DOCTORAL THESIS

Draught and Infection Risk Control in Modern Educational and Office Spaces

Martin Kiil

Draught and Infection Risk Control in Modern Educational and Office Spaces

MARTIN KIIL

TAL
TECH
PRESS

TALLINN UNIVERSITY OF TECHNOLOGY
School of Engineering
Department of Civil Engineering and Architecture
This dissertation was accepted for the defence of the degree 30/06/2025

Supervisor: Tenured Full Professor Jarek Kurnitski
                             School of Engineering
                             Tallinn University of Technology
                             Tallinn, Estonia

Co-supervisor: Senior Researcher Raimo Simson
                             School of Engineering
                             Tallinn University of Technology
                             Tallinn, Estonia

Opponents: Prof Lars Ekberg
                             Chalmers University of Technology
                             Göteborg, Sweden

                             Prof Panu Mustakallio
                             Aalto University
                             Espoo, Finland

Defence of the thesis: 19/08/2025, Tallinn

Declaration:
Hereby I declare that this doctoral thesis, my original investigation and achievement, submitted for the doctoral degree at Tallinn University of Technology has not been submitted for doctoral or equivalent academic degree.

Martin Kiil

                                          _____
                                                                  signature

Tõmbus- ja nakkusriski ohjamine kaasaegsetel haridus- ja büroopindadel

MARTIN KIIL

TALTECH KIRJASTUS

Contents

List of publications

The list of author's publications, on the basis of which the thesis has been prepared:

I   Kiil, M.; Simson, R.; Thalfeldt, M.; Kurnitski, J. (2020). A Comparative Study on Cooling Period Thermal Comfort Assessment in Modern Open Office Landscape in Estonia. *Atmosphere* 2020, 11(2), 127 DOI: https://doi.org/10.3390/atmos11020127

II Kiil, M.; Simson, R.; Thalfeldt, M.; Kurnitski, J. (2024). Overheating and air velocities in modern office buildings during heating season. *Indoor Air* 2024 DOI: https://doi.org/10.1155/2024/9992937

III Kiil, M.; Valgma, I.; Võsa, K.-V.; Simson, R.; Mikola, A.; Tark, T.; Kurnitski, J. (2023). Ventilation effectiveness in classroom infection risk control. The 11th International Conference on Indoor Air Quality, Ventilation & Energy Conservation in Buildings (IAQVEC2023) DOI: https://doi.org/10.1051/e3sconf/202339601043

IV Kiil, M.; Mikola, A.; Võsa K.V.; Simson, R.; Kurnitski, J. (2024). Ventilation effectiveness and incomplete mixing in air distribution design for airborne transmission. *Building and Environment* 2024 DOI: https://doi.org/10.1016/j.buildenv.2024.112207

Author's contribution to the publications

The author of the thesis is the principal author, the composer of the manuscripts, and responsible for data analysis of the publication I to IV. The author prepared agreements with the building owners, performed the measurements, analysed the data, and formalized the results of the publications I and II.

The lead supervisor professor Jarek Kurnitski conceived and designed the experiments performed in publications. Raimo Simson contributed to writing the papers. Professor Martin Thalfeldt contributed to composing publications I and II. Alo Mikola contributed mostly to publications III and IV. Teet Tark and Indrek Valgma assisted with III paper. Karl-Villem Võsa developed the visualization methods for the results in publications III and IV.

Introduction

Indoor thermal conditions significantly affect occupant comfort levels. Local thermal comfort and draught rates have been extensively studied, with most research conducted under controlled conditions rather than in real work environments. Thermal comfort in Estonian office buildings has been scarcely explored.

This thesis presents and discusses results from five Tallinn office buildings, varying in HVAC system designs and room elements. The study involved on-site thermal comfort and draught assessments, alongside occupant surveys. Findings reveal that standard-based thermal comfort criteria may not fully reflect occupant experiences, and the choice of specific room conditioning units does not consistently ensure a draught-free, comfortable environment. Short- and long-term data revealed significant overheating during the heating season, despite low air velocities. Occupants were comfortable at lower clo values (0.7 clo). Elevated temperature setpoints were used to mitigate draught, contributing to overheating. As a solution, adjusting room temperature control based on outdoor mean temperatures and supply air temperature based on extract air temperatures is proposed.

The benefits of proper classroom ventilation for health and learning outcomes are well-documented. However, many studies continue to report issues with air quality, air exchange rates, and air velocities. This thesis examines typical Estonian classroom air distribution systems using an air distribution laboratory at Tallinn University of Technology. CO_2 tracer gas decay was employed to measure air change efficiency, while the continuous dose method was used to assess contaminant removal effectiveness. Draught measurements were also conducted in the mock-up classroom using air velocity probes to provide evidence whether the high ventilation effectiveness and low draught risk can be achieved simultaneously.

Airborne respiratory infections impose considerable socio-economic costs. Effective ventilation design for airborne transmission remains a challenge due to the non-uniform air distribution in spaces, despite ventilation standards assuming well-mixed conditions. This study developed a new method to quantify infection risk by measuring ventilation effectiveness with point-source tracer gas tests in 22 rooms, mimicking an infector's location. Results showed that calculating ventilation effectiveness from average concentration at breathing height required higher ventilation rates than traditional methods, with discrepancies ranging up to 39% in large open-plan offices. Ventilation effectiveness values ranged from 0.5 to 1.4, indicating significant room for improvement.
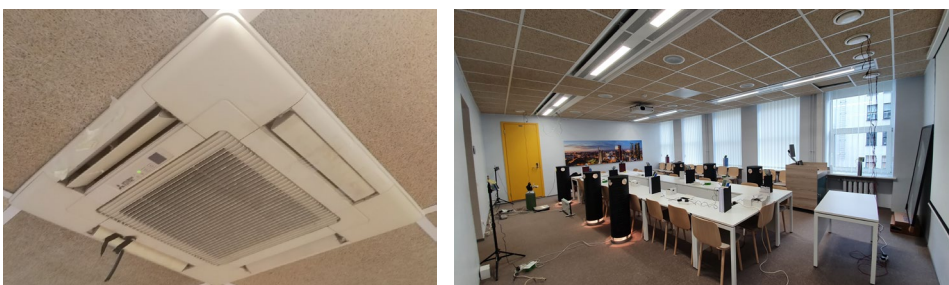

Figure 1. Modified airflow distribution of a fan coil unit to avoid draught (left). Point source ventilation effectiveness measurements in a meeting room to replicate an airborne viral situation using CO_2 tracer gas method (right).

Research questions and methods

RQ1 – How typical HVAC settings perform in terms of indoor air temperature and draught in typical office buildings in Estonia? **Method** – Field measurements in 5 office buildings in Tallinn.

RQ2 – How typical air distribution system layouts perform in terms of change efficiency and contaminant removal effectiveness while maintaining air velocity criterion in a classroom? **Method** – Measurements in a mock-up classroom.

RQ3 – Whether the air distribution systems provide presumed fully mixing ventilation criterion? **Method** – Field measurements of point source ventilation effectiveness for breathing pane in typical non-residential room types.

RQ4 – How to calculate required ventilation rate supplied by the ventilation system in case of inadequate air exchange and viral situation? **Method** – Target ventilation rate calculation method for non-mixing air distribution and infection risk-based ventilation.

Achieving objectives

The thesis is based on peer-reviewed journal articles and conference paper (Figure 2). Indoor air temperature and draught risk is investigated in Publications I and II, including up to 80 measurement points in open office settings in five office buildings in Tallinn, Estonia. Both indoor air temperatures and air velocities are measured during cooling season. In Publication II, heating season measurements are covered. In addition, indoor air temperature and supply air temperature are studied in two of the five office buildings. In Publication I and II, the measurement results are compared with occupant thermal sensation using indoor climate questionnaire forms. Draught risk assessment is extended to Publication III, which focuses on both air exchange efficiency and contaminant removal effectiveness measurements to assess infection risk in a mock-up classroom. These experiments are extended to an additional 20 non-residential typical rooms in Publication IV, which provides calculation methods for target ventilation rate in case of viral situation. These non-residential settings include various rooms, such as classroom, dressing room, fitness, gym, restaurant, bar, meeting room and open office. Finally, the calculation of required ventilation rate is improved by iterative method of spatial variation.
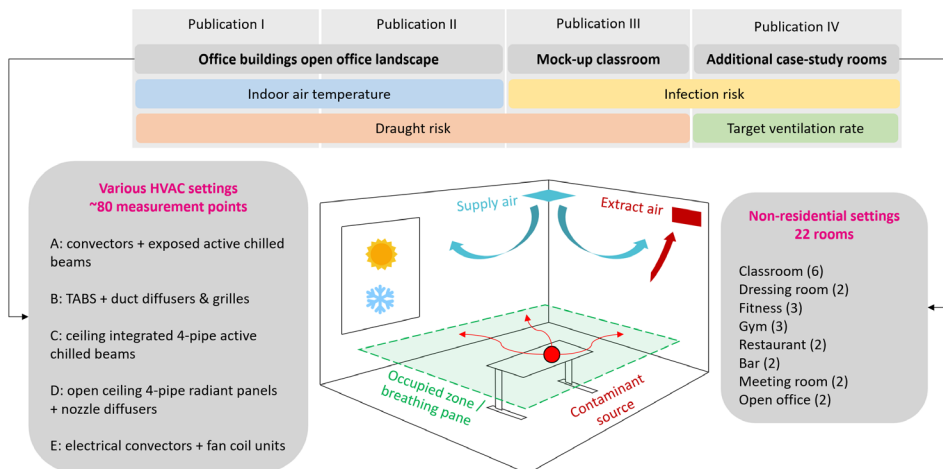

Figure 2. Main structure of the thesis.

Novelty and practical outcomes

Field measurements from office buildings provided valuable feedback on real HVAC systems operation and indicated some fundamental problems which solving will require actions in design and operation. Some buildings experienced higher indoor air temperatures during heating season compared to cooling season (3/5 did not meet the comfort criterion). Higher air velocities causing draught were compensated with elevated supply air temperatures, resulting in overheating risk. The results from heating period indicate better alignment with clo values reduced from 1.0 to 0.7 which may represent occupants' adaptation to overheating. Four-pipe radiant panels performed best, following active chilled beams with the potential to meet the Cat II requirements achieving air velocity and room air temperature simultaneously. TABS maintained similar air velocities with active chilled beams but experienced overheating during winter. Fan coil units with considerably higher velocities performed worst during cooling period.

Results revealed that room air temperature, supply air temperature and air velocities were not adequately controlled in studied office buildings. Therefore, a practical recommendation for temperature control improvement algorithm in building automation system was proposed. Using running mean outdoor temperature and including midseason definition for supply air temperature control based on extract air temperature can help to avoid draught or overheating.

Ventilation effectiveness analyses with local air quality index and contaminant removal effectiveness showed that fully mixing is not a case in mixing ventilation with a point source, although air change efficiency determined with equally distributed source showed fully mixing conditions. It was shown that point source ventilation effectiveness values can be used as a correction factor for mixing ventilation airflow rate. Our results enable to propose default values for contaminant removal effectiveness in mixing ventilation ranging from 0.5–0.8 depending on space category and room size. Measured ventilation effectiveness values higher than 1.0 demonstrate that better ventilation effectiveness than in fully mixed conditions can been achieved with carefully designed air distribution systems.

New method taking into account special differences in concentration and corresponding infection risk was developed and tested for target ventilation rate determination. In this method, infection risk was quantified at breathing height for each measurement point, and the required ventilation rate to meet a specified risk level was calculated based on tracer gas measurements from a few point source locations. This methodology facilitates the optimization of air distribution systems for effective infection control. This spatial variation iterative calculation method requiring quanta data provided in all cases less conservative results for required ventilation rate than a simple calculation from an average concentration.

These theses contribute to the goal of avoiding draught and maintaining high ventilation effectiveness simultaneously that was reasonably achievable in many studied cases. Risk assessment model based on basic reproduction number aims not to eliminate but considerably reduce the infection risk in shared indoor spaces. Infection risk-based ventilation research conducted in this thesis has been a part of post-COVID ventilation design method development already published by Nordic Ventilation Group and REHVA. This method is proposed to be included in the ongoing revision of EN 16798-1:2019 standard.

Limitations and future work

Interpretation of the findings of the thermal comfort study is most applicable in heating-dominated climatic conditions. Only several HVAC setting investigated not covering the full spectrum of systems found in real-world office buildings. Additionally, development of advanced indoor climate survey systems and integrating clothing monitoring into HVAC control systems and occupant feedback could be promising research topics.

Measurement conditions and validity. Because of complexity of air flow patterns development in a room, affected by air jets, internal and solar heat gains, geometry etc., contaminant removal effectiveness measurement strictly applies only for those conditions in a room at measurement time. This makes it highly important to conduct measurements in typical, representative situations. Internal heat gains are to be organised to the room, supply air temperature controlled, and the ventilation rate to be adjusted close to values under interest, because Archimedes number that is used to describe non-isothermal jets should not change significantly to keep the same air distribution patterns.

Room categories was not comprehensively studied for instance to find the best possible ventilation effectiveness values. Such analyses can be recommended for future studies because the results show high variations – there could be a substantial improvement potential in many cases. Additional complexity is working with a point source which can have many possible locations in a room. In this study a tracer gas was injected into the dummy that is a simplification compared for instance to breathing manikin. While some guidance on how to select relevant source locations was possible to provide, this topic evidently deserves future research efforts to ensure correct and practical application for ventilation design purposes. In addition, tracer gas experiments are more reliable in smaller rooms with lower ceilings than in larger and higher or partly open spaces.

In general, future joint topics could include integrating draught and infection risk management:

- Within demand-based HVAC systems in dynamic environments (both educational and office spaces) while avoiding oversizing.
- In case of retrofitting existing buildings.
- Into HVAC design and selection tools as both measurement methods for air velocity and tracer gas are difficult to use during the planning phase of a new building.
- While balancing multiple factors including architectural functionality, thermal comfort, ventilation acoustics, indoor climate control automation, energy efficiency, cost-effectiveness, etc.

Notations

Abbreviations and terms

CFD	computational fluid dynamics
HVAC	heating, ventilation, and air conditioning
ICC	indoor climate category
ICQ	indoor climate questionnaire
TABS	thermally activated building systems
TC	thermal comfort
VAV	variable air volume

Symbols

A	net floor area of the room (m²)
ACH	air change per hour (1/h)
C	average quanta concentration in the breathing zone (quanta/m³)
C_{avg}	time-averaged quanta concentration (quanta/m³)
C_0	quanta concentration in the supply air (quanta/m³)
C_e	quanta concentration in the extract air (quanta/m³)
C_{ex}	concentration in the exhaled breath of infector (quanta/m³)
C_i	quanta concentration at the location i (quanta/m³)
C_{res}	respiratory convective heat exchange (W/m²)
$CADR$	clean air delivery rate (m³/h)
CRE	contaminant removal effectiveness, (-)
D	duration of the occupancy (exposure) (h)
D_i	dilution ratio (-)
D_{inf}	the total interaction time when an infectious individual is in the vicinity of any susceptible persons during the whole pre-symptomatic infectious period (h)
DR	draught rate (%)
E	quanta emission rate (quanta/h)
ε^a	air change efficiency (%)
ε_P^a	local air change index (%)
$\varepsilon^c = CRE$	contaminant removal effectiveness (-)
ε_P^c	local air quality index (-)
ε_b^j	point source ventilation effectiveness of measurement j (-)
ε_b	point source ventilation effectiveness for the breathing zone (-)
$\varepsilon_{P,i}$	local air quality index at the measurement point i (-)
ε_b	ventilation effectiveness (contaminant removal effectiveness) $\varepsilon_b = 1$ for fully mixed conditions (-)
ε_b^j	point source ventilation effectiveness of measurement with source location j (-)
$\varepsilon_{b,loc}$	ventilation effectiveness taking into account the spatial variation of concentration (-)

$\varepsilon_{b,loc}^{j}$	point source ventilation effectiveness of measurement with source location j taking into account the spatial variation of concentration (-)
f_v	fraction of the local population who are vaccinated, $f_v = 0$ for no vaccination (-)
Θ_{rm}	outdoor running mean air temperature (°C)
g	solar radiation transmittance through window glass (-)
h	room height (m)
I	number of infectious persons (-)
k	virus decay (1/h)
k_f	filtration removal rate (1/h)
k_{UV}	disinfection by upper room ultraviolet germicidal irradiation UVGI (1/h)
K	number of measurement points (-)
λ	first-order loss rate coefficient (1/h)
λ_{dep}	deposition onto surfaces (1/h)
λ_{rest}	other removal mechanisms than ventilation (1/h)
λ_v	outdoor air change rate, i.e., removal rate due to ventilation (1/h)
m	number of tracer gas experiments with different point source locations (-)
M	metabolic rate (met)
n	number of quanta inhaled (quanta)
η_s	facial mask efficiency for a susceptible person (-)
η_i	facial mask efficiency for infected person (-)
η_f	filter efficiency (-)
η_v	the efficacy of the vaccine against becoming infectious, $\eta_v = 1$ for ideal protection (-)
N	total number of occupants (-)
N_c	number of disease cases (-)
N_s	number of susceptible persons in the room (-)
p	probability of infection for a susceptible person (-)
p_i	probability of infection for a susceptible person at location i (-)
PMV	predicted mean vote (-)
PPD	predicted percentage dissatisfied (%)
q	quanta emission rate per infectious person (quanta/h)
q_q	quanta emission specific ventilation rate for occupancy per person [l/(s·person)]
q_r	removal rate of virus decay and deposition [l/(s·m³)]
Q	outdoor and non-infectious supply air target ventilation rate for the breathing zone (m³/h)
Q_{act}	actual measured design ventilation rate supplied by the ventilation system (l/(s m²))
Q_b	volumetric breathing rate of an occupant (m³/h)
Q_s	ventilation rate supplied by ventilation air distribution system (m³/h)
$Q_{s,loc}$	ventilation rate supplied by ventilation air distribution system taking

	into account the spatial variation of concentration (m³/h)
$q_{V,bz}$	breathing zone ventilation rate (m³/h)
$q_{V;ODA}$	outdoor air ventilation rate (m³/h)
R	event reproduction number (-)
R_0	basic reproduction number that describes the spread of an epidemic in the population (-)
R_i	fraction of the reproduction number (-)
RH	relative humidity (%)
t	time (h)
t_i	indoor air temperature (°C)
t_o	operative temperature (°C)
t_{sup}	supply air temperature (°C)
Tu	turbulence intensity (-)
τ_n	nominal time constant (h)
$\bar{\tau}_r$	air change time for all the air in the room
$\bar{\tau}_P$	local mean age of air (h)
U	thermal transmittance [W/(m²×K)]
V	volume of the room (m³)
v_a	air velocity (m/s)
WWR	window-to-wall ratio (-)

1 Background

In Estonia, research on thermal comfort TC and occupant satisfaction during the cooling season is nearly absent. Existing studies in office buildings primarily focus on heating season performance and energy efficiency. Indoor thermal conditions significantly impact occupant comfort. This thesis hypothesizes that, despite the appearance and capabilities of heating, ventilation, and air conditioning (HVAC) systems in open office environments, a considerable number of occupants remain dissatisfied with TC conditions. The primary objective is to identify factors contributing to poor temperature and air velocity v_a control and to offer recommendations for managing these parameters in design and operation to achieve comfort. The hypothesis suggests that v_a, indoor air temperature (t_i), and supply air temperature (t_{sup}) are not effectively controlled in current design and operational practices. Additionally, it is possible that standard responses to indoor climate complaints, such as adjusting controller setpoints, have led to excessively high indoor temperatures outside the optimal comfort range. For determining the issues described, field measurements and indoor climate surveys in 5 office buildings in Tallinn, including up to 80 measurement points, were performed.

The next focus of this thesis is to evaluate ventilation effectiveness simultaneously with draught risk in a mock-up classroom. Main findings of the experiments indicated that the ventilation solutions do not always guarantee the expected efficiency, or the v_a values do not maintain the required limits in the occupied zone. As airborne respiratory infections result in significant socio-economic costs, ventilation effectiveness was additionally studied in multiple non-residential room typologies. The final goal of the thesis was to provide a practical calculation method for the required ventilation rate supplied by the ventilation system in case of inadequate air exchange or viral situation. This fills the gap that exists in understanding how to apply ventilation effectiveness to airborne transmission from a point source.

In this chapter, a brief overview of TC, draught, ventilation effectiveness, and calculation of infection risk fundamentals is provided.

1.1 Thermal comfort and draught

Modern low-energy office buildings require efficient HVAC systems to maintain a comfortable and healthy indoor environment. Key design factors, particularly façade elements such as window size, layout, and glazing, significantly affect HVAC performance and thermal conditions. Studies have shown that window-to-wall ratios, especially around 25% for triple-glazed windows, optimize cooling loads and energy efficiency in cold climates [1,2]. Higher glazing ratios lead to increased cooling demands, necessitating larger cooling units, greater airflow, or lower supply air temperatures, which also raise the risk of draught. Draught has been identified as a primary discomfort source, even when other thermal conditions are satisfactory [2–5]. Occupant positions and densities in offices often differ significantly from initial designs, creating dynamic conditions that complicate HVAC system design for stable thermal environments. Open office layouts, commonly used to allow flexible workspace allocation [6], require careful HVAC planning to maintain adequate conditions across various configurations. In modern buildings, achieving both comfort and health while reducing energy use is essential to meet European Union energy efficiency targets [7].

In temperate climates, mechanical ventilation and active cooling are standard. However, these systems do not always ensure satisfactory thermal conditions [8].

Achieving high occupant satisfaction remains challenging, making (TC) a critical factor in modern office design [9,10]. During the conceptual and detailed design stages, decisions on HVAC strategies, system types, and components often lack a clear link to occupant satisfaction [11–14]. Even with precise design, installation, and operation, indoor climate dissatisfaction persists [15–19], indicating several critical factors in design and commissioning. Meeting individual preferences is particularly difficult in open-plan offices, where controllers usually serve large zones [20].

In offices, water-based room cooling solutions vary with cooling load, cooling source type, and interior design, and can be classified by supply water temperature: low-temperature units (e.g., fan coils) and high-temperature systems (e.g., thermally activated building systems (TABS), passive and active cooling beams combined with ventilation terminals) [21,22]. High-temperature cooling is often favoured in low-energy buildings for improved cooling plant efficiency [22]. Most studies on these systems are based on computational fluid dynamics CFD simulations or lab environments [23,24, 33–37,25–32], with real-world research primarily in warm climates [38–41]. In temperate and cold climates, limited studies exist. For instance, Pfafferott et al. [42] found 41% summer discomfort in German low-energy offices with TABS, revealing a gap between perceived and standard-measured comfort. Hens [4] also noted that standards, such as Fanger's predicted mean vote PMV and percentage of dissatisfied occupants PPD [43], may underestimate dissatisfaction, suggesting caution in interpreting thermal comfort findings.

Proper application of control strategies, design, installation, and maintenance of room cooling and ventilation systems are essential to ensure a stable indoor climate without temperature fluctuations or draughts during the cooling season [44–50]. Since occupant satisfaction with thermal conditions depends on various factors (e.g., gender, age, health), temperature and air movement measurements alone are often insufficient [48,51–54]. Surveys are typically needed to identify issues and gain a complete view of thermal comfort. Studies indicate that predicted and actual thermal comfort can vary [4,42,53], with female occupants generally reporting higher dissatisfaction rates [52,55–58].

Indoor environmental conditions significantly affect workplace comfort and symptoms among occupants [59–61]. Poor indoor climate is associated with reduced productivity and well-being [62–65], prompting codes and standards to set requirements for workplace conditions [60,66–69]. Uncomfortable thermal conditions can impair cognitive performance, reducing concentration, memory, and reaction times. Hence, comfortable environments enhance productivity and learning outcomes, with evidence linking thermal comfort to improved learning performance [70,71].

European and international standards provide guidelines for measuring thermal environmental variables, design criteria, and assessing TC in buildings. Key standards include EN 16798-1 [72] and EN 16798-2 [73], which set requirements for indoor environmental parameters and HVAC design. EN ISO 7730 [74] offers methods for predicting thermal sensation and discomfort, while EN ISO 7726 [75] details methods for TC assessment. These standards use a heat balance comfort model, incorporating physiological factors to calculate the PMV and the PPD, along with an adaptive model [76,77]. EN ISO 7730 accounts for factors like t_i, relative humidity (RH), v_a, radiation, metabolic rate M, and clothing insulation, all crucial to TC [78]. Clothing insulation is measured in clo units, with 1 clo equalling 0.155 K·m²·W^{-1}, representing the insulation needed for a person at 1.2 met engaged in sedentary activity to maintain TC in a room

at +22 °C with 0.1 m/s air movement. A default value of 1.0 clo is used for heating seasons and 0.5 clo for cooling seasons.

Although prior studies highlight energy savings through optimized temperature control [79–81], they often overlook key TC factors essential for effective control strategies. Local thermal discomfort, primarily due to v_a [48], is a common HVAC issue, with studies showing a strong correlation between t_i and air movement [82–86]. Draught perception is heightened with pulsating rather than steady airflow, emphasizing the need for airflow stability in ventilation design [87]. Supply air fluctuations can lead to dissatisfaction [86], making it crucial to select t_{sup} that balance draught comfort, ventilation effectiveness, and energy efficiency [88].

1.2 Ventilation effectiveness

Enhancing ventilation effectiveness enables significant improvement in indoor air quality without increasing the overall air change rate, thereby avoiding the associated rise in the capital costs and energy consumption. Ventilation effectiveness broadly refers to performance indices that characterize a ventilation system's ability to facilitate air exchange within a space and to remove airborne contaminants efficiently (Figure 3). [89]
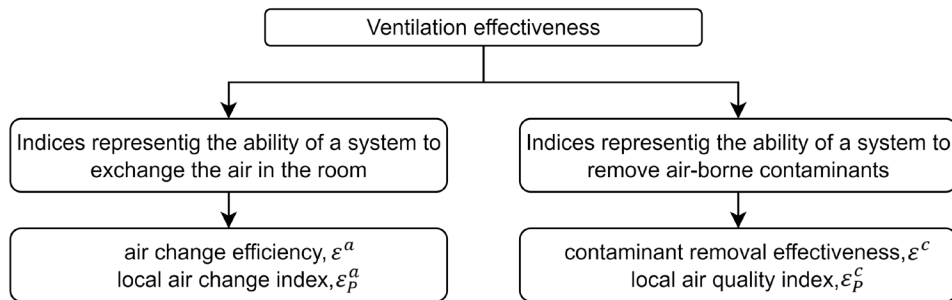

Figure 3. Ventilation effectiveness indices. [89]

Air distribution is crucial for air quality, affecting how effectively contaminated indoor air is replaced with fresh air. Studies show that poor air quality in classrooms reduces student performance and negatively impacts health, increasing risks of asthma, absenteeism, and respiratory issues [90–95]. Adequate air change rates improve these outcomes [96–99]. Mixing air distribution, the oldest and most common method, aims to achieve uniform pollutant removal and temperature distribution in occupied zones [100,101]. Novoselac and Srebic [102] found that overlapping results in the occupied and breathing zones reduce the required number of measurement points. Kosonen and Mustakallio [103,104] analysed mixing and displacement ventilation in a mock-up classroom, with CFD simulations showing that heat gains in rooms with mixed ventilation significantly impact air distribution and draught.

Ventilation combined with particle filtration and air disinfection helps mitigate long-range airborne transmission by reducing infectious aerosol levels in shared spaces [105]. Ventilation dilutes indoor airborne pathogens by mixing non-infectious air, significantly lowering transmission risk [106]. However, achieving effective ventilation at practical air change rates depends not only on the rates but also on ventilation effectiveness [89]. This thesis addresses the challenge that standard ventilation criteria

– based on perceived air quality, pollutant thresholds, or airborne transmission – will provide a target ventilation rate at fully mixed conditions. In practice, mechanical (or natural) ventilation creates non-uniform air distribution [107], leading to contaminant concentration variations. This non-uniformity can undermine infection risk assessments, as the Wells-Riley model assumes a uniform aerosol distribution, potentially underestimating risk [108–110].

Ventilation effectiveness can account for non-uniform concentration, with summarized values for various air distribution systems available in reviews [100,111]. However, these values are typically based on distributed sources like bioeffluents or CO_2 emissions from all occupants, not a point source, such as an infector. Distributed sources are relatively uniform and easily managed by mixing ventilation, often assuming contaminant removal effectiveness value of 1.0. In contrast, airborne transmission involves a single infector acting as a point source, with varying potential locations in a room, making typical ventilation effectiveness values less applicable.

Ventilation effectiveness reflects a system's capacity to exchange room air or remove airborne contaminants. The former is categorized into air change efficiency ε^a and local air change index ε_P^a, while the latter is divided into contaminant removal effectiveness ε^c (CRE) and local air quality index ε_P^c. The age of air is a useful metric for evaluating ventilation effectiveness. The local mean age of air $\bar{\tau}_P$ in the exhaust is always equal to the nominal time constant τ_n. The ε^a can be calculated by the ratio between the lowest possible mean age of air and the actual room mean age of air $\bar{\tau}_r$ as shown in Equation (1). The upper limit of ε^a is 100% for piston flow, with 50%-100% indicating displacement flow, 50% representing fully mixed flow, and below 50% suggesting short-circuiting flow. To calculate the ε_P^a at a specific point, τ_n is divided by $\bar{\tau}_P$, shown in Equation (2). [89]

$$\varepsilon^a = \frac{\tau_n}{\bar{\tau}_r} \cdot 100 = \frac{\tau_n}{2\langle\bar{\tau}\rangle} \cdot 100, \text{ (\%)} \tag{1}$$

$$\varepsilon_P^a = \frac{\tau_n}{\bar{\tau}_P} \cdot 100, \text{ (\%)} \tag{2}$$

The determination of airflow rates using the tracer gas dilution method follows EN ISO 12569:2017 [112], while methods for characterizing ventilation conditions via local mean ages of air are outlined in ISO 16000-8:2007 [113]. The ε^c can be calculated by the ratio shown in Equation (3) between the steady-state of the exhaust concentration c_e and the steady-state mean concentration of the room $\langle c \rangle$. Equation (4) calculates ε_P^c, representing contaminant concentration at point P. In both cases, the supply air concentration c_{sup} is subtracted from the extract air concentration c_{ext} and from either the mean concentration $\langle\bar{c}\rangle$ or the local point concentration c_P [89]. According to EN 16798-3:2017 [114], Equation (3) is also used as ventilation effectiveness.

$$\varepsilon^c = \frac{c_e}{\langle c \rangle} = \frac{(c_{ext} - c_{sup})}{(\langle\bar{c}\rangle - c_{sup})}, \text{ (-)} \tag{3}$$

$$\varepsilon_P^c = \frac{c_e}{c_P} = \frac{(c_{ext} - c_{sup})}{(c_P - c_{sup})}, \text{ (-)} \tag{4}$$

The breathing zone ventilation rate $q_{V,bz}$, divided by the ε^c from Equation (3), represents the required volume flow of outdoor air at the room's supply diffusers, as shown in Equation (5):

$$q_{V;ODA} = \frac{q_{V,bz}}{\varepsilon^c}, \text{ (m}^3\text{/h)} \tag{5}$$

The outdoor air ventilation rate $q_{V,ODA}$ can be calculated as the infection risk-based ventilation rate [115]. Instead of using the mean concentration in the breathing zone shown in Equation (3), we utilize local breathing zone values demonstrated in Equation (4). When the contaminant source is a point source, such as an infectious individual, these local values should serve as the denominator in Equation (5) to apply the recently proposed infection risk-based design method [115]. This method incorporates quanta emission data to simplify the direct calculation of ventilation rates for standard room types, yielding the design ventilation airflow rate Q_s for the actual air distribution setup, as illustrated in Equations (6) to (8) [116]. However, laboratory classroom experiments involving various ventilation layouts indicated that ε^a values were consistently 10–20% more efficient than corresponding point source ε^c values in case of mimicking a mixing ventilation scenario. Furthermore, using the average of two or more source locations, rather than relying on a single-point measurement, is recommended to provide a sufficiently conservative correction factor (ε_b) for dimensioning ventilation rates Q_s.

$$Q_s = \frac{Q}{\varepsilon_b}, \text{(m}^3\text{/h)} \tag{6}$$

where ε_b represents point source ventilation effectiveness for breathing zone. Notation b is used to refer to the point source while ε^c values are measured with distributed source. ε_b can be calculated as [117]:

$$\varepsilon_b = \frac{1}{\frac{\Sigma_{i=1}^{m}\left(\frac{1}{\varepsilon_b^j}\right)}{m}}, \text{(-)} \tag{7}$$

where ε_b^j stands for point source ventilation effectiveness of measurement with source location j calculated from m experiments in (two or more) different point source locations. Equation (8) shows the calculation of ε_b^j:

$$\varepsilon_b^j = \frac{1}{\frac{\Sigma_{i=1}^{K}\left(\frac{1}{\varepsilon_{P,i}}\right)}{K}}, \text{(-)} \tag{8}$$

Here, the point source location j ventilation effectiveness based on the average concentration on breathing plane is calculated based on local air quality index measurement points $\varepsilon_{P,i}$, similarly to Equation (4) and K represents the number of measurement point.

1.3 Modelling of infection risk

The COVID-19 pandemic, caused by SARS-CoV-2, created a global health crisis, disrupting public health systems, economies, and daily life worldwide. This event has highlighted the essential role of indoor air quality and effective ventilation in preventing respiratory infections [105,118,119]. Studies show COVID-19 primarily spreads via aerosols, which remain airborne longer and travel farther than the initially recommended 2-meter distancing [120,121]. The pandemic has accelerated the need for specific ventilation guidelines tailored to respiratory infection risks in shared indoor spaces [122,123]. Lichtner and Kriegel [124] found that classroom ventilation could result in air quality up to five times worse than expected. Other studies underscore the link between ventilation strategy and airborne disease transmission [120,125]. Recently, an infection

risk-based ventilation method was introduced [115], which requires adjusting fully mixed ventilation equations by point source effectiveness for realistic air distribution [126]. Figure 4 illustrates the impact of outdoor air ventilation on virus concentration within a room. Under fully mixed ventilation, pollutant concentration is assumed to be uniform throughout the space. However, in practice, concentrations are higher near the source. A fully mixed condition typically establishes at distances of approximately 1.5 meters from an infected individual engaged in activities such as speaking or coughing [127]. Consequently, general ventilation should be complemented by physical distancing, and distances less than 1.5 meters require additional measures such as personal protective equipment or localized ventilation solutions. [115]
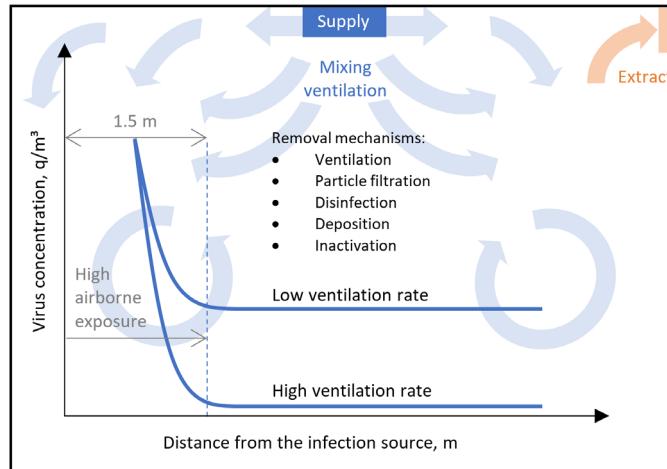

Figure 4. Illustration of how a viral load of an infectious person leads to aerosol concentration in a room. At about 1.5 m distance from the source the virus concentration has decreased to a constant level depending on the emission rate and removal mechanisms. [115]

Many studies have analysed spatial non-uniform concentrations due to air distribution patterns, using CFD simulations [128] or detailed measurements [107] to assess infection risk at various points. Tan [129] found that indoor aerosol concentration variation is substantial and should be considered in risk assessments, while Jan [130] used CFD with a modified Wells-Riley model to quantify individual occupant risk, revealing significant spatial variation. Son [131] demonstrated experimentally that floor extracts enhance vertical airflow, reducing PM2.5 at breathing height. Singer [132] showed that ceiling diffusers provide effective mixing with cooled or neutral air but lose effectiveness when heating. A CFD simulation of CO_2 distribution in a naturally ventilated classroom during winter revealed significant variation based on different opening configurations [133]. These studies illustrate effective air distribution designs and lower-risk occupant locations, but the methodologies are too complex for routine ventilation design. CO_2, validated as a tracer gas for ventilation effectiveness measurements [89,112,113,134,135], offers a simpler alternative to complex CFD simulations, although a practical, robust design method for ventilation remains needed.

To establish a general ventilation criterion based on infection risk, the Wells-Riley model, calibrated for SARS-CoV-2 quanta emission rates, is applied. Infection probability is estimated for typical public spaces using ventilation rates defined in EN 16798-1 [72],

Categories I to III. The infection risk for different room types and activities is calculated using the standard Wells-Riley model, adapted for airborne transmission of COVID-19 by incorporating appropriate source strength (quanta emission rate, *E*, in quanta/h). A quantum is defined as the dose of airborne particles required to infect susceptible individual with the chance of 63%. This aerosol-based infection risk model follows the original Wells-Riley formulation [136,137], as further developed by Gammaitoni and Nucci [138]. In this framework, the probability of infection *p* is related to the number of inhaled quanta (*n*), as described in Equation (9) [115]:

$$p = \frac{N_c}{N_s} = 1 - e^{-n} = 1 - e^{-\frac{IqQ_bD}{Q}} = 1 - e^{-CQ_bD}, \text{ (-)} \tag{9}$$

where:
- p probability of infection for a susceptible person (-)
- N_c number of disease cases (-)
- N_s number of susceptible persons in the room (-)
- I number of infectious persons (-)
- n number of quanta inhaled (quanta)
- q quanta emission rate per infectious person (quanta/h)
- Q_b volumetric breathing rate of an occupant (m3/h)
- Q ventilation rate for the breathing zone (m3/h)
- D duration of the occupancy (h)
- C quanta concentration in the room (quanta/m3)

The number of susceptible individuals does not distinguish between high- and low-risk populations. However, more stringent probability thresholds can be applied for high-risk groups. To account for vaccinated individuals, the number of susceptible may be adjusted by assuming 100% vaccine efficacy. If no vaccinated persons are present, the number of susceptible is defined as $N_s = N - I$, where *N* is the total number of occupants, and *I* is the number of infectious individuals. The quanta inhaled (*n*, in quanta) is determined by the time-averaged quanta concentration C_{avg} (quanta/m³), the occupant's volumetric breathing rate Q_b (m³/h), and the duration of exposure *D* (h) [115]:

$$n = C_{avg}Q_bD, \text{ (quanta)} \tag{10}$$

In Equation (10), both the breathing rate and the quanta emission rate are assumed to be constant, representing average values over the exposure period. In reality, however, individual behaviours, such as coughing or not coughing, can introduce variability in emissions, even at the same breathing rate. The model assumes that emissions originate solely from breathing or speaking, and that the concentration of quanta in exhaled air is independent of the breathing rate or respiratory activity. When a person wears a mask, the mask efficiency η_s for the susceptible individual reduces the amount of quanta inhaled [115]:

$$n = C_{avg}Q_b(1 - \eta_s)D, \text{ (quanta)} \tag{11}$$

The airborne quanta concentration increases over time from an initial value of zero, following a "one minus exponential" curve, characteristic of the dynamic response of a fully mixed indoor environment to a constant emission source. A single-zone fully mixed mass balance model is used to estimate the concentration in the room [115]:

$$\frac{dC}{dt} = \frac{E}{V} - \lambda C \tag{12}$$

where:

> E quanta emission rate (quanta/h)
>
> V volume of the room (m³)
>
> λ first-order loss rate coefficient [139] for quanta/h due to the summed effects of ventilation (λ_v, 1/h), deposition onto surfaces (λ_{dep}, 1/h) and virus decay (k, 1/h) and filtration by a portable air cleaner if applied (k_f, 1/h) and upper room ultraviolet germicidal irradiation UVGI (k_{UV}, 1/h), $\lambda = \lambda_v + \lambda_{dep} + k + k_f + k_{UV}$, 1/h)

A fully mixed mass balance model does not account for spatial variations in concentration within the room, potentially leading to uncertainties. The ventilation loss rate coefficient includes all virus-free air supplied to the room, such as outdoor air ventilation, infiltration, virus-free air from recirculation, and transfer air from other rooms. In the single-zone model used in this study, recirculation is not considered, which would require a multi-zone model. In public spaces with human occupancy, ventilation is typically balanced, or the supply airflow rate exceeds the extract rate, meaning no transfer air enters the room. Therefore, in the following analysis, ventilation is treated solely as outdoor air ventilation. The quanta emission rate is generated by I infected individuals, and when accounting for facial mask efficiency, the emission rate can be described as [115]:

$$E = (1 - \eta_i)Iq, \text{ (quanta/h)} \tag{13}$$

where:

> η_i facial mask efficiency for infected person, 0 for no mask (-).

The filtration efficiency of a facial mask worn by an infectious individual may differ from that of a mask worn by a susceptible person, even if the masks are nominally identical. This is due to differences in particle size and moisture content, with exhaled droplets being larger and more water-laden than inhaled, evaporated particles. For example, Ueki et al. [140] reported worst-case mask efficiencies of 0.5 for infected persons and 0.3 for susceptible individuals. A surface deposition loss rate of 0.3 1/h is used, based on findings by Thatcher et al. and Diapouli et al. [141,142], though values may range from 0.24 to 1.5 1/h, depending on particle size. Coleman et al. [143] found that fine aerosols (≤5 μm) accounted for 85% of viral load, supporting the use of a lower deposition loss rate. For virus decay in the absence of sunlight, Fears et al. [144] observed no decay over 16 hours at 53% relative humidity, whereas van Doremalen et al. [145] reported a half-life of 1.1 h, corresponding to a decay rate of $k = \ln(2) / t_1/_2 = 0.63$ 1/h. An average value of 0.32 1/h from these studies is used in this analysis. For portable air cleaners, the filtration removal rate (k_f) is calculated as $k_f = (Q_f \times \eta_f) / V$, where Q_f is the airflow through the filter, η_f is the filter efficiency, and V is the room volume [115]:

$$k_f = \frac{Q_f \eta_f}{V}, \text{ (1/h)} \tag{14}$$

For portable air cleaners equipped with high-efficiency particulate air (HEPA) filters, the clean air delivery rate CADR (m³/h) is typically specified, and the filtration removal rate k_f can be calculated using $k_f = CADR / V$, where V is the room volume. It is important

to note that both filter efficiency and *CADR* are particle size-dependent and should be estimated based on the size distribution of virus-laden particles. The following calculation examples are performed without the inclusion of air cleaners. Assuming the initial quanta concentration is zero at the start of occupancy, Equation (12) is solved to determine the average concentration C_{avg} as follows [115]:

$$C(t) = \frac{E}{\lambda V}\left(1 - e^{-\lambda t}\right), \text{ (quanta/m}^3) \tag{15}$$

$$C_{avg} = \frac{1}{D}\int_0^D C(t)\, dt = \frac{E}{\lambda V}\left[1 - \frac{1}{\lambda D}\left(1 - e^{-\lambda D}\right)\right], \text{ (quanta/m}^3) \tag{16}$$

where:

  t time (h).

Assuming steady-state conditions, Equations (15) and (16) simplify, with the terms in round and square brackets reducing to unity.

$$C_{avg} = \frac{E}{\lambda V}, \text{ (quanta/m}^3) \tag{17}$$

Example applications of these simplified equations can be found in studies analysing the Skagit Valley Chorale outbreak [146] and SARS-CoV-2 quanta emission rates [147]. Buonanno et al. [148] report that quanta emission rates range widely, from 3 to 270 quanta/h, depending on activity level – higher values are associated with loud speaking, shouting, singing, and elevated metabolic rates (see Table 1). While quanta emissions follow probability distributions, fixed values, specifically the 66th percentile, can be used for scenarios with constant parameters (ventilation, occupancy, activity, and emission), as suggested by Buonanno et al. [148]. In this study, more conservative 90th percentile values are applied due to high uncertainty in emission estimates. Using fixed quanta values is justified here because the analysis focuses on steady-state ventilation airflow rate sizing under constant occupancy and emission conditions. Quanta values in Table 1 can be compared with those for other infectious diseases, such as 1–10 quanta/h for common cold/rhinovirus [149], and 0.1–0.2 quanta/h on average, with a maximum of 630 quanta/h, for influenza [150]. These comparisons show that SARS-CoV-2 emission rates during rest and silent breathing are of a similar magnitude. Volumetric breathing rates, which also vary by activity, are presented in Table 2. [115].

Table 1. 90th percentile SARS-CoV-2 quanta emission rates for different activities. [148]

Activity	Quanta emission rate q, quanta/(h·pers)
Resting, oral breathing	3.1
Heavy activity, oral breathing	21
Light activity, speaking	42
Light activity, singing (or loudly speaking)	270

In this thesis, time-averaged quanta emission rates derived from the activities listed in Table 1 are used: 5 quanta/h for office work and classroom occupancy (assuming 5% of the time spent speaking), 15 quanta/h for restaurants (30% speaking), 21 quanta/h for sports activities, and 19 quanta/h for meeting rooms (40% speaking). Accordingly, the classroom scenarios are based on one infectious student, and cases involving an infectious teacher, with extended speaking durations, are not considered. [115]

Table 2. Volumetric breathing rates. [151,152]

Activity	Breathing rate Q_b, m³/h
Standing (office, classroom)	0.54
Talking (meeting room, restaurant)	1.10
Light exercise (shopping)	1.38
Heavy exercise (sports)	3.30

While Equations (9), (10), and (15) allow for the estimation of infection probability in a fully mixed room, they do not directly yield the ventilation rate required to achieve a specified probability. The ventilation rate must instead be determined iteratively – by selecting an initial value, calculating the resulting probability, and adjusting the rate until the desired probability is obtained. However, under steady-state conditions, it is possible to derive a direct equation for ventilation sizing. Using the Wells-Riley model, with its history and modifications [158], the infection probability p relates to the number of quanta inhaled n shown in Equation (9). By substituting Equation (11) into Equation (9), the expression can be reformulated as follows [115]:

$$p = 1 - e^{-C_{avg}Q_b(1-\eta_s)D}, \text{(-)} \tag{18}$$

Assuming steady state conditions and substituting C_{avg} from Equation (17) and E from Equation (13), while recognizing that the outdoor air ventilation rate is given by $Q = \lambda_v V$, the equation becomes [115]:

$$p = 1 - e^{-\frac{EQ_b(1-\eta_s)D}{\lambda V}} = 1 - e^{-\frac{(1-\eta_i)IqQ_b(1-\eta_s)D}{Q+(\lambda_{dep}+k+k_f+k_{UV})V}}, \text{(-)} \tag{19}$$

Rearranging Equation (19) to solve for the outdoor air ventilation rate Q, (m³/h) yields [115]:

$$Q = \frac{(1-\eta_i)IqQ_b(1-\eta_s)D}{\ln\left(\frac{1}{1-p}\right)} - \left(\lambda_{dep} + k + k_f + k_{UV}\right)V, \text{(m³/h)} \tag{20}$$

Therefore, in the absence of masks, air cleaners, and with one infectious individual present, Equation (20) simplifies as follows [115]:

$$Q = \frac{qQ_bD}{\ln\left(\frac{1}{1-p}\right)} - \left(\lambda_{dep} + k\right)V, \text{(m³/h)} \tag{21}$$

Equation (21) enables the calculation of the required outdoor ventilation rate per infectious individual for a specified probability of infection and quanta emission rate. It illustrates that lower acceptable infection probabilities necessitate higher ventilation rates, and that larger room volumes contribute positively. The ventilation requirement may become zero or negative if other removal mechanisms (represented on the right-hand side of the equation) are sufficient to eliminate the virus. Determining the target infection probability involves various considerations. A more robust method, as recommended in [153] and [154], is to use the event reproduction number R, defined as the number of secondary cases per infector. The number of decease cases can be expressed using reproduction number R and the number of infectious individuals I ($R = N_c / I$). Given that the number of new cases $N_c = p \cdot N_s$, the acceptable individual infection probability for a specific room can be calculated as Equation (22). In addition, vaccinated susceptible persons in the room can be taken into account [115]:

$$p = \frac{RI}{N_s} = \frac{RI}{(N-I)(1-f_v\eta_v)}, \ (\text{-}) \qquad (22)$$

where:

R event reproduction number, i.e. number of people who become infected per infectious occupant (-)

f_v fraction of the local population who are vaccinated, $f_v = 0$ for no vaccination (-)

η_v the efficacy of the vaccine against becoming infectious, $\eta_v = 1$ for ideal protection (-)

To ensure the basic reproduction number R_0 for airborne transmission of COVID-19 remains below 1, thereby preventing sustained transmission within the population, the event reproduction number R must be less than R_0, as susceptible individuals may be exposed to multiple transmission events [115,154]. It has been demonstrated that a single infector in any room creates the highest total removal rate required to maintain the target number of new disease cases per infector [155,156], making this scenario relevant for exposure design. The risk assessment model [155], which aims for secondary attack rates $R_0 \leq 1$, is applied according to Equation (23). This model calculates an acceptable room-specific R during a single occupancy period, assuming the infection rate (i.e., infections per unit time) remains constant over the pre-symptomatic infectious period. It incorporates exposure across out-of-home events by introducing an average interaction time [157] between the infector and susceptible occupants over the infectious period.

$$\frac{R}{R_0} \cong \frac{D}{D_{inf}} \quad \Longrightarrow \quad R \leq \frac{D}{D_{inf}} \quad when \ \ R_0 \leq 1 \qquad (23)$$

where:

D_{inf} total interaction time when an infectious individual is in the vicinity of any susceptible persons during the whole pre-symptomatic infectious period (h)

R_0 basic reproduction number describing the spread of an epidemic in the population (-)

The pre-symptomatic infectious period, typically lasting approximately 2.5 days, generally ends with the onset of symptoms, at which point the infectious individual self-isolates or is otherwise removed from contact with susceptible individuals. For instance, if an infectious person spends a total of 20 hours in proximity to others during this period (in public transport or at work/school), then to maintain $R_0 \leq 1$, the individual must not infect more than 1 person, corresponding to an average infection rate of $R = 1/20 = 0.05$ infections per hour. [155]

Equation (20) is reordered as ln $(1 / 1 - p)$ is moved to the left side, as shown in Equation (24) [155]:

$$\ln\left(\frac{1}{1-p}\right) = \frac{(1-\eta_i)IqQ_b(1-\eta_s)D}{Q+(\lambda_{dep}+k+k_f+k_{UV})V}, \ (\text{m}^3/\text{h}) \qquad (24)$$

Then both sides are raised to the power of e (as $e^{\ln(x)} = x$), as presented in Equation (25) [155]:

$$\frac{1}{1-p} = e^{\frac{(1-\eta_i)IqQ_b(1-\eta_s)D}{Q+(\lambda_{dep}+k+k_f+k_{UV})V}} \qquad (25)$$

Equation (25) can be simplified using the Taylor approximation of the exponential function $e^n \cong 1 + n$ at low doses. The Taylor approximation offers acceptable accuracy at low infection probabilities, with an error of approximately 2.4% at p = 0.05 and 4.7% at p = 0.1. Applying an additional approximation, $1 / (1 - p) \approx 1 + p$, valid when $|p| \ll 1$, Equation (25) is expressed as [155]:

$$1 + p = 1 + \frac{(1 - \eta_i)IqQ_b(1 - \eta_s)D}{Q + (\lambda_{dep} + k + k_f + k_{UV})V} \tag{26}$$

Equation (26) can be rearranged to solve for the ventilation rate Q, using $p = RI / N_s$ from Equation (22) as [155]:

$$Q = \frac{(1 - \eta_i)qQ_b(1 - \eta_s)DN_s}{R} - (\lambda_{dep} + k + k_f + k_{UV})V, \text{(m}^3\text{/h)} \tag{27}$$

This equation provides a straightforward method for calculating ventilation rates based on infection risk, using default values for quanta emission rate, breathing rate, and exposure duration. In scenarios where no face masks are used and ventilation is the sole removal mechanism, Equation (27) simplifies as follows [155]:

$$Q = \frac{qQ_bDN_s}{R} - (\lambda_{dep} + k)V, \text{(m}^3\text{/h)} \tag{28}$$

The quanta emission and breathing rates [155] can be substituted into Equation (28) to derive simplified space category specific target ventilation rate Equation (29) for typical occupied environments, where Q is expressed as litre per second (l/s).

$$Q = q_q(N - 1) - q_rV, \text{(l/s)} \tag{29}$$

where:

q_q quanta emission specific ventilation rate for occupancy per person [l/(s·person)]

q_r removal rate of virus decay and deposition [l/(s·m³)]

The first term in Equation (29), denoted as q_q, represents the quanta emission-specific ventilation rate, which depends solely on the viral load and acceptable risk level, and can therefore be recalculated for other respiratory viruses. The second term, q_r, accounts for removal mechanisms such as surface deposition and virus decay, both of which are virus-specific parameters. In scenarios involving portable air cleaners or ultraviolet disinfection, an additional removal term $(k_f + k_{UV}) \cdot V / 3.6$ must be included, as derived from Equation (27). The following default values are used to define the scenario for calculating q_q and q_r values presented in Table 3. Finally, target ventilation rate Q from Equation (29) can be used in the Equation (6) to calculate the ventilation rate supplied by the air distribution system [155]:

Table 3. Virus specific ventilation parameters q_q and q_r in Equation (29). [155]

Space category	q_q, l/(s·person)	q_r, l/(s·m³)
Classroom	10	0.24
Office	23	0.24
Assembly hall	30	0.24
Meeting room	40	0.24
Restaurant	40	0.24
Gym	70	0.24

2 Methods

The chapter describes the measurement methods of thermal comfort and ventilation effectiveness indices. Reference office buildings and conduction of measurements in open office landscape with data analysis are explained in terms of thermal comfort and draught. It explains, how field measurements were performed and analysed to find answer for the research question 1. Assessment of ventilation effectiveness includes the explanation of case-study rooms and the methodology of CO_2 tracer gas experiments. In turn, this provides methods for research questions 2 to 4 to support the description of tracer gas measurements for ultimately calculating target ventilation rate.

2.1 Thermal comfort and draught measurements

The research methodology is structured into three key stages: measurements, analysis and recommendations (Figure 5). Standard-based methods [72,158,159] were used to measure and calculate TC parameters and to perform an online indoor climate questionnaire ICQ survey. The mobile and flexible TC measuring probe set [160] used in this thesis was designed for research and development purposes. To provide recommendations for temperature control curves, yearly t_i and t_{sup} data of two representative office buildings (C and E) was analysed retrospectively.
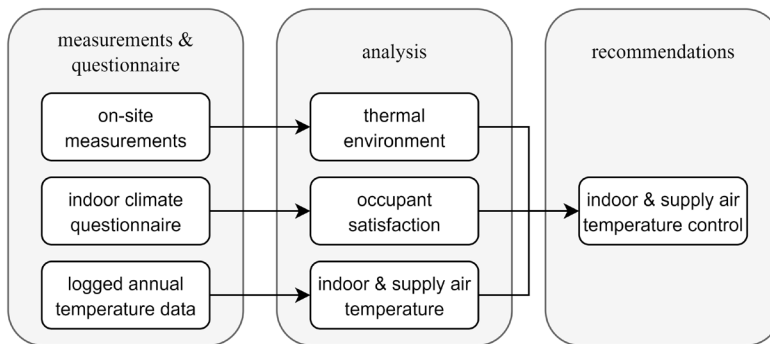

Figure 5. Flow chart of research methodology.

2.2 Office buildings selected for thermal comfort measurements

The five modern office buildings studied in Tallinn (labelled A to E), were selected for compliance with Estonian energy efficiency regulations established in 2007 [161], covering criteria such as air tightness, wall insulation, window glazing, and HVAC performance. All buildings were equipped with dedicated outdoor air balanced ventilation systems with heat recovery. Most used mixing ventilation, while Building B employed impinging jet ventilation. Heating and cooling systems varied: Buildings A and C used district heating, Building B featured low-temperature heating with a ground-source heat pump, Building D used a gas boiler, and Building E had electrical heating convectors. Cooling was provided by high-temperature cooling in most buildings, with active chilled beams, TABS, and ceiling panels for room conditioning. Fan coils were used in Building E. Buildings C and D had room conditioning units for both heating and cooling.

Table 4 provides general information on the reference buildings, detailing the measurement scope and building envelope characteristics, including thermal transmittance U values for walls, windows, ground floors, and roofs, along with specific heat loss of external envelopes and window-to-wall ratios WWR. Measurements were conducted on the highest floors of Buildings A, B, C, and D, and on the lowest floors of Buildings B and D. Slab temperatures were assumed close to t_i, so their effect on operative temperature was excluded, as heat transmission through building envelopes in these low-energy buildings is minimal compared to heat gains from glazed surfaces, thus having a limited effect on thermal comfort. Various HVAC systems (Table 5) were examined in the measurement zones, including some of the latest solutions in Estonia's construction market.

Temperature control in the buildings was based on seasonal setpoints for winter and summer, with manual adjustment required during the midseason. In the heating season, Buildings A, C, and D operated based on a heating curve tied to outdoor temperatures, with room control following a lower limit setpoint. Building B maintained a constant heating curve. During the cooling season, Buildings A, C, and D did not use activate heating if t_i fell below the heating setpoint, and cooling systems (except for free cooling) were disabled in the heating season. In contrast, Building B allowed both heating during cooling season and cooling during heating season via buffer tanks. In Building E, heating was manually controlled with electrical convectors, and multi-split fan coils were available for winter use. Ventilation t_{sup} in air handling unit was controlled by extract air temperature curves in all buildings except E, where manual adjustments were made. In Buildings A and C, the actual t_{sup} leaving from active chilled beams (induced with room air) to the room was not measured and analysed. Building managers reported multiple modifications to the initial setpoints based on occupant feedback. Building B's TABS was deactivated for heating during daytime when supplemental supply air heating was used. In Building C, preheating was often supported by 4-pipe active chilled beams, as turning off ventilation effectively turned off heating during non-working hours. HVAC design across all buildings stipulated that open windows would reduce system performance. No window openings were observed during measurements.

Table 4. General building information of reference objects.

Bldg	Year of Constr.	Net Floor Area (m²) / appr. Total Measured Area (%)	Number of Floors / Number of Measured Floors	Thermal Transmittance W/(m²·K)	Specific Heat Loss of External Envelopes W/(m²·K) / Window-to-Wall Ratio / Glazing g Value
A	2015	10800 / 30	13 / 4	U_{window} 0.80 / U_{wall} 0.18 / U_{roof} 0.09 / U_{floor} 0.14	*H/A 0.50 / WWR 0.69 / g 0.25*
B	2018	7000 / 20	5 / 3	U_{window} 0.83 / U_{wall} 0.12 / U_{roof} 0.09 / U_{floor} 0.13* (*above ambient air)	*H/A 0.31 / WWR 0.59 / g 0.24*
C	2017	18900 / 10	14 / 2	U_{window} 0.65 / U_{wall} 0.10 / U_{roof} 0.10 / U_{floor} 0.15	*H/A 0.30 / WWR 0.38 / g 0.30*
D	2018	13900 / 100 (available office space)	2 / 2	U_{window} 1.0 / U_{wall} 0.15 / U_{roof} 0.14 / U_{floor} < 0.15	*H/A < 0.20 / WWR < 0.25 / g 0.30*
E	Recons. 2014 (1982)	5300 / 20	6 / 1	U_{window} > 1.2 / U_{wall} > 0.25 / U_{roof} N/A / U_{floor} N/A	*H/A > 0.50 / WWR 0.90 / g 0.40*

Table 5. Room design solutions for heating, ventilation, and air conditioning in reference buildings.

Bldg	Heating	Ventilation	Cooling
A	Water-based convectors (height 300 mm, length 700–1800 mm) below the windowsill. Installed room unit heating power 18 W/m². Outdoor temperature compensated heating curve with room controllers. Switching seasons manually.	Mixing ventilation 1.4 l/(s×m²) using active exposed chilled beams (effective length 2700–3300 mm) mounted in the open ceiling (height 2.75 m) for supply and circular valves (Ø 125 mm) for extract air (height 2.7 m). Extract air temperature-based t_{sup} control. Switching seasons manually.	Active exposed chilled beams (effective length 2700–3300 mm) mounted in the open ceiling (height 2.75 m). Installed room unit sensible cooling power 52 W/m². Flow rate control with room controllers. Switching seasons manually.

B	Thermally active building system (slab, room height 3.0 m). Installed heating power 43 W/m². Constant flow temperature, flow rate control with zone controllers. Switching seasons manually.	Impinging jet ventilation 1.4 l/(s×m²) including duct diffusers (Ø 160–315 mm, nozzle angle 120–180 °C) for supply (height 2.7–2.8 m), mounted in the open ceiling to the perimeter of rooms. Wall and ceiling grilles with plenum box serving supply and extract air (height 2.8 m on cornice, 2.6 m for ribbed suspended ceiling). Extract air temperature-based tsup control with additional supply air heating option. Switching seasons manually.	Thermally active building system (slab, room height 3.0 m). Installed sensible cooling power 41 W/m². Flow rate control with zone controllers. Switching seasons manually.
C	4-pipe active ceiling integrated chilled beams (effective length 900–1500 mm) mounted in suspended ceiling (height 2.7 m). Installed room unit heating power 17 W/m². Outdoor temperature compensated heating curve with room controllers. Switching seasons manually.	Mixing ventilation 1.7 l/(s×m²) using 4-pipe ceiling integrated chilled beams (effective length 900–1500 mm) for supply air and circular valves (Ø 100 mm) for extract air (height 2.7 m). Extract air temperature-based tsup control with pre-heating mode. Switching seasons manually.	4-pipe active ceiling integrated chilled beams (effective length 900–1500 mm) mounted in suspended ceiling (height 2.7 m). Installed room unit sensible cooling power 46 W/m². Flow rate control with room controllers. Switching seasons manually.
D	4-pipe radiant panels mounted in the open ceiling on the height of 2.4 m. Installed room unit heating power 24 W/m². Outdoor temperature compensated heating curve with room controllers. Switching seasons manually.	Mixing ventilation 2.1 l/(s×m²). Rectangular nozzle diffusers including directionally adjustable nozzles (plates 160 × 160 / 200 × 200 mm) mounted on plenum box for supply air and circular plate (Ø 200–250 mm) combined with plenum box for extract air in the open ceiling (height 2.7 m). Extract air temperature-based tsup control. Switching seasons manually.	4-pipe radiant panels mounted in the open ceiling on the height of 2.4 m. Installed room unit sensible cooling power 10 W/m². Flow rate control with room controllers. Switching seasons manually.
E	Electrical convectors (height 200 mm, length 1500 mm) in front of windows. Installed room unit heating power 60 W/m². Manual local setpoint control.	Mixing ventilation 1.3 l/(s×m²) with circular supply and extract air diffusers (Ø 160–250 mm) mounted in the suspended ceiling (height 2.5–2.7 m). Manual setpoint control. (Supply air is not chilled)	Multi-split fan coil units (without heating function) mounted in the suspended ceiling (height 2.7 m). Installed total cooling power 78 W/m². Manual local setpoint control.

Room conditioning unit photos (Figure 6) in buildings were taken with permission from building managers. Measurements were conducted consecutively at workplace locations within the occupied zone, targeting areas with the highest expected air velocities based on air jet assessments and manager feedback. Table 6 provides details on these critical measurement points, including floor plan callouts, sectional views, and dimensions of the office modules where measurements took place.
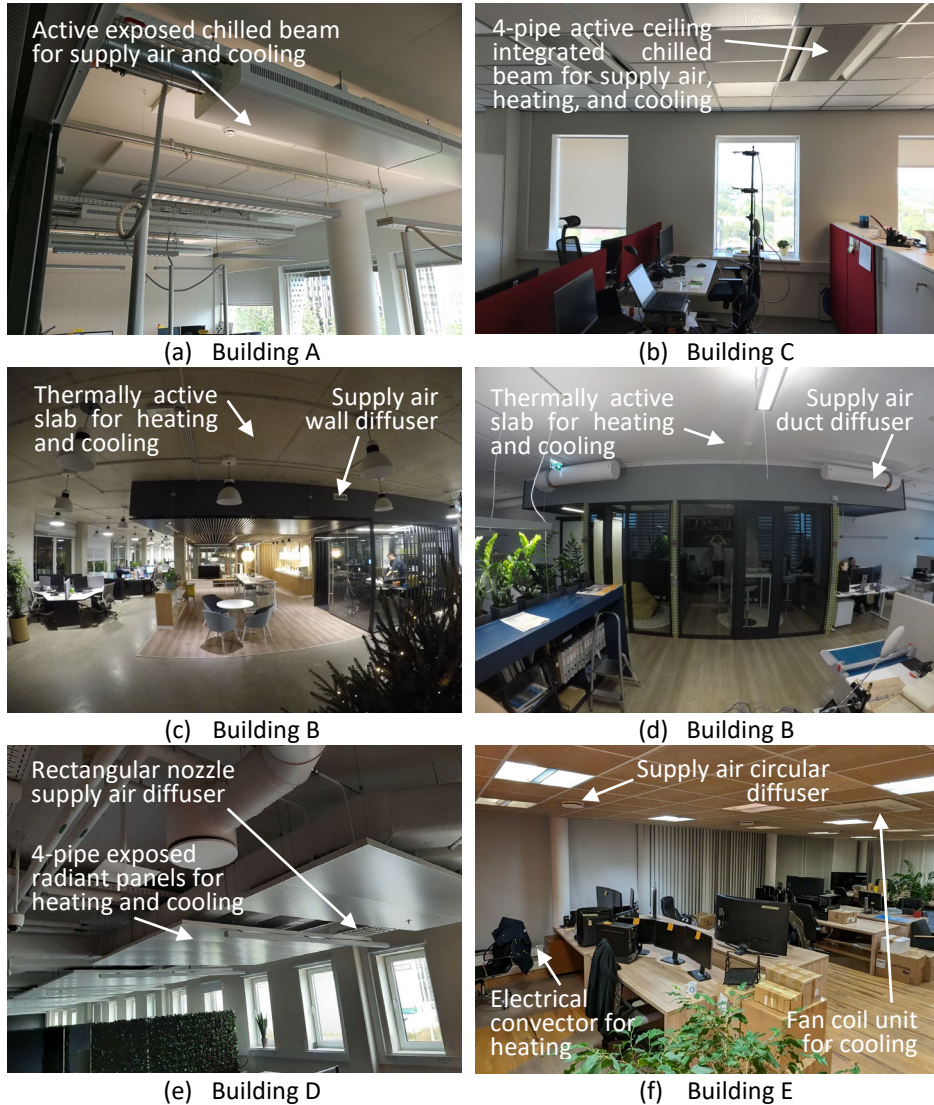
Figure 6. Room conditioning units: (a) Building A – active exposed chilled beam for supply air and cooling, (b) Building C – 4-pipe active ceiling integrated chilled beam for supply air, heating, and cooling, (c-d) Building B – thermally active slab for heating and cooling, supply air wall diffuser, and supply air duct diffuser, (e) Building D – 4-pipe exposed radiant panels for heating and cooling and rectangular nozzle supply air diffuser, and (f) Building E – supply air circular air diffusers, electrical convector for heating, and fan coil unit for cooling.

Table 6. Floor plan call outs and section views illustrating the critical locations of measurement points (yellow dots/cylinders). The blue arrows depict the potential air flow paths which may generate draught, the grey arrow represents the circulation air.
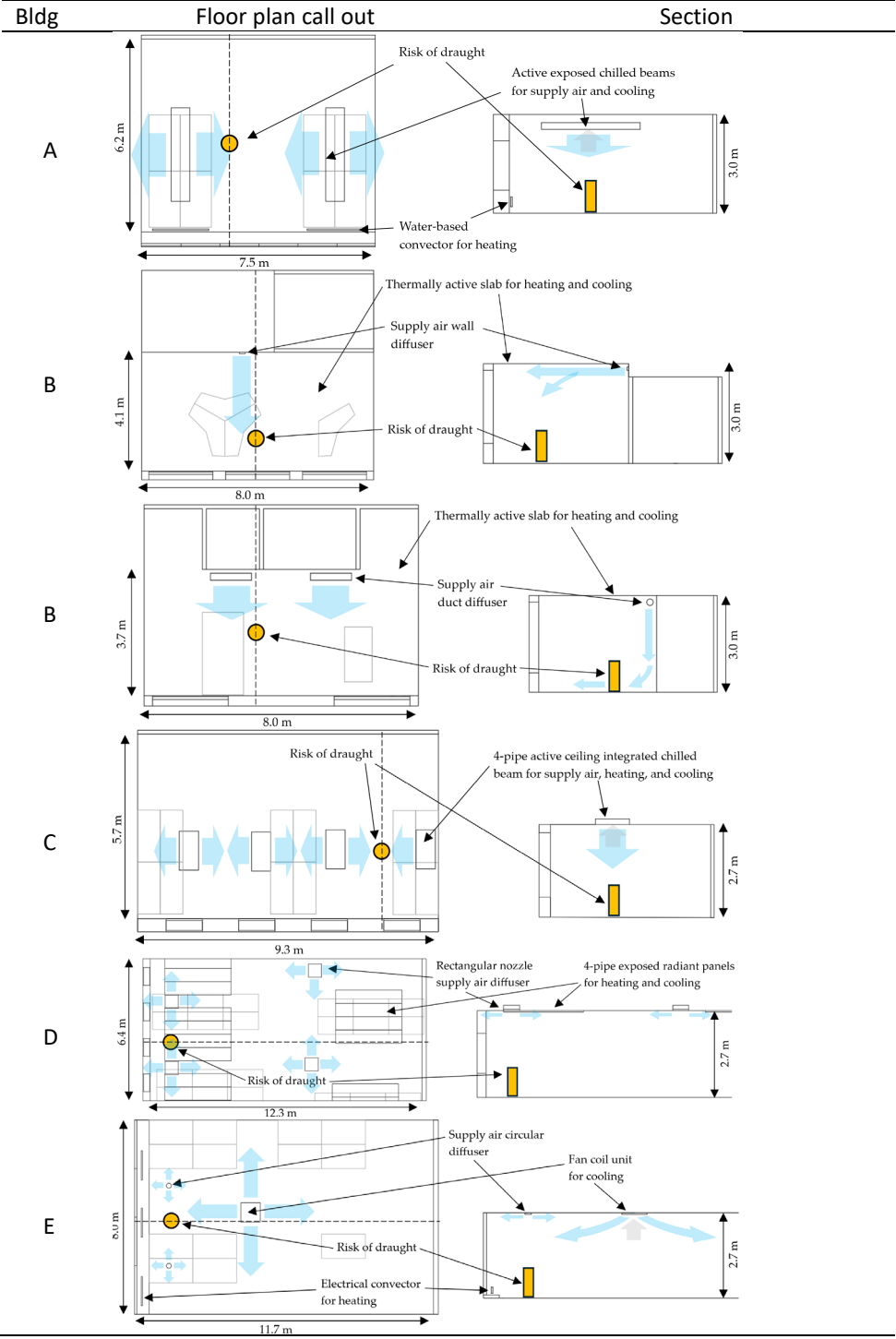
2.3 Thermal comfort measurements in open office landscape

This study's experimental measurements were conducted using the Dantec Dynamics ComfortSense system [162], designed for precise multi-point measurement of v_a, t_i, RH, and t_o (Table 7). Nearly 80 measurement points were analysed, with a tripod-mounted setup placed on a mobile frame (Figure 7). Following ISO 7726 [75], probes were set at heights of 0.1 m, 0.6 m, and 1.1 m from seated level to measure draught. As small temperature vertical differences were observed, results from 1.7 m and 2.0 m probes excluded from analysis. RH probe, not height-specific per standards, was placed at 0.6 m, aligning with the t_o probe at a 30° angle to represent the abdomen level of a seated person [75]. For thermal calculations, a metabolic rate of 1.2 met was assumed, with clothing insulation set to 0.5 clo for cooling and 1.0 clo for heating as per EN 16798-1 [72]. Turbulence intensity (Tu) and draught rate DR were calculated at 1.1 m, and predicted mean vote PMV with predicted percentage dissatisfied PPD at 0.6 m. Probes connected to the 54N90 ComfortSense main frame [160] used 7 out of 16 channels, with data stored in ComfortSense software [162] (version 4) on a laptop. For each measurement, occupants were temporarily replaced by a measurement tripod for a duration of three minutes, with a sampling rate of 20 Hz, in accordance with the EN 15726:2011 [163] methodology.
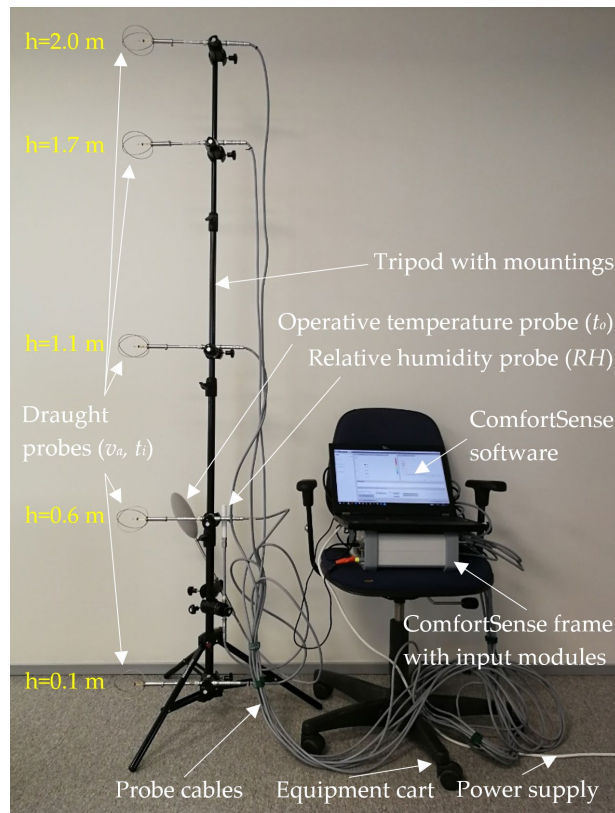

Figure 7. Measuring equipment setup including draught probes, an operative temperature probe and a relative humidity probe mounted on the tripod. Probes are connected through cables with the frame equipped with power supply. ComfortSense software provides the measured data for the analysis.

Table 7. Specifications of measuring equipment: draft and temperature, relative humidity, and operative temperature probes. [160]

	54T33 Draft Probe	54T37 Relative Humidity Probe	54T38 Operative Temperature Probe
Range	0.05…5 m/s −20…+80 °C	0…100 %	0…+45 °C
Accuracy	±0.02 m/s ±0.2 K	+1.5 %	±0.2 K

Measurements were conducted by the author with assistance from graduate students. Building HVAC systems were functioning normally, with internal gains from occupants, office equipment, and lighting in typical use. No significant HVAC design or construction issues were observed. Following ISO 7726 [75] guidelines, measurements aimed to reflect conditions related to occupant complaints. Rooms were occupied, but occupants vacated workspaces during measurement setup to prevent any influence on results. Measurements were conducted nearly simultaneously, using a single portable measurement stand moved between locations. Results were assessed according to the indoor climate categories ICC in EN 16798-1 [72]. Cooling season measurements took place on workdays in August (Table 8), while heating season measurements were performed under typical winter conditions (Table 9). Measurement days were chosen with building owners to ensure a notable temperature difference between indoor and outdoor environments.

Table 8. Time of cooling period measurements in workplaces and weather information from the Estonian Weather Service. [164]

Building	Time of Measurements	Weather Conditions	Maximum Outdoor Temp. °C	Mean Outdoor Temp. °C
A	06.08.2019 before midday	cloudy skies showers	+20.9	+15.2
B	14.08.2019 after midday	cloudy skies no precipitation	+19.7	+13.8
C	12.08.2019 after midday	cloudy skies light showers	+22.0	+17.3
D	29.08.2019 after midday	sunny skies no precipitation	+26.5	+20.6
E	05.08.2019 after midday	cloudy skies no precipitation	+19.7	+13.8

Table 9. Time of heating period measurements in workplaces and weather information from the Estonian Weather Service. [164]

Building	Time of Measurements	Weather Conditions	Maximum Outdoor Temp. °C	Mean Outdoor Temp. °C
A	21.02.2020 after midday	cloudy skies light showers	+2.7	+0.5
B	17.12.2018 after midday	cloudy skies light showers	−4.0	−2.1
C	17.02.2020 before midday	cloudy skies showers	+4.5	+6.2
D	18.02.2020 after midday	cloudy skies light showers	+6.0	+5.0
E	14.02.2020 after midday	partly cloudy skies no precipitation	−2.5	+0.1

To study occupant satisfaction, we conducted an online ICQ via Google Forms [165], in alignment with some organizations' paperless policies. The questionnaire, based on EN 15251 [158], included questions assessing TC sensation and added inquiries on age, gender, work environment (open office or private office), and the time spent at desks. Additional questions addressed draught sensation over the past month and throughout all seasons. In Building C, the ICQ could not be completed for heating season due to a COVID-19 outbreak. Measurements were conducted simultaneously with the ICQ, though responses were received within days. Measurement and questionnaire results were analysed as separate samples.

Due to instances of t_i exceeding expectations, concurrent assessment of t_i and t_{sup} was required. To analyse these variables, retrospective yearly data was collected from workspaces in Buildings C and E. In Building C, data from the room controller and duct temperature sensor served as a reference for t_{sup}, while in Building E, data from a HOBO Data Logger was utilized. Table 10 lists the logging equipment employed.

Table 10. Measuring equipment specification: temperature logger [166]*, room temperature controller* [167]*, duct temperature sensor.* [168]*.*

	HOBO Data Logger U12-013	HLS 44 Room Controller	Duct Temperature Sensor NTC5k
Range	−20…+70 °C	0…+50 °C	−30…+80 °C
Accuracy	±0.35 K	±0.5 K	±0.5 K

To improve the evaluation of annual t_i and t_{sup} data across heating, cooling, and midseason (+10 to +15 °C) conditions, the running mean outdoor temperature (Θ_{rm}) equation from EN 16798-1:2019 [72] was applied. Hourly t_i and t_{sup} analyses in Building C utilized 2020 data [164], while 15-minute interval data was available for Building E. The data was filtered to display results exclusively for occupied hours.

2.4 Classroom ventilation effectiveness maintaining air velocities

Methods of air change efficiency ε^a, contaminant removal effectiveness ε^c (CRE), including v_a measurements used in the experiments, are described below. The tests were conducted in a mock-up classroom within the air distribution laboratory at Tallinn University of Technology. Data visualization was performed using the SciPy and matplotlib libraries in Python. The experiments were conducted in an open-ceiling mock-up classroom with a room height of 3.8 m and a floor area of 5.2 × 8.7 m (45 m²). An air change rate of 240 l/s (5.3 l/s × m², 5 1/h) according to EVS 906 [169] (Estonian National Annex for EN 16798-3 [114]) was provided to accommodate 29 students and one teacher [169]. Ventilation layouts used in the experiments are illustrated in Figure 8, including grilles (GR) and ceiling diffusers (CD) as solutions used in renovation in Tallinn schools [170] and duct diffusers (D240↓) as a more modern solution for comparison. Extract air setups included both a single location (V1) and six points (V2) distributed evenly throughout the room.
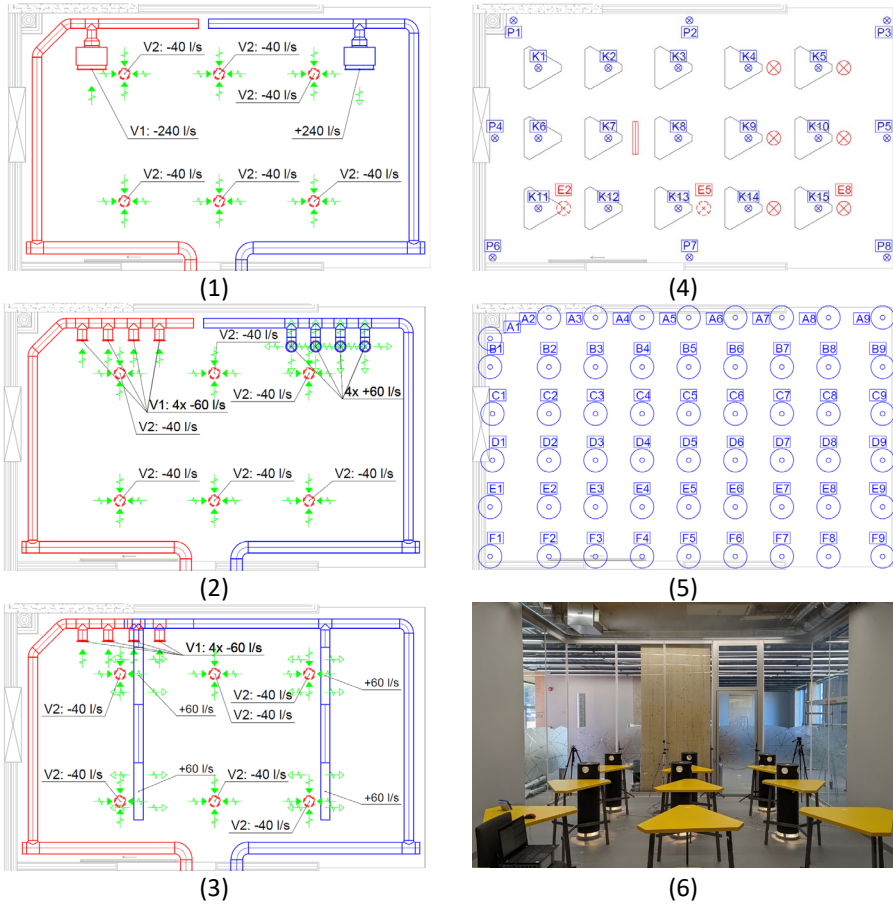
Figure 8. Ventilation layouts and measurement equipment used in the experiments: (1) grille (GR), (2) circular diffuser (CD), (3) duct diffuser (D240↓), (4) "K" and "P"-labelled data loggers for occupied zone and room perimeter with the location of thermal mannequins (E2, E5 and E8 as contaminant source), (5) draught probes' measurement points (A1 to F9) and (6) photo of the mock-up classroom. V1 and V2 in the (1) to (3) layouts represent single and six extraction options.

To assess ε^a and *CRE*, CO_2 was used as a tracer gas for the concentration decay method and the continuous dose method, respectively. Calibrated dataloggers were employed to measure CO_2 concentrations: 15 placed at table level (breathing plane, h = 1.1 m), 8 around the perimeter (h = 1.1 m), 1 in the supply air duct for fresh air reference concentration, 1 in the extraction duct for single-point extraction, and 6 for multiple extraction points (Figure 8). A scale was used to measure gas dosage. Air diffusers were balanced and measured for each layout using a differential pressure manometer. Additionally, to evaluate draught risk, each ventilation layout was measured at a height of 1.1 m using a set of 6 v_a probes positioned at 1 m intervals. The same draught probes were used as in previously described TC campaign (Table 7). Experiments were conducted with an indoor temperature t_i of +22.7 ±0.8 °C and a t_{sup} of +19.9 ±0.7 °C, maintaining a Δt between t_i and t_{sup} of ~4 K. Measurement equipment specifications are detailed in Table 11.

Table 11. Specifications of measuring equipment : CO_2 concentration logger [171]*, differential pressure sensor* [172]*, gas mass weighing scale.* [173]*.*

	Aranet4 Data Logger	Testo 440 dP	Kern FKB weight
Range	0…9999 ppm	−150…+150 hPa	0.002…65 kg
Accuracy	±30 ppm + ±3 %	<100 Pa ±0.05 Pa	±0.001 kg

The placement of 180 W thermal mannequins (red circle with a cross) and an additional 1 kW electrical convector (red rectangle) to imitate the rest of the heat gain of occupants not covered by the thermal mannequins is shown in Figure 8 (4). Before conducting the ε^a assessment experiments, the room was filled with tracer gas to achieve a fully mixed state. In contrast, during *CRE* experiments, gas was continuously injected as a contaminant throughout the test. A CO_2 tank connected to a dummy served as the contaminant source, positioned in three different locations (Figure 8).
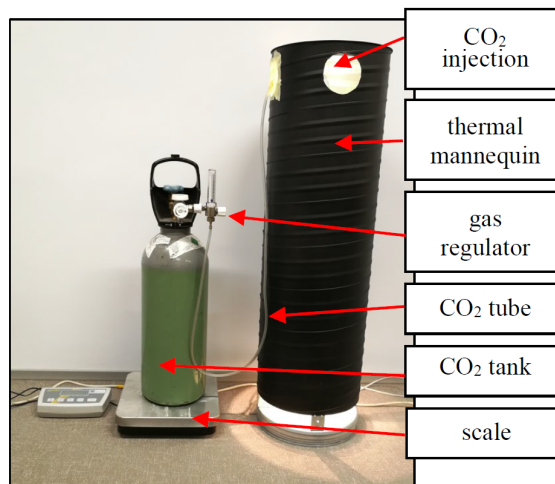

Figure 9. CO_2 tank connected with a thermal mannequin used as a contaminant source.

2.5 Case-study rooms of ventilation effectiveness measurements

In addition to the mock-up classroom laboratory described earlier, an extended campaign of ventilation effectiveness experiments was conducted in multiple typical shared indoor spaces. The rooms were selected in modern or renovated non-residential buildings equipped with mechanical supply and exhaust ventilation systems with heat recovery (without recirculation mode activated, if available) in Tallinn and Helsinki. Typical spaces in educational, office, and sports facilities, featured mainly ceiling-mounted mixing ventilation systems. To comprehensively assess mixing ventilation performance, both previously reported data and original measurements from this thesis were used. Laboratory mock-ups, including Classroom 1 [115,155,174] and Open Office 2 [174], were measured at Tallinn University of Technology. Classrooms 2 to 5 [175] consist of a large space divisible into three smaller classrooms. Measurements for the canteen, restaurant, bar, and nightclub were conducted on a cruise ship [176] docked in Helsinki. Additional measurements were taken in dressing rooms, fitness rooms, gyms, and meeting rooms. Details on air distribution, floor area (A), height (h), and design ventilation rates (Q_{act}) are provided in Table 12.

The experiments were conducted under controlled conditions simulating normal operation, without occupants, to minimize external influences. Thermal dummies were used to replicate internal heat gains from occupants, generating convective plumes similar to humans. However, they do not replicate close-proximity exhalation airflows and concentration fields, making them suitable only for long-range transmission experiments. CO_2 injection within the dummy, simulating an infector, was adjusted with a gas regulator and weighted using a scale. HVAC staff ensured that design airflow rates were maintained by setting the BMS system to 100% airflow and holding temperature setpoints for occupied hours. According to BMS sensors, room temperatures were approximately +22°C, with supply air temperatures between +18 to +20°C.

In laboratory tests, the effect of point source location was examined by repeating measurements with different point source placements, though this process is time-consuming. In field measurements, 2- or 3-point source locations were used, representing typical occupant positions, where one was placed as far as possible from the extract points, and another was positioned in the centre of the room.

Table 12. Description of the case study rooms.

Classroom 1
Wall diffuser[1]
45.0 m², h = 3.8 m
Q_{act} = 5.3 L/s·m²

Classroom 2
Ceiling swirl diff.
42.5 m², h = 2.9 m
Q_{act} = 3.8 L/s·m²

Classroom 3
Ceiling swirl diffusers
30.5 m², h = 2.9 m
Q_{act} = 6.2 L/s·m²

Classroom 4
Ceiling swirl diff.
56.5 m², h = 2.9 m
Q_{act} = 3.9 L/s·m²

Classroom 5
Ceiling swirl diffusers
129.5 m², h = 2.9 m
Q_{act} = 3.9 L/s·m²

Classroom 6
Ceiling diffusers
45.1 m², h = 2.9 m
Qact = 4.0 L/s·m²

Dressing room 1
Ceiling diffusers
145.0 m², h = 2.8 m
Q_{act} = 8.1 L/s·m²

Dressing room 2
Ceiling diffusers
318.0 m², h = 2.5 m
Q_{act} = 6.9 L/s·m²

Fitness 1
Conical ceiling diff.
173.5 m², h = 3.5 m
Q_{act} = 5.2 L/s·m²

Fitness 2
Wall diffusers
117.0 m², h = 4.6 m
Q_{act} = 6.4 L/s·m²

Fitness 3
Duct diffusers
153.0 m², h = 3.4 m
Q_{act} = 4.9 L/s·m²

Gym 1
Ceiling swirl diff.
217.5 m², h = 6.0 m
Q_{act} = 9.2 L/s·m²

Gym 2
Conical wall diffusers
331.0 m², h = 6.0 m
Q_{act} = 6.0 L/s·m²

Gym 3
Conical ceiling diff.
987.0 m², h = 8.0 m
Q_{act} = 4.1 L/s·m²

Canteen
Ceiling diffusers
242 m², h = 2.5 m
Q_{act} = 1.8 L/s·m²

Restaurant
Ceiling diffusers
135.0 m², h = 3.1 m
Qact = 4.2 L/s·m²

Bar
Ceiling diffusers
203.0 m², h = 3.1 m
Q_{act} = 3.7 L/s·m²

Nightclub
Ceiling diffusers
492.0 m², h = 4.5 m
Q_{act} = 3.8 L/s·m²

Meeting room 1
Active chilled beams
52.5 m², h = 3.2 m
Q_{act} = 3.8 L/s·m²

Meeting room 2
Ceiling swirl diff.
23.5 m², h = 2.7 m
Q_{act} = 6.4 L/s·m²

Open office 1
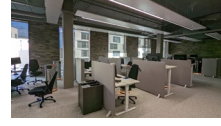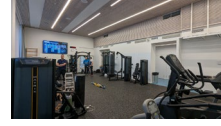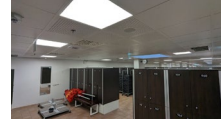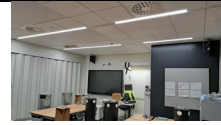Active chilled beams
45.0 m², h = 3.8 m
Q_{act} = 2.0 L/s·m²

Open office 2
Ceiling diffusers,
ceiling panels
242.0 m², h = 2.7 m
Q_{act} = 2.3 L/s·m²

[1] *ceiling diffusers, duct diffusers, single and multiple extracts in other cases*

2.6 Point source CO₂ tracer gas experiments

No strong correlation was observed between ε^a and *CRE* based on the mock-up classroom laboratory experiments. Local ventilation effectiveness for contaminant removal indicated that fully mixed conditions do not apply when a point source is present, despite air change efficiency calculated with an evenly distributed source suggesting fully mixed conditions. Consequently, the development of an infection risk-based ventilation method was explored using a continuously dosed tracer gas point source approach.

To evaluate the impact of incomplete mixing in ventilation design for airborne transmission, average concentration at a height of 1.1 m (representing seated breathing height) or, ultimately, local concentrations were used as shown in Figure 11. In general, two approaches were applied:

- Using the average concentration *C* in the breathing zone and calculating the event reproduction number *R* based on exposure scenarios and a risk assessment model.
- Applying a new method where local concentrations C_i are used to calculate the local air quality index and fractional event reproduction number R_i, leading to an iterative solution of the *R* equation. This approach accounts for spatial variations in infection risk with a new ventilation effectiveness parameter $\varepsilon_{b,loc}$.

To determine the target ventilation rate, input data from quanta emission and the risk assessment model was used [132]. This model aims to keep secondary attack rates below 1.0 during the "subclinical infectious period," thereby slowing epidemic spread. The necessary ventilation rate supplied by the air distribution system is calculated from local air quality index values, assessed through tracer gas measurements.

Ventilation effectiveness values, ε_b, were computed based on the average concentration *C* at 1.1 m height, as well as in the supply and extract air (Figure 10) and compared with iteratively calculated, $\varepsilon_{b,loc}$ values, which incorporate spatial infection risk variation. This comparison allowed recalculation of the fully mixed target ventilation rate to reflect the actual ventilation requirements of the distribution system, accounting for non-uniform concentration and infection risk. The developed methodology was tested using tracer gas measurements with a constant injection method across 22 rooms, utilizing 2–3 point source locations per room.
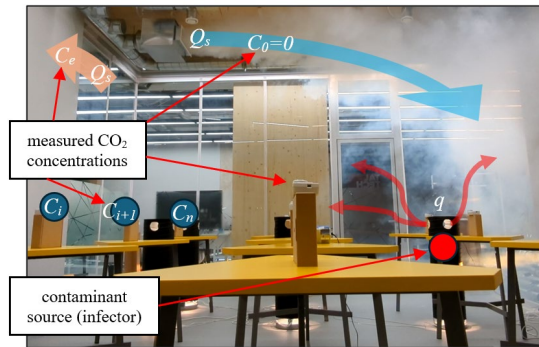
Figure 10. Measuring CO₂ concentrations at 1.1 m height of sitting person and in the supply and extract air.
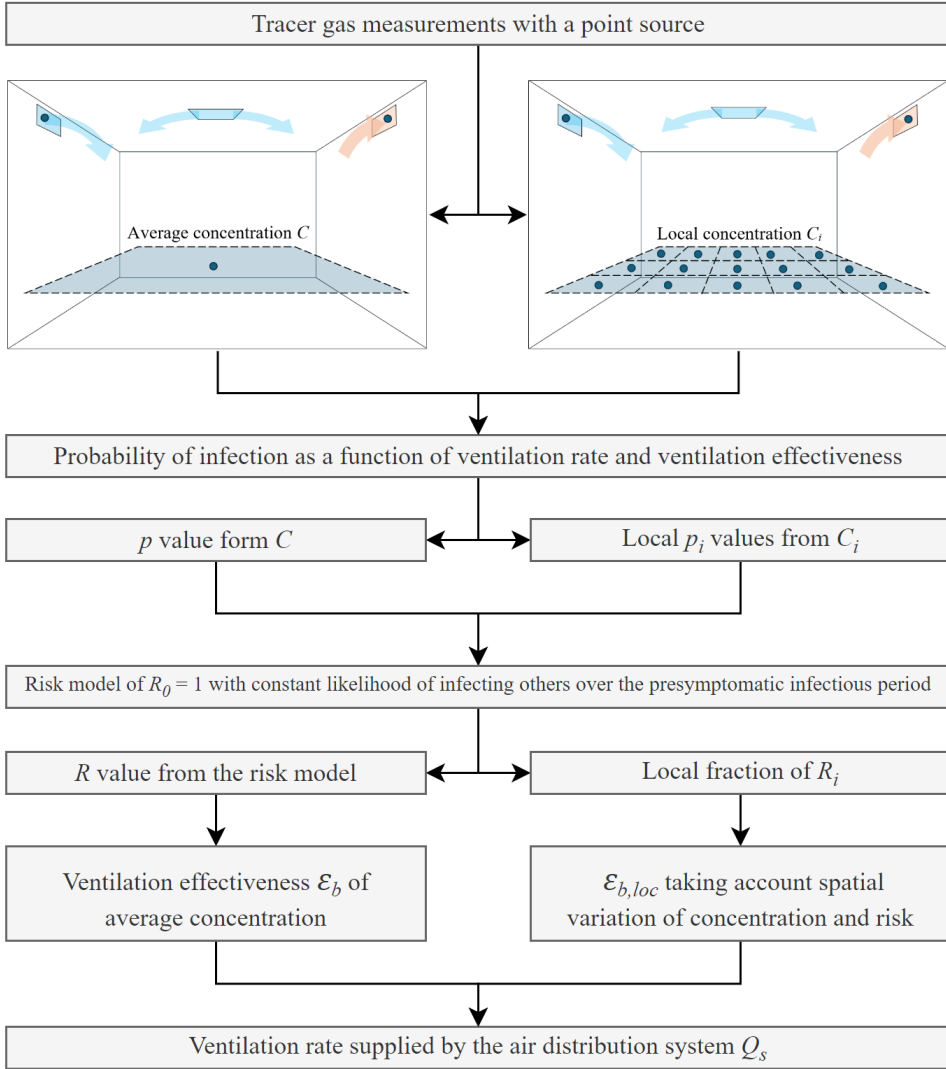
Figure 11. Flow chart of the research methodology in the development the new method as the right path in the figure, to take the spatial variation of the infection risk into account in the air distribution design.

The primary source of uncertainty in our measurements arises from the CO_2 sensor's accuracy, which includes errors of ±30 ppm ± 3% of the measured value, an additional 1% due to sensor non-linearity, and ±30 ppm from CO_2 level fluctuations under quasi-steady-state conditions. The total relative uncertainty for the calculated ventilation effectiveness indices ranges from 3% to 12% according to Equation (30), with higher relative errors occurring in tests with lower absolute CO_2 concentrations within the rooms measured. This issue is particularly notable in large rooms, where achieving practical CO_2 dosing levels during field measurements is challenging.

$$u_T = \frac{H^2}{i} \sqrt{\sum \left(\frac{u_j}{\left(\varepsilon_b^j\right)^2} \right)^2} \tag{30}$$

where

u_T total uncertainty of ventilation effectiveness (-)

H harmonic mean value of the point source ventilation effectiveness at all source locations (-)

i number of point source locations (-)

u_j uncertainty of point source ventilation effectiveness of measurement with source location j (-)

ε_b^j point source ventilation effectiveness of measurement with source location j (-)

In Figure 12, an example of the measurement setup layout for a larger teaching space, Classroom 5, is presented. The impact of different source locations is analysed and visualized in the results chapter. The number of measurements in each studied room is also presented within the results.
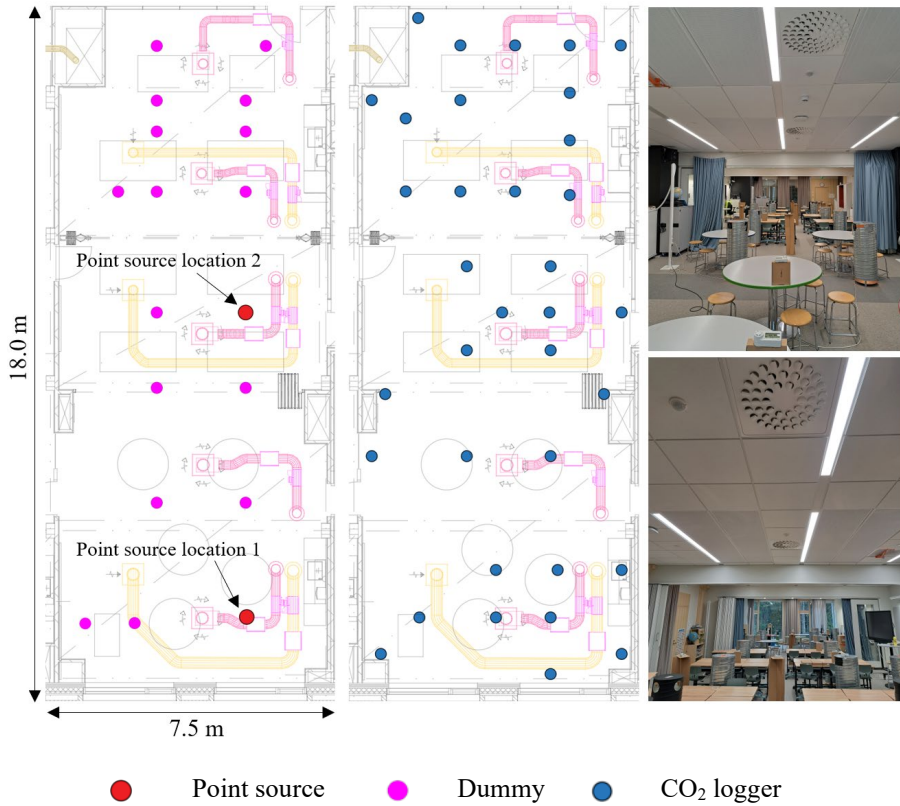
Figure 12. An example of the measurement setup in Classroom 5: locations of the point source, dummies and measurement points. Upper right photo from the façade and lower right photo to the façade direction.

Room- and virus-specific parameters needed to calculate the target ventilation rate Q under fully mixed conditions at a specified risk level are listed in Table 13. Room volume V, occupancy N_s, and the number of concentration measurement points K are presented in the same order as in Table 12. Previously described virus-specific risk parameters presented in the background chapter are provided [155]. These parameters allow calculation of required ventilation rates, though adjusting parameter values does not significantly alter relative differences between cases, as shown by exposure risk analyses [177]. Deposition and decay rates, λ_{dep} and k, remain constant across all rooms.

The quanta emission rates applied were: 4 quanta/(h·person) for classrooms, 6 quanta/(h·person) for fitness, gym, and office rooms, and 10 quanta/(h·person) for dressing rooms, restaurants, bars, and meeting rooms. Breathing rates used were 0.57 m³/h for classrooms, 0.6 m³/h for open offices, 0.65 m³/h for dressing rooms, bars, and restaurants, and 1.92 m³/h for fitness and gym. An occupancy duration of 2 hours was assumed, except for 6 hours in classrooms and 9 hours in meeting rooms and open offices. Interaction times for an infectious individual near susceptible persons were set to 16 hours and 22.5 hours in meeting rooms and open offices, respectively. The reproduction number R used was 0.089, except for 0.375 in classrooms and 0.4 in open offices. For virus control, occupancy reductions were applied as follows: 33% in dressing rooms, 50% in meeting rooms, and 80% in open offices. Room-specific R values, based on a pre-symptomatic infectious period of 2.5 days [155], are also provided in Table 13.

Table 13. Description of the infection risk-based target ventilation rate parameters in fully mixed conditions in the case study rooms.

Room	V (m³)	N_s (-)	K (-)	q (quanta/ h·pers)	Q_b (m³/h)	D (h)	D_{inf} (h)	λ_{dep} (1/h)	k (1/h)	R (-)
Classroom 1	171	29	15	4	0.57	6	16	0.24	0.63	0.375
Classroom 2	123	24	18	4	0.57	6	16	0.24	0.63	0.375
Classroom 3	88	12	15	4	0.57	6	16	0.24	0.63	0.375
Classroom 4	164	24	14	4	0.57	6	16	0.24	0.63	0.375
Classroom 5	376	49	29	4	0.57	6	16	0.24	0.63	0.375
Classroom 6	131	24	12	4	0.57	6	16	0.24	0.63	0.375
Dressing room 1	406	28	22	10	0.65	2	16	0.24	0.63	0.089
Dressing room 2	795	37	20	10	0.65	2	16	0.24	0.63	0.089
Fitness 1	607	32	20	6	1.92	2	16	0.24	0.63	0.089
Fitness 2	538	17	13	6	1.92	2	16	0.24	0.63	0.089
Fitness 3	520	19	13	6	1.92	2	16	0.24	0.63	0.089
Gym 1	1305	24	30	6	1.92	2	16	0.24	0.63	0.089
Gym 2	1986	24	35	6	1.92	2	16	0.24	0.63	0.089
Gym 3	7896	48	34	6	1.92	2	16	0.24	0.63	0.089
Canteen	605	20	16	10	0.65	2	16	0.24	0.63	0.089
Restaurant	419	27	14	10	0.65	2	16	0.24	0.63	0.089
Bar	629	37	16	10	0.65	2	16	0.24	0.63	0.089
Nightclub	2214	93	16	10	0.65	2	16	0.24	0.63	0.089
Meeting room 1	168	12	13	10	0.65	9	22.5	0.24	0.63	0.089
Meeting room 2	69	7	20	10	0.65	9	22.5	0.24	0.63	0.089
Open office 1	171	6	7	6	0.6	9	22.5	0.24	0.63	0.4
Open office 2	450	21	25	6	0.6	9	22.5	0.24	0.63	0.4

3 Results and discussion

This chapter presents the main findings and the discussion of the results of the t_i and v_a measurements supported by the ICQ reports. The thermal comfort topic is concluded with the t_i and t_{sup} control recommendation. This covers the research question 1 in this thesis, explaining how typical HVAC room unit settings perform in Estonian office buildings. Ventilation effectiveness indices results are explained with the infection risk-based target ventilation rate calculations, providing response and solutions for research questions 2 to 4. The results illustrate, whether the ventilation effectiveness can be maintained with v_a simultaneously. Secondly, the results of the case-study rooms compared to mixing ventilation criteria are provided. Finally, the calculation of the required ventilation rate supplied by the ventilation system in case of inadequate air exchange or viral situation is demonstrated.

3.1 Indoor air temperature and draught in open offices

Short-term v_a and t_i measurements were conducted during both heating and cooling seasons in areas with reported or anticipated thermal discomfort, as detailed in Table 6 of the methods section. These measurements, performed following standard procedures in carefully selected locations, aim to provide representative v_a results. The results across all buildings and measurement locations are summarized for each building. Figure 13 presents v_a and t_i values during the measurement period as box-and-whisker plots, with minimum and maximum values at the whiskers' ends, the first and third quartiles as the lower and upper box lines, the median as the central line, and the mean v_a and t_i value marked by a cross for each measurement location.

During the heating season, the on-site v_a measurements indicate better performance compared to the cooling season. Buildings B and E achieve v_a values within the II ICC for heating, while the other three buildings meet the I ICC. For cooling, only Building D remains in the I ICC, while Building C reaches the III ICC once in the heating season and three times in the cooling season, along with Buildings B, C, and E. Variability in v_a results is greater during the cooling season, except in Building D.
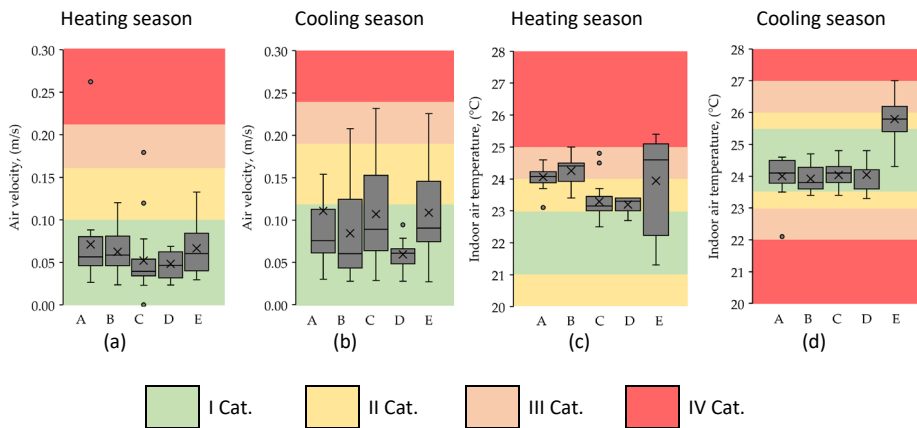
Figure 13. Air velocities recorded during the on-site measurements in the heating (a) and cooling season (b) and indoor air temperatures in the heating (c) and cooling season (b) in Building A to E.

The ICQ survey results for the cooling season's thermal environment are summarized in Table 14 and Figure 14 (a). Due to a sample size below the recommended minimum [178], the findings carry high uncertainty. Most respondents worked in open offices. Building E recorded the least favourable t_i, while Building D had the most satisfactory t_i. In general, discomfort was more frequently associated with warmer than cooler temperatures. For 83% of Building A respondents, t_i was suitable, though some found it warm or slightly cool. In Building B, 90% found t_i suitable. In Building C, 75% found t_i suitable, though 20% perceived it as too warm. Building D respondents, all in open offices, found t_i suitable. In Building E, only one-third found t_i suitable, with the rest reporting it as slightly warm or hot.

The heating season ICQ survey, Table 15 and Figure 14 (b), conducted in four buildings (excluding Building C due to COVID-19), suggested that complaints may be overrepresented due to the low response rate. In Buildings A and D, approximately one-third of respondents reported draught, a high frequency given the measured air velocities at 1.1 m were below 0.1 m/s. Counting only frequent complaints, draught would affect less than 20% of respondents across all buildings, aligning with measured results. Air velocities were slightly higher at 0.1 m, particularly in Building D, possibly due to cold draught from windows. Despite t_i at +23 to +24 °C, higher supply air temperature t_{sup} may have been used to offset draught complaints, potentially increasing t_i and heating costs, and lowering RH. Buildings B and E, both overheated, had minimal draught complaints. Most respondents were either satisfied with or preferred a higher temperature, which corresponds to the prevalence of neutral or slightly cool responses, generally below 20%. In Building A, with t_i at +24 °C, a preference for slightly cool temperatures was observed, with 26% wanting warmer and 22% preferring cooler conditions. Building B had the highest t_i with 89% neutral responses. In Buildings D and E, high preferences for increased temperature (43% and 39%, respectively) were noted despite t_i exceeding +23 °C. This suggests occupants have adapted to higher t_i levels and may prefer warmer conditions if draught is present. All measured t_i values exceeded the expected comfort temperature of +22 °C, suggesting clothing levels may be less than the standard 1.0 clo assumed for heating seasons. This phenomenon is further examined in long-term t_i and t_{sup} measurements in Section 3.2.

Table 14. Summary of the indoor climate questionnaire for cooling period.

Building	A	B	C	D	E
No. of respondents	36	29	20	8	22
Male/Female	19/17	18/11	6/14	3/5	14/8
Age	Majority 26-35 and 36-45	Majority 26-35 and 36-45	26-35 and older	Majority 26-35	Majority 26-35
Location	Mostly open office	Mostly open office	Open office	Open office	Mostly open office
Working hours	Mostly whole workday	52% half workday	2/3 whole workday	Mostly half workday	Mostly whole workday
Temperature	84% satisfied, but both cool and warm reported	90% satisfied	75% satisfied	Mostly satisfied	64% satisfied, but warm reported

Table 15. Summary of the indoor climate questionnaire for heating period.

Building	A	B	C[1]	D	E
No. of respondents	23	18	-	21	18
Male/Female	5/18	8/10	-	5/16	8/10
Age	Majority 26-35 and 36-45	Majority 26-35 and 36-45	-	Majority 26-35	Majority 26-35
Location	Mostly open office	Open office	-	Mostly open office	Mostly open office
Working hours	Mostly whole workday	2/3 whole workday	-	Mostly whole workday	2/3 whole workday
Temperature	78% satisfied, but both cool and warm reported	95% satisfied	-	76% satisfied, but preferences for lower and higher temperature	88% satisfied
Draught	30% dissatisfied, draught reported both in summer and winter	No draught complaints, while few noted more draught in the summer season	-	33% dissatisfied, no draught complaints from summer	No draught complaints

[1] *data unavailable due to COVID-19 outbreak*
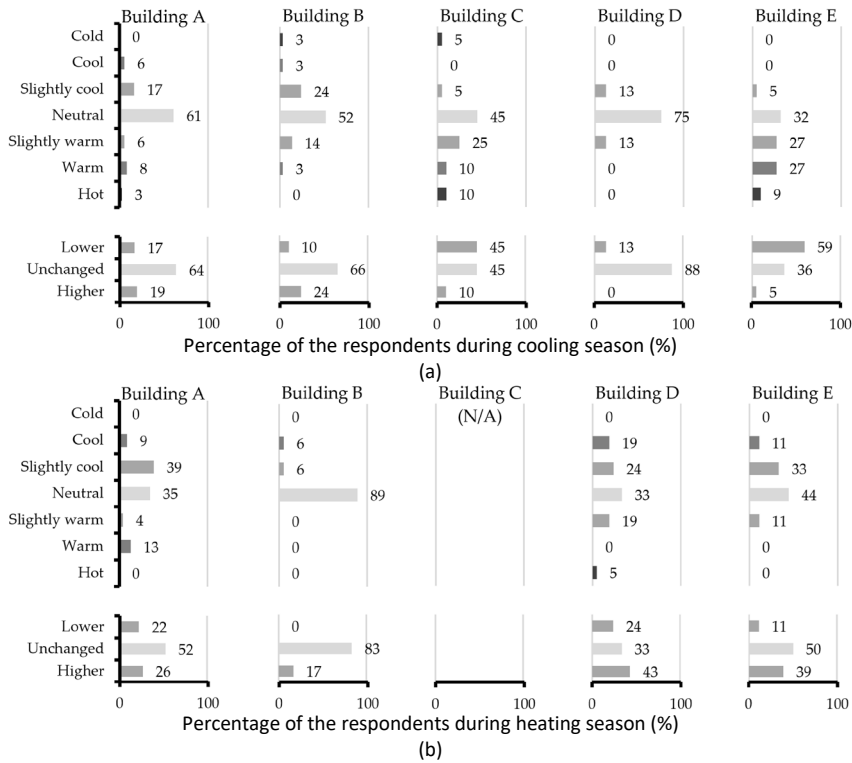
Figure 14. Indoor climate questionnaire results for indoor air temperature. The upper y-axis represents air temperature sensation question as lower stands for verification question. Cooling season – upper Figure (a), heating season – lower Figure (b).

The on-site measurements revealed a risk of draught during the cooling season across all buildings. Avoiding fan coil units does not inherently ensure a draught-free thermal environment. Although Building D, equipped with radiant panels for heating and cooling with nozzle diffusers for ventilation, exhibited the lowest draught risk. In Building E, the draught risk associated with fan coil units was mitigated by taped air distribution vanes (Figure 1 left) and strategic workstation placement to avoid direct airflow, possibly resulting in higher indoor temperatures. In Building A, airflows for open ceiling active chilled beams were adjusted manually to minimize draught, while in Building C, some suspended ceiling active chilled beams had paper covers over nozzles. These adjustments were responses to complaints or workspace layout changes, potentially leading to ineffective use of floor space. This suggests that design or construction inaccuracies or user-based thermal settings may not fully meet v_a and draught risk requirements. The v_a limits in EN 16798-1:2019 [72] assume +23°C and a Tu of 40%. Figure 15 (a) and (b) left show that Tu exceeded this default, contributing to local TC dissatisfaction, although higher t_i values measured in most locations tended to reduce occupant dissatisfaction. Figure 15 (a) and (b) right indicate a slight downward trend for values calculated using default assumptions compared to the calculated DR based on actual t_i and Tu results.

Compared to the cooling season, Building A, with open ceiling chilled beams for cooling and wall-mounted radiators, showed slightly better v_a and DR results during

the heating season. While it met I ICC in most areas in summer, heating season measurements indicated higher t_i values, placing it within II and III ICC. Building B, equipped with impinging jet ventilation and TABS, was notably overheated during heating, with an average t_i above +24°C. Building C, similar to Building A with active chilled beams, performed better in the heating season in terms of v_a and DR, with I ICC achieved in most cases and only occasional II and III ICC results. Building D, with radiant ceiling panels, maintained I ICC across both summer and cooling season measurements. Building E, with fan coil units, was identified as the least favourable setup for cooling season conditions. Although v_a was not problematic during the heating season, measured Tu exceeded the standard-recommended 40% [72].
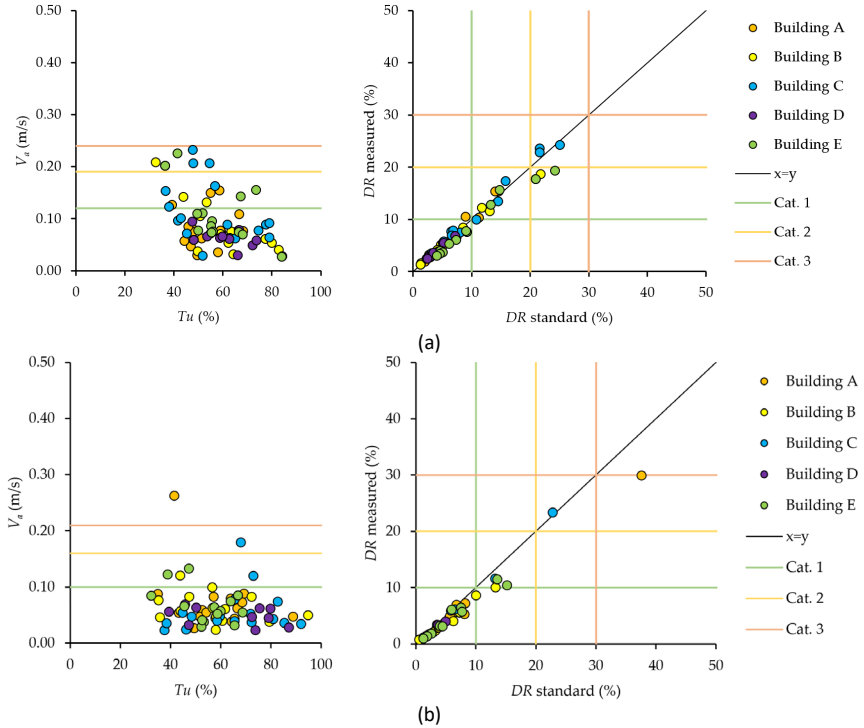
Figure 15. Air velocity and turbulence intensity (upper left – cooling season, lower left – heating season). Draught rate correlation in measured and standard-based [72] conditions according (upper right – cooling season, lower right – heating season).

While short-term measurements cannot capture temperature fluctuations, year-round data on t_i and ventilation t_{sup} were analysed for two representative buildings to contextualize on-site findings and questionnaire responses. This phased study approach, starting with immediate on-site evaluations and extending to long-term environmental monitoring, establishes a comprehensive framework for examining indoor climate control and occupant comfort in office settings. This approach underscores both the complexity of managing indoor environments and the importance of integrating immediate and extended data for effective building management.

3.2 Room air and supply air temperature control in open offices

To analyse the temperature difference between t_i and t_{sup}, general recommendations for dry cooling systems are available, including guidelines for condensation prevention in active and passive chilled beams [179]. CR 1752:1998 [180] provides guidelines on temperature differences between t_{sup} and air temperature in the breathing zone to ensure sufficient ventilation. Midseason conditions were defined using the Θ_{rm} formula B.2 from EN 16798-1 [72], with outdoor air temperatures between +10 °C and +15 °C. The ICC temperature boundaries for midseason were established by merging the lower limits of the heating season and the upper limits of the cooling season, as shown in Figure 16, Figure 17 and Figure 19. In Figure 16, t_i values for a typical floor are presented as cumulative frequency curves from occupied hours, while t_{sup} values are marked as grey dots. The horizontal axis represents relative time (0–100%) across all three seasons, with each season's width reflecting its duration. The heating season is defined considerably longer than both cooling and midseason.
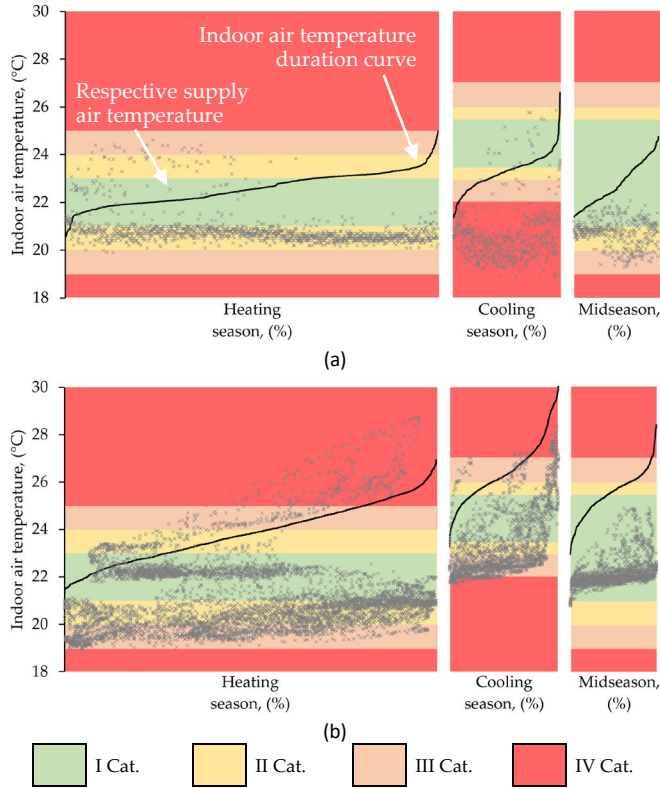
Figure 16. Yearly duration curves of indoor air temperature in Building C (a) and Building E (b) and respective supply air temperatures for heating, cooling and midseason compared to recommended [72] indoor climate category values.

Recommendations from the *Rehva Guidebook* No. 5 [179] were used to determine the suitable temperature range for maintaining comfort and controlling draught risk, as shown in Figure 17. In Building C, t_{sup} during the heating season generally ranged between +20 and +21 °C. Scattered t_{sup} points above the t_i duration curve in heating mode are due to the use of a 4-pipe active chilled beam system for heating. These

higher t_{sup} values often occurred at the start of the workday, especially on Monday mornings when heating setpoints had been lowered over the weekend. The gap between t_i and t_{sup} is more noticeable during the cooling season, with greater variability in t_{sup} values. During midseason, t_{sup} values are more dispersed than in winter but remain consistently below t_i. Thus, in Building C, higher t_{sup} values occur when additional heat is required from the ventilation system for space heating, although this is not the case during the cooling season. The few instances of high t_{sup} during cooling could be due to the cooling coil being inactive for some reason. In midseason, t_{sup} consistently stays lower than t_i.

In Building E, the t_i duration curves range from the lower limit of I ICC and exceed the upper limit of III ICC, indicating prolonged overheating periods throughout the year. Similar to Building C, t_{sup} remains well below t_i during midseason. Across all seasons, scattered t_{sup} values exceed the recommended limit of 3 °C below t_i, increasing draught risk. The winter discrepancy between two clusters of t_{sup} values is due to varying setpoints across calendar years. During the cooling season, t_{sup} values are also notably high. In midseason, where the temperature difference is most stable, t_{sup} remains consistently below t_i. As clarified earlier, Building E employed a systematic approach to workstation placement to avoid draught-prone areas near fan coil units. However, the analysis of t_i and t_{sup} reveals significant deficiencies in t_i control and indicates manual adjustments in t_{sup} settings.
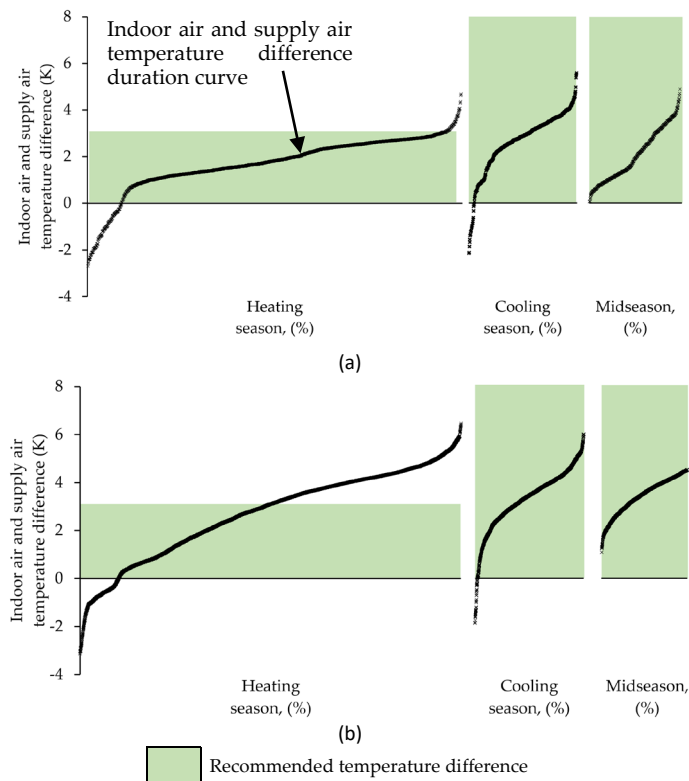

Figure 17. Yearly duration curve of the indoor air temperature and ventilation supply air difference for heating, cooling and midseason compared to recommended [179] *values in Building C (a) and Building E (b).*

To account for occupants' acceptance of t_i values between +23 to +25 °C, compared to the neutral temperature of +22 °C at 1.0 clo, a new classification criterion for t_i was calculated based on a proposed clothing value of 0.7 clo, in accordance with EN 16798-1:2019 [72], assuming v_a of 0.1 m/s. Note that the temperature scale difference between the heating and cooling season graphs for 0.7 clo is due to differing RH values of 40% in heating and 60% in cooling seasons.

With the 0.7 clo criterion applied for heating season, the majority of measurement points in Buildings A, B, C, and D fall within the II ICC, as shown in Figure 18 (a). In Building E, there is a broader temperature range, though only one position reaches the III ICC. For the cooling season provided in the Figure 18 (b), the 0.7 clo criterion yields worse results in all five buildings, indicating that 0.5 clo better aligns with occupant perceptions.

Figure 18 (and Figure 13) show no substantial differences in measured temperatures between heating and cooling seasons in Buildings A and B. In Building B, average t_i values were slightly higher in winter compared to summer measurements. In Buildings A to D, average t_i values were closer to cooling season averages than to recommended heating period setpoints. Two hypotheses may explain this: first, raising the t_{sup} setpoint might effectively prevent draught complaints; second, occupants may have adjusted their clothing to a lower clo value than the standard 1.0 clo. Figure 18 illustrates that by adjusting the clo value from 1.0 to 0.7, t_i values fall within the I ICC for 79% of the measurement period, compared to 18% initially. Thus, it is likely that temperature control in the studied buildings aligns with a clothing value of 0.7 clo in heating and 0.5 clo in cooling seasons, resulting in only a 1 °C difference between the temperature scales for these season.
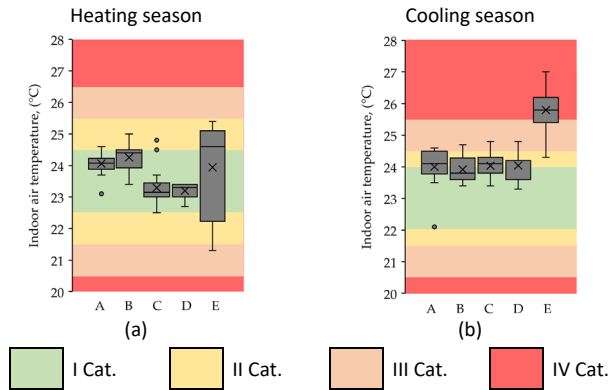
Figure 18. Indoor air temperatures recorded during on-site measurements in the heating (a) and the cooling (b) season on the 0.7 clo temperature scale in Buildings A to E.

One approach to improving t_i control is to apply comfort temperature ranges based on Θ_{rm}. However, this was not implemented in the building automation and control systems in any of the studied buildings. Using Θ_{rm} enables setting seasonal temperature ranges, which were not evident in the measured results, as shown in Figure 18. Based on Figure 19, optimal energy efficiency can be achieved by operating at the lower red line during the heating season and the upper blue line during the cooling season. The dashed red line indicates the heating threshold during the cooling season (heating should largely be avoidable with precise t_{sup} control), while the dashed blue line shows the cooling threshold during the heating season (which can be met with free cooling if available and if necessary).

The grey dotted line represents a *PMV* value of 0, which can serve as the t_i setpoint with a deadband, forming the basis for a control strategy using Θ_{rm}. In the midseason, the shaded area represents *PMV* = 0 with clothing adaptation, meaning that occupants are expected to adjust clothing within a range of 0.5–1.0 clo as needed. The lower (b) figure illustrates the conditions in the buildings, assuming a likely 0.7 clo clothing level during the heating season.
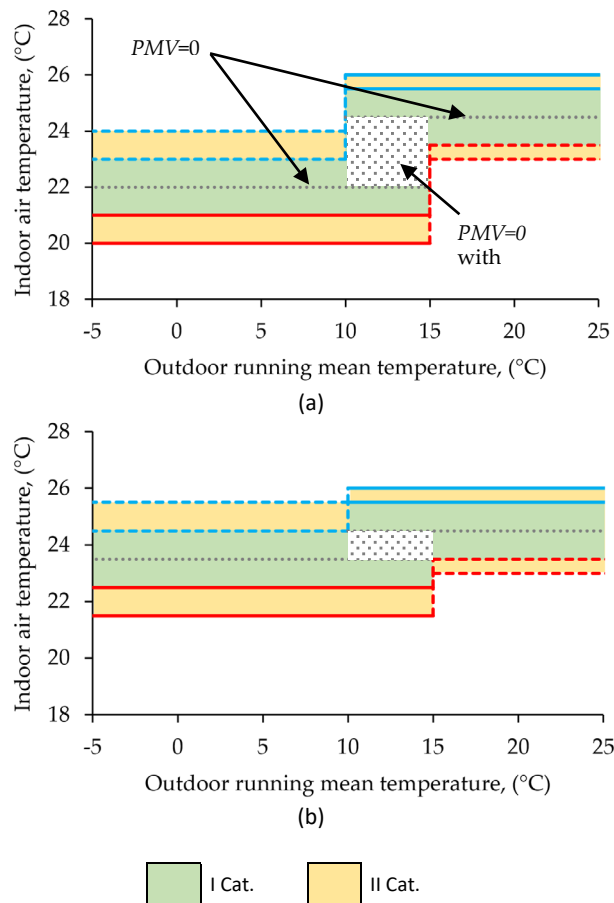
Figure 19. Room air temperature control recommendations for heating and cooling seasons, (a) based on the standard 1.0/0.5 clo and based on the estimated 0.7./0.5 clo in the measured buildings.

Since the temperature control shown in Figure 19 (a) was not implemented in any of the buildings, these values were converted into controller setpoints for practical application, as detailed in Table 16. The formula for Θ_{rm}, along with three setpoints and deadband values, should be programmed into the controllers. For example, in I ICC, at $\Theta_{rm} < 10$ °C, the controller setpoint is +22 ±1 °C. The ±1 °C indicates a deadband of 2 °C, resulting in a heating threshold of +21 °C. Values in Table 16 are rounded to the nearest 0.5 °C, with the cooling deadband slightly reduced due to the effect of relative humidity on *PMV*. Table 16 assumes ideal control accuracy, therefore, minor adjustments may be necessary in practice, depending on the system, to ensure that temperature remains within the green or yellow zones shown in Figure 19 (a).

Table 16. Controller setpoint and deadband values as a function of outdoor running mean temperature converted from Figure 19 (a).

Outdoor running mean temperature, °C	Controller setpoint, Category I	Controller setpoint, Category II
<10 (heating)	22 ±1	22 ±2
10–15 (midseason)	23.25 ±2.25	23 ±3
>15 (cooling)	24.5 ±1	24.5 ±1.5

Another observed challenge was controlling t_{sup}, which potentially contributed to elevated t_i. In Buildings A and C, where constant air volume systems with chilled beams are used, t_{sup} is seasonally adjusted, ranging from +18 to +20 °C during the cooling season and from +19 to +21 °C during the heating season [179]. In impinging jet ventilation (Building B), t_{sup} should be set 1 to 2 K lower than for mixing ventilation to avoid short circuits caused by buoyancy-driven upward airflow [89,181]. A minimum t_{sup} of +18 °C is recommended for impinging jet systems. Additionally, when impinging jet ventilation is combined with a high-temperature cooling system, the airflow may shift to a mixing system [182].

To achieve effective t_{sup} control for the supply air and room conditioning units studied, a recommended t_{sup} curve, based on design values from *Rehva Guidebook* No. 5 [179], was proposed, as supported by the measurement results in Building C shown in Figure 20. This curve aims to balance the prevention of overheating with the avoidance of draught discomfort. The proposed t_{sup} control method is effective when room conditioning units are designed to maintain low v_a values. However, in practice, t_{sup} adjustments in the studied buildings were made manually and inconsistently according to the season [5], often increasing gradually during both heating and cooling seasons to mitigate draught complaints.

Figure 20. Recommendation for a control curve of ventilation supply air setpoint depending on the ventilation extract air temperature.

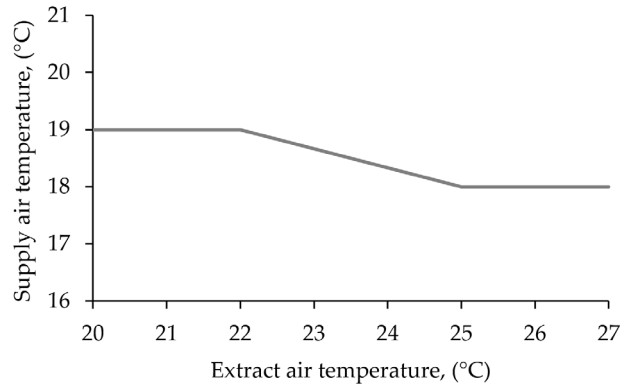## 3.3 Classroom air change efficiency and contaminant removal effectiveness

This section presents and discusses the primary results from the mock-up classroom experiments. Not all analysed ventilation layouts are included in the results. For instance, duct diffusers set at horizontal 2 x 60°, upward 120°↑, and upward 240°↑ configurations performed less effectively in terms of ε_b values compared to the downward 240°↓ setting. The 120°↓ downward duct diffuser configuration showed air velocities up to 0.45 m/s in the occupied zone. It was observed that increasing t_{sup} to match t_i did not significantly affect the performance of these ventilation setups. Table 17 provides the calculated values of ε^a, with minimum and maximum ε_P^a, calculated ε^c using Equation (3), with ε_b using Equation (7) and (8) (derived from ε_P^c values), and measured v_a, excluding perimeter values. The ε_P^a results as color maps are shown in Figure 21, ε_P values in Figure 22, and measured v_a values in Figure 23. In Table 17, the values of ε^c and ε_b^j differ because ε_b^j is calculated based on the average concentration of the 50% of measurement points with the highest contaminant levels. However, the results in Table 18 (Classroom 1) including Figure 32 to Figure 34 are derived from across all measurement points.

Table 17. Results of calculated air change efficiency (ε^a) and local air change index (ε_P^a), calculated ventilation effectiveness of contaminant removal (ε^c) and point source ventilation effectiveness of measurements with positions of 1-3 (ε_b^j) with point source ventilation effectiveness (ε_b), and measured air velocity (v_a) for grille (GR), circular diffuser (CD), and downward 240° duct diffuser (D240°↓) supply comparing single (V1) and six (V2) extraction layouts in the occupied zone on the breathing plane.

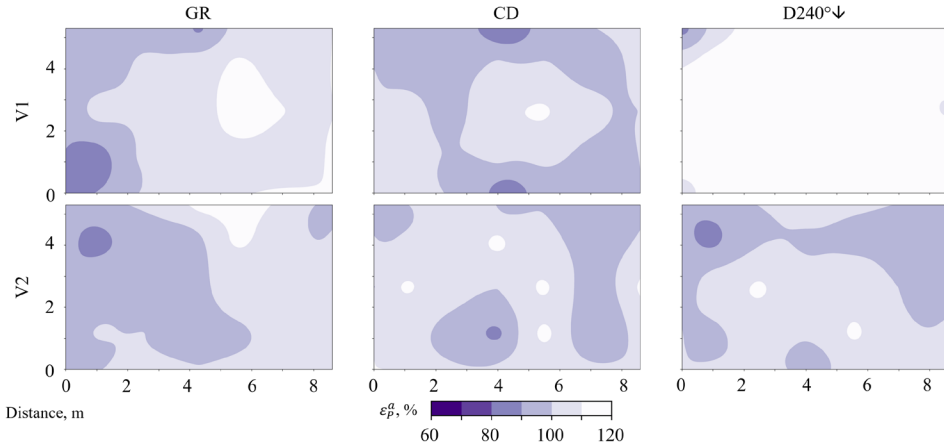| Experiment		Air change efficiency, local air change index			Contaminant removal effectiveness, point source ventilation effectiveness for the breathing zone						Av. point source vent. effectiveness	Air velocity	
					Pos. 1 (E2)		Pos. 2 (E5)		Pos. 3 (E8)				
		ε^a %	$\varepsilon_{P,min}^a$ %	$\varepsilon_{P,max}^a$ %	ε^c -	ε_b^1 -	ε^c -	ε_b^2 -	ε^c -	ε_b^3 -	ε_b -	v_a m/s	$v_{a,max}$ m/s
GR	V1	51	92	107	1.06	0.88	1.07	0.85	1.06	0.98	0.90	0.09	0.40
	V2	50	94	106	0.90	0.65	0.98	0.82	1.09	1.03	0.83		
CD	V1	50	97	106	1.73	1.51	1.62	1.39	1.20	1.12	1.34	0.10	0.31
	V2	51	94	107	1.34	1.17	1.23	1.01	1.05	0.97	1.05		
D240°↓	V1	56	107	124	1.09	1.02	0.97	0.87	0.87	0.82	0.91	0.11	0.21
	V2	50	94	106	1.09	1.03	1.00	1.00	0.99	0.98	1.00		

Figure 21. Results of calculated local air change index representing mock-up classroom breathing plane colour-maps from CO$_2$ concentration decay method measurements. Grille (GR), circular diffuser (CD), and duct diffuser (D240°↓) compared with single (V1) and six (V2) extraction (for measurement grid and equipment, see Figure 8).

In all cases, the ε^a results align closely with the theoretical mixing ventilation benchmark of 50%. The lowest calculated $\varepsilon^a_{P,min}$ values reached 92% based on measurements, with the duct diffuser option featuring a single extraction showing improved air change efficiency and local air change index. Generally, as seen in Figure 21, ε^a_P remains relatively uniform across various layout settings, except for the duct diffuser with single extraction. According to Equation (5) and the average ε^a results indicating a mixing ventilation state (ε^a = 50%), increasing the air change rate would be unnecessary.

Comparing ε^c results, greater contaminant removal effectiveness was observed across all cases when the contaminant source was positioned centrally at P2 (E5). The results in the middle column of Figure 22 show some symmetry, with grille setups featuring six extractions in P3 (E8), all circular diffusers, and both P1 (E2) duct diffuser setups displaying less contaminant spread. For the duct diffuser layouts, CO$_2$ concentrations were more dispersed around the source at the central P2 (E5) position. The distribution becomes more diffused in the grille option, except for P3 (E8) with six extractions. The most critical areas were observed with duct diffuser settings when the contaminant source was positioned in P3 (E8). For the grille with six extractions (V2) and duct diffuser with single extraction (D240°↓), ε^c values of 0.90 at P1 (E2) and 0.87 at P3 (E8), respectively, were recorded. However, ε_b results for positions 1 to 3 showed more variation, with the central P2 (E5) position offering no distinct advantage. The lowest ε_b value at position P1 (E2) was 0.65 for the grille with six extractions, 0.82 at P2 (E5) for the same grille layout (0.85 for one extraction), and 0.82 at P3 (E8) for the duct diffuser with single extraction. Notably, the circular diffuser with a single extract achieved an ε_b of 1.51 at position P1 (E2), 1.39 at P2 (E5), and 1.12 at P3 (E8). For general ventilation efficiency in the mock-up classroom (ε^c = 1 for mixing ventilation), a ventilation rate increase of 11% is recommended for the grille with six extractions (ε^c = 0.90) at position 1 (E2). At position 2 (E5), lower ε^c values could be rounded to 1.0. For the duct diffuser with single extract (ε^c = 0.87), a rate increase of 11% is also suggested. However, for duct diffusers, the ventilation rate could be reduced theoretically.
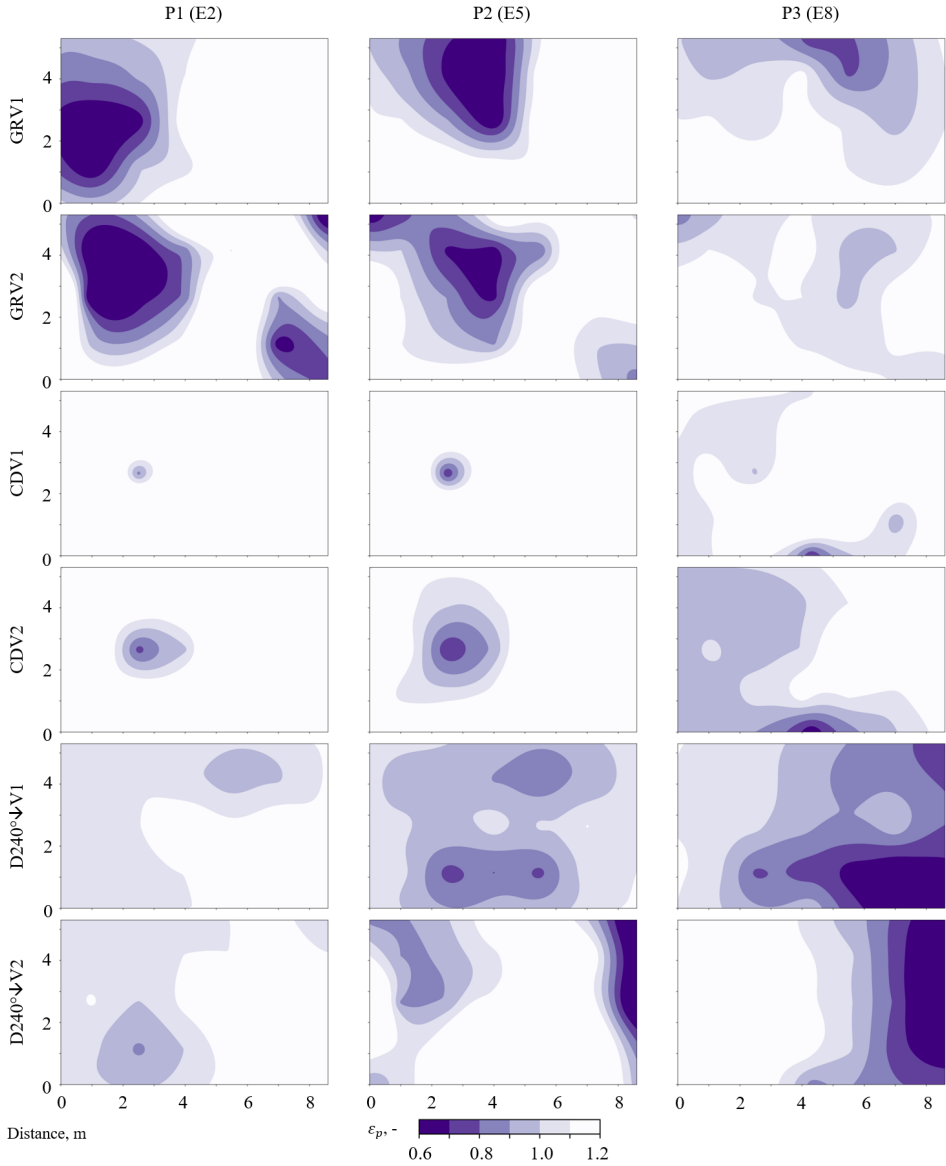
Figure 22. Measured local air quality index from which point source ventilation effectiveness can be calculated, representing mock-up classroom breathing plane colour-maps from continuous injection method. Grille (GR), circular diffuser (CD), and duct diffuser (D240°⬇) compared with single (V1) and six (V2) extraction for each contaminant source position P1-P3 (for measurement grid and equipment, see Figure 8).

Based on ε_b, adjustments to ventilation rates of up to 14% (ε_b = 0.88 in P1 for grille with single extract) and up to 54% (ε_b = 0.65 in P1 for six extractions) may be needed. A more moderate approach could use an average of three contaminant source positions, resulting in required increases of 11% and 20% for the grille. For duct diffusers, this approach would suggest a 22% increase for single extraction (ε_b = 0.82 in P3) and a 2% increase for six extractions (ε_b = 0.98 in P3). Using the average ε_b values

from multiple positions rather than the lowest single measurement would likely prevent excessive over-dimensioning of the ventilation rate, offering a conservative yet practical approach.

The Category I, II, and III thresholds for v_a are 0.10, 0.16, and 0.21 m/s in winter and 0.12, 0.19, and 0.24 m/s in summer, respectively [72]. Measured air velocities at breathing height within the occupied zone reached maximum values of 0.40 m/s for the grille, 0.31 m/s for the circular diffuser, and 0.21 m/s for the duct diffuser, with average v_a values recorded at 0.09 m/s, 0.10 m/s, and 0.11 m/s, respectively. Figure 8 shows that the grille and circular diffuser plots indicate the highest draught risk at the border of the occupied zone and along the room perimeter. Within the occupied zone, the duct diffuser reaches 0.21 m/s in one area, corresponding to Category III, while the rest of the zone generally satisfies Category II standards.
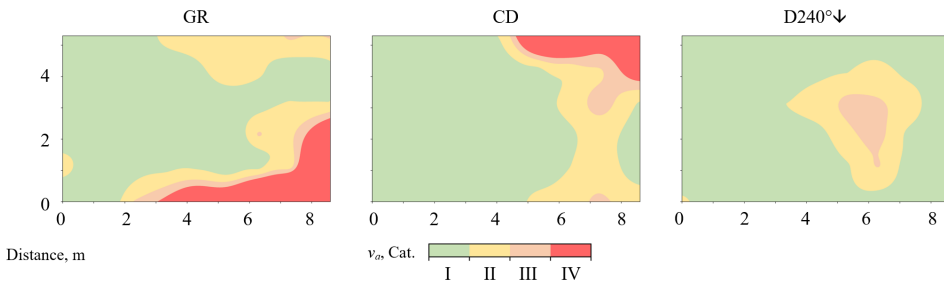
Figure 23. Results of measured air velocity representing a mock-up classroom breathing plane colour-maps. Green stands for I Category (<0.10 m/s), yellow for II Category (0.10-0.16 m/s), light red for III Category (0.16-0.21 m/s), and dark red for IV Category (>0.21 m/s) during summer [72]. Grille (GR), circular diffuser (CD), and duct diffuser (D240°↓) are compared (for measurement grid and equipment, see Figure 8).

Further measurements are essential, particularly as the $\varepsilon_b > 1$ observed for circular diffusers was unexpected. Similarly, increasing extraction points from 1 to 6 sometimes reduced performance (for grille and circular diffusers) but improved it in the case of duct diffusers. These results are encouraging, demonstrating that ε_b values equal to or exceeding 1 are achievable. This could reduce the need for increased ventilation rates, which often lead to higher draught risk, as well as increased spatial requirements and energy costs. In conclusion, additional research on ventilation effectiveness is critical, especially for infection risk-based ventilation design.

3.4 Calculation of infection risk-based target ventilation rate

The Wells-Riley model is applicable for long-range aerosol transmission under fully mixed conditions. However, in scenarios of incomplete mixing with a single infector (point source), the concentration C may vary throughout the room. This concentration can be measured with tracer gas at specific points of interest at breathing height, denoted as C_i to C_n (Figure 24).
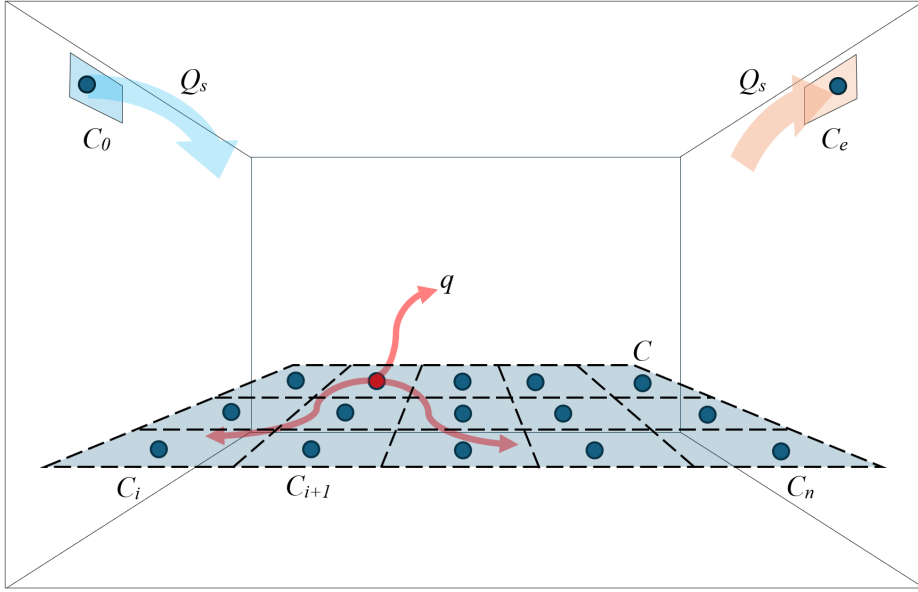
Figure 24. Concentrations in the room and extract air in the case of incomplete mixing. Red arrows show one possible location of an infector that can be located at any point; therefore the measurements are to be repeated with multiple infector locations.

An explicit Equation (31) for ventilation rate under steady-state conditions, at a specified infection risk probability and fully mixed air distribution, has been derived [115]. This approach can also be adapted for conditions of incomplete mixing. The quanta concentration *C,* at steady state, can be determined from the pollutant mass balance as follows:

$$Iq = C_e \lambda_v V + C \lambda_{rest} V \tag{31}$$

where:

   C_e quanta concentration in the extract air (quanta/m^3)
   C average quanta concentration in the breathing zone (quanta/m^3)
   V volume of the room (m^3)
   λ_v outdoor air change rate, i.e., removal rate due to ventilation (1/h)
   λ_{rest} removal mechanisms other than ventilation (1/h)

Similarly to the Equation (3), the ratio of concentrations C_e and C is expressed through ventilation effectiveness as in Equation (32), as defined in EN 16798-3:2017 [114] (contaminant removal effectiveness in *Rehva Guidebook* No. 2 [89]):

$$\varepsilon_b = \frac{C_e - C_0}{C - C_0} \tag{32}$$

where:
   C_0 quanta concentration in the supply air (quanta/m^3)

By substituting ε_b into Equation (31) and noting that the ventilation rate supplied by the air distribution system is $Q_s = \lambda_v V$, one obtains Equation (33):

$$C = \frac{Iq}{\varepsilon_b Q_s + \lambda_{rest} V} \tag{33}$$

where:

Q_s ventilation rate supplied by the ventilation air distribution system (m³/h)

The probability of infection can be calculated using Equation (34), based on Equation (19), by substituting C from Equation (33) into Equation (9):

$$p = 1 - e^{-\frac{Iq Q_b D}{\varepsilon_b Q_s + \lambda_{rest} V}} \tag{34}$$

Given that N_s susceptible individuals are exposed to C, the reproduction number R (new cases per infectious person) can be calculated as Equation (35):

$$R = \frac{p N_s}{I} \tag{35}$$

For a specified R value, the breathing zone ventilation rate Q can be derived from Equation (34), because Equation (36):

$$Q = \varepsilon_b Q_s \tag{36}$$

where:

Q target ventilation airflow rate for the breathing zone (m³/h)

The Q matches the rate under fully mixed conditions ($C = C_e$ and ε_b = 1). To determine the relevant R value, the exposure scenario (on or more infectors) and risk assessment concept, must be defined. Equations (34) to (36) align with the Equation (9) provided earlier [115]. The ventilation rate Q_s supplied by the air distribution system can be calculated if ε_b is known or measured. Since ε_b and Q_s results apply to specific point source locations, multiple tests with different point source placements are required to obtain representative values.

3.5 New method – calculation of infection risk from local concentration values

To assess the impact of using average concentration values rather than local concentrations, considering spatial variation of concentration C, infection probability can be calculated for each measured location i. In this case, the quanta concentration C_i at location i under steady-state conditions is derived from the pollutant mass balance as Equation (37):

$$Iq = C_e \lambda_v V + C_i \lambda_{rest} V \tag{37}$$

where:

C_e quanta concentration in the extract air (quanta/m³)
C_i quanta concentration at the location i (quanta/m³)
V volume of the room (m³)
λ_v outdoor air change rate, i.e., removal rate due to ventilation (1/h)
λ_{rest} other removal mechanisms than ventilation (1/h)

The local air quality index is defined similarly to the Equation (4) as Equation (38):

$$\varepsilon_{P,i} = \frac{C_e - C_0}{C_i - C_0} \tag{38}$$

By substituting $\varepsilon_{P,i}$ into Equation (37) and noting that the ventilation rate supplied by the system is $Q_{s,loc} = \lambda_v V$, we obtain Equation (39):

$$C_i = \frac{Iq}{\varepsilon_{P,i} Q_{s,loc} + \lambda_{rest} V} \tag{39}$$

where:

$Q_{s,loc}$ ventilation rate supplied by the ventilation air distribution system taking into account the spatial variation of concentration (m^3/h)

The probability of infection at location i can then be calculated by substituting C_i from Equation (39) into Equation (9), as seen in Equation (40):

$$p_i = 1 - e^{-\frac{Iq Q_b D}{\varepsilon_{P,i} Q_{s,loc} + \lambda_{rest} V}} \tag{40}$$

If $N_{s,i}$ susceptible persons are exposed to C_i at location i, R_i (new disease cases per infectious person) can be calculated according to the Equation (41):

$$R_i = \frac{p_i N_{s,i}}{I} \tag{41}$$

The total R value is derived from the exposure of all susceptible individuals as Equation (42):

$$R = \sum_i R_i \tag{42}$$

For a specified R value, the ventilation rate $Q_{s,loc}$ provided by the air distribution system can be iteratively solved using Equations (40) to (42). Ventilation effectiveness can then be calculated based on the target ventilation rate for the breathing zone, assuming fully mixed conditions as in Equation (43):

$$\varepsilon_{b,loc} = \frac{Q}{Q_{s,loc}} \tag{43}$$

where:

Q target ventilation airflow rate for the breathing zone (m^3/h)

$\varepsilon_{b,loc}$ ventilation effectiveness taking into account the spatial variation of concentration (-)

The target ventilation rate for the breathing zone Q is equivalent to the ventilation rate under fully mixed conditions and is calculated using Equations (34) to (36), with $\varepsilon_b = 1$.

The use of CO_2 as a tracer gas for evaluating ventilation effectiveness is well-established [89,112,113,134]. To calculate local air quality index values at measurement points, CO_2 is injected at a constant rate, and stabilized steady-state concentration values are applied in Equation (38). Ventilation effectiveness ε_b measures a system's capacity to remove airborne contaminants [89]. To compute ε_b using a conventional method based on average concentration, values are averaged

from experiments across various point source locations j (ε_b^j) according to Equations (44) and (45). For each point source j, ventilation effectiveness based on average concentration in the breathing zone is calculated from local air quality index measurements using Equation (38) at each measurement point $\varepsilon_{P,i}$.

$$\varepsilon_{b,loc}^j = \frac{1}{\dfrac{\sum_{i=1}^K \left(\dfrac{1}{\varepsilon_{P,i}}\right)}{K}} \tag{44}$$

For the room, ventilation effectiveness taking into account the spatial variation of concentration is calculated as the weighted average of reciprocals from m experiments with different point source locations as Equation (45):

$$\varepsilon_{b,loc} = \frac{1}{\dfrac{\sum_{i=1}^m \left(\dfrac{1}{\varepsilon_{b,loc}^j}\right)}{m}} \tag{45}$$

3.6 Ventilation effectiveness and target ventilation rate calculated from average and local concentration in case study rooms

The novel new ventilation effectiveness parameter $\varepsilon_{b,loc}$, which reflects spatial concentration and risk variation with a single value is especially useful for cases with significant concentration differences. To validate this approach, tracer gas measurements were conducted in real buildings and a mock-up lab at Tallinn University of Technology. Data from previous CO_2 tracer gas studies [115,155,174,183,184] were also analysed. The study includes 22 rooms in various non-residential settings (classrooms, open-plan offices, meeting rooms, gyms, restaurants), with ceiling-based mixing ventilation. Findings indicate trends and significant variations in ventilation effectiveness based on air distribution type, room size, and air change rate.

To illustrate the spatial concentration distribution and highlight air distribution performance trends, $\varepsilon_{P,i}$ values are visualized in selected rooms. In each room, $\varepsilon_{P,i}$ values were calculated at 1.1 m height across K measurement points using Equation (38) (see Table 13). The resulting values were used to create linearly interpolated colour plots, shown in Figure 25 to Figure 31, generated with SciPy and Matplotlib libraries in Python. The effect of the point source not fully mixed by the mixing ventilation system, which is designed for distributed source removal, is clearly visible in the laboratory-measured Office 1 setup (Figure 25). Although active chilled beams generated high induction airflow and promoted good mixing, higher concentration zones still formed near the point source across all three measured locations. Depending on the use of single or multiple extract points, ε_b ranged from 0.89 to 0.96, slightly below the ideal fully mixed value of 1.0.
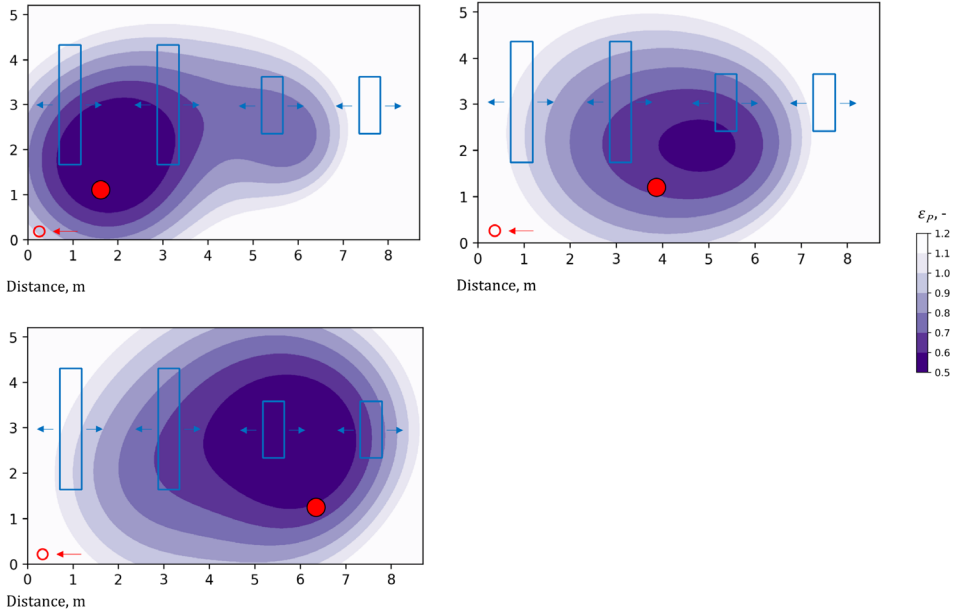
Figure 25. Local air quality index values in Office 1 (45.1 m²) depending on the emission source location marked with red circle.

Figure 26 illustrates the impact of extract air device placement in a relatively small, 25-person classroom. This setup includes two ceiling diffusers with plenum boxes, 12 concentration measurement points at a height of 1.1 m, and one measurement from the extract air duct. With source locations both near and far from the extract points, distinct high and low concentration zones emerged, resulting in ε_b^j values of 0.90 and 1.67, and an overall ε_b of 1.17. This indicates that local exhaust positioning enhances ventilation effectiveness and that source locations should avoid proximity directly beneath the extract during measurements. A similar effect has been observed in Classroom 3 [175] and Meeting Room 1 [155].
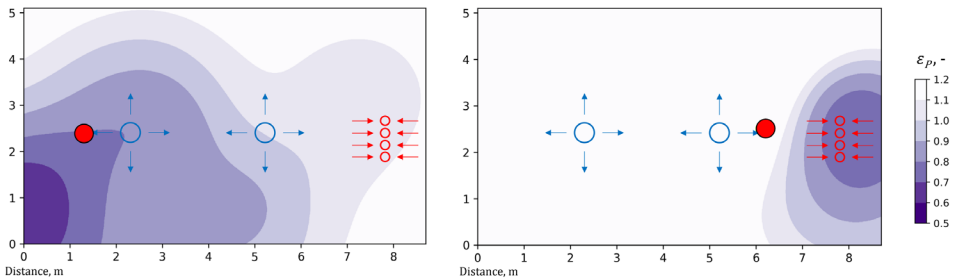
Figure 26. Local air quality index values with left and right locations of point source in Classroom 6 of 45.1 m². Emission source is marked with red circle.

Figure 27 presents an extreme case of Fitness 1 where the source was positioned directly beneath the room's only exhaust, resulting in a high ε_b^j of 1.86, effectively creating a local extract effect. However, a different source location revealed contaminant accumulation, indicating inadequate air distribution – air jets from ceiling diffusers

failed to reach floor level, causing short-circuiting with a ε_b^j of 0.53. The substantial variation in ε_b^j values suggests that averaging might not yield reliable results. However, the calculated ε_b of 0.79 reflects poor air distribution performance. In contrast, a similar Fitness 2 room in Figure 28 demonstrates effective air distribution, with ε_b^j values of 1.34 and 1.04, both exceeding fully mixed conditions, leading to an overall ε_b of 1.17. Here, the air distribution was organized with wall diffusers and extract grilles.
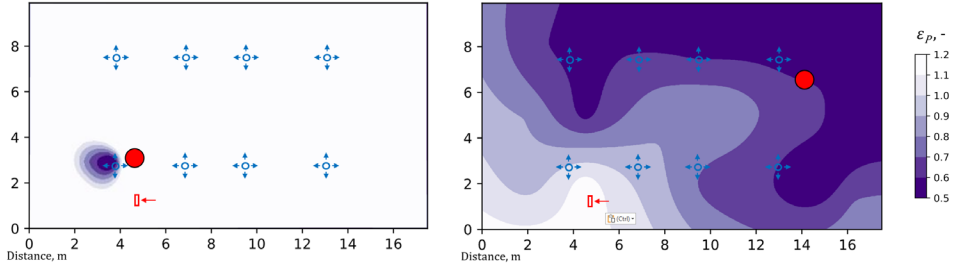
Figure 27. Local air quality index values with left and right locations of point source in Fitness 1 of 173.5 m². Emission source is marked with red circle.
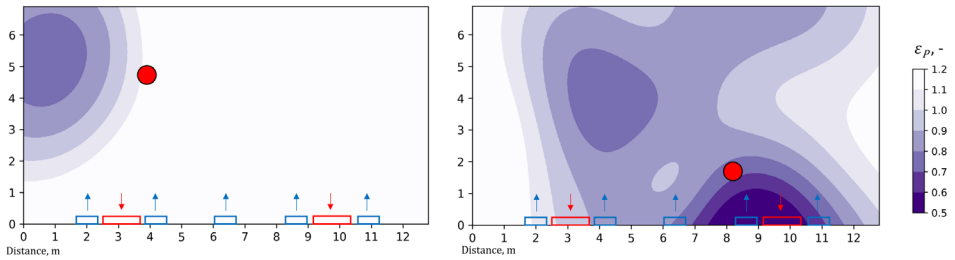
Figure 28. Local air quality index values with left and right locations of point source in Fitness 2 of 117.0 m². Emission source is marked with red circle.

In larger gym spaces with similar *ACH*, ε_b values both below and above 1.0 were observed, similar to those in fitness rooms. Gym 1 experienced short-circuiting due to insufficient jet throw length, resulting in one of the lowest measured ε_b values of 0.49 (Figure 29). In the slightly larger Gym 2, all three measurements yielded ε_b^j values above 1.0, with an overall ε_b of 1.17 (Figure 30). However, in the upper left setup, higher concentrations were noted around the source, indicating poor mixing in this area. In contrast, in the upper right configuration, with the source placed centrally, the tracer gas was efficiently removed, resulting in breathing zone concentrations significantly lower than those in the extract duct.
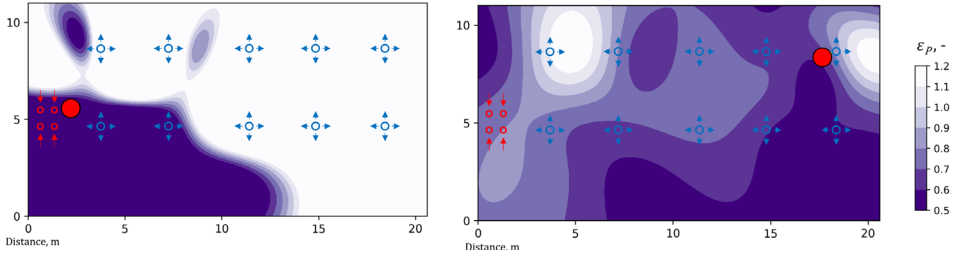
Figure 29. Local air quality index values with left and right locations of point source in the gym (Gym 1) of 217.5 m². Emission source marked with red circle.
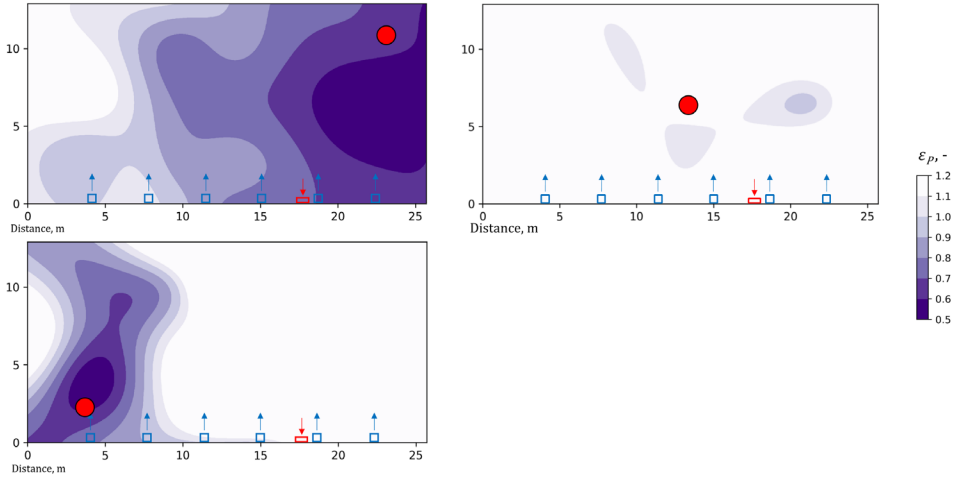
Figure 30. Local air quality index values with three locations of point source in the gym (Gym 2) of 331 m². Emission source marked with red circle.

While Fitness 1 and Gym 1, which utilized ceiling diffusers, experienced short-circuiting, Fitness 2 and Gym 2, equipped with wall diffusers, demonstrated greater effectiveness than fully mixed ventilation. This observation should not be regarded as a general rule but rather highlights the importance of controlling throw length in ceiling diffusers. In the largest gym, Gym 3, also using ceiling diffusers, conditions nearly achieved full mixing, with ε_b 0.99 (Figure 31).
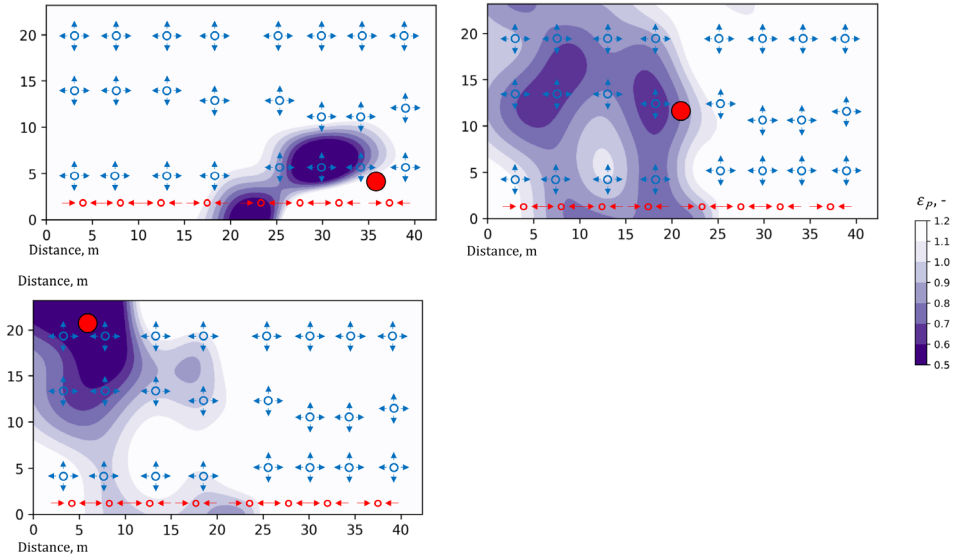
Figure 31. Local air quality index values with three locations of point source in the gym (Gym 3) of 987 m². Emission source marked with red circle.

The remaining measurement results are summarized in Table 18, showing that ε_b values both below and above 1 were recorded in classrooms, dressing rooms, fitness areas, gyms, and meeting rooms. In certain instances, such as Classroom 1 and Classroom 3, higher ventilation rates resulted in increased ventilation effectiveness, while the opposite was observed in cases like Gym 1 and Gym 3, suggesting that ventilation rates were sufficient to influence airflow patterns in these spaces. In offices with lower ventilation rates (2–2.3 l/s·m² compared to 4–9 l/s·m² in other rooms), ε_b values remained below 1, as did those for restaurants and bars where interior design disrupted air distribution.

Furthermore, measurements indicated that spatial concentration differences are a factor in all cases involving a point contaminant source, making it essential to understand how infection risk is elevated in high-concentration areas and reduced in low-concentration areas. This spatial variation is not accounted for in ε_b and Q_s calculations, which are based on average concentration at 1.1 m height. Therefore, Table 18 includes $\varepsilon_{b,loc}^{j}$ and $Q_{s,loc}$, iteratively calculated using Equation (39) to Equation (42) based on local concentrations at each measurement point. The difference, $\Delta Q_s = (Q_s − Q_{s,loc}) / Q_{s,loc} \cdot 100\%$, represents the percentage discrepancy between these two airflow rates. Since ΔQ_s is positive in all cases, this adjustment for spatial infection risk variation results in lower required airflow rates. While this difference is minor in many cases, in some larger spaces it exceeds 10%, reaching a maximum of 39% in the large open-plan Office 2, where the greatest concentration disparities were observed.

Table 18. Comparison of the required ventilation airflow rates supplied by the air distribution system Q_s based on the measured ventilation effectiveness ε_b and iteratively calculated $Q_{s,loc}$ and $\varepsilon_{b,loc}$ which take into account the spatial difference.

Room	ε_b^j -	ε_b -	Q_s m³/s	$\varepsilon_{b,loc}^j$ -	$\varepsilon_{b,loc}$ -	$Q_{s,loc}$ m³/s	Q m³/s	ΔQ_s %
Classr. 1	0.97, 0.97, 1.00	0.98	0.258	0.99, 0.98, 1.00	0.99	0.255	0.253	+1.4
Classr. 1	0.84, 0.95, 1.09	0.95	0.267	0.85, 0.95, 1.09	0.96	0.264	0.253	+1.0
Classr. 1	1.53, 1.43, 1.12	1.34	0.189	1.55, 1.46, 1.12	1.35	0.187	0.253	+1.0
Classr. 1	1.28, 1.17, 1.00	1.14	0.222	1.29, 1.18, 1.02	1.15	0.219	0.253	+1.1
Classr. 1	1.13, 0.98, 0.91	1.00	0.252	1.13, 0.98, 0.92	1.00	0.252	0.253	+0.2
Classr. 1	1.09, 0.89, 1.09	1.01	0.249	1.10, 0.89, 1.10	1.02	0.248	0.253	+0.4
Classr. 2	0.82	0.82	0.262	0.82	0.82	0.261	0.213	+0.2
Classr. 3	0.95, 1.77	1.24	0.081	0.95, 1.78	1.24	0.081	0.100	+0.4
Classr. 4	0.73	0.73	0.279	0.73	0.73	0.278	0.204	+0.7
Classr. 5	0.72, 0.76	0.74	0.547	0.74, 0.80	0.77	0.529	0.406	+3.5
Classr. 6	0.90, 1.67	1.17	0.181	0.90, 1.71	1.18	0.179	0.212	+1.1
Dress. 1	1.64, 1.03	1.26	0.823	1.69, 1.05	1.30	0.803	0.755	+2.6
Dress. 2	0.95, 1.27, 1.03	1.07	1.685	1.00, 1.47, 1.15	1.18	1.527	1.799	+10.4
Fitn. 1	0.53, 1.86	0.79	2.624	0.54, 1.93	0.84	2.560	2.157	+2.5
Fitn. 2	1.34, 1.04	1.17	0.934	1.35, 1.04	1.18	0.930	1.094	+0.4
Fitn. 3	0.64, 1.05	0.79	1.570	0.67, 1.06	0.82	1.510	1.242	+4.0
Gym 1	0.56, 0.43	0.49	2.904	0.72, 0.44	0.55	2.575	1.413	+12.8
Gym 2	1.12, 1.12, 1.28	1.17	1.069	1.19, 1.18, 1.33	1.23	1.017	1.248	+5.1
Gym 3	1.52, 0.97, 0.74	0.99	1.563	1.68, 1.00, 1.07	1.18	1.307	1.548	+19.6
Canteen	0.97	0.97	0.684	1.10	1.10	0.605	0.666	+13.1
Restaur.	0.56, 0.87	0.68	1.465	0.59, 0.90	0.71	1.400	0.996	+4.6
Bar	0.64, 0.76	0.70	1.938	0.67, 0.79	0.72	1.865	1.351	+3.9
Nightcl.	0.70, 0.50	0.59	5.521	0.79, 0.56	0.66	4.950	3.243	+11.5
Meet. 1	0.83, 1.37	1.04	0.431	0.84, 1.38	1.04	0.430	0.447	+0.1
Meet. 2	0.90, 0.96	0.93	0.288	0.91, 0.96	0.93	0.288	0.268	+0.2
Office 1	0.87, 1.02, 0.99	0.96	0.098	0.94, 1.17, 1.10	1.07	0.088	0.094	+10.8
Office 1	0.80, 1.08, 0.99	0.94	0.100	0.95, 1.16, 1.02	1.03	0.091	0.094	+9.9
Office 1	0.83, 0.98, 0.88	0.89	0.105	0.88, 1.06, 1.02	0.98	0.096	0.094	+9.6
Office 2	0.37, 0.69	0.48	0.657	0.56, 0.81	0.66	0.474	0.315	+38.8

The airflow data in Table 18 is converted to units of l/s per m² of floor area in Figure 32, facilitating comparison of the required ventilation rates for air distribution systems in the measured rooms. Significant variations in required ventilation rates within the same room type are observed, attributed to differences in ventilation effectiveness, occupancy, and room volume.
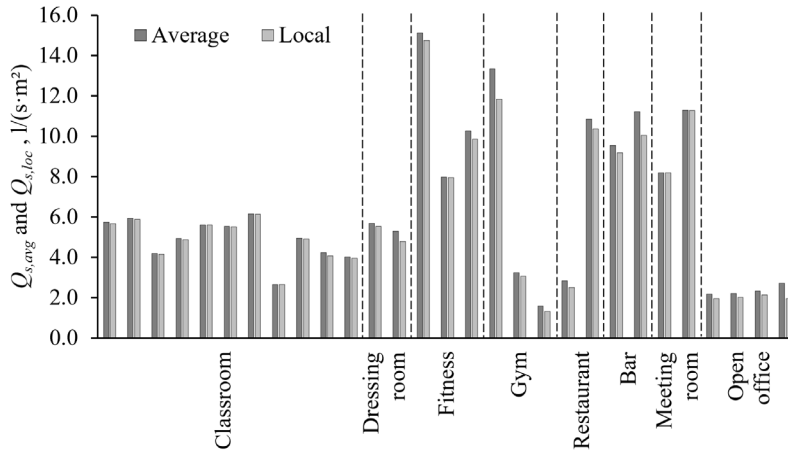
Figure 32. Required ventilation rates to be supplied by air distribution systems in the measured rooms calculated from average and local concentrations.

Figure 32 compares the required ventilation rates with the ICC I and II specified in EN 16798-1:2019 [72]. Perceived air quality airflow rates for categories I and II include both an occupant component (I category – 10 l/(s·person); II category – 7 l/(s·person)) and a floor area component for low-polluting buildings (I category – 1.0 l/(s·m²); II category – 0.7 l/(s·m²)).
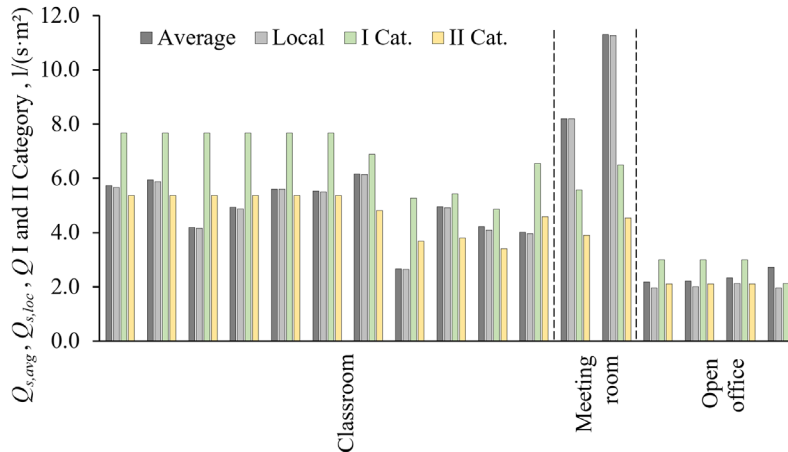
Figure 33. Required ventilation rates to be supplied by air distribution systems calculated from average and local concentrations compared to EN 16798-1 [72] category I and II ventilation rates.

As shown in Figure 33, ventilation rates based on infection risk in classrooms and open offices generally fall between category I and II levels. In contrast, meeting rooms require significantly higher infection-risk-based ventilation rates, indicating that reducing occupancy and employing advanced air distribution methods could be effective solutions.

While infection-risk-based ventilation rates vary with quanta values, measured ventilation effectiveness remains a specific parameter of the air distribution system and can be consistently used in relative risk reduction assessments. Figure 34 illustrates the

variation in ventilation effectiveness across the room categories measured. Values above 1.0 indicate that well-designed air distribution systems achieved higher ventilation effectiveness than in fully mixed conditions. Among the measured spaces, bars and the large open plan Office 2 were the only areas where values above 1.0 were not obtained. For bars, this was clearly an issue of air distribution design, whereas in large open plan offices, values near 1.0 are challenging to achieve due to relatively low ventilation rates.
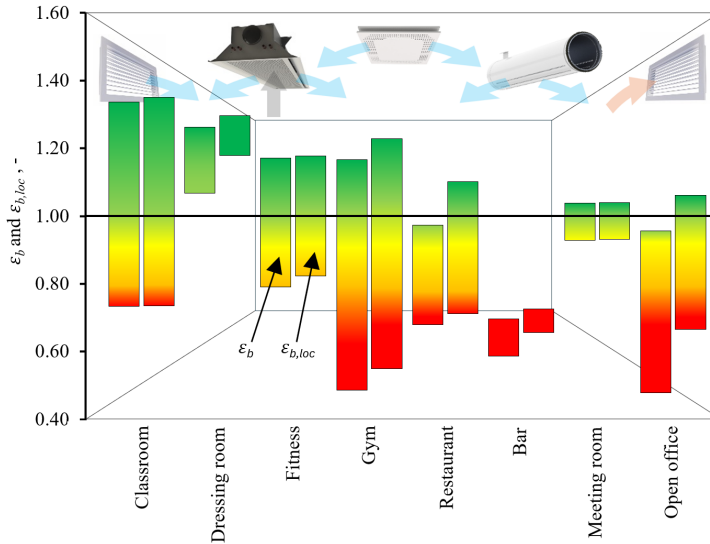
Figure 34. Variation of ventilation effectiveness in measured room categories calculated from average (left columns, conventional method) and local concentrations (right columns, new method).

3.7 Discussion on point source contaminant removal effectiveness

In this thesis, new method for considering ventilation effectiveness in the design of ventilation systems for airborne transmission, was developed. While previous studies have analysed local concentrations of tracer gas or particles and created infection risk maps, this study advances by introducing a new parameter, $\varepsilon_{b,loc}$, which quantifies spatial variations in concentration and infection risk based on the fraction of R_i. The primary innovation of this method is the introduction of a ventilation effectiveness indicator that captures spatial concentration and risk variation with a single parameter. Compared to traditional ventilation effectiveness calculations based on average concentrations, this method improves accuracy, particularly in cases with large concentration variations.

In practical application, several factors must be considered. Quanta emission rates, which vary widely, are required to calculate the ventilation rate for a specified risk level. However, from a methodological standpoint, ventilation effectiveness is an intrinsic parameter of the air distribution system, applicable regardless of emission source intensity. Thus, differences between cases are not significantly impacted by quanta values, similar to other quanta-based methods: while there is uncertainty in absolute risk, relative changes can be accurately assessed for different rooms and ventilation setups.

Measurement conditions and validity are also critical for ventilation effectiveness. Due to the complexity of airflow patterns influenced by air jets, internal and solar heat gains, geometry, and other factors, contaminant removal effectiveness strictly applies only to the conditions present at the time of measurement. Thus, measurements should be conducted in typical, representative scenarios. Internal heat gains should be set up, t_{sup} controlled, and ventilation rates adjusted to match expected values, as significant changes in the Archimedes number (which describes non-isothermal jets) could alter air distribution patterns.

Moreover, working with a point source introduces complexity, as a point source can occupy various locations in a room. In this thesis, tracer gas was released inside a dummy, a simplification compared to using a breathing manikin. This was appropriate here, as the focus was on long-range transmission rather than the close-proximity exhalation concentration field. While some guidance is provided on selecting relevant source locations, this area warrants further research to ensure effective and practical application in ventilation design.

The suitability of contaminant removal effectiveness as an indicator for ventilation effectiveness in describing spatial concentration differences is also open to discussion. Another commonly used indicator in studies is the dilution ratio D_i of the exhaled breath from an infector. Although D_i was not applied in this thesis, the equations could be reformulated to replace the local air quality index with the dilution ratio. To achieve this, the source term in Equation (9) could be expanded as follows to Equation (46):

$$Iq = IQ_b C_{ex} \qquad (46)$$

where:

C_{ex} concentration in the exhaled breath of infector (quanta/m³)

Using the definition of D_i, it can be demonstrated by substituting C_i from Equation (39) that D_i serves as an alternative indicator to the local air quality index $\varepsilon_{P,i}$ as in Equation (47):

$$D_i = \frac{C_{ex}}{C_i} = \frac{q}{Q_b C_i} = \frac{\varepsilon_{P,i} Q_{s,loc} + \lambda_{rest} V}{IQ_b}, \text{ (-)} \qquad (47)$$

Thus, D_i does not provide a more generalizable value, as it remains similarly sensitive to heat gains and airflow rates, particularly when the Archimedes number changes.

Existing standards recommend for contaminant removal effectiveness a default value of 1.0 for mixing ventilation (cool air) that applies for distributed source (occupants in the room). In the case of design for airborne transmission (ASHRAE 241, revision of EN 16798-1) calculation of ε needs to be revisited because of the point source (infector) and the issue of average concentration on the breathing level. Infector means a point source, and mixing ventilation with distributed source is not necessary mixing ventilation in the case of the point source. Point source evidently reduces the average and increases the variations of local values. Conservative values generally <1 should be taken into account in the design if air distribution system specific values are not available. This provides also a motivation for manufactures to develop more efficient air distribution methods that can be rewarded with higher values if measured or CFD simulated. For this purpose, default values shown in Table 19 are proposed to be used if measured or simulated values are not available.

Table 19. Default point source contaminant removal effectiveness values for mixing ventilation to be used if measured or CFD simulated results are not available.

Space category	Room size m²	ε_b -	Room size m²	ε_b -
Classroom	<60	0.9	>60	0.8
Meeting room	<50	0.9	>50	0.8
Office	<60	0.8	>60	0.7
Restaurant	<100	0.8	>100	0.7
Fitness and gym	<150	0.9	>150	0.8

   In this context, a long-term ambition could be that manufacturers begin to report contaminant removal effectiveness within their product selection software for typical applications. The development towards this would likely involve multiple stages: initially, expanding and refining standardised example values (e.g. similar to the table values in CR 1752 [180]), then integrating these into manufacturer-specific selection tools. Measured values for typical room layout cases can be reported as a first step. In the long term, the calculation models need to be developed to provide these values. It must be acknowledged that generating such product-specific effectiveness data would require a substantial number of measurements and high-resolution CFD simulations across a wide range of representative cases, along with ongoing calibration and validation. Nonetheless, such an initiative would align with a more application-relevant ventilation performance metrics and could lead to more informed product selection and system design choices.

4 Conclusions

In this thesis, thermal comfort and draught rate in five office buildings in Tallinn using both measurements and occupant questionnaires were assessed. Secondly, next to air velocity, ventilation effectiveness indices – air change efficiency and contaminant removal effectiveness were examined in a mock-up classroom. And finally, based on additional field measurements, a new method for ventilation effectiveness application in ventilation design for airborne transmission was proposed.

Providing response to research question 1 in this thesis, open office landscape thermal comfort findings indicate that achieving consistent thermal comfort in modern open-plan offices remains challenging due to variations in room conditioning systems and design practices. Overall, the results showed that thermal comfort categories were inconsistently met across buildings. For example, air and operative temperatures in Building E nearly fell below category III during the heating season, while Buildings A–D achieved between category I and III. However, significant overheating was observed in three out of five buildings during the heating season, with temperatures of 23–25 °C. This led to an assumption of occupant adaption of clothing levels to 0.7 clo, a factor that improved comfort ratings in certain buildings but underscored the need for improved temperature control.

Active chilled beams and radiant panels performed variably across buildings, with only the open ceiling chilled beams in Building A meeting category II requirements. Ceiling radiant panels in Building D achieved category I performance, suggesting that proper air distribution and correct sizing are crucial to meet higher comfort standards. Additionally, inadequate air velocity control and the absence of specific questions on draught discomfort in surveys were notable limitations affecting comfort assessment. To address these issues, future designs could incorporate air distribution tailored to occupant needs, with controls adjusted based on outdoor running mean and extract air temperatures. This approach could mitigate heating period overheating and overall draught, balancing occupant comfort and energy efficiency.

Mock-up classroom measurements were conducted to reply to research question 2 of the thesis. Comparisons were made across supply grille, circular diffuser, and duct diffuser configurations with single and six extract terminal layouts. No strong correlation was observed between air change efficiency and contaminant removal effectiveness. Local ventilation effectiveness for contaminant removal indicated that full mixing does not occur with a point source, even though air change efficiency, measured with an evenly distributed source, suggested fully mixed conditions. The circular diffuser yielded unexpectedly high ventilation effectiveness values (>1), while six extraction points did not consistently outperform a single extraction element. Point source ventilation effectiveness was calculated as the average of measurements from multiple contaminant source locations. This conservative value enables recalculating fully mixed airflow rates to align with actual ventilation distribution solutions.

While traditional ventilation effectiveness values rely on tracer gas measurements with a distributed source, the developed method utilizes a few point source locations representing an infector, accounting for spatial concentration variations due to air distribution patterns. The innovation of this method is the introduction of a new ventilation effectiveness parameter, $\varepsilon_{b,loc}$, which captures the impact of spatial concentration variations and associated airborne infection risk in a single metric.

This study demonstrated that infection risk can be quantified at each measurement point at breathing height, allowing calculation of the necessary ventilation rate for a specified risk level based on ventilation effectiveness from tracer gas measurements using a few point source locations. The new method requires the quanta emission rate as input. However, results showed minimal variation across studied cases regardless of the quanta values applied. Using two or three locations for point source, tracer gas measurements provided representative results. Contaminant locations should be ideally positioned at typical occupant spots, one far from extracts and another in the room centre, while locations directly beneath extracts should be avoided. A simple ventilation effectiveness calculation based on average concentration at breathing height, without quanta data, produced conservative results, yielding lower ventilation effectiveness and higher required ventilation rates than iterative calculations with the new method that accounts for spatial concentration differences and infection risk.

In many cases, the difference in required ventilation rates calculated with the new method versus average concentration was only a few percent. In total for large spaces, additional air flow exceeded 10%, with a maximum difference of 39% observed in a large open-plan office with significant concentration variations. Ventilation effectiveness varied widely across room types, ranging from 0.5 to 1.4. In the light of research question 3, values above 1.0 indicate that carefully designed air distribution systems can achieve better effectiveness than fully mixed conditions. Higher ventilation rates did not consistently enhance ventilation effectiveness, suggesting that rates were already sufficient to control airflow patterns. Only in large open-plan offices was it challenging to achieve values close to 1.0 due to relatively low ventilation rates.

The outcome of research question 4 has potential applications in ventilation standards and air distribution calculation tools. Ideally, the new method could be integrated into tools calculating air jet throw length and airflow patterns, enabling future reports to incorporate ventilation effectiveness values that consider spatial concentration differences and infection risk. As the simple ventilation effectiveness calculation based on average concentration provided conservative results, it appears suitable for practical design purposes, though it may lead to oversizing in certain cases.

4.1 Limitations

The findings of the thermal comfort study are most applicable in heating-dominated climatic conditions. HVAC settings investigated do not cover the full spectrum of systems found in real-world office buildings. Secondly, draught and ventilation effectiveness measurement conditions and validity. Because of complexity of air flow patterns in a room, affected by air jets, internal and solar heat gains, geometry etc., contaminant removal effectiveness measurement applies only for those conditions in a room at measurement time. Therefore, it is highly important to conduct measurements in typical representative situations. Internal heat gains should be well organised in the room, supply air temperature controlled, and the ventilation rate to be adjusted close to values under interest as Archimedes number that is used to describe non-isothermal jets should not change significantly to keep the same air distribution patterns.

Additional complexity is measuring with a point source which can have many possible positions in a room. In this thesis a tracer gas was injected inside the dummy that is a simplification compared for instance to breathing manikin. In general, tracer

gas experiments are more reliable in smaller rooms with lower ceilings than in larger, higher or partly open spaces. Finally, measurement methods for air velocity and tracer gas are difficult to use during the planning phase of a new building.

4.2 Future work

To begin with, development of advanced indoor climate survey systems could be one major topic for further research. For example, integrating clothing monitoring into HVAC control systems and occupant feedback using modern sensors and appliances, such as smartphones and smartwatches etc. In general, room categories were not comprehensively studied for instance to find the best possible ventilation effectiveness values. Such analyses can be recommended for future studies because the results show high variations – there could be a substantial improvement potential in many cases. While some guidance on how to select relevant source locations was possible to provide, this topic evidently deserves future research efforts to ensure correct and practical application for ventilation design purposes. To sum up, future topics could include integrating draught and infection risk management:

- Within demand-based HVAC systems in dynamic environments while avoiding oversizing.
- With a lack of installation space in case of retrofitting existing buildings.
- Into HVAC design and selection tools as both measurement methods for air velocity and tracer gas are difficult to use during the planning phase of a new building.
- While balancing wider spectrum of building design factors including architectural functionality, thermal comfort, ventilation acoustics, indoor climate control automation, energy efficiency, cost-effectiveness, etc.

4.3 Practical HVAC design outcomes

The main practical outcomes of this thesis are as follows:

- Four-pipe radiant panels performed best, followed by active chilled beams with the potential to meet the Cat II requirements achieving suitable air velocity and room air temperature simultaneously.
- TABS maintained similar air velocities with active chilled beams but experienced overheating during winter.
- Fan coil units performed wo<rst during the cooling period.
- Using running mean outdoor temperature including midseason definition for both room air temperature and supply air temperature control, while using extract air temperature to adjust supply air temperature can help to avoid draught or overheating.
- Point source ventilation effectiveness values can be used as a correction factor for mixing ventilation airflow rate.
- Spatial variation iterative calculation method requiring quanta data provided less conservative results for required ventilation rate, avoiding over dimensioning.
- The goal of avoiding draught and maintaining high ventilation effectiveness simultaneously is achievable. However, the aim is not to eliminate but considerably reduce the infection risk in shared indoor spaces.

This work is a part of post-COVID ventilation design method already published by Nordic Ventilation Group and REHVA. The method is proposed to be included in EN 16798-1:2019 standard.

References

1. Pikas, E.; Thalfeldt, M.; Kurnitski, J.; Liias, R. Extra cost analyses of two apartment buildings for achieving nearly zero and low energy buildings. *Energy* **2015**, *84*, 623–633, doi:10.1016/J.ENERGY.2015.03.026.
2. Kähkönen, E. Draught, radiant temperature asymmetry and air temperature–a comparison between measured and estimated thermal parameters. *Indoor Air* **1991**, *1*, 439–447.
3. FANGER, P.O.; Christensen, N.K. Perception of draught in ventilated spaces. *Ergonomics* **1986**, *29*, 215–235.
4. Hens, H.S.L.C. Thermal comfort in office buildings: Two case studies commented. *Build. Environ.* **2009**, *44*, 1399–1408.
5. Kiil, M.; Mikola, A.; Thalfeldt, M.; Kurnitski, J. Thermal comfort and draught assessment in a modern open office building in Tallinn. In Proceedings of the E3S Web of Conf.; **2019**; Vol. 111.
6. Shahzad, S.S.; Brennan, J.; Theodossopoulos, D.; Hughes, B.; Calautit, J.K. Energy efficiency and user comfort in the workplace: Norwegian cellular vs. British open plan workplaces. *Energy Procedia* **2015**, *75*, 807–812.
7. Yang, L.; Yan, H.; Lam, J.C. Thermal comfort and building energy consumption implications–a review. *Appl. Energy* **2014**, *115*, 164–173.
8. Seppᵋnen, O. Ventilation strategies for good indoor air quality and energy efficiency. *Int. J. Vent.* **2008**, *6*, 297–306.
9. Jafarpur, P.; Berardi, U. Effects of climate changes on building energy demand and thermal comfort in Canadian office buildings adopting different temperature setpoints. *J. Build. Eng.* **2021**, *42*, 102725.
10. Frontczak, M.; Schiavon, S.; Goins, J.; Arens, E.; Zhang, H.; Wargocki, P. Quantitative relationships between occupant satisfaction and satisfaction aspects of indoor environmental quality and building design. *Indoor Air* **2012**, *22*, 119–131.
11. Gärtner, J.A.; Gray, F.M.; Auer, T. Assessment of the impact of HVAC system configuration and control zoning on thermal comfort and energy efficiency in flexible office spaces. *Energy Build.* **2020**, *212*, 109785.
12. De Dear, R. Thermal comfort in practice. *Indoor Air* **2004**, *14*, 32–39.
13. Sansaniwal, S.K.; Mathur, J.; Mathur, S. Review of practices for human thermal comfort in buildings: present and future perspectives. *Int. J. Ambient Energy* **2022**, *43*, 2097–2123.
14. Zhao, W.; Lestinen, S.; Mustakallio, P.; Kilpeläinen, S.; Jokisalo, J.; Kosonen, R. Experimental study on thermal environment in a simulated classroom with different air distribution methods. *J. Build. Eng.* **2021**, *43*, 103025.
15. Cheung, T.; Schiavon, S.; Graham, L.T.; Tham, K.W. Occupant satisfaction with the indoor environment in seven commercial buildings in Singapore. *Build. Environ.* **2021**, *188*, 107443.
16. Licina, D.; Yildirim, S. Occupant satisfaction with indoor environmental quality, sick building syndrome (SBS) symptoms and self-reported productivity before and after relocation into WELL-certified office buildings. *Build. Environ.* **2021**, *204*, 108183.

17. Dong, Z.; Zhao, K.; Ren, M.; Ge, J.; Chan, I.Y.S. The impact of space design on occupants' satisfaction with indoor environment in university dormitories. *Build. Environ.* **2022**, *218*, 109143.

18. Nkini, S.; Nuyts, E.; Kassenga, G.; Swai, O.; Verbeeck, G. Evaluation of occupants' satisfaction in green and non-green office buildings in Dar es Salaam-Tanzania. *Build. Environ.* **2022**, *219*, 109169.

19. Võsa, K.-V.; Ferrantelli, A.; Kurnitski, J. Cooling Thermal Comfort and Efficiency Parameters of Ceiling Panels, Underfloor Cooling, Fan-Assisted Radiators, and Fan Coil. *Energies* **2022**, *15*, 4156.

20. Chen, W.; Deng, Y.; Cao, B. An experimental study on the difference in thermal comfort perception between preschool children and their parents. *J. Build. Eng.* **2022**, *56*, 104723.

21. Rhee, K.-N.; Olesen, B.W.; Kim, K.W. Ten questions about radiant heating and cooling systems. *Build. Environ.* **2017**, *112*, 367–381.

22. Saber, E.M.; Tham, K.W.; Leibundgut, H. A review of high temperature cooling systems in tropical buildings. *Build. Environ.* **2016**, *96*, 237–249.

23. Schellen, L.; Loomans, M.G.L.C.; De Wit, M.H.; Olesen, B.W.; van Marken Lichtenbelt, W.D. Effects of different cooling principles on thermal sensation and physiological responses. *Energy Build.* **2013**, *62*, 116–125.

24. Maula, H.; Hongisto, V.; Koskela, H.; Haapakangas, A. The effect of cooling jet on work performance and comfort in warm office environment. *Build. Environ.* **2016**, *104*, 13–20.

25. Gao, S.; Wang, Y.A.; Zhang, S.M.; Zhao, M.; Meng, X.Z.; Zhang, L.Y.; Yang, C.; Jin, L.W. Numerical investigation on the relationship between human thermal comfort and thermal balance under radiant cooling system. *Energy procedia* **2017**, *105*, 2879–2884.

26. Cen, C.; Jia, Y.; Liu, K.; Geng, R. Experimental comparison of thermal comfort during cooling with a fan coil system and radiant floor system at varying space heights. *Build. Environ.* **2018**, *141*, 71–79.

27. Kolarik, J.; Toftum, J.; Olesen, B.W.; Jensen, K.L. Simulation of energy use, human thermal comfort and office work performance in buildings with moderately drifting operative temperatures. *Energy Build.* **2011**, *43*, 2988–2997.

28. Fonseca, N. Experimental study of thermal condition in a room with hydronic cooling radiant surfaces. *Int. J. Refrig.* **2011**, *34*, 686–695.

29. Li, R.; Yoshidomi, T.; Ooka, R.; Olesen, B.W. Field evaluation of performance of radiant heating/cooling ceiling panel system. *Energy Build.* **2015**, *86*, 58–65.

30. Saber, E.M.; Iyengar, R.; Mast, M.; Meggers, F.; Tham, K.W.; Leibundgut, H. Thermal comfort and IAQ analysis of a decentralized DOAS system coupled with radiant cooling for the tropics. *Build. Environ.* **2014**, *82*, 361–370.

31. Chiang, W.-H.; Wang, C.-Y.; Huang, J.-S. Evaluation of cooling ceiling and mechanical ventilation systems on thermal comfort using CFD study in an office for subtropical region. *Build. Environ.* **2012**, *48*, 113–127.

32. Mustakallio, P.; Bolashikov, Z.; Kostov, K.; Melikov, A.; Kosonen, R. Thermal environment in simulated offices with convective and radiant cooling systems under cooling (summer) mode of operation. *Build. Environ.* **2016**, *100*, 82–91.

33. Cehlin, M.; Karimipanah, T.; Larsson, U.; Ameen, A. Comparing thermal comfort and air quality performance of two active chilled beam systems in an open-plan office. *J. Build. Eng.* **2019**, *22*, 56–65.

34. Kim, T.; Kato, S.; Murakami, S.; Rho, J. Study on indoor thermal environment of office space controlled by cooling panel system using field measurement and the numerical simulation. *Build. Environ.* **2005**, *40*, 301–310.

35. Fredriksson, J.; Sandberg, M.; Moshfegh, B. Experimental investigation of the velocity field and airflow pattern generated by cooling ceiling beams. *Build. Environ.* **2001**, *36*, 891–899.

36. Rhee, K.-N.; Shin, M.-S.; Choi, S.-H. Thermal uniformity in an open plan room with an active chilled beam system and conventional air distribution systems. *Energy Build.* **2015**, *93*, 236–248.

37. Koskela, H.; Häggblom, H.; Kosonen, R.; Ruponen, M. Air distribution in office environment with asymmetric workstation layout using chilled beams. *Build. Environ.* **2010**, *45*, 1923–1931.

38. Indraganti, M.; Ooka, R.; Rijal, H.B. Thermal comfort in offices in summer: Findings from a field study under the 'setsuden'conditions in Tokyo, Japan. *Build. Environ.* **2013**, *61*, 114–132.

39. De Vecchi, R.; Candido, C.; de Dear, R.; Lamberts, R. Thermal comfort in office buildings: Findings from a field study in mixed-mode and fully-air conditioning environments under humid subtropical conditions. *Build. Environ.* **2017**, *123*, 672–683.

40. Azad, A.S.; Rakshit, D.; Wan, M.P.; Babu, S.; Sarvaiya, J.N.; Kumar, D.K.; Zhang, Z.; Lamano, A.S.; Krishnasayee, K.; Gao, C.P. Evaluation of thermal comfort criteria of an active chilled beam system in tropical climate: A comparative study. *Build. Environ.* **2018**, *145*, 196–212.

41. He, Y.; Li, N.; Huang, Q. A field study on thermal environment and occupant local thermal sensation in offices with cooling ceiling in Zhuhai, China. *Energy Build.* **2015**, *102*, 277–283.

42. Pfafferott, J.Ü.; Herkel, S.; Kalz, D.E.; Zeuschner, A. Comparison of low-energy office buildings in summer using different thermal comfort criteria. *Energy Build.* **2007**, *39*, 750–757.

43. Fanger, P.O. Thermal comfort. Analysis and applications in environmental engineering. *Therm. Comf. Anal. Appl. Environ. Eng.* **1970**.

44. Yang, Z.; Ghahramani, A.; Becerik-Gerber, B. Building occupancy diversity and HVAC (heating, ventilation, and air conditioning) system energy efficiency. *Energy* **2016**, *109*, 641–649.

45. Mathews, E.H.; Botha, C.P.; Arndt, D.C.; Malan, A. HVAC control strategies to enhance comfort and minimise energy usage. *Energy Build.* **2001**, *33*, 853–863.

46. Simmonds, P. The utilisation of optimal design and operation strategies in lowering the energy consumption in office buildings. *Renew. energy* **1994**, *5*, 1193–1201.

47. Guo, W.; Zhou, M. Technologies toward thermal comfort-based and energy-efficient HVAC systems: A review. In Proceedings of the 2009 IEEE international conference on systems, man and cybernetics; IEEE, **2009**; pp. 3883–3888.

48. Fanger, P.O.; Christensen, N.K. Perception of draught in ventilated spaces. *Ergonomics* **1986**, *29*, 215–235, doi:10.1080/00140138608968261.

49. Shahrestani, M.; Yao, R.; Cook, G.K. Decision making for HVAC&R system selection for a typical office building in the UK. *Ashrae Trans* **2012**, *118*, 222–229.

50. Nemethova, E.; Stutterecker, W.; Schoberer, T. Thermal Comfort and HVAC Systems Operation Challenges in a Modern Office Building–Case Study. *Sel. Sci. Pap. Civ. Eng.* **2016**, *11*, 103–114.

51. Choi, J.-H.; Loftness, V.; Aziz, A. Post-occupancy evaluation of 20 office buildings as basis for future IEQ standards and guidelines. *Energy Build.* **2012**, *46*, 167–175.

52. Karjalainen, S. Thermal comfort and gender: a literature review. *Indoor Air* **2012**, *22*, 96–109.

53. Schellen, L.; Loomans, M.G.L.C.; de Wit, M.H.; Olesen, B.W.; van Marken Lichtenbelt, W.D. The influence of local effects on thermal sensation under non-uniform environmental conditions—Gender differences in thermophysiology, thermal comfort and productivity during convective and radiant cooling. *Physiol. Behav.* **2012**, *107*, 252–261.

54. Rupp, R.F.; Vásquez, N.G.; Lamberts, R. A review of human thermal comfort in the built environment. *Energy Build.* **2015**, *105*, 178–205.

55. Kolarik, J.; Toftum, J.; Olesen, B.W. Operative temperature drifts and occupant satisfaction with thermal environment in three office buildings using radiant heating/cooling system. In Proceedings of the Healthy Buildings Europe 2015. **2015**.

56. Griefahn, B.; Künemund, C. The effects of gender, age, and fatigue on susceptibility to draft discomfort. *J. Therm. Biol.* **2001**, *26*, 395–400.

57. Maykot, J.K.; Rupp, R.F.; Ghisi, E. A field study about gender and thermal comfort temperatures in office buildings. *Energy Build.* **2018**, *178*, 254–264.

58. Maula, H.; Hongisto, V.; Östman, L.; Haapakangas, A.; Koskela, H.; Hyönä, J. The effect of slightly warm temperature on work performance and comfort in open-plan offices–a laboratory study. *Indoor Air* **2016**, *26*, 286–297.

59. Mujan, I.; Anđelković, A.S.; Munćan, V.; Kljajić, M.; Ružić, D. Influence of indoor environmental quality on human health and productivity-A review. *J. Clean. Prod.* **2019**, *217*, 646–657.

60. Al Horr, Y.; Arif, M.; Kaushik, A.; Mazroei, A.; Katafygiotou, M.; Elsarrag, E. Occupant productivity and office indoor environment quality: A review of the literature. *Build. Environ.* **2016**, *105*, 369–389.

61. Sundell, J. On the history of indoor air quality and health. *Indoor Air* **2004**, *14*, 51–58.

62. Wargocki, P.; Djukanovic, R. Simulations of the Potential Revenue from Investment in Improved Indoor Air Quality in an Office Building. *ASHRAE Trans.* **2005**, *111*.

63. Fisk, W.J.; Rosenfeld, A.H. Estimates of improved productivity and health from better indoor environments. *Indoor Air* **1997**, *7*, 158–172.

64. Valancius, R.; Jurelionis, A.; Dorosevas, V. Method for cost-benefit analysis of improved indoor climate conditions and reduced energy consumption in office buildings. *Energies* **2013**, *6*, 4591–4606.

65. Djukanovic, R.; Wargocki, P.; Fanger, P.O. Cost-benefit analysis of improved air quality in an office building. In Proceedings of the Proceedings of Indoor Air 2002; Citeseer, **2002**; Vol. 1, pp. 808–813.

66. Leaman, A.; Bordass, B. Productivity in buildings: the 'killer'variables. In *Creating the productive workplace*; Taylor & Francis, **2006**; pp. 181–208 ISBN 0203696883.

67. Lan, L.; Wargocki, P.; Lian, Z. Thermal effects on human performance in office environment measured by integrating task speed and accuracy. *Appl. Ergon.* **2014**, *45*, 490–495.

68. Lamb, S.; Kwok, K.C.S. A longitudinal investigation of work environment stressors on the performance and wellbeing of office workers. *Appl. Ergon.* **2016**, *52*, 104–111.

69. Seppänen, O.A.; Fisk, W. Some Quantitative Relations between Indoor Environmental Quality and Work Performance or Health. *HVAC&R Res.* **2006**, *12*, 957–973.

70. Jiang, J.; Wang, D.; Liu, Y.; Xu, Y.; Liu, J. A study on pupils' learning performance and thermal comfort of primary schools in China. *Build. Environ.* **2018**, *134*, 102–113.

71. Seppanen, O.; Fisk, W.J.; Lei, Q.H. Effect of temperature on task performance in office environment. **2006**.

72. EN Standard. 16798-1. Energy performance of buildings—Ventilation for buildings—Part 1: Indoor environmental input parameters for design and assessment of energy performance of buildings addressing indoor air quality. *Therm. Environ. Light. Acoust. M1-6.(16798-1).* **2019**.

73. EN 16798-2: 2019 Energy Performance of Buildings—Ventilation for Buildings—Part 2: Interpretation of the Requirements in EN 16798-1—Indoor Environmental Input Parameters for Design and Assessment of Energy Performance of Buildings Addressing Indoor Air Quali. *Therm. Environ. Light. Acoust. (Module M1-6).* **2019**.

74. EN ISO 7730:2005 Ergonomics of the thermal environment — Analytical determination and interpretation of thermal comfort using calculation of the PMV and PPD indices and local thermal comfort criteria. **2005**.

75. EN ISO 7726:1998 Ergonomics of the thermal environment - Instruments for measuring physical quantities. **1998**.

76. Geshwiler, M. ASHRAE Pocket Guide for Air Conditioning, Heating, Ventilation, Refrigeration (IP Edition). *ASHRAE, Atlanta, United States.* **2005**.

77. ASHRAE Standard 55. American National Standards Institute/American Society of Heating, Refrigerating and Air-Conditioning Engineers. **2020**.

78. Gao, S.; Ooka, R.; Oh, W. Experimental investigation of the effect of clothing insulation on thermal comfort indices. *Build. Environ.* **2021**, *187*, 107393.

79. Hoyt, T.; Arens, E.; Zhang, H. Extending air temperature setpoints: Simulated energy savings and design considerations for new and retrofit buildings. *Build. Environ.* **2015**, *88*, 89–96.

80. Raftery, P.; Li, S.; Jin, B.; Ting, M.; Paliaga, G.; Cheng, H. Evaluation of a cost-responsive supply air temperature reset strategy in an office building. *Energy Build.* **2018**, *158*, 356–370.

81. Hawila, A.A.-W.; Merabtine, A.; Chemkhi, M.; Bennacer, R.; Troussier, N. An analysis of the impact of PMV-based thermal comfort control during heating period: A case study of highly glazed room. *J. Build. Eng.* **2018**, *20*, 353–366.

82. Griefahn, B.; KÜNEMUND, C.; Gehring, U.; MEHNERT, P. Drafts in cold environments the significance of air temperature and direction. *Ind. Health* **2000**, *38*, 30–40.

83. Griefahn, B.; Künemund, C.; Gehring, U. The impact of draught related to air velocity, air temperature and workload. *Appl. Ergon.* **2001**, *32*, 407–417.

84. Griefahn, B.; Künemund, C.; Gehring, U. Evaluation of draught in the workplace. *Ergonomics* **2002**, *45*, 124–135.

85. Pinto, D.; Rocha, A.; Simões, M.L.; Almeida, R.M.S.F.; Barreira, E.; Pereira, P.F.; Ramos, N.M.M.; Martins, J.P. An innovative approach to evaluate local thermal discomfort due to draught in semi-outdoor spaces. *Energy Build.* **2019**, *203*, 109416.

86. Borowski, M.; Łuczak, R.; Halibart, J.; Zwolińska, K.; Karch, M. Airflow Fluctuation from Linear Diffusers in an Office Building: The Thermal Comfort Analysis. *Energies* **2021**, *14*, 4808.

87. Tawackolian, K.; Lichtner, E.; Kriegel, M. Draught perception in intermittent ventilation at neutral room temperature. *Energy Build.* **2020**, *224*, 110268.

88. Ahmed, K.; Hasu, T.; Kurnitski, J. Actual energy performance and indoor climate in Finnish NZEB daycare and school buildings. *J. Build. Eng.* **2022**, *56*, 104759.

89. Mundt, M.; Mathisen, H.M.; Moser, M.; Nielsen, P. V Ventilation effectiveness: Rehva guidebooks. **2004**.

90. Duffield, T.J. School ventilation. Its effect on the health of the pupil. *Am. J. Public Health* **1927**, *17*, 1226–1229.

91. Toyinbo, O.; Shaughnessy, R.; Turunen, M.; Putus, T.; Metsämuuronen, J.; Kurnitski, J.; Haverinen-Shaughnessy, U. Building characteristics, indoor environmental quality, and mathematics achievement in Finnish elementary schools. *Build. Environ.* **2016**, *104*, 114–121.

92. d'Ambrosio Alfano, F.R.; Bellia, L.; Boestra, A.; van Dijken, F.; Ianniello, E.; Lopardo, G.; Minichiello, F.; Romagnoni, P.; da Silva, M.C.G. *Indoor Environment and Energy Efficiency in Schools*; Rehva, Federation of European Heating and Air-conditioning Associations. **2010**.

93. Johnson, D.L.; Lynch, R.A.; Floyd, E.L.; Wang, J.; Bartels, J.N. Indoor air quality in classrooms: Environmental measures and effective ventilation rate modeling in urban elementary schools. *Build. Environ.* **2018**, *136*, 185–197.

94. Stafford, T.M. Indoor air quality and academic performance. *J. Environ. Econ. Manage.* **2015**, *70*, 34–50.

95. Simons, E.; Hwang, S.-A.; Fitzgerald, E.F.; Kielb, C.; Lin, S. The impact of school building conditions on student absenteeism in upstate New York. *Am. J. Public Health* **2010**, *100*, 1679–1686.

96. Wargocki, P.; Wyon, D.P. The effects of moderately raised classroom temperatures and classroom ventilation rate on the performance of schoolwork by children (RP-1257). *Hvac&R Res.* **2007**, *13*, 193–220.

97. Wargocki, P.; Wyon, D.P. Providing better thermal and air quality conditions in school classrooms would be cost-effective. *Build. Environ.* **2013**, *59*, 581–589.

98. Salthammer, T.; Uhde, E.; Schripp, T.; Schieweck, A.; Morawska, L.; Mazaheri, M.; Clifford, S.; He, C.; Buonanno, G.; Querol, X. Children's well-being at schools: Impact of climatic conditions and air pollution. *Environ. Int.* **2016**, *94*, 196–210.

99. Bakó-Biró, Z.; Clements-Croome, D.J.; Kochhar, N.; Awbi, H.B.; Williams, M.J. Ventilation rates in schools and pupils' performance. *Build. Environ.* **2012**, *48*, 215–223.

100. Cao, G.; Awbi, H.; Yao, R.; Fan, Y.; Sirén, K.; Kosonen, R.; Zhang, J.J. A review of the performance of different ventilation and airflow distribution systems in buildings. *Build. Environ.* **2014**, *73*, 171–186.

101. Müller, D.; Kandzia, C.; Kosonen, R.; Melikov, A.K.; Nielsen, P.V. *Mixing Ventilation Guide on mixing air distribution design*; Rehva, Federation of European Heating and Air-conditioning Associations. **2013**.

102. Novoselac, A.; Srebric, J. Comparison of air exchange efficiency and contaminant removal effectiveness as IAQ indices. *Trans. Soc. Heat. Refrig. Air Cond. Eng.* **2003**, *109*, 339–349.

103. Mustakallio, P.; Kosonen, R. Indoor air quality in classroom with different air distribution systems. *Indoor Air* **2011**, 5–10.

104. Kosonen, R.; Mustakallio, P. Ventilation in classroom: a Case-study of the performance of different air distribution methods. In Proceedings of the Proceedings of 10th REHVA World Congress-Clima. **2010**.

105. Morawska, L.; Cao, J. Airborne transmission of SARS-CoV-2: The world should face the reality. *Environ. Int.* **2020**, *139*, 105730.

106. Makris, R.; Kopic, C.; Schumann, L.; Kriegel, M. A Comprehensive Index for Evaluating the Effectiveness of Ventilation-Related Infection Prevention Measures with Energy Considerations: Development and Application Perspectives. *Indoor Air* **2024**, *2024*.

107. Zhang, S.; Lin, Z. Dilution-based evaluation of airborne infection risk-Thorough expansion of Wells-Riley model. *Build. Environ.* **2021**, *194*, 107674.

108. Aliabadi, A.A.; Rogak, S.N.; Bartlett, K.H.; Green, S.I. Preventing airborne disease transmission: review of methods for ventilation design in health care facilities. *Adv. Prev. Med.* **2011**, *2011*, 124064.

109. Ai, Z.T.; Melikov, A.K. Airborne spread of expiratory droplet nuclei between the occupants of indoor environments: A review. *Indoor Air* **2018**, *28*, 500–524.

110. Asadi, S.; Bouvier, N.; Wexler, A.S.; Ristenpart, W.D. The coronavirus pandemic and aerosols: Does COVID-19 transmit via expiratory particles? *Aerosol Sci. Technol.* **2020**, *54*, 635–638.

111. Yang, B.; Melikov, A.K.; Kabanshi, A.; Zhang, C.; Bauman, F.S.; Cao, G.; Awbi, H.; Wigö, H.; Niu, J.; Cheong, K.W.D. A review of advanced air distribution methods-theory, practice, limitations and solutions. *Energy Build.* **2019**, *202*, 109359.

112. ISO/TC 163; CEN/TC 89 ISO 12569:2017 Thermal performance of buidlings and materials. *Determ. Specif. airflow rate Build. - Tracer gas dilution method* **2017**.

113. ISO/TC 146 ISO 16000-8:2007 Indoor air - Part 8: *Determ. local mean ages air Build. Charact. Vent. Cond.* **2007**.

114. EN Standard. 16798-3. Energy performance of buildings - Ventilation for buildings - Part 3: For non-residential buildings. *Perform. Requir. Vent. room-conditioning Syst. (Modules M5-1, M5-4).* **2017**.

115. Kurnitski, J.; Kiil, M.; Wargocki, P.; Boerstra, A.; Seppänen, O.; Olesen, B.; Morawska, L. Respiratory infection risk-based ventilation design method. *Build. Environ.* **2021**, *206*, 108387.

116. Nordic Ventilation Group; Rehva Technology and Research Committee COVID-19 Task Force Nordic Ventilation Group proposal for post-COVID target ventilation rates. Health-based target ventilation rates and design method for reducing exposure to airborne respiratory infectious diseases. *Rehva* **2022**.

117. Kiil, M.; Mikola, A.; Võsa, K.-V.; Simson, R.; Kurnitski, J. Point source Ventilation Effectiveness of mixing ventilation solutions used in non-residential Settings. In Proceedings of the Indoor Air , July 7-11, 2024, Honolulu, Hawaii, USA; E3S Web of Conferences [forthcoming]. **2024**.

118. Flahault, A.; Calmy, A.; Costagliola, D.; Drapkina, O.; Eckerle, I.; Larson, H.J.; Legido-Quigley, H.; Noakes, C.; Kazatchkine, M.; Kluge, H. No time for complacency on COVID-19 in Europe. *Lancet* **2023**, *401*, 1909–1912.

119. Li, Y.; Cheng, P.; Liu, L.; Li, A.; Jia, W.; Zhang, N. Predicting building ventilation performance in the era of an indoor air crisis. In Proceedings of the Building Simulation; National Library of Medicine, **2023**; Vol. 16, pp. 663–666.

120. Li, Y.; Leung, G.M.; Tang, J.W.; Yang, X.; Chao, C.Y.; Lin, J.Z.; Lu, J.W.; Nielsen, P.V.; Niu, J.; Qian, H. Role of ventilation in airborne transmission of infectious agents in the built environment-a multidisciplinary systematic review. *Indoor Air* **2007**, *17*, 2–18.

121. Gormley, M.; Marawska, L.; Milton, D. It is time to address airborne transmission of coronavirus disease 2019 (COVID-19). *Clin. Infect. Dis.* **2020**, *71*, 2311–2313.

122. Qian, H.; Miao, T.; Liu, L.; Zheng, X.; Luo, D.; Li, Y. Indoor transmission of SARS-CoV-2. *Indoor Air* **2021**, *31*, 639–645.

123. Morawska, L.; Allen, J.; Bahnfleth, W.; Bennett, B.; Bluyssen, P.M.; Boerstra, A.; Buonanno, G.; Cao, J.; Dancer, S.J.; Floto, A. Mandating indoor air quality for public buildings. *Science (80-.).* **2024**, *383*, 1418–1420.

124. Lichtner, E.; Kriegel, M. Pathogen spread and air quality indoors-ventilation effectiveness in a classroom. **2021**.

125. Zhang, J. Integrating IAQ control strategies to reduce the risk of asymptomatic SARS CoV-2 infections in classrooms and open plan offices. *Sci. Technol. Built Environ.* **2020**, *26*, 1013–1018.

126. Rehva Health-based target ventilation rates and design method for reducing exposure to airborne respiratory infectious diseases. REHVA proposal for post-COVID target ventilation rates. *Rehva* **2023**.

127. Liu, L.; Li, Y.; Nielsen, P.V.; Wei, J.; Jensen, R.L. Short-range airborne transmission of expiratory droplets between two people. *Indoor Air* **2017**, *27*, 452–462.

128. Su, W.; Yang, B.; Melikov, A.; Liang, C.; Lu, Y.; Wang, F.; Li, A.; Lin, Z.; Li, X.; Cao, G. Infection probability under different air distribution patterns. *Build. Environ.* **2022**, *207*, 108555.

129. Tan, S.; Zhang, Z.; Maki, K.; Fidkowski, K.J.; Capecelatro, J. Beyond well-mixed: A simple probabilistic model of airborne disease transmission in indoor spaces. *Indoor Air* **2022**, *32*, e13015.

130. Yan, Y.; Li, X.; Fang, X.; Tao, Y.; Tu, J. A spatiotemporal assessment of occupants' infection risks in a multi-occupants space using modified Wells–Riley model. *Build. Environ.* **2023**, *230*, 110007.

131. Son, S.; Jang, C.-M. Effects of internal airflow on IAQ and cross-infection of infectious diseases between students in classrooms. *Atmos. Environ.* **2022**, *279*, 119112.

132. Singer, B.C.; Zhao, H.; Preble, C. V; Delp, W.W.; Pantelic, J.; Sohn, M.D.; Kirchstetter, T.W. Measured influence of overhead HVAC on exposure to airborne contaminants from simulated speaking in a meeting and a classroom. *Indoor Air* **2022**, *32*, e12917.

133. Vouriot, C.V.M.; van Reeuwijk, M.; Burridge, H.C. Robustness of point measurements of carbon dioxide concentration for the inference of ventilation rates in a wintertime classroom. *Indoor Environ.* **2024**, *1*, 100004.

134. Batterman, S. Review and extension of CO2-based methods to determine ventilation rates with application to school classrooms. *Int. J. Environ. Res. Public Health* **2017**, *14*, 145.

135. Chung, K.-C.; Hsu, S.-P. Effect of ventilation pattern on room air and contaminant distribution. *Build. Environ.* **2001**, *36*, 989–998.

136. Noakes, C.J.; Sleigh, P.A. Mathematical models for assessing the role of airflow on the risk of airborne infection in hospital wards. *J. R. Soc. Interface* **2009**, *6*, S791–S800.

137. Nicas, M.; Nazaroff, W.W.; Hubbard, A. Toward understanding the risk of secondary airborne infection: emission of respirable pathogens. *J. Occup. Environ. Hyg.* **2005**, *2*, 143–154.

138. Gammaitoni, L.; Nucci, M.C. Using a mathematical model to evaluate the efficacy of TB control measures. *Emerg. Infect. Dis.* **1997**, *3*, 335.

139. Yang, W.; Marr, L.C. Dynamics of airborne influenza A viruses indoors and dependence on humidity. *PLoS One* **2011**, *6*, e21481.

140. Ueki, H.; Furusawa, Y.; Iwatsuki-Horimoto, K.; Imai, M.; Kabata, H.; Nishimura, H.; Kawaoka, Y. Effectiveness of face masks in preventing airborne transmission of SARS-CoV-2. *MSphere* **2020**, *5*.

141. Thatcher, T.L.; Lai, A.C.K.; Moreno-Jackson, R.; Sextro, R.G.; Nazaroff, W.W. Effects of room furnishings and air speed on particle deposition rates indoors. *Atmos. Environ.* **2002**, *36*, 1811–1819.

142. Diapouli, E.; Chaloulakou, A.; Koutrakis, P. Estimating the concentration of indoor particles of outdoor origin: A review. *J. Air Waste Manage. Assoc.* **2013**, *63*, 1113–1129.

143. Coleman, K.K.; Tay, D.J.W.; Tan, K. Sen; Ong, S.W.X.; Koh, M.H.; Chin, Y.Q.; Nasir, H.; Mak, T.M.; Chu, J.J.H.; Milton, D.K. Viral Load of SARS-CoV-2 in Respiratory Aerosols Emitted by COVID-19 Patients while Breathing, Talking, and Singing. *medRxiv* **2021**.

144. Fears, A.C.; Klimstra, W.B.; Duprex, P.; Hartman, A.; Weaver, S.C.; Plante, K.C.; Mirchandani, D.; Plante, J.A.; Aguilar, P. V; Fernandez, D. Comparative dynamic aerosol efficiencies of three emergent coronaviruses and the unusual persistence of SARS-CoV-2 in aerosol suspensions. *medRxiv* **2020**.

145. Van Doremalen, N.; Bushmaker, T.; Morris, D.H.; Holbrook, M.G.; Gamble, A.; Williamson, B.N.; Tamin, A.; Harcourt, J.L.; Thornburg, N.J.; Gerber, S.I. Aerosol and surface stability of SARS-CoV-2 as compared with SARS-CoV-1. *N. Engl. J. Med.* **2020**, *382*, 1564–1567.

146. Miller, S.L.; Nazaroff, W.W.; Jimenez, J.L.; Boerstra, A.; Buonanno, G.; Dancer, S.J.; Kurnitski, J.; Marr, L.C.; Morawska, L.; Noakes, C. Transmission of SARS-CoV-2 by inhalation of respiratory aerosol in the Skagit Valley Chorale superspreading event. *Indoor Air* **2020**.

147. Buonanno, G.; Stabile, L.; Morawska, L. Estimation of airborne viral emission: Quanta emission rate of SARS-CoV-2 for infection risk assessment. *Environ. Int.* **2020**, *141*, 105794.

148. Buonanno, G.; Morawska, L.; Stabile, L. Quantitative assessment of the risk of airborne transmission of SARS-CoV-2 infection: prospective and retrospective applications. *Environ. Int.* **2020**, *145*, 106112.

149. Sun, Y.; Wang, Z.; Zhang, Y.; Sundell, J. In China, students in crowded dormitories with a low ventilation rate have more common colds: evidence for airborne transmission. *PLoS One* **2011**, *6*, e27140.

150. Bueno de Mesquita, P.J.; Noakes, C.J.; Milton, D.K. Quantitative aerobiologic analysis of an influenza human challenge-transmission trial. *Indoor Air* **2020**, *30*, 1189–1198.

151. Adams, W.C. Measurement of breathing rate and volume in routinely performed daily activities. *Final Rep. Contract.* **1993**.

152. Binazzi, B.; Lanini, B.; Bianchi, R.; Romagnoli, I.; Nerini, M.; Gigliotti, F.; Duranti, R.; Milic-Emili, J.; Scano, G. Breathing pattern and kinematics in normal subjects during speech, singing and loud whispering. *Acta Physiol.* **2006**, *186*, 233–246.

153. Morawska, L.; Allen, J.; Bahnfleth, W.; Bluyssen, P.M.; Boerstra, A.; Buonanno, G.; Cao, J.; Dancer, S.J.; Floto, A.; Franchimon, F. A paradigm shift to combat indoor respiratory infection. *Science (80-.).* **2021**, *372*, 689–691.

154. Shen, J.; Kong, M.; Dong, B.; Birnkrant, M.J.; Zhang, J. A systematic approach to estimating the effectiveness of multi-scale IAQ strategies for reducing the risk of airborne infection of SARS-CoV-2. *Build. Environ.* **2021**, *200*, 107926.

155. Kurnitski, J.; Kiil, M.; Mikola, A.; Vosa, K.-V.; Aganovic, A.; Schild, P.; Seppänen, O. Post-COVID ventilation design: Infection risk-based target ventilation rates and point source ventilation effectiveness. *Energy Build.* **2023**, *296*, 113386.

156. Guo, Y.; Zhang, N.; Hu, T.; Wang, Z.; Zhang, Y. Optimization of energy efficiency and COVID-19 pandemic control in different indoor environments. *Energy Build.* **2022**, *261*, 111954.

157. The Lancet COVID-19 Commission *Proposed Non-infectious Air Delivery Rates (NADR) for Reducing Exposure to Airborne Respiratory Infectious Diseases. November 2022*. **2022**.

158. EN 15251:2007 Indoor environmental input parameters for design and assessment of energy performance of buildings addressing indoor air quality, thermal environment, lighting and acoustics. **2007**.

159. Standard, I.S.O. 7726 (1998) "Ergonomics of the thermal environment-Instruments for measuring physical quantities." *Int. Organ. Stand. Geneva, Switz.* **1998**.

160. Dantec Dynamics A/S ComfortSense Probes Available online: https://www.dantecdynamics.com/product-category/thermal-comfort/comfortsense-probes/.

161. Regulation nr 258 Minimum energy performance requirements. **2007**.

162. Dantec Dynamics ComfortSense specification Available online: https://www.dantecdynamics.com/solutions/thermal-comfort/comfortsense/ (accessed on Nov 23, 2023).

163. EN 15726:2011 Ventilation for buildings - Air diffusion - Measurements in the occupied zone of air-conditioned/ventilated rooms to evaluate thermal and acoustic conditions. **2011**.

164. EMHI Observation data Available online: https://www.ilmateenistus.ee/ilm/ilmavaatlused/vaatlusandmed/tunniandmed/?lang=en (accessed on Mar 16, 2020).

165. Google Forms Available online: https://www.google.com/forms/about/.

166. Onset Computer Corporation HOBO Temperature/Relative Humidity/2 External Channel Data Logger Available online: https://www.onsetcomp.com/products/data-loggers/u12-013/.

167. Produal International Room controller HLS 44 Available online: https://www.produal.com/sku-1150250.html.

168. WOLF Anlagen-Technik GmbH & Co. KG Duct Temperature Sensor NTC5k Available online: https://www.wolf.eu/fileadmin/Wolf_Daten/Dokumente/Technische_Dokus_E N/Airhandling/CONTROL_SYSTEM_AIR_HANDLING_-_WRS-K_201806.pdf.

169. EVS/TC 27 EVS 906:2018 Ventilation for non-residential buildings. *Perform. Requir. Vent. room-conditioning Syst. Est. Natl. Annex EVS-EN 16798-32017.* **2017**.

170. Tark, T.; Valgma, I. Audit of ventilation systems in educational institutions in Tallinn. **2021**.

171. SAF Tehnika JSC Aranet4 TDSPC0H3 data logger Available online: https://aranet.com/about-us/.

172. Testo SE & Co. KGaA Testo 440 dP datasheet Available online: https://www.testo.com/en-US/testo-440-dp/p/0560-4402.

173. KERN & SOHN GmbH Kern FKB datasheet Available online: https://www.kern-sohn.com/en/FKB.

174. Kiil, M.; Simson, R.; Võsa, K.-V.; Kesküll, A.; Kurnitski, J. Assessment of SARS-CoV-2 Transmission in Room with Mixing Ventilation Using CO2 Tracer Gas Technique. In Proceedings of the Healthy Buildings America 2021, Honolulu, Hawaii, USA, January 18-20, 2022; International Society of Indoor Air Quality and Climate (ISIAQ). **2021**.

175. Mikola, A.; Kiil, M.; Võsa, K.-V.; Ejaz, M.F.; Kilpeläinen, S.; Kosonen, R.; Kurnitski, J. Ventilation effectiveness measurements and CFD simulations in classrooms for infection risk control. In Proceedings of the 17th Roomvent Conference, April 22-25, 2024, Stockholm, Sweden; E3S Web of Conferences. **2024**.

176. Mikola, A.; Kiil, M.; Võsa, K.-V.; Kurnitski, J. Infection Risk-Based Ventilation Assessment in Cruise Ship Common Spaces Using Tracer Gas. In Proceedings of the 17th Roomvent Conference, April 22-25, 2024, Stockholm, Sweden; E3S Web of Conferences. **2024**.

177. Jones, B.; Sharpe, P.; Iddon, C.; Hathway, E.A.; Noakes, C.J.; Fitzgerald, S. Modelling uncertainty in the relative risk of exposure to the SARS-CoV-2 virus by airborne aerosol transmission in well mixed indoor air. *Build. Environ.* **2021**, *191*, 107617.

178. Wang, J.; Wang, Z.; de Dear, R.; Luo, M.; Ghahramani, A.; Lin, B. The uncertainty of subjective thermal comfort measurement. *Energy Build.* **2018**, *181*, 38–49, doi:10.1016/J.ENBUILD.2018.09.041.

179. Virta, M.; Butler, D.; Gräslund, J.; Hogeling, J.; Kristiansen, E.L.; Reinikainen, M.; Svensson, G. *Chilled beam application guidebook*; Rehva, Federation of European Heating and Air-conditioning Associations, **2007**; ISBN 1523115777.

180. 156, C. CR 1752:1998 Ventilation for buildings. *Des. criteria indoor Environ.* **1998**.

181. Skistad, H.; Mundt, E.; Nielsen, P. V.; Hagström, K.; Railio, J. *Displacement Ventilation in Non-industrial Premises*; Rehva, Federation of European Heating and Air-conditioning Associations. **2004**.

182. Virta, M.; Hovorka, F.; Kurnitski, J.; Litiu, A. *HVAC in Sustainable Office Buildings*; Rehva, Federation of European Heating and Air-conditioning Associations. **2012**.

183. Aganovic, A.; Cao, G.; Kurnitski, J.; Melikov, A.; Wargocki, P. Zonal modeling of air distribution impact on the long-range airborne transmission risk of SARS-CoV-2. *Appl. Math. Model.* **2022**, *112*, 800–821.

184. Kiil, M.; Valgma, I.; Võsa, K.-V.; Simson, R.; Mikola, A.; Tark, T.; Kurnitski, J. Ventilation effectiveness in classroom infection risk control. In Proceedings of the E3S Web of Conferences; EDP Sciences, **2023**; Vol. 396, p. 1043.

185. OpenAI GPT-4 Technical Report, Dec 2024 Available online: http://arxiv.org/abs/2303.08774.

Acknowledgements

Abstract

Draught and infection risk control in modern educational and office spaces

Thermal comfort and draught rates have been widely studied, mostly under controlled conditions rather than in real-world settings. Proper building design should balance thermal comfort and energy efficiency, but dissatisfaction with indoor conditions often leads to corrective actions that increase energy consumption. Given the complexity of modern HVAC systems, evaluating whether design intent is achieved in new office buildings is essential. In Estonia, research on office thermal comfort is limited. Although ventilation benefits for health and learning in classrooms are well-known, issues with air quality, air change rates, and velocities persist. Achieving effective ventilation at reasonable air change rates is challenging due to non-uniform air distribution patterns.

This thesis presents thermal comfort and draught rate assessments in five modern office buildings in Tallinn, each with distinct HVAC systems. All buildings, less than six years old, were equipped with outdoor air ventilation and room conditioning units. Measurements included draught, room, and supply air temperatures, alongside occupant surveys, to evaluate system performance against actual conditions. Both short- and long-term data highlighted operational issues, suggesting areas for improvement. Additionally, typical Estonian classroom air distribution was studied in a lab setting using CO_2 tracer gas to assess air change efficiency and contaminant removal. A new ventilation effectiveness method was also developed and tested in 22 rooms, utilizing point-source measurements to quantify infection risk, providing a novel single-parameter indicator for spatial concentration and risk assessment.

Results indicate that standard thermal comfort criteria do not fully align with actual occupant experiences. Excessive overheating was noted during the heating season, despite low air velocities. Radiant ceiling panels had the lowest velocities, while active chilled beams met category II standards. Thermally activated systems showed the most overheating, with occupants satisfied at lower temperatures (23–25 °C) due to lighter clothing (0.7 clo). The mock-up classroom air distribution efficiency varied, with contaminant removal effectiveness ranging from 0.6 to 1.7, influenced by source location. Ceiling diffusers and vertical supply grilles posed a higher draught risk, while perforated duct diffusers showed acceptable air velocities. Full mixing was not achieved with point sources, indicating the need for increased air change rates to ensure adequate ventilation effectiveness. The extended non-residential room type study indicated, that simple ventilation effectiveness calculations at breathing height consistently required higher ventilation rates compared to quanta-based methods.

Choosing a specific room conditioning unit or system does not necessarily ensure a better thermal environment without draught. While some HVAC systems in this study should theoretically enhance comfort, this was not consistently the case across buildings. To reduce overheating, a control suggestions for adjusting room temperature control based on outdoor mean temperature and supply air temperature based on extract air temperature was proposed. A ventilation effectiveness measurement method for the breathing zone using at least two point sources is suggested for infection risk-based design. In some large spaces, required ventilation rates exceeded 10%, with a maximum difference of 39%, indicating room for improvement. Ventilation effectiveness values from 0.5 to 1.4 show significant potential for optimization.

Lühikokkuvõte

Tõmbus- ja nakkusriski juhtimine kaasaegsetel haridus- ja büroopindadel

Soojuslikku mugavust ja tõmbust on laialdaselt uuritud, enamasti kontrollitud tingimustes, vähem tegelikes töötingimustes. Korrektne hoone projekteerimine peaks tasakaalustama soojuslikku mugavust ja energiatõhusust, kuid rahulolematus soojusliku sisekliimaga viib sageli parandusmeetmeteni, mis suurendavad energiatarbimist. Arvestades kaasaegsete kütte-, ventilatsiooni- ja jahutussüsteemide (KVJ) keerukust, on oluline hinnata, kas uutes büroohoonetes on projekteerimise eesmärk saavutatud. Kuigi ventilatsiooni eelised tervisele ja õppetööle klassiruumides on hästi teada, on endiselt probleeme õhuvahetuse efektiivsuse ja tõmbusega. Tõhusa ja mugava ventilatsiooni samaaegne saavutamine on ebaühtlaste õhujaotusmustrite tõttu keeruline ülesanne.

Käesolevas doktoritöös esitatakse soojusliku mugavuse ja tõmbuse mõõtmistulemused viies Tallinna kaasaegses büroohoones, millest igaühel on erinevad KVJ-süsteemid. Uuritud hooned olid varustatud mehaaniliste sissepuhke-väljatõmbe ventilatsiooni- ja ruumi konditsioneerimisseadmetega. Mõõtmised hõlmasid tõmbust ja ruumi õhu- ning sissepuhkeõhu temperatuure ja kasutajate küsitlusi. Nii lühi- kui ka pikaajalised andmed tõid esile mitmeid toimivuse parendamise võimalusi. Lisaks uuriti Eesti tüüpilist klassiruumi õhujaotust laboritingimustes, kasutades CO_2 märkegaasi meetodit, et hinnata õhuvahetuse efektiivsust ja saasteainete eemaldamise efektiivsust. Samuti töötati välja ja katsetati kokku 22 ruumis uut meetodit, kasutades nakkusriski kvantifitseerimiseks punktallika mõõtmisi, pakkudes uudset üheparameetrilist indikaatorit ruumilise kontsentratsiooni ja riskihindamise jaoks.

Tulemused näitavad, et standardsed soojusliku mugavuse kriteeriumid ei pruugi olla kasutajatega kooskõlas. Vaatamata madalatele õhukiirustele täheldati kütteperioodil liigset üle kütmist. Kiirguspaneelidega fikseeriti väikseimad kiirused, samas kui aktiivjahutustalad vastasid II kategooria standarditele. Enim kasulikku põrandapinda kaotati tõmbust vältides ventilaatorkonvektoritega jahutades. Termoaktiveeritud tarinditega süsteem näitas kõige enam ülekuumenemist, kus kasutajad olid rahul õhutemperatuuridega (23–25 °C) tänu õhemale riietusele (0,7 clo). Klassiruumi saasteainete eemaldamise efektiivsus oli vahemikus 0,6 kuni 1,7, mida mõjutas saasteallika asukoht. Taldrikplafoonid ja vertikaalsed restid kujutasid endast suuremat tõmbuse riski, samas kui suudmikanalitel oli vastuvõetav õhukiirus. Punktallikatega ei saavutatud täielikku segunemist, mis viitab vajadusele suurendada ventilatsiooni, et tagada piisav õhuvahetus. Laiendatud mitteeluruumide uuring näitas, et lihtsad ventilatsiooni efektiivsuse arvutused hingamiskõrgusel nõuavad järjekindlalt kõrgemaid ventilatsioonimäärasid võrreldes *quanta*-põhiste meetoditega.

Konkreetne ruumi KVJ-süsteem ei taga tingimata paremat keskkonda vältides tõmbust. Talvise ülekütmise vähendamiseks pakuti välja juhtimissoovitused õhutemperatuuri reguleerimiseks vastavalt libisevale välisõhu keskmisele õhutemperatuurile ja sissepuhkeõhu temperatuurile väljatõmbetemperatuuri järgi. Nakkusriskipõhiseks projekteerimiseks on soovitatav kasutada hingamistsooni ventilatsiooni efektiivsuse mõõtmise meetodit, kasutades vähemalt kahte punktallikat. Suuremates ruumides ületasid nõutavad ventilatsioonimäärad 10%, kusjuures maksimaalne erinevus oli 39%, mis näitab parendusruumi. Ventilatsiooni efektiivsuse väärtused 0,5–1,4 näitavad märkimisväärset optimeerimispotentsiaali.

Appendix 1

Article

A Comparative Study on Cooling Period Thermal Comfort Assessment in Modern Open Office Landscape in Estonia

Martin Kiil [1],*, Raimo Simson [1] , Martin Thalfeldt [1] and Jarek Kurnitski [1,2]

[1] Department of Civil Engineering and Architecture, Tallinn University of Technology, Ehitajate tee 5, 19086 Tallinn, Estonia; raimo.simson@taltech.ee (R.S.); martin.thalfeldt@taltech.ee (M.T.); jarek.kurnitski@taltech.ee (J.K.)
[2] School of Engineering, Aalto University, Otakaari 4, 02150 Espoo, Finland
* Correspondence: martin.kiil@taltech.ee

check for updates

Abstract: Local thermal comfort and draught rate has been studied widely. There has been more meaningful research performed in controlled boundary condition situations than in actual work environments involving occupants. Thermal comfort conditions in office buildings in Estonia have been barely investigated in the past. In this paper, the results of thermal comfort and draught rate assessment in five office buildings in Tallinn are presented and discussed. Studied office landscapes vary in heating, ventilation and cooling system parameters, room units, and elements. All sample buildings were less than six years old, equipped with dedicated outdoor air ventilation system and room conditioning units. The on-site measurements consisted of thermal comfort and draught rate assessment with indoor climate questionnaire. The purpose of the survey is to assess the correspondence between heating, ventilation and cooling system design, and the actual situation. Results show, whether and in what extent the standard-based criteria for thermal comfort is suitable for actual usage of the occupants. Preferring one room conditioning unit type or system may not guarantee better thermal environment without draught. Although some heating, ventilation and cooling systems observed in this study should create the prerequisites for ensuring more comfort, results show that this is not the case for all buildings in this study.

1. Introduction

Modern low energy office buildings require energy efficient heating, ventilation, and air conditioning (HVAC) systems which can provide comfortable and healthy indoor environment. In temperate climate countries, mechanical ventilation and active cooling systems are common practice in such buildings. However, mechanical HVAC systems do not always provide satisfactory thermal conditions [1]. It is important to properly apply control strategies, design and install room cooling units and ventilation supply air elements, as well as to operate and maintain the systems to provide comfortable indoor climate without temperature fluctuations and draught risk in the cooling season [2–8]. Office plans, in terms of occupant positions and density, can be very different from initial design and vary significantly, resulting in changing conditions and dynamic settings which makes it difficult to design the systems adequately to ensure stable thermal environment. Open office layout design is used commonly in most office buildings mainly to allow flexibility in workspaces allocation [9]. This creates a difficult task for HVAC systems design, requiring careful planning to assure adequate conditions in the occupied zone in different layout cases.

As occupant satisfaction with thermal environment is dependent on many factors, such as gender, age, health, activity, mood, and other physiological and psychological factors, assessing thermal comfort (TC) based on temperature and air movement measurements is usually not sufficient for adequate estimation [6,10–13]. Thus, evaluation by questioning the occupants is usually also needed to specify the problems and get a comprehensive overview of the TC situation. Studies on office workers thermal sensation have shown that the predicted TC and actual sensation can differ significantly [12,14,15]. For example, gender specific analysis indicates higher dissatisfaction rates for female occupants [11,16–19]. Recent research has widely focused on individual perception of TC [20–22], developed methods to analyze the preferences for TC using machine learning algorithms [23,24] and adapt systems to provide preferable personal comfort by implementing Personalized Comfort Systems [20–22,25]. Utilization of such systems in buildings requires paradigm shifts in occupant interaction with HVAC systems as well as system design practices, integration of advanced controls and information technologies solutions [26,27].

In addition to the individual preferences and system specific aspects influencing thermal comfort (TC), there are many building related design factors that can affect the performance of HVAC systems and in turn influence the thermal environment. Of these factors, façade design, namely window sizes, layout, and glazing parameters, can have large impact on cooling load as well as radiant temperature asymmetry and thus major influence on the overall thermal conditions in the office [28,29]. Thalfeldt et al. [28] showed the importance of façade design by analyzing the effect on office buildings energy efficiency and cooling load in cold climate countries. Window-to-wall ratio (*WWR*) of 0.25 was found optimal for triple glazing window solutions. Larger glazing results in higher cooling loads and increase the need for larger room cooling units, higher cooled airflow rates or lower supply air temperatures to maintain the room temperature. The latter factors also increase the risk of draught in occupied spaces. In several studies, draught rate (*DR*) has been identified as the main cause of discomfort even if other thermal environment factors are at satisfactory levels [6,15,29,30].

Depending mainly on the cooling load, cooling plant solution, and interior design, different water based room cooling solutions are used in offices, which can be classified by supply water temperature as low temperature room cooling units e.g., fan coil units and high temperature units, such as thermally active building systems (TABS), passive cooling beams, or active cooling beams, combined with ventilation supply air terminals [31,32]. In low energy buildings, high temperature cooling is usually preferred to achieve higher energy efficiency for cooled water production by cooling plants [32]. The performance of these systems is extensively analyzed in various recent studies. Most of the research is based on either computer simulations, mainly computational fluid dynamics (CFD) studies or studies conducted in controlled laboratory environments [33–47]. The research in real office settings is mainly focused on buildings located in warm and hot climate countries, dominated by cooling need [48–51]. To the knowledge of the authors, only few extensive studies have been carried out in cold and temperate climates and in low energy buildings. In Germany, Pfafferott, Herkel, Kalz, and Zeuschner [14] have conducted research on summertime TC in 12 low energy office buildings which are passively cooled with local heat sink based TABS. Results showed, that 41% of occupants were dissatisfied with thermal environment in summer, but assessment, according to the standard CEN EN 15251 [52], showed measured indoor temperature-based classification relative to the indoor climate category I (highest) and II, indicating a gap between perceived and assessed TC conditions and the need for more detailed comfort assessment. Hens [15] investigated TC in two office buildings in Belgium cooled with active chilled beams and air-cooling systems. He found that the Fanger [53] predicted mean vote (*PMV*)/predicted percentage dissatisfied (*PPD*) curve underestimated the actual number of dissatisfied occupants and that standards should not be considered as absolute references. It was also concluded that one should be very careful when interpreting the results of TC studies.

The theoretical knowledge involved or access to expert engineers during office building design is feasible and implemented in practice in Estonia. However, the volatile quality of different parts of the design, building phase simplifications with budget cuts and the contradiction between the

initial task and the actual situation leads to a risk of an outcome failure regarding TC for the occupant. In the Estonian construction market, great emphasis is given on diplomas, professional certificates, software for both building information modeling (BIM), and product selection programs integrating BIM solutions in the building process. In reality, during the construction process the HVAC designer and after the warranty period, the constructor retreat. Therefore, in a short period of time during the design a huge effort is invested in the project definition, while after the realization phase much of the expert advice is ignored. Otherwise, complaints regarding draught or room temperature were not topical issues. In Estonia as well, in-depth research on cooling season TC and occupant satisfaction is practically non-existent, a few studies in office buildings have been conducted with the main focus on heating season performance and mostly aimed towards energy efficiency analysis. The conducted studies indicate problems and dissatisfaction with thermal environment but lack the detail to specify the causes and details of occupants' thermal conditions and HVAC systems performance in terms of room equipment.

Regardless of the design and performance of the HVAC systems installed in actual open offices, the hypothesis of this study proposes that high proportion of occupants are dissatisfied with the TC conditions. The goal of this study is to determine, whether the thermal sensation dissatisfaction of the occupants in modern office spaces is verifiable and in accordance with the valid standard criteria. This paper aims to fill the gap of summer TC assessment by extensive field studies and thorough occupant survey in modern office buildings in Estonia, a temperate climate country. We have investigated four recently constructed and one reconstructed office buildings with open plan office layouts designed with different ventilation and cooling solutions, including mixing and displacement ventilation, TABS, radiant cooling panels, fan coil units, and active cooling beams. The on-site measurements conducted in the offices consist of high resolution and accuracy temperature and air velocity measurements with *DR* and TC calculations, which are described in the following chapter.

2. Methods

The flow chart of research methodology is shown in Figure 1. Section of methods is divided between description of reference objects, measurement set-up and equipment specifications, data analysis, and indoor climate questionnaire (ICQ). We used standard-based [52,54,55] methods in this study to measure and calculate TC parameters and to perform an online ICQ survey. The TC measuring probe and tripod mobile and flexible kit set [56] we used was designed for research and development purposes.
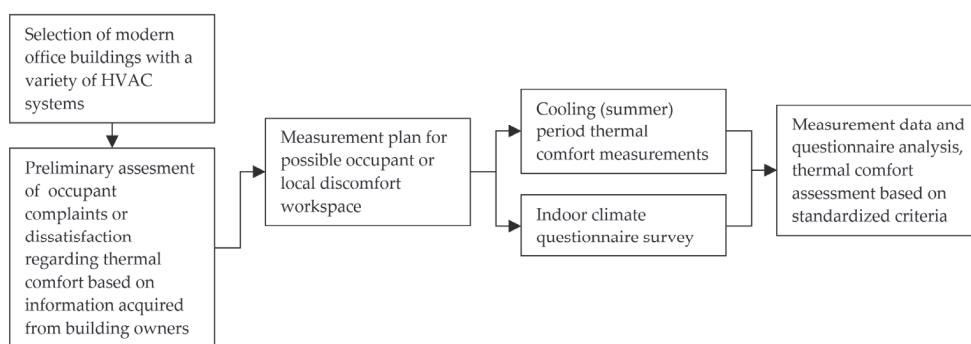
Figure 1. Flow chart of research methodology.

2.1. Reference Objects

General information regarding reference objects are provided in Table 1. The scope and range of measurement points with main building envelope characteristics, such as thermal transmittance for

main surfaces, such as walls, windows, floors on ground and roofs are listed with specific heat loss of external envelopes and window-to-wall ratios.

Table 1. General building information of reference objects.

Bldg	Year of Constr.	Net Floor Area (m²)/appr. Total Measured Area (%)	No of Floors/ No of Measured Floors	Thermal Transmittance W/(m² × K)	Specific Heat Loss of External Envelopes W/(m² × K)/Window-to-Wall Ratio/Glazing g Value
A	2015	10,800/30	13/4	U_{window} 0.80/U_{wall} 0.18 U_{roof} 0.09/U_{floor} 0.14	H/A 0.50 WWR 0.69 g 0.25
B	2018	7000/20	5/3	U_{window} 0.83/U_{wall} 0.12 U_{roof} 0.09/U_{floor} 0.13* (*above ambient air)	H/A 0.31 WWR 0.59 g 0.24
C	2017	18,900/10	14/2	U_{window} 0.65/U_{wall} 0.10 U_{roof} 0.10/U_{floor} 0.15	H/A 0.30 WWR 0.38 g 0.30
D	2018	13,900/100 (available office space)	2/2	U_{window} 1.0/U_{wall} 0.15 U_{roof} 0.14/U_{floor} < 0.15	H/A < 0.20 WWR < 0.25 g 0.30
E	Reconstr, 2014 (1982)	5300/20	6/1	U_{window} > 1.2/U_{wall} > 0.25 U_{roof} N/A/U_{floor} N/A	H/A > 0.50 WWR 0.90 g 0.40

In Buildings A, B, C, and D, measurements were also taken on the highest floor and in Buildings B and D on the lowest floor. The temperature of slabs was considered to be close to t_i and therefore the impact on operative temperature was not accounted for, as heat transmission through the building envelope in such low energy buildings is negligible compared to the heat gains through glazed surfaces and have little effect on TC. A variety of HVAC systems was involved in measurements zones (Table 2) including new and innovative solutions in the Estonian construction market.

Table 2. Heating, ventilation, and air conditioning room design solutions of reference objects.

Bldg.	Heating	Ventilation	Cooling
A	Water-based convectors (height 300 mm, length 700–1800 mm) below the windowsill. Installed room unit heating power 18 W/m².	Mixing ventilation 1.4 l/(s × m²) using active exposed chilled beams (effective length 2700–3300 mm) mounted in the open ceiling (height 2.75 m) for supply and circular valves (Ø 125 mm) for extract air (height 2.7 m).	Active exposed chilled beams (effective length 2700–3300 mm) mounted in the open ceiling (height 2.75 m). Installed room unit sensible cooling power 52 W/m².
B	Thermally active building system (slab, room height 3.0 m). Installed heating power 43 W/m².	Displacement ventilation 1.4 l/(s × m²) including duct diffusers (Ø 160–315 mm, nozzle angle 120–180 °C) for supply (height 2.7–2.8 m), mounted in the open ceiling to the perimeter of rooms. Wall and ceiling grilles with plenum box serving extract air (height 2.8 m on cornice, 2.6 m for ribbed suspended ceiling).	Thermally active building system (slab, room height 3.0 m). Installed sensible cooling power 41 W/m².
C	4-pipe active ceiling integrated chilled beams (effective length 900–1500 mm) mounted in suspended ceiling (height 2.7 m). Installed room unit heating power 17 W/m².	Mixing ventilation 1.7 l/(s × m²) using 4-pipe ceiling integrated chilled beams (effective length 900–1500 mm) for supply air and circular valves (Ø 100 mm) for extract air (height 2.7 m).	4-pipe active ceiling integrated chilled beams (effective length 900–1500 mm) mounted in suspended ceiling (height 2.7 m). Installed room unit sensible cooling power 46 W/m².
D	4-pipe radiant panels mounted in the open ceiling on the height of 2.4 m. Installed room unit heating power 24 W/m².	Mixing ventilation 2.1 l/(s × m²). Rectangular diffusers including directionally adjustable nozzles (plates 160 × 160 / 200 × 200 mm) mounted on plenum box for supply air and circular plate (Ø 200–250 mm) combined with plenum box for extract air in the open ceiling (height 2.7 m).	4-pipe radiant panels mounted in the open ceiling on the height of 2.4 m. Installed room unit sensible cooling power 10 W/m².
E	Electrical convectors (height 200 mm, length 1500 mm) in front of windows. Installed room unit heating power 60 W/m².	Mixing ventilation 1.3 l/(s × m²) with circular supply and extract air valves (Ø 160–250 mm) mounted in the suspended ceiling (height 2.5–2.7 m).	Multi-split fan coil units (without heating function) mounted in the suspended ceiling (height 2.7 m). Installed total cooling power 78 W/m². (Ventilation supply air is not chilled)

Ø: diameter of air diffuser connection duct.

The buildings involved in this study were chosen from a range of modern office spaces in Tallinn. First criteria for reference objects was the correspondence with the Estonian energy efficiency regulations, which were first set in 2007 [57]. This created the prerequisites for new buildings and

HVAC systems criteria, such as envelope related parameters, such as air tightness, external wall insulation thickness, window glazing solutions, and HVAC system parameters, e.g., effectiveness of room units and energy sources, heat recovery effectiveness, specific fan power of ventilation units etc. Buildings A and B have high temperature heating systems and district heating. Building B is using low temperature heating and a ground source heat pump, Building D has high temperature heating water produced and a gas boiler and electrical heating convectors are installed in Building E. All of the studied buildings are equipped with dedicated outdoor air ventilation systems with heat recovery. Ventilation air distribution methods were classified as mixing ventilation, except for Building B, where supply air systems were built in a way to support displacement ventilation method. Buildings A and C were using active chilled beams for supply air distribution. Buildings A, C, and D are built with chillers to supply the cooling system. In all Buildings, except for E, high temperature cooling is used in room conditioning units as supply air is dehumidified in the air handling units. Multi-split fan coil units with refrigerant without the option of heating function were in operation in Building E. Room conditioning units in Buildings C and D, including the Building B with thermally active buildings system, operated both for heating and cooling purposes.

2.2. Measurement Equipment

Experimental measurements in this study were carried out with a TC measurement system Dantec Dynamics ComfortSense [56]. The system is designed for high quality multi-point measurements of v_a, t_i, RH, and t_o. The set is equipped with software, what allows easy setup for measuring sequence and positions giving researchers a comprehensive overview if the measured data. Measurement equipment probe data is described in Table 3.

Table 3. Specifications of measuring equipment [56].

	54T33 Draft Probe	54T37 Relative Humidity Probe	54T38 Operative Temperature Probe
Image			
Range	0.05–5 m/s −20 °C to +80 °C	0–100%	0 to +45 °C
Accuracy	±0.02 m/s ±0.2 K	+1.5%	±0.2 K

The set is mounted on a tripod including five draft probes, one humidity and one t_o probe. For a sitting position, ISO standard [55] recommends measuring heights for ankle level 0.1 m, abdomen level 0.6 m, and head level 1.1 m. Conformably to Fanger and Christensen [6], mean v_a and standard deviation at three heights around the sitting occupant body were measured according to heights shown on Figure 2. RH probe was set at 1.0 m as a fixed height for measuring has not been fixed for measurements. The t_o probe was mounted with the angle of 30° at the height of 0.6 m as the abdomen level of a sitting person [55].
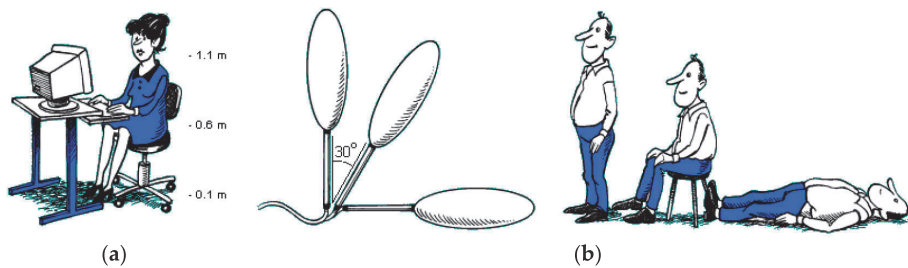
Figure 2. Recommended air velocity probe heights behind the feet, elbow, and neck for a sitting person (**a**); Recommended operative temperature probe person's angle factor to their surroundings (**b**) [58].

Probes were connected with 54N90 ComfortSense main frame [56], using 7 channels of 16. Main frame was in turn connected with laptop computer where the measurement data was stored using ComfortSense software version 4, (Dantec Dynamics A/S, Skovlunde, Denmark) [56]. Measurement period of 180 seconds as the least time recommended [59] was used.

2.3. Data Analysis

Measurement data, including t_i, v_a, *RH*, and t_o was recorded with the sampling rate 20 Hz with ComfortSense [56] and processed in Microsoft Excel. TC parameters are calculated for each measurement positions with equations for *Tu*, *DR*, *PMV*, and *PPD* followed. To assess *DR*, the fluctuation rate of v_a is described as *Tu*, which is calculated by [59]

$$Tu = \frac{SD}{v_a} \times 100 \ (\%), \tag{1}$$

where *SD* is standard deviation of measured local mean v_a (m/s) for one measurement. With t_i, v_a, and *Tu*, the percentage of people predicted to be dissatisfied because of draught may be calculated as [60]

$$DR = (34 - t_i) \times (v_a - 0.05)^{0.62} \times (0.37 \times v_a \times Tu + 3.14) \ (\%) \tag{2}$$

To predict the mean value of the subjective ratings of a group of people in a given environment, *PMV* index is used. Consisting of a set of parameters with sub-formulas, the *PMV* equation is given by [60]

$$PMV = [0.303 \times \exp(-0.036 \times M) + 0.028] \times [(M - W) - H_d - E_c - C_{res} - E_{res}] \tag{3}$$

The *PMV* index in Equation (3) was calculated using Equations (4)–(11). In the equations provided, *M* (W/m^2) is metabolic rate and *W* (W/m^2) is the effective mechanical power. Assumption of metabolic rate 1.2 met for sedentary activity for summer season provided in EN 16798-1 was used. Sedentary activity does not suppose producing effective mechanical power, therefore 0 (W/m^2) was used in analysis. The next symbol H_d in Equation (3) represents dry heat loss, which is found as

$$H_d = \frac{(mt_{sk} - t_{cl})}{I_{cl}} \left(W/m^2 \right), \tag{4}$$

where mt_{sk} is mean skin temperature [°C] and in Equation (4), t_{cl} is expressed using t$_o$ and calculated through iterative process, by

$$t_{cl} = 35.7 - 0.028 \times (M - W) - I_{cl} \times \{3.96 \times 10^{-8} \times f_{cl} \times [(t_{cl} + 273)^4 - (t_o + 273)^4] + I_{cl} \times f_{cl} \times h_c \times (t_{cl} - t_o)\} \ (°C) \tag{5}$$

In Equation (5), I_{cl} [(m^2 × K)/W] is the clothing insulation, f_{cl} is the clothing surface area factor, v_{ar} (m/s) is the relative air velocity, h_c [W/(m^2 × K)] is the convective heat transfer coefficient, and t_{cl} (°C) is the

clothing surface temperature. Clothing unit 0.5 clo for summer season provided in EN 16798-1 was used in calculations. Equation (5) includes h_c, which is given as

$$h_c = 2.38 \times |t_{cl} - t_i|^{0.25} \quad \text{for} \quad 2.38 \times |t_{cl} - t_i|^{0.25} > 12.1 \times \sqrt{v_{ar}} \quad \text{and}$$
$$12.1 \times \sqrt{v_{ar}} \quad \text{for} \quad 2.38 \times |t_{cl} - t_i|^{0.25} < 12.1 \times \sqrt{v_{ar}} \left[\text{W} / \left(\text{m}^2 \times \text{K} \right) \right], \tag{6}$$

where v_{ar} was set equal to the v_a as occupants were intended to be stationary sensing draught. Equation (5) includes f_{cl}, which is calculated by

$$f_{cl} = 1.00 + 1.290 \times I_{cl} \text{ for } I_{cl} \leq 0.078 \text{ and}$$
$$1.05 + 0.645 \times I_{cl} \text{ for } I_{cl} > 0.078 \tag{7}$$

Continuing the *PMV* index calculation, in Equation (3), evaporative heat exchange at the skin, when the person experiences a sensation of thermal neutrality E_c given as

$$E_c = 3.05 \times 10^{-3} \times [5733 - 6.99 \times (M - W) - p_a] + 0.42 \times (M - W - 58.15) \text{ (W/m}^2\text{)}, \tag{8}$$

where p_a is the water vapor partial pressure [Pa], calculated using measured *RH* by

$$p_a = \frac{RH}{100} \times 479 + (11.52 + 1.62 \times t_i)^2 \text{(Pa)}, \tag{9}$$

In addition, Equation (3) for *PMV* includes respiratory convective heat exchange C_{res}, calculated as

$$C_{res} = 0.0014 \times M \times (34 - t_i) \text{ (W/m}^2\text{)}, \tag{10}$$

and Equation (3) includes also respiratory evaporative heat exchange E_{res}, given as

$$E_{res} = 1.72 \times 10^{-5} \times M \times (5867 - p_a) \text{ (W/m}^2\text{)}, \tag{11}$$

Finally, to predict the rate of people dissatisfied in a thermal environment, the *PPD* index is used. Knowing *PMV*, *PPD* can be calculated as [60]

$$PPD = 100 - 95 \times \exp(-0.03353 \times PMV^4 - 0.2179 \times PMV^2) \tag{12}$$

Measured values are shown in Building result figures in the results chapter and used in Equations (1) and (2) for calculating *Tu* and *DR*, and in Equations (3) and (12) to calculate *PMV* and *PPD*.

2.4. Indoor Climate Questionnaire

To study occupant satisfaction we provided online questionnaires to the employees of the measured office spaces. As some organizations involved in this study are moving towards policy of a paperless work management, we used Google Forms [61] application. In addition to standard CEN EN 15251 [52] suggestions, we added also questions about age, gender, amount of time behind the desk during workday, and the working environment regarding cabinet or open office plan. The ICQ is presented in Appendix A.

2.5. On-Site Measurements

This section provides an overview of the TC measurement time and weather information (Table 4), followed by measurement results with calculated TC indicative parameters *Tu*, *DR*, *PMV*, and *PPD*. ICQ survey results are summarized at the end of the results sections.

Table 4. Time of measurements and weather information from the Estonian Weather Service [62].

Building	Time of Measurements	Weather Conditions	Maximum Outdoor Temp. °C	Mean Outdoor Temp. °C
A	06.08.2019 before midday	cloudy skies showers	+20.9	+15.2
B	14.08.2019 after midday	cloudy skies no precipitation	+19.7	+13.8
C	12.08.2019 after midday	cloudy skies light showers	+22.0	+17.3
D	29.08.2019 after midday	sunny skies no precipitation	+26.5	+20.6
E	05.08.2019 after midday	cloudy skies no precipitation	+19.7	+13.8

The experiments were carried out on regular workdays during August. Measurements were taken by two persons, by the main author of this article assisted by graduate students in different buildings. HVAC systems were in regular performance mode without disfunctions or failures recorded. Internal gains by occupants, office equipment, and lighting were in use by default as some desks were empty by unused space, duties, or vacation. No serious defects in HVAC design or construction were observed. Although, some air flow and velocity aspects were noticeable. As in Buildings A and C, active beams were in use, occupants were not always placed sitting according to rule of thumbs, according to the architectural layout, or number of persons. Possible air flow obstacles by lighting fixture (Figure 3a) were noticed with open ceiling in Building A. *DR* risk was also predictable in building E (Figure 3b) where some vanes were taped to closed position. *DR* risk was more carefully considered in Buildings B and D.

(a)   (b)

Figure 3. Possible air flow obstacles with open active beam solution (**a**); modified airflow distribution with fan coil unit (**b**).

3. Results

Based on on-site measurements, the summary of v_a in each measurement position are shown below for each Building. According to three heights provided in Figure 2, v_a values during measurement period are shown with box and whiskers plot. Minimum and maximum are at the end of the whiskers, the lower and the upper line of the box are first and third quartiles, the line between is median and the cross shows mean v_a value of the measurement in one position.

On the box and whiskers plot, the category of the indoor climate category is colored according to the lowest criteria achieved during measurements, meaning if one of the three height is in III category, the measurement point is placed in the least, III category. In the table part on the result figures below the box and whiskers plot, measured values and calculated parameters are colored according to the

category reached to be more easily distinguishable. *Tu* and *RH* measured values are not colored as being not categorized. Nonetheless, measurement point indoor climate category is defined by the inferior measured value or calculated parameter reached altogether.

3.1. Building A Results

The v_a results and TC parameters in Building A equipped with open ceiling active chilled beams are provided below in Figure 4. In Building A, in 2/3 of the measured positions the v_a was below the first indoor climate category threshold. Five positions met the II category requirement and in one position the v_a was above the category II threshold. Measurement No 14 was taken in an office space with unusually high internal gains, where also multi-split fan coil units were additionally added to the environment due to the specifics of the lessee. The results of t_i and v_a including *DR*, *PMV,* and *PPD* are placed in the first category mainly.

		1	2	3	4	5	6	7	8	9	10	11	12	13	14	15	16	17	18
$t_{i(1.1\,m)}$	°C	24.5	23.7	23.8	24.1	24.5	24.6	24.1	24.0	24.5	24.4	23.6	24.2	23.5	22.1	24.2	23.9	23.8	24.5
$v_{a(1.1\,m)}$	m/s	0.07	0.08	0.04	0.05	0.03	0.07	0.06	0.07	0.06	0.15	0.15	0.08	0.11	0.61	0.07	0.08	0.13	0.08
$Tu_{(1.1\,m)}$	%	65.3	47.9	58.0	46.9	49.5	59.4	44.3	55.0	51.4	58.7	55.0	68.3	66.6	48.2	47.9	45.9	39.1	58.9
$DR_{(1.1\,m)}$	%	4.7	5.2	0.0	0.0	0.0	4.3	1.9	4.2	2.7	15.3	15.4	5.3	10.5	100.0	4.3	5.7	10.3	4.9
$t_{i(0.6\,m)}$	°C	24.2	23.5	23.6	23.9	24.2	24.3	23.9	23.8	23.8	24.2	23.5	23.9	23.3	22.2	24.1	23.8	23.7	24.4
$t_{o(0.6\,m)}$	°C	24.7	23.7	23.8	24.3	24.6	24.7	24.2	24.1	24.6	24.7	23.9	24.1	23.6	22.9	24.2	24.2	24.1	24.7
$v_{a(0.6\,m)}$	m/s	0.04	0.08	0.03	0.02	0.03	0.09	0.06	0.07	0.03	0.15	0.08	0.05	0.12	0.43	0.04	0.06	0.10	0.08
$RH_{(0.6\,m)}$	%	50.5	52.8	54.4	52.6	51.7	52.1	51.7	52.1	50.9	52.1	55.9	53.4	49.4	52.7	52.5	53.2	55.3	54.0
$PMV_{(0.6\,m)}$	–	0.0	−0.3	−0.2	−0.1	0.0	0.0	−0.1	−0.2	0.0	−0.2	−0.2	−0.1	−0.4	−1.3	−0.1	−0.1	−0.2	0.0
$PPD_{(0.6m)}$	%	5.0	6.4	6.0	5.2	5.0	5.0	5.2	5.5	5.0	5.5	5.7	5.3	8.6	39.2	5.3	5.2	5.5	5.0

I Cat.　　II Cat.　　III Cat.　　IV Cat.

Figure 4. Building A air velocity results in measurement points 1–18 and the thermal comfort parameters.

3.2. Building B Results

The v_a results and TC parameters of Building B with slab-based TABS system are given below in Figure 5. Building B had more measured points in the second category by *PMV* and *PPD* compared to Building A. *DR* met the II category in four measurement positions. Positions 4–8 were in an office, where the ventilation rate had been doubled by the request of the lessee. These four measurements stand out above the others. Regarding the other four buildings observed, displacement ventilation effect can be seen, as v_a fluctuates more near the floor.

		1	2	3	4	5	6	7	8	9	10	11	12	13	14	15	16
$t_{i(1.1\,m)}$	°C	23.5	23.7	23.8	23.5	24.3	23.8	23.9	24.3	23.6	23.6	24.2	23.4	23.8	24.7	24.0	24.6
$v_{a(1.1\,m)}$	m/s	0.03	0.04	0.08	0.06	0.20	0.13	0.10	0.05	0.03	0.21	0.05	0.06	0.05	0.14	0.07	0.04
$Tu_{(1.1\,m)}$	%	64.2	82.9	63.4	77.4	36.4	53.3	50.7	79.9	84.2	32.6	102.3	48.1	62.2	43.9	58.9	49.7
$DR_{(1.1\,m)}$	%	0.0	0.0	5.1	3.2	17.7	12.3	8.5	1.3	0.0	18.7	1.6	2.5	1.3	11.5	4.2	0.0
$t_{i(0.6\,m)}$	°C	23.4	23.5	23.6	23.5	24.1	23.7	23.7	24.1	24.1	23.5	24.0	23.1	23.4	24.5	23.8	24.4
$t_{o(0.6\,m)}$	°C	23.4	23.9	24.1	23.5	24.4	23.8	24.0	24.3	23.6	23.7	24.5	23.3	23.8	24.7	24.3	24.3
$v_{a(0.6\,m)}$	m/s	0.02	0.04	0.09	0.11	0.13	0.12	0.11	0.06	0.02	0.19	0.03	0.07	0.04	0.10	0.06	0.03
$RH_{(0.6\,m)}$	%	49.5	50.5	49.3	50.9	46.5	45.9	45.7	45.9	46.8	47.8	47.4	48.5	46.9	47.5	49.0	47.6
$PMV_{(0.6\,m)}$	-	−0.4	−0.2	−0.2	−0.4	−0.2	−0.4	−0.3	−0.1	−0.3	−0.6	−0.1	−0.4	−0.3	0.0	−0.1	−0.1
$PPD_{(0.6\,m)}$	%	8.1	6.2	5.6	8.1	6.1	7.9	6.6	5.4	7.1	12.2	5.1	8.8	6.8	5.0	5.3	5.3

■ I Cat.　　■ II Cat.　　■ III Cat.　　■ IV Cat.

Figure 5. Building B air velocity results in measurement points 1–16 and the thermal comfort parameters.

3.3. Building C Results

Building C was equipped with suspended ceiling active chilled beams and the results of v_a and parameters of TC are presented below in Figure 6. *PMV*, *PPD*, and t_i were similar to Buildings A and

B, at the same time v_a and DR were measured at two positions in the II category and three times in the III category. The v_a is more fluctuating on the height of the sitting person neck.

		1	2	3	4	5	6	7	8	9	10	11	12	13	14	15	16	17	18	19
$t_{i(1.1\,m)}$	°C	24.8	24.3	24.3	24.1	23.8	24.1	23.7	23.9	23.8	24.1	23.4	23.7	23.4	24.3	24.3	24.4	24.0	24.3	24.0
$v_{a(1.1\,m)}$	m/s	0.06	0.07	0.08	0.06	0.16	0.04	0.08	0.09	0.21	0.06	0.21	0.12	0.15	0.03	0.10	0.23	0.10	0.09	0.09
$Tu_{(1.1\,m)}$	%	62.8	45.2	74.6	65.0	56.8	105.3	66.4	77.6	54.5	79.0	47.9	37.9	36.6	51.8	41.7	47.7	42.9	79.0	61.8
$DR_{(1.1\,m)}$	%	3.0	3.9	5.5	2.9	17.4	0.0	5.8	7.7	23.5	3.5	22.8	9.9	13.5	0.0	6.6	24.2	7.5	7.8	6.9
$t_{i(0.6\,m)}$	°C	24.5	24.1	24.0	23.9	23.9	23.9	23.4	23.9	23.9	24.0	23.5	23.5	23.4	24.0	24.2	24.3	23.9	24.2	23.8
$t_{o(0.6\,m)}$	°C	24.8	24.4	24.5	24.3	24.0	24.0	23.7	24.1	24.3	24.3	23.8	23.9	23.7	23.9	24.5	24.7	24.3	24.3	24.2
$v_{a(0.6\,m)}$	m/s	0.07	0.07	0.12	0.11	0.11	0.06	0.10	0.12	0.16	0.06	0.13	0.12	0.14	0.05	0.07	0.14	0.08	0.08	0.09
$RH_{(0.6\,m)}$	%	53.3	57.5	57.3	58.0	57.7	58.0	56.7	57.0	56.0	56.2	56.5	56.5	57.0	52.0	54.2	53.6	54.0	52.5	54.5
$PMV_{(0.6\,m)}$	-	0.1	0.0	−0.1	−0.1	−0.2	−0.1	−0.3	−0.2	−0.3	−0.1	−0.3	−0.3	−0.4	−0.2	0.0	−0.1	−0.1	−0.1	−0.1
$PPD_{(0.6\,m)}$	%	5.2	5.0	5.1	5.2	6.0	5.4	6.4	5.7	6.9	5.1	7.2	6.5	8.3	5.8	5.0	5.2	5.1	5.2	5.3

■ I Cat. ■ II Cat. ■ III Cat. ■ IV Cat.

Figure 6. Building C air velocity results in measurement points 1–19 and the thermal comfort parameters.

3.4. Building D Results

Equipped with radiant cooling panels, results of v_a and parameters of TC in Building D are showed below in Figure 7. Compared to other buildings, Building D with the least number of positions had the best results on all analyzed parameters. In all cases, I category DR was achieved. At all times, mean v_a remained below 0.10 m/s being more fluctuating near the floor.

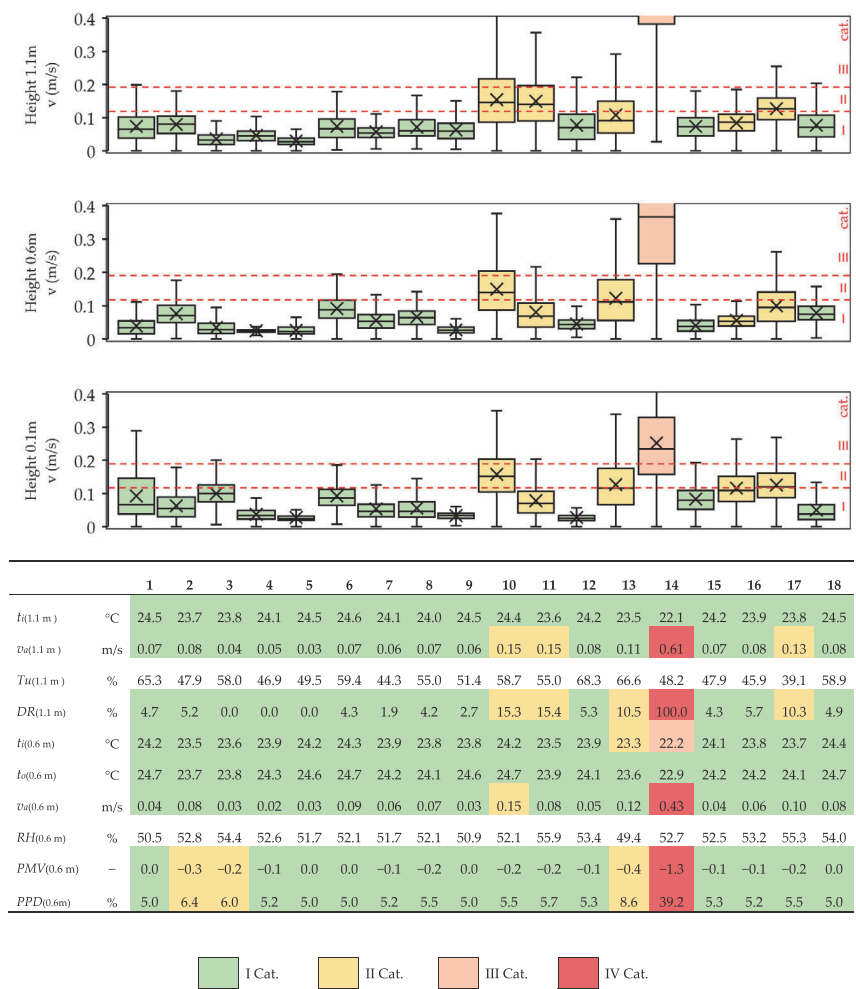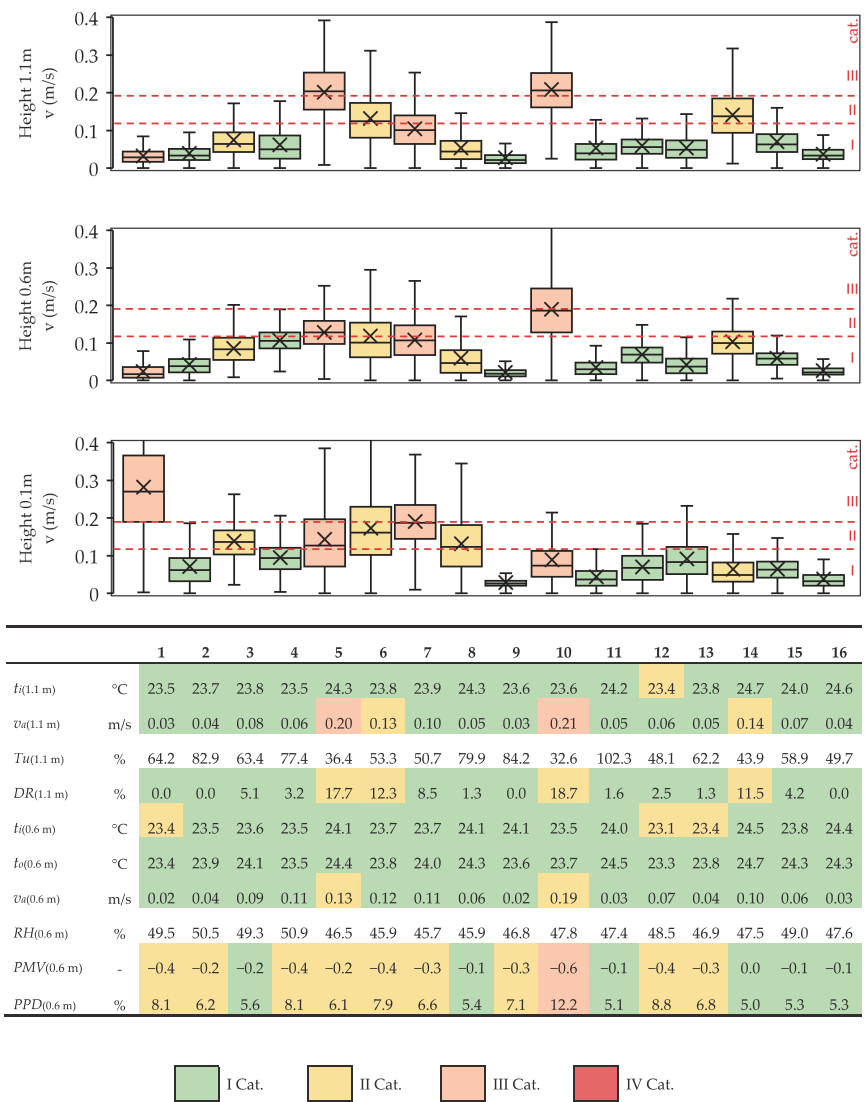|		1	2	3	4	5	6	7	8	9	10	11
$t_{i(1.1\,m)}$	°C	24.8	24.2	24.2	24.2	24.2	24.2	23.3	23.6	24.5	23.9	23.4
$v_{a(1.1\,m)}$	m/s	0.07	0.09	0.08	0.05	0.03	0.06	0.06	0.03	0.06	0.07	0.06
$Tu_{(1.1\,m)}$	%	53.5	47.5	66.6	72.1	66.1	73.6	62.7	84.2	58.8	59.9	48.1
$DR_{(1.1\,m)}$	%	3.2	6.8	5.5	0.0	0.0	2.4	2.9	0.0	2.9	3.6	2.5
$t_{i(0.6\,m)}$	°C	24.4	24.0	24.1	24.0	24.1	24.1	23.4	23.4	23.4	23.5	23.1
$t_{o(0.6\,m)}$	°C	24.3	23.8	24.0	24.0	24.0	24.0	23.1	23.6	24.8	23.7	23.3
$v_{a(0.6\,m)}$	m/s	0.06	0.07	0.07	0.06	0.03	0.06	0.05	0.02	0.08	0.09	0.07
$RH_{(0.6\,m)}$	%	58.0	57.8	57.2	57.4	57.8	58.0	59.9	46.8	57.2	59.7	48.5
$PMV_{(0.6\,m)}$	-	0.0	−0.2	−0.1	−0.1	−0.1	−0.1	−0.4	−0.3	0.1	−0.2	−0.4
$PPD_{(0.6\,m)}$	%	5.1	5.7	5.4	5.4	5.4	5.3	8.5	7.3	5.1	6.1	8.8

I Cat.   II Cat.   III Cat.   IV Cat.

Figure 7. Building D air velocity results in measurement points 1–11 and the thermal comfort parameters.

3.5. *Building E Results*

According to the results, Building E achieved the worst TC values by categories. *DR* was in the II category in 4 positions of 14, t_i was in III category four times. *PMV* and *PPD* second category was not reached 5 times. Fluctuations of v_a were random depending on the height. The v_a results and TC parameters in Building E, with fan coil units mounted in the suspended ceiling, are compared below in Figure 8.

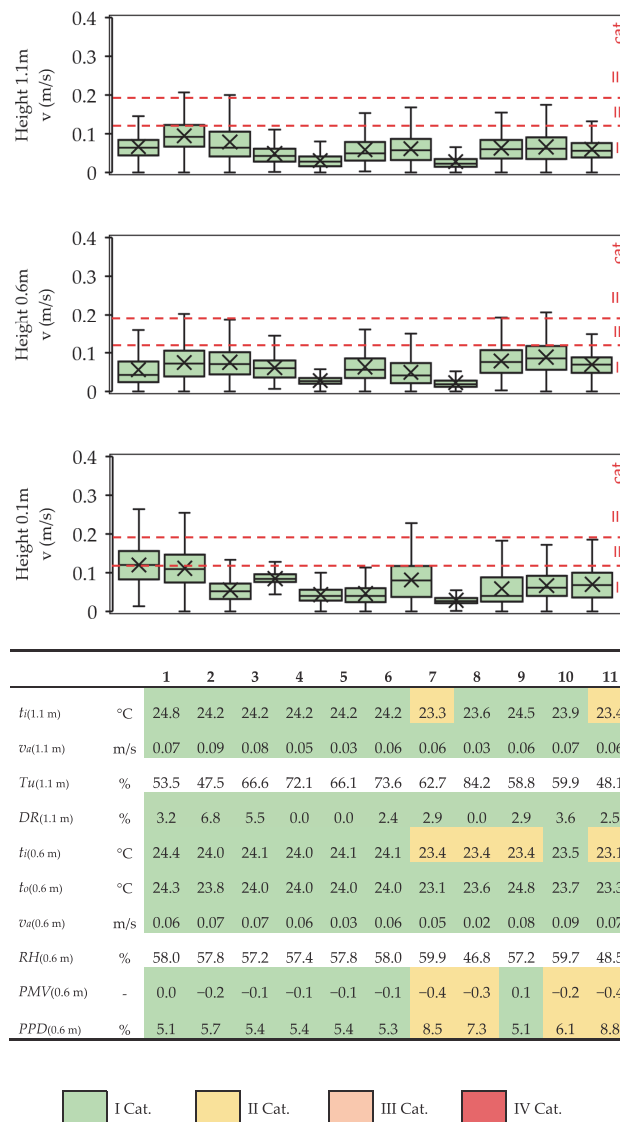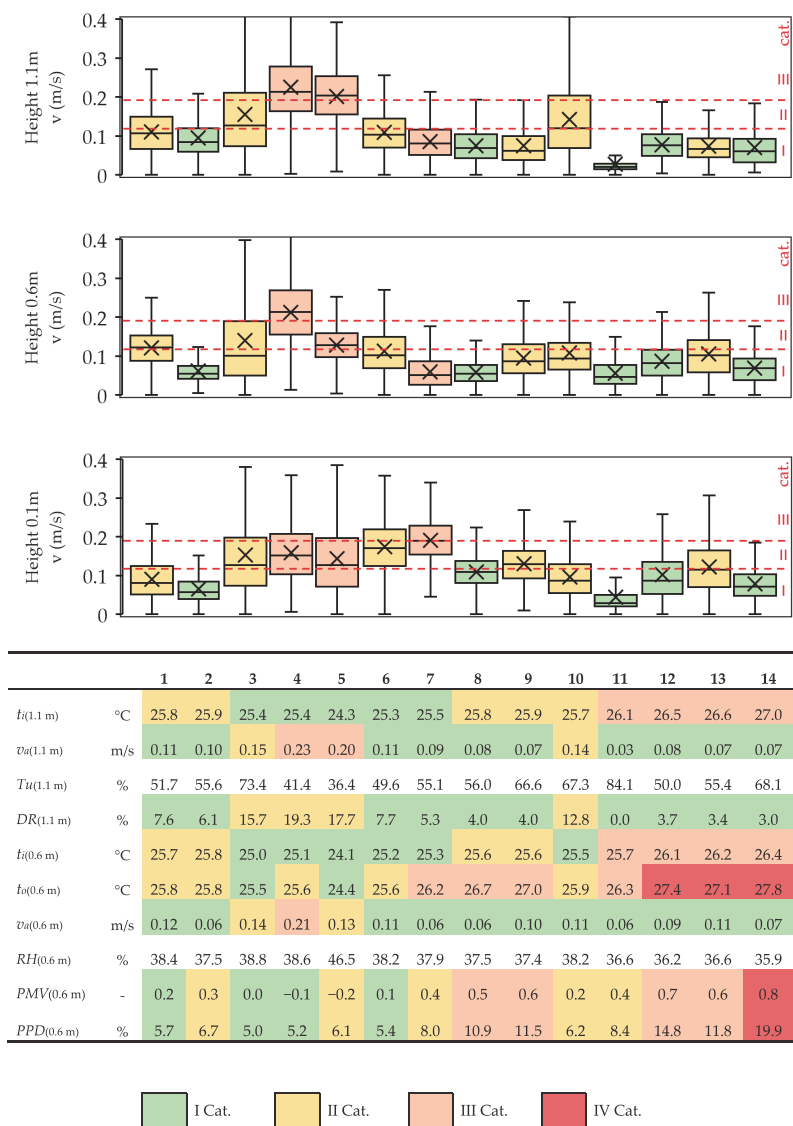|		1	2	3	4	5	6	7	8	9	10	11	12	13	14
$t_{i(1.1\,m)}$	°C	25.8	25.9	25.4	25.4	24.3	25.3	25.5	25.8	25.9	25.7	26.1	26.5	26.6	27.0
$v_{a(1.1\,m)}$	m/s	0.11	0.10	0.15	0.23	0.20	0.11	0.09	0.08	0.07	0.14	0.03	0.08	0.07	0.07
$Tu_{(1.1\,m)}$	%	51.7	55.6	73.4	41.4	36.4	49.6	55.1	56.0	66.6	67.3	84.1	50.0	55.4	68.1
$DR_{(1.1\,m)}$	%	7.6	6.1	15.7	19.3	17.7	7.7	5.3	4.0	4.0	12.8	0.0	3.7	3.4	3.0
$t_{ii(0.6\,m)}$	°C	25.7	25.8	25.0	25.1	24.1	25.2	25.3	25.6	25.6	25.5	25.7	26.1	26.2	26.4
$t_{o(0.6\,m)}$	°C	25.8	25.8	25.5	25.6	24.4	25.6	26.2	26.7	27.0	25.9	26.3	27.4	27.1	27.8
$v_{a(0.6\,m)}$	m/s	0.12	0.06	0.14	0.21	0.13	0.11	0.06	0.06	0.10	0.11	0.06	0.09	0.11	0.07
$RH_{(0.6\,m)}$	%	38.4	37.5	38.8	38.6	46.5	38.2	37.9	37.5	37.4	38.2	36.6	36.2	36.6	35.9
$PMV_{(0.6\,m)}$	-	0.2	0.3	0.0	−0.1	−0.2	0.1	0.4	0.5	0.6	0.2	0.4	0.7	0.6	0.8
$PPD_{(0.6\,m)}$	%	5.7	6.7	5.0	5.2	6.1	5.4	8.0	10.9	11.5	6.2	8.4	14.8	11.8	19.9

I Cat.   II Cat.   III Cat.   IV Cat.

Figure 8. Building E air velocity results in measurement points 1–14 and the thermal comfort parameters.

3.6. Results of the Indoor Climate Questionnaire

Based on ICQ survey, summary of the results for thermal environment are shown below in Figure 9, the ICQ results for *PMV* and *PPD* are presented below in Figure 10. The highest number of answers were in the Building A with 36 responses divided between all age groups equally between men and women. A total of 83% were working in open office layout and 86% were spending most of the day at their workplace. For 83% of the respondents, t_i was described as suitable. Meanwhile, 6 occupants found it to be warm and 7 slightly cooler. A total of 89% had not or had perceived slight odor, 72% did not find lighting fixtures or sunlight to be disturbing, and 81% found ICQ to be suitable or better. A total of 61% perceived overall acoustics and 36% perceived other noises to be disturbing. Roughly half of the respondents rarely felt eye problems, headaches, or concentration matters and

64% rarely felt nasal or throat irritation. Extra comments mentioned occasional lack of ventilation and air dryness.
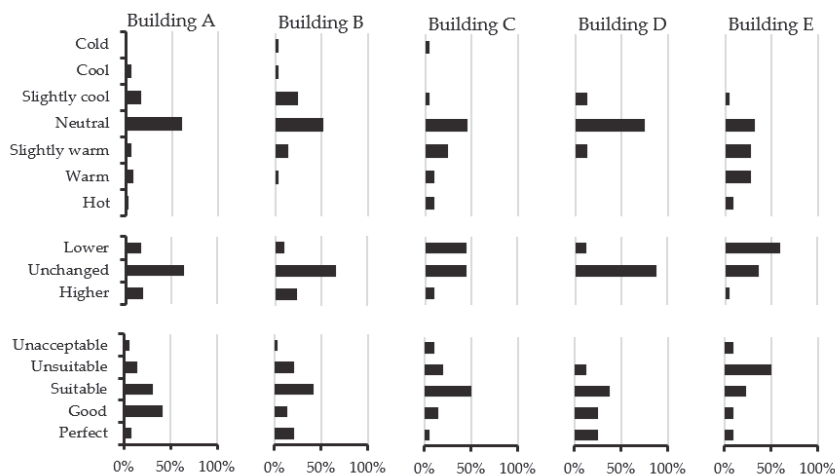

Figure 9. Indoor climate questionnaire results for indoor air temperature. The descriptions of y-axis are the room air temperature sensation question (upper) and verification questions (middle and lower) from the indoor climate questionnaire (see Appendix A).
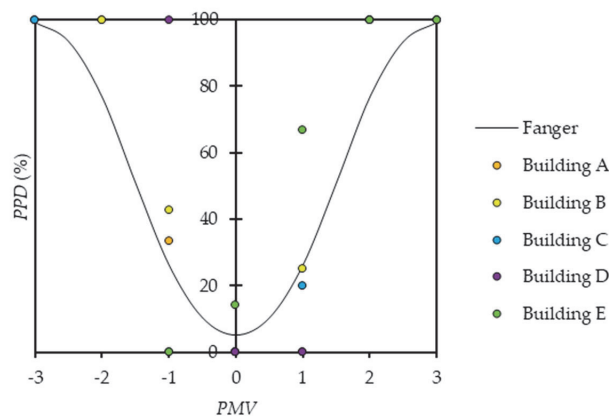

Figure 10. Indoor climate questionnaire results for predicted percentage of dissatisfied and predicted mean vote.

Respondents in the Building B were 38% females, 2/3 aged between 26–35 or 36–45 and 1/2 spending half of the workday behind the desk. A total of 72% of them working in open office environment. Ninety percent found t_i to be suitable. A total of 13 of the 29 respondents did not perceive odor. Lighting was disturbing for 21% and sunlight for 14%, meanwhile 14% were dissatisfied with ICQ. Seven percent did not find room acoustics and 17% general noise in office to be disturbing. Half of the respondents had rarely felt eye dryness or irritation, occur headaches or fatigue, and felt nasal problem or dry throat. A total of 62% had rarely felt concentration problems.

Seventy percent of the 20 ICQ respondents in Building C were women. Answers were divided between the age of 26 to 65 with the majority of them working in open office landscape, 2/3 working behind their desk most of the day. Perceived as too warm by 20%, t_i was suitable by 75% of the

occupants. Ninety percent had not perceived or had perceived slight odor. A total of 70% did not find lighting equipment to be disturbing and 75% was not disturbed by the sunlight. Forty percent of the respondents found air quality to be not suitable or unacceptable. A total of 85% perceived colleagues' speech and overall room acoustic to be somewhat disturbing, while 65% claimed other noises to be distracting. A total of 1/3 had rarely felt eye problems, occurred headaches, or tiredness. A total of 45% had rarely felt nasal or throat irritation and 20% had rarely had concentration issues. Extra comments mentioned lower fresh air rate in the end of the day.

Building D had only 8 responses for the online ICQ all of them working in the open office. For the majority of the answers, t_i was suitable. Odor was rarely noticed, lighting or sunlight was not disturbing. ICQ was suitable or better, while room acoustics was more disturbing than other noises. Nasal issues were more often to occur compared to eye dryness or headaches and concentration issues. Extra comments noted that open office may be cheaper option for the employer being unsuitable for the employees.

A total of 2/3 of the 22 respondents in Building E were in the second age group between 26–35 years and 36% in overall were females. A total of 77% of the tenants were working in an open office environment, while 2/3 of them were spending most of their day behind the desk. One-third found t_i to be suitable and 2/3 claimed the t_i to be slightly warm, warm, or hot. Fifty percent perceived weak or moderate odor. Room lighting equipment did not disturb 82% and the sun did not disturb 60% of the respondents. A total of 2/3 marked ICQ suitable, good, or very good. Room acoustic level was not claimed to be disturbing for 40% and other noise for 23% of the respondents. Fifty percent had rarely felt eye dryness or irritation, 64% had rarely occur headaches or fatigue, 82% had rarely felt nasal problems or dry throat, and 50% mentioned concentration issues sometimes, often, or all the time. Extra comments noted that air quality decreases in the second phase of the day and the missing option for opening windows was also described as a disadvantage.

Number of respondents of the ICQ is below the least recommended sample size [63], therefore the results of the ICQ include higher uncertainty (Figure 10). Thermal sensation voted by occupants covers significantly wider range than *PMV* calculated from measurements. Majority of the respondents were working in open office. The most unsatisfying t_i was in the Building E and the most suitable t_i was in the Building D. In general, unsuitable t_i was perceived more as warmer than cooler. In Buildings A, B, and D the t_i was perceived suitable for over 80% of the employees, while it was 67% in the Building E and the 60% in the Building C.

4. Discussion

The on-site measurement results showed, that the during cooling summertime *DR* risk can be stated in all observed buildings. Preconception of avoiding fan coil units for cooling does not immediately guarantee a superior thermal environment without draught. However, draught risk was the lowest in Building D with radiant cooling panels as room conditioning units.

Possible causes, v_a and *DR* was not significantly higher in the case of fan coil units in Building E was the taping of air distribution vanes (Figure 3b) and also positioning of the working stations was carried out avoiding direct draught from the fan coil units. This could explain the higher thermal environment temperatures. The induced airflow rate is manually adjustable for open ceiling active chilled beams in Building A and was adjusted into different positions for avoiding possible draught between two beams in various places. In Building C, few suspended ceiling active chilled beams had paper covers blocking air flow from the nozzles. These modifications were made due to the complaints, decrease in productivity or spatial plan and the layout of the workspaces. Described modifications in Buildings A, C, and E refer to possible ineffective floor space areas. Therefore, whether the design or construction may have been inaccurate or user-based thermal environment setpoints do not meet the requirements for v_a and *DR*.

The v_a limit values in EN 16798−1:2019 [54] have been calculated assuming t_o +23 °C and *Tu* 40%. Figure 11a illustrates that the *Tu* is considerably higher than the default value, which increases the

unsatisfaction with local TC. However, the measured t_o was higher than the default value in most of the measured positions in all buildings, which decreases the number of dissatisfied. Figure 11b shows that, in general, the *DR* calculated based on measured t_o and *Tu* is in the same scale with the one calculated with the default values.
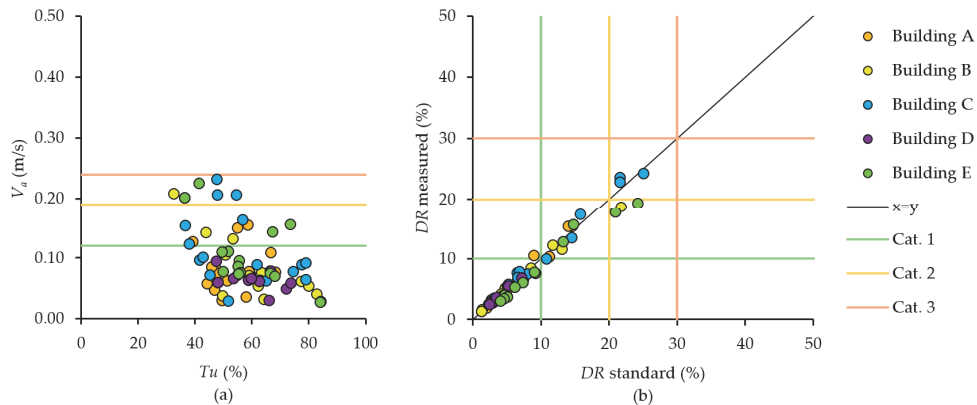

Figure 11. Air velocity and turbulence intensity results according to maximum air velocity categories I–III in summer (**a**); Draught rate correlation in measured and standard-based [54] conditions according to draught rate categories I–III (**b**).

In further analysis of this study t_i will be more deeply discussed, foreseeing to include transitional period and heating period measurements, façade inspection and t_i periodical data analysis in the reference buildings. Therefore, the performance of the cooling units according to t_i could be more clearly presented by period or duration curve. Periodical data analysis on t_i is mandatory as t_i presented in this study reflects only a fragment of the thermal environment. Positioning TC measurement values on periodical t_i data can indicate TC measurement accuracy and dispersion. IQC survey number of respondents also needs additional attention, how to achieve a higher response rate.

There are several limitations to this work. Authors had no control over the boundary conditions during measurements. This study only focuses on a few office spaces in five different building in Tallinn. More further studies of actual work environment need to be performed in order to be able to draw general conclusions about studied room conditioning solutions air distribution performance.

5. Conclusions

This study was based on TC measurements in open office environments in Tallinn. First or second category measured general thermal comfort in four buildings out of five were still inconvenient for significant number of occupants because of local thermal discomfort caused by draught and by some additional dissatisfaction indicated by questionnaires. Questionnaire survey showed deviation from predicted *PPD* in both directions. Some small occupant groups were either more satisfied or less satisfied at slightly cool or slightly warm thermal sensation, but at neutral sensation the results were more consistent. Less satisfied occupant groups exposed to higher air velocities has likely affected their satisfaction reported in thermal sensation questions because there was no specific draught question available.

Temperature measurements showed that air and operative temperature was the worst in Building E which was close to drop out from category III, while measurement results in Buildings A–D remained in between I and II category. According to the questionnaire over 80% of the employees in Buildings A, B, and C, and 75% in Building D were thermally satisfied. In the Building E, 59% of occupants found the thermal environment unsuitable or unacceptable. Generally, the average thermal satisfaction of occupants was well in line with the measurements.

Air velocity and draught rate measurements showed that modern offices do not necessarily reach to generally expected good indoor climate category II air velocity and draught rate values. A room conditioning solution with suspended ceiling active chilled beams in Building C, displacement ventilation in Building B with TABS and fan coil units in Building E showed category III performance only. Open ceiling active chilled beams in Building A corresponded to category II requirements and ceiling panels for room conditioning in Building D showed superior Category I performance. Category II and III results with active chilled beams indicate that dedicated air distribution solution together with proper design and sizing is needed to reach category II.

We found that existing standards do not provide enough detailed questionnaire for the assessment of occupant dissatisfaction. Our results suggest that questionnaire could be an easier compliance assessment method compared to measurements, which need an expensive equipment and carefully selected measurement days. For the compliance assessment with the measurement, there is more guidance needed especially how to select relevant measurement conditions and locations for draught rate measurement. Future office buildings with open-plan layouts revealed to be demanding environments where careful air distribution design is needed in order to meet comfort requirements.

Nomenclature

A	net floor area (m^2)
C_{res}	respiratory convective heat exchange (W/m^2)
DR	draught rate (%)
E_c	evaporative heat exchange at the skin, when the person experiences a sensation of thermal neutrality (W/m^2)
E_{res}	respiratory evaporative heat exchange (W/m^2)
f_{cl}	clothing surface area factor
g	solar radiation transmittance through window glass
H	heat loss (W/K)
H_d	dry heat loss (W/m^2)
h_c	convective heat transfer coefficient [W/(m$^2 \times$ K)]
HVAC	heating, ventilation, and air conditioning
I_{cl}	clothing insulation [(m$^2 \times$ K)/W]
ICQ	indoor climate questionnaire
M	metabolic rate (W/m^2)
mt_{sk}	mean skin temperature (°C)
p_a	water vapor partial pressure (Pa)
PMV	predicted mean vote
PPD	predicted percentage dissatisfied (%)
RH	relative humidity (%)
SD	standard deviation
TABS	thermally active building systems

TC	thermal comfort
t_{cl}	clothing surface temperature (°C)
t_i	indoor air temperature (°C)
t_o	operative temperature (°C)
Tu	turbulence intensity
U	thermal transmittance [W/(m^2×K)]
v_a	air velocity (m/s)
v_{ar}	relative air velocity (m/s)
W	effective mechanical power (W/m^2)
WWR	window-to-wall ratio

Appendix A

The ICQ form is for online survey is provided below.

1. Gender—( ) Female, ( ) Male
2. Age—( ) 18–25, ( ) 26–35, ( ) 36–45, ( ) 46–55, ( ) 56–65, ( ) 66+
3. Workstation—( ) Private office (max 3 people), ( ) Open office
4. Which amount of the workday you spend at your desk—( ) Whole workday, ( ) Half of the workday (up to 4–5 h), ( ) Few hours (max 1–2 h)
5. In which zone do you spend the most of your workday (1–n in picture)—( ) 1–n
6. How do you rate you thermal sensation (choose neutral if you do not want a change in temperature)—( ) Hot, ( ) Warm, ( ) Slightly warm, ( ) Comfortable, ( ) Slightly cool, ( ) Cool, ( ) Cold
7. How do you perceive odor intensity—( ) No odor, ( ) Weak, ( ) Moderate, ( ) Strong, ( ) Very strong, ( ) Unbearable
8. Would you prefer the room temperature to be—( ) Higher, ( ) Unchanged, ( ) Lower
9. Does the room lighting disturb working—( ) Yes, ( ) No
10. Does the sunlight disturb working—( ) Yes, ( ) No
11. Please rate (room temperature is)—( ) Perfect, ( ) Good, ( ) Suitable, ( ) Unsuitable, ( ) Unbearable
12. Please rate (air quality is)—( ) Perfect, ( ) Good, ( ) Suitable, ( ) Unsuitable, ( ) Unbearable
13. How do you perceive acoustic level (colleagues' speech and overall room acoustics)—( ) Does not disturb at all, ( ) Rarely disturbs, ( ) Sometimes disturbs, ( ) Often disturbs, ( ) Disturbs all the time
14. How do you perceive other noise in your workplace—( ) Does not disturb at all, ( ) Rarely disturbs, ( ) Sometimes disturbs, ( ) Often disturbs, ( ) Disturbs all the time
15. Whether and how often have you experienced the following symptoms (eye dryness or irritation)—( ) Never, ( ) Rarely, ( ) Sometimes, ( ) Often, ( ) All the time
16. Whether and how often have you experienced the following symptoms (headache or fatigue)—( ) Never, ( ) Rarely, ( ) Sometimes, ( ) Often, ( ) All the time
17. Whether and how often have you experienced the following symptoms (nasal or throat dryness or irritation)—( ) Never, ( ) Rarely, ( ) Sometimes, ( ) Often, ( ) All the time
18. Whether and how often have you experienced the following symptoms (concentration problems)—( ) Never, ( ) Rarely, ( ) Sometimes, ( ) Often, ( ) All the time

References

1. Seppanen, O. Ventilation Strategies for Good Indoor Air Quality and Energy Efficiency. *Int. J. Vent.* **2008**, *6*, 297–306.
2. Yang, Z.; Ghahramani, A.; Becerik-Gerber, B. Building occupancy diversity and HVAC (heating, ventilation, and air conditioning) system energy efficiency. *Energy* **2016**, *109*, 641–649. [CrossRef]
3. Mathews, E.H.; Botha, C.P.; Arndt, D.C.; Malan, A.G. HVAC control strategies to enhance comfort and minimise energy usage. *Energy Build.* **2001**, *33*, 853–863. [CrossRef]
4. Simmonds, P. The Utilization of Optimal-Design and Operation Strategies in Lowering the Energy-Consumption in Office Buildings. *Renew. Energy* **1994**, *5*, 1193–1201. [CrossRef]
5. Guo, W.; Zhou, M. Technologies toward thermal comfort-based and energy-efficient HVAC systems: A review. In Proceedings of the 2009 IEEE International Conference on Systems, Man and Cybernetics, San Antonio, TX, USA, 11–14 October 2009; pp. 3883–3888.
6. Fanger, P.O.; Christensen, N.K. Perception of draught in ventilated spaces. *Ergonomics* **1986**, *29*, 215–235. [CrossRef] [PubMed]

7.　Shahrestani, M.; Yao, R.M.; Cook, G.K. Decision Making for HVAC&R System Selection for a Typical Office Building in the UK. *Ashrae Trans.* **2012**, *118*, 222–229.

8.　Nemethova, E.; Stutterecker, W.; Schoberer, T. Thermal Comfort and HVAC Systems Operation Challenges in a Modern Office Building—Case Study. *Sel. Sci. Pap. J. Civ. Eng.* **2016**, *11*, 103–114. [CrossRef]

9.　Shahzad, S.S.; Brennan, J.; Theodossopoulos, D.; Hughes, B.; Calautit, J.K. Energy Efficiency and User Comfort in the Workplace: Norwegian Cellular vs. British Open Plan Workplaces. *Energy Procedia* **2015**, *75*, 807–812. [CrossRef]

10.　Choi, J.H.; Loftness, V.; Aziz, A. Post-occupancy evaluation of 20 office buildings as basis for future IEQ standards and guidelines. *Energy Build.* **2012**, *46*, 167–175. [CrossRef]

11.　Karjalainen, S. Thermal comfort and gender: A literature review. *Indoor Air* **2012**, *22*, 96–109. [CrossRef]

12.　Schellen, L.; Loomans, M.G.L.C.; de Wit, M.H.; Olesen, B.W.; Lichtenbelt, W.D.V. The influence of local effects on thermal sensation under non-uniform environmental conditions-Gender differences in thermophysiology, thermal comfort and productivity during convective and radiant cooling. *Physiol. Behav.* **2012**, *107*, 252–261. [CrossRef] [PubMed]

13.　Rupp, R.F.; Vasquez, N.G.; Lamberts, R. A review of human thermal comfort in the built environment. *Energy Build.* **2015**, *105*, 178–205. [CrossRef]

14.　Pfafferott, J.U.; Herkel, S.; Kalz, D.E.; Zeuschner, A. Comparison of low-energy office buildings in summer using different thermal comfort criteria. *Energy Build.* **2007**, *39*, 750–757. [CrossRef]

15.　Hens, H.S.L.C. Thermal comfort in office buildings: Two case studies commented. *Build. Environ.* **2009**, *44*, 1399–1408. [CrossRef]

16.　Kolarik, J.; Toftum, J.; Olesen, B.W. Operative temperature drifts and occupant satisfaction with thermal environment in three office buildings using radiant heating/ cooling system. In Proceedings of the Healthy Buildings Europe 2015, Eindhoven, The Netherlands, 18–20 May 2015.

17.　Griefahn, B.; Kunemund, C. The effects of gender, age, and fatigue on susceptibility to draft discomfort. *J. Therm. Biol.* **2001**, *26*, 395–400. [CrossRef]

18.　Maykot, J.K.; Rupp, R.F.; Ghisi, E. A field study about gender and thermal comfort temperatures in office buildings. *Energy Build.* **2018**, *178*, 254–264. [CrossRef]

19.　Maula, H.; Hongisto, V.; Ostman, L.; Haapakangas, A.; Koskela, H.; Hyona, J. The effect of slightly warm temperature on work performance and comfort in open-plan offices - a laboratory study. *Indoor Air* **2016**, *26*, 286–297. [CrossRef]

20.　Wang, Z.; de Dear, R.; Luo, M.H.; Lin, B.R.; He, Y.D.; Ghahramani, A.; Zhu, Y.X. Individual difference in thermal comfort: A literature review. *Build. Environ.* **2018**, *138*, 181–193. [CrossRef]

21.　Kim, J.; Zhou, Y.X.; Schiavon, S.; Raftery, P.; Brager, G. Personal comfort models: Predicting individuals' thermal preference using occupant heating and cooling behavior and machine learning. *Build. Environ.* **2018**, *129*, 96–106. [CrossRef]

22.　Pazhoohesh, M.; Zhang, C. A satisfaction-range approach for achieving thermal comfort level in a shared office. *Build. Environ.* **2018**, *142*, 312–326. [CrossRef]

23.　Enescu, D. A review of thermal comfort models and indicators for indoor environments. *Renew. Sustain. Energy Rev.* **2017**, *79*, 1353–1379. [CrossRef]

24.　Laftchiev, E.; Nikovski, D. An IoT system to estimate personal thermal comfort. In Proceedings of the 2016 IEEE 3rd World Forum on Internet of Things (WF-IoT), Reston, VA, USA, 12–14 December 2016; pp. 672–677.

25.　Ghahramani, A.; Castro, G.; Karvigh, S.A.; Becerik-Gerber, B. Towards unsupervised learning of thermal comfort using infrared thermography. *Appl. Energy* **2018**, *211*, 41–49. [CrossRef]

26.　Jung, W.; Jazizadeh, F. Human-in-the-loop HVAC operations: A quantitative review on occupancy, comfort, and energy-efficiency dimensions. *Appl. Energy* **2019**, *239*, 1471–1508. [CrossRef]

27.　Shi, J.; Yu, N.P.; Yao, W.X. Energy efficient building HVAC control algorithm with real-time occupancy prediction. In Proceedings of the 8th International Conference on Sustainability in Energy and Buildings, Turin, Italy, 11–13 September 2017.

28.　Thalfeldt, M.; Pikas, E.; Kurnitski, J.; Voll, H. Facade design principles for nearly zero energy buildings in a cold climate. *Energy Build.* **2013**, *67*, 309–321. [CrossRef]

29.　Kähkönen, E. Draught, Radiant Temperature Asymmetry and Air Temperature – a Comparison between Measured and Estimated Thermal Parameters. *Indoor Air* **1991**, *1*, 439–447. [CrossRef]

30. Kiil, M.; Mikola, A.; Thalfeldt, M.; Kurnitski, J. Thermal comfort and draught assessment in a modern open office building in Tallinn. *E3S Web Conf.* **2019**, *111*, 02013. [CrossRef]

31. Rhee, K.N.; Olesen, B.W.; Kim, K.W. Ten questions about radiant heating and cooling systems. *Build. Environ.* **2017**, *112*, 367–381. [CrossRef]

32. Saber, E.M.; Tham, K.W.; Leibundgut, H. A review of high temperature cooling systems in tropical buildings. *Build. Environ.* **2016**, *96*, 237–249. [CrossRef]

33. Schellen, L.; Loomans, M.G.L.C.; de Wit, M.H.; Olesen, B.W.; Lichtenbelt, W.D.V.M. Effects of different cooling principles on thermal sensation and physiological responses. *Energy Build.* **2013**, *62*, 116–125. [CrossRef]

34. Maula, H.; Hongisto, V.; Koskela, H.; Haapakangas, A. The effect of cooling jet on work performance and comfort in warm office environment. *Build. Environ.* **2016**, *104*, 13–20. [CrossRef]

35. Gao, S.; Wang, Y.A.; Zhang, S.M.; Zhao, M.; Meng, X.Z.; Zhang, L.Y.; Yang, C.; Jin, L.W. Numerical investigation on the relationship between human thermal comfort and thermal balance under radiant cooling system. *Energy Procedia* **2017**, *105*, 2879–2884. [CrossRef]

36. Cen, C.; Jia, Y.H.; Liu, K.X.; Geng, R.X. Experimental comparison of thermal comfort during cooling with a fan coil system and radiant floor system at varying space heights. *Build. Environ.* **2018**, *141*, 71–79. [CrossRef]

37. Kolarik, J.; Toftum, J.; Olesen, B.W.; Jensen, K.L. Simulation of energy use, human thermal comfort and office work performance in buildings with moderately drifting operative temperatures. *Energy Build.* **2011**, *43*, 2988–2997. [CrossRef]

38. Fonseca, N. Experimental study of thermal condition in a room with hydronic cooling radiant surfaces. *Int. J. Refrig.* **2011**, *34*, 686–695. [CrossRef]

39. Li, R.L.; Yoshidomi, T.; Ooka, R.; Olesen, B.W. Field evaluation of performance of radiant heating/cooling ceiling panel system. *Energy Build.* **2015**, *86*, 58–65. [CrossRef]

40. Saber, E.M.; Iyengar, R.; Mast, M.; Meggers, F.; Tham, K.W.; Leibundgut, H. Thermal comfort and IAQ analysis of a decentralized DOAS system coupled with radiant cooling for the tropics. *Build. Environ.* **2014**, *82*, 361–370. [CrossRef]

41. Chiang, W.H.; Wang, C.Y.; Huang, J.S. Evaluation of cooling ceiling and mechanical ventilation systems on thermal comfort using CFD study in an office for subtropical region. *Build. Environ.* **2012**, *48*, 113–127. [CrossRef]

42. Mustakallio, P.; Bolashikov, Z.; Kostov, K.; Melikov, A.; Kosonen, R. Thermal environment in simulated offices with convective and radiant cooling systems under cooling (summer) mode of operation. *Build. Environ.* **2016**, *100*, 82–91. [CrossRef]

43. Cehlin, M.; Karimipanah, T.; Larsson, U.; Ameen, A. Comparing thermal comfort and air quality performance of two active chilled beam systems in an open-plan office. *J. Build. Eng.* **2019**, *22*, 56–65. [CrossRef]

44. Kim, T.; Kato, S.; Murakami, S.; Rho, J. Study on indoor thermal environment of office space controlled by cooling panel system using field measurement and the numerical simulation. *Build. Environ.* **2005**, *40*, 301–310. [CrossRef]

45. Fredriksson, J.; Sandberg, M.; Moshfegh, B. Experimental investigation of the velocity field and airflow pattern generated by cooling ceiling beams. *Build. Environ.* **2001**, *36*, 891–899. [CrossRef]

46. Rhee, K.N.; Shin, M.S.; Choi, S.H. Thermal uniformity in an open plan room with an active chilled beam system and conventional air distribution systems. *Energy Build.* **2015**, *93*, 236–248. [CrossRef]

47. Koskela, H.; Haggblom, H.; Kosonen, R.; Ruponen, M. Air distribution in office environment with asymmetric workstation layout using chilled beams. *Build. Environ.* **2010**, *45*, 1923–1931. [CrossRef]

48. Indraganti, M.; Ooka, R.; Rijal, H.B. Thermal comfort in offices in summer: Findings from a field study under the 'setsuden' conditions in Tokyo, Japan. *Build. Environ.* **2013**, *61*, 114–132. [CrossRef]

49. De Vecchi, R.; Candido, C.; de Dear, R.; Lamberts, R. Thermal comfort in office buildings: Findings from a field study in mixed-mode and fully-air conditioning environments under humid subtropical conditions. *Build. Environ.* **2017**, *123*, 672–683. [CrossRef]

50. Azad, A.S.; Rakshit, D.; Wan, M.P.; Babu, S.; Sarvaiya, J.N.; Kumar, D.E.V.S.K.; Zhang, Z.; Lamano, A.S.; Krishnasayee, K.; Gao, C.P.; et al. Evaluation of thermal comfort criteria of an active chilled beam system in tropical climate: A comparative study. *Build. Environ.* **2018**, *145*, 196–212. [CrossRef]

51. He, Y.D.; Li, N.P.; Huang, Q. A field study on thermal environment and occupant local thermal sensation in offices with cooling ceiling in Zhuhai, China. *Energy Build.* **2015**, *102*, 277–283. [CrossRef]

52. CEN EN 15251:2007. *European Committee for Standardization, Indoor Environmental Input Parameters for Design and Assessment of Energy Performance of Buildings Addressing Indoor Air Quality, Thermal Environment, Lighting and Acoustics*; European Committee for Standardization: Brussels, Belgium, 2007.

53. Fanger, P.O. *Thermal Comfort, Analysis and Applications in Environmental Engineering*; Danish Technical Press: Manhattan, KS, USA, 1970.

54. CEN EN 16798-1:2019. *Energy Performance of Buildings—Ventilation for Buildings—Part 1: Indoor Environmental Input Parameters for Design and Assessment of Energy Performance of Buildings Addressing Indoor Air Quality, Thermal Environment, Lighting and Acoustics—Module M1-6*; European Committee for Standardization: Brussels, Belgium, 2019.

55. ISO 7726:1998. *Ergonomics of the Thermal Environment—Instruments for Measuring Physical Quantities*; International Organization for Standardization: Geneva, Switzerland, 1998.

56. Dantec Dynamics. *ComfortSense specification*; Dantec Dynamics A/S, A Nova Instruments Company: Denmark, Skovlunde, 2019; Available online: http://www.dantecdynamics.jp/docs/products-and-services/thermal-comfort/PI264_ComfortSense.pdf (accessed on 5 June 2019).

57. Ministry of Economic Affairs and Communications. Estonian Regulation No 258: Minimum Requirements for Energy Performance. *Riigi Teataja* **2007**, *72*, 445.

58. Thermal Comfort. Innova AirTech Instruments A/S. 2002. Available online: http://www.labeee.ufsc.br/sites/default/files/disciplinas/Thermal%20Booklet.pdf (accessed on 10 July 2019).

59. CEN EN 15726:2011. *Ventilation for Buildings—Air Diffusion—Measurements in the Occupied Zone of Air-Conditioned/Ventilated Rooms to Evaluate Thermal and Acoustic Conditions*; European Committee for Standardization: Brussels, Belgium, 2011.

60. ISO 7730:2005. *Ergonomics of the Thermal Environment—Analytical Determination and Interpretation of Thermal Comfort Using Calculation of the PMV and PPD Indices and Local Thermal Comfort Criteria*; International Organization for Standardization: Geneva, Switzerland, 2005.

61. Google. Google Forms. Google Inc., Mountain View (CA), USA. 2019. Available online: https://www.google.com/forms/about/ (accessed on 1 July 2019).

62. EMHI. Observation Data. Estonian Weather Service: Tallinn, Estonia. 2019. Available online: https://www.ilmateenistus.ee/ilm/ilmavaatlused/vaatlusandmed/tunniandmed/?lang=en (accessed on 15 September 2019).

63. Wang, J.Y.; Wang, Z.; de Dear, R.; Luo, M.H.; Ghahramani, A.; Lin, B.R. The uncertainty of subjective thermal comfort measurement. *Energy Build.* **2018**, *181*, 38–49. [CrossRef]

Appendix 2

WILEY

Research Article

Overheating and Air Velocities in Modern Office Buildings During Heating Season

Martin Kiil [ID],[1] **Raimo Simson** [ID],[1,2] **Martin Thalfeldt** [ID],[1] and **Jarek Kurnitski** [ID][1,2]

[1]*Department of Civil Engineering and Architecture, Tallinn University of Technology, Ehitajate tee 5, 19086 Tallinn, Estonia*
[2]*School of Engineering, Aalto University, Otakaari 4, 02150 Espoo, Finland*

Correspondence should be addressed to Martin Kiil; martin.kiil@taltech.ee

Proper design and operation of buildings are expected to result in optimal thermal comfort and energy performance at the same time. If occupants are not satisfied with thermal conditions, corrective actions by building managers and maintenance staff may lead to elevated room temperatures with evident energy penalties. Because of complicated technical systems and control logic, it is worth studying how well the design intent has been realised in new office buildings. In this study, thermal comfort was analysed by measurements of draught, room, and supply air temperature as well as with occupant questionnaire surveys in five modern office buildings. Both short- and long-term measurements were conducted to demonstrate problems in the operation and to find potential solutions for improvement. The results revealed an issue of excessive overheating during the heating season despite generally low air velocities. Radiant ceiling panels had the lowest velocities in both summer and winter, while buildings with active chilled beams showed the potential to meet Category II air velocity and temperature requirements. The building with thermally activated building systems experienced the most overheating during the heating season. Occupants were satisfied with the heating season temperatures of 23°C–25°C that can be attributed to lighter clothing (0.7 clo) instead of the standard 1.0 clo. Ventilation supply air and indoor temperature analyses indicate that elevated setpoints have been used to compensate for draught, resulting in overheating. As a measure of improvement to avoid overheating, we propose control curves for room temperature based on the outdoor running mean temperature and for supply air temperature based on the extract air temperature.

Keywords: ceiling panels; chilled beams; cooling season; heating season; running mean temperature; TABS; thermal comfort

1. Introduction

Indoor environmental conditions have a significant influence on the symptoms and comfort of occupants in the workplace [1–3]. Poor indoor climate is linked to decreased productivity and diminished well-being among workers [4–7]. To mitigate adverse health effects on building occupants, building codes, regulations, and standards have established requirements for working conditions in built environments [2, 8–11]. In modern buildings, ensuring both healthy and comfortable conditions while minimizing energy consumption, it is essential to meet European Union (EU) targets for building energy efficiency [12]. Notably, research provides evidence that thermal comfort (TC) in buildings can impact learning performance [13, 14]. Uncomfortable thermal conditions have been shown to affect cognitive performance among occupants negatively

[15], resulting in reduced concentration, impaired memory, and slower reaction times. Conversely, when occupants experience comfort, their cognitive performance improves, leading to enhanced productivity and learning outcomes.

European and international standards are available for measurement of thermal environmental variables, for design criteria, and assessment of TC in buildings. Key standards include EN 16798-1 [16] and EN 16798-2 [17], which outline requirements for indoor environmental parameters and heating, ventilation, and air conditioning (HVAC) design. EN ISO 7730 [18] provides methods for predicting general thermal sensation and discomfort levels, while EN ISO 7726 [19] offers methods for assessing TC.

The standards employ a body heat balance-based comfort model and consider physiological factors to calculate the predicted mean vote (PMV) index and the percentage

of dissatisfied occupants (PPD) as well as an adaptive comfort model [20, 21]. EN ISO 7730 outlines a TC assessment methodology that takes into account various factors, including indoor air temperature (t_i), relative humidity (RH), air velocity (v_a), radiation, metabolic rate, and clothing insulation, which all influence TC significantly [22]. Clothing insulation is measured in clo units, where 1 clo represents a thermal resistance of $0.155 \, \mathrm{K \cdot m^2 \cdot W^{-1}}$, it is determined based on the insulation required for a person engaged in sedentary activity at 1.2 met to maintain thermal equilibrium in a normally ventilated room at 22°C with an air movement of 0.1 m/s. A default value of 1.0 clo is used for occupants' clothing during the heating season and 0.5 clo during the cooling season.

Despite the well-established standards, it is still challenging to achieve high occupant satisfaction, making TC a critical consideration in the design of modern office buildings [23, 24]. In the conceptual and detailed design, many decisions on the selection of HVAC strategies, system types, and components are made, in which the connection to occupant satisfaction is not easy to understand [25–28]. Even with very careful design, installation, and operation of HVAC systems, occupants may still experience dissatisfaction with the indoor climate [29–33], showing that critical aspects in the design, commissioning, and operation are not necessarily known. Satisfying individual preferences is a special challenge in open-plan offices where controllers typically serve large zones [34].

The main objective of the study is to find reasons for poor temperature and air velocity control and to provide recommendations on how to handle air velocity and temperature parameters in the design and operation to enable good comfort and energy performance at the same time. The main hypothesis in this study is that v_a, t_i, and supply air temperature (t_{sup}) are the parameters that are not well controlled in the current design and operation practices. Our previous study, [35] showed high air velocities and dissatisfaction in the cooling season. In this study, we focus on the same buildings in the heating season and conduct long-term measurements in some buildings to analyse why t_i and t_{sup} in operation are far from optimal. It is possible that typical actions in handling indoor climate complaints have been changing the controller setpoints, resulting in too high t_i out of the expected comfort range. Some roles may be also attributed to controllers that are not programmed to change the setpoints according to the outdoor running mean temperature (Θ_{rm}) and extract air. Another specific hypothesis tested in this study is that occupants adjust their clothing in the case of high winter temperatures and report high satisfaction rates.

Local thermal discomfort caused by v_a [36] can be a main issue for the unexpected operation of HVAC, as extensive studies in various settings have shown a strong correlation between t_i and its movement dynamics [37–41]. Perception of draught is stronger when air movement is pulsating rather than constant at the same v_a, highlighting the importance of airflow stability in ventilation design [42]. Fluctuations in airflow from supply air terminals can lead to occupant dissatisfaction, even with a properly designed ventilation air distribution system [41]. Given that t_{sup} can exacerbate the negative impact of fluctuating airflow, it is crucial to operate with appropriate t_{sup} that satisfies draught, air change efficiency, and energy performance simultaneously [43]. Previous studies have shown significant energy savings through optimal temperature control strategies [44–46], but these studies often overlook detailed aspects of TC, which in principle work as enabling aspects for such control strategies.

This study measured air distribution and TC in modern office landscapes in Tallinn. Five buildings with nearly 80 measurement points were analysed, each equipped with different HVAC systems common in heating dominating North-Europe. The study design combines results from the previous cooling season study [35], to analyse differences between seasons and to understand the reasons for elevated temperatures and air velocities. In comparison to the previous analysis of the summer season, a retrospective analysis of available characteristic yearly data for t_i and t_{sup} was conducted, supplemented with an indoor climate questionnaire (ICQ) on main indoor climate aspects. The hypothesis of the impact of clothing adaption on comfort perception was studied with 0.7 clo to explain the contradictory satisfaction levels of occupants with increased t_i values. Based on existing guidelines and recommendations for air distribution methods, we propose optimal setpoint curves for t_i and t_{sup}. Considering the multitude of factors influencing measurement results in real office environments, this study can provide some insights for future studies and the development of measurement methods.

2. Methods

This section provides an overview of the reference office buildings, measurement equipment, measurements conducted, and the ICQ survey employed in the study. The research methodology is structured into three key stages: measurements, analysis, and recommendations (Figure 1). Local TC measurements followed the same plan as the cooling season study [35], and the results were analysed in conjunction with the ICQ feedback. In addition to the previous study, we analysed retrospectively yearly t_i and t_{sup} data of two representative buildings. Finally, recommendations for temperature control curves are presented.

2.1. Reference Buildings. Five modern office buildings in Tallinn under the study (Table 1) are denoted by letters from A to E. The buildings were equipped with dedicated outdoor air-balanced ventilation systems with heat recovery and used mostly mixing ventilation and impinging jet ventilation (B). The buildings had different heating and cooling systems (Table 2). Room conditioning units included high-temperature cooling and low-temperature heating thermally active building systems (TABS) active chilled beams, ceiling panels, and fan coils. Room conditioning units in B, C, and D were operated for both heating and cooling purposes, while the other two had separated units for heating and cooling.

The temperature control was based on winter and summer temperature setpoints, but in the midseason, the only
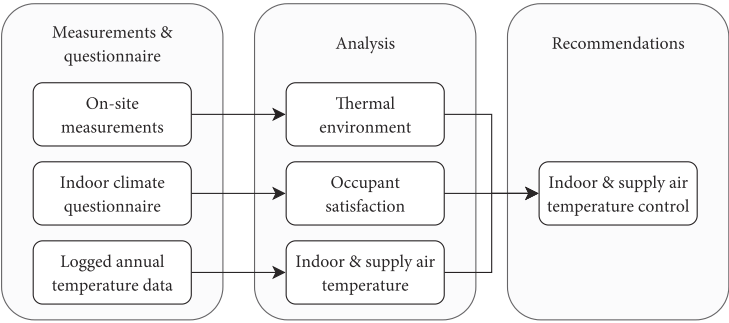
FIGURE 1: Flow chart of research methodology.

TABLE 1: General building information of reference objects [35].

Bldg	Year of constr.	Net floor area (m²)/ appr. total measured area (%)	Number of floors/ number of measured floors	Thermal transmittance (W/(m²·K))	Specific heat loss of external envelopes (W/(m²·K)/window-to-wall ratio/glazing g value)
A	2015	10800/30	13/4	U_{window} 0.80/U_{wall} 0.18 U_{roof} 0.09/U_{floor} 0.14	H/A 0.50 WWR 0.69 g 0.25
B	2018	7000/20	5/3	U_{window} 0.83/U_{wall} 0.12 U_{roof} 0.09/U_{floor} 0.13* (*above ambient air)	H/A 0.31 WWR 0.59 g 0.24
C	2017	18900/10	14/2	U_{window} 0.65/U_{wall} 0.10 U_{roof} 0.10/U_{floor} 0.15	H/A 0.30 WWR 0.38 g 0.30
D	2018	13900/100 (available office space)	2/2	U_{window} 1.0/U_{wall} 0.15 U_{roof} 0.14/U_{floor} < 0.15	H/A < 0.20 WWR < 0.25 g 0.30
E	Reconstr. 2014 (1982)	5300/20	6/1	U_{window} > 1.2/U_{wall} > 0.25 U_{roof} N/A/U_{floor} N/A	H/A > 0.50 WWR 0.90 g 0.40

option possible to set or change setpoints was manual control. In the heating season, the heating system operates according to the heating curve (buildings A, C, and D) depending on the outdoor air temperature and the room controller operates according to the heating (lower limit) setpoint. In Building B, the heating temperature curve remains constant. If t_i drops below the heating setpoint during the cooling season, no heating is applied in buildings A, C, and D, whereas cooling plants (except free cooling) are set not to operate during the heating season. In building B, both heating during the cooling season and cooling during the heating season are available from buffer tanks. In building E, electrical convectors are controlled manually, and multi-split fan coils are available for use during winter. The ventilation t_{sup} was controlled by extracting air temperature curves, except for building E where the setpoint was changed manually. According to building managers, both the designed and the built setpoints had been modified for many times, mostly based on complaints from occupants. In building B, TABS was not applied for heating during the daytime when additional supply air heating was used. Building C

often used ventilation-supported preheating with four-pipe active chilled beams as switching off ventilation practically turned heating off during nonworking hours. The design solutions for all the buildings stipulated that the opening of windows limits or reduces the performance of HVAC systems. During the on-site measurements, window opening was not observed.

Figure 2 displays photos of room conditioning units in each building. These photos were obtained with permission from the building managers and owners. Measurements were conducted consecutively in workplaces where the highest air velocities could be expected based on air jet assessment and building managers' feedback. These critical measurement point locations are shown in Table 3, where floor plan callouts, sectional views, and dimensions of office modules, where measurements were conducted, are presented.

2.2. Measuring Equipment. The TC measuring system (Figure 3) used for the previous summertime study [35] was also employed for the current measurements, including

TABLE 2: Room design solutions for heating, ventilation, and air conditioning in reference buildings [35].

Bldg	Heating	Ventilation	Cooling
A	Water-based convectors (height 300 mm, length 700–1800 mm) below the windowsill. Installed room unit heating power 18 W/m². Outdoor temperature compensated heating curve with room controllers. Switching seasons manually.	Mixing ventilation $1.4\,l/(s \times m^2)$ using active exposed chilled beams (effective length 2700–3300 mm) mounted in the open ceiling (height 2.75 m) for supply and circular valves (Ø 125 mm) for extract air (height 2.7 m). Extract air temperature-based t_{sup} control. Switching seasons manually.	Active exposed chilled beams (effective length 2700–3300 mm) mounted in the open ceiling (height 2.75 m). Installed room unit sensible cooling power 52 W/m². Flow rate control with room controllers. Switching seasons manually.
B	Thermally active building system (slab, room height 3.0 m). Installed heating power 43 W/m². Constant flow temperature and flow rate control with zone controllers. Switching seasons manually.	Impinging jet ventilation $1.4\,l/(s \times m^2)$ including duct diffusers (Ø 160–315mm, nozzle angle 120°C –180°C) for supply (height 2.7–2.8 m), mounted in the open ceiling to the perimeter of rooms. Wall and ceiling grilles with plenum box serving supply and extract air (height 2.8 m on cornice, 2.6 m for ribbed suspended ceiling). Extract air temperature-based t_{sup} control with additional supply air heating option. Switching seasons manually.	Thermally active building system (slab, room height 3.0 m). Installed sensible cooling power 41 W/m². Flow rate control with zone controllers. Switching seasons manually.
C	Four-pipe active ceiling integrated chilled beams (effective length 900–1500 mm) mounted in suspended ceiling (height 2.7 m). Installed room unit heating power 17 W/m². Outdoor temperature compensated heating curve with room controllers. Switching seasons manually.	Mixing ventilation $1.7\,l/(s \times m^2)$ using four-pipe ceiling integrated chilled beams (effective length 900–1500 mm) for supply air and circular valves (Ø 100 mm) for extract air (height 2.7 m). Extract air temperature-based t_{sup} control with preheating mode. Switching seasons manually.	Four-pipe active ceiling integrated chilled beams (effective length 900–1500 mm) mounted in suspended ceiling (height 2.7 m). Installed room unit sensible cooling power 46 W/m². Flow rate control with room controllers. Switching seasons manually.
D	Four-pipe radiant panels mounted in the open ceiling on the height of 2.4 m. Installed room unit heating power 24 W/m². Outdoor temperature compensated heating curve with room controllers. Switching seasons manually.	Mixing ventilation $2.1\,l/(s \times m^2)$. Rectangular nozzle diffusers including directionally adjustable nozzles (plates 160 × 160/200 × 200 mm) mounted on plenum box for supply air and circular plate (Ø 200–250 mm) combined with plenum box for extract air in the open ceiling (height 2.7 m). Extract air temperature-based t_{sup} control. Switching seasons manually.	Four-pipe radiant panels mounted in the open ceiling on the height of 2.4 m. Installed room unit sensible cooling power 10 W/m². Flow rate control with room controllers. Switching seasons manually.
E	Electrical convectors (height 200 mm, length 1500 mm) in front of windows. Installed room unit heating power 60 W/m². Manual local setpoint control.	Mixing ventilation $1.3\,l/(s \times m^2)$ with circular supply and extract air diffusers (Ø 160–250 mm) mounted in the suspended ceiling (height 2.5–2.7 m). Manual setpoint control. (supply air is not chilled).	Multisplit fan coil units (without heating function) mounted in the suspended ceiling (height 2.7 m). Installed total cooling power 78 W/m². Manual local setpoint control.

v_a, t_i, RH, and operative temperature (t_o). The probe data listed in Table 4 was recorded using the ComfortSense software version 4 on a laptop connected to the 54N90 Comfort-Sense frame [47]. Due to the occurrence of internal t_i exceeding expectations, there was a need to assess t_i concurrently with t_{sup}. To analyse the t_i and t_{sup}, we collected retrospective yearly data from a workplace in buildings C and E. In building C, we used data from the room controller and the duct temperature sensor as a reference for t_{sup}. In building E, HOBO Data Logger measurement data was used. Table 4 below shows the logging equipment used.

A comprehensive measurement campaign was conducted encompassing nearly 80 measurement points. We used a tripod-mounted equipment setup, with the frame and recording software placed on a mobile chair (Figure 3). According to ISO standard [19], probe heights of 0.1, 0.6, and 1.1 m from a seated person were used to measure draught. The upper 1.7 m and 2.0 m probe data are not analysed in this study. The vertical temperature difference was not critical in any building. In Figure 4 and in Appendix B in the Supporting Information section, we report temperatures from 0.6 and 1.1 m with very small differences. The same is applied for 0.1 m. RH probe height is not defined by the standard and was placed on the same level of 0.6 m with the t_o probe, the height of which was set to be the abdomen point of a sitting person, with the angle of 30° to mimic a sitting person [19].
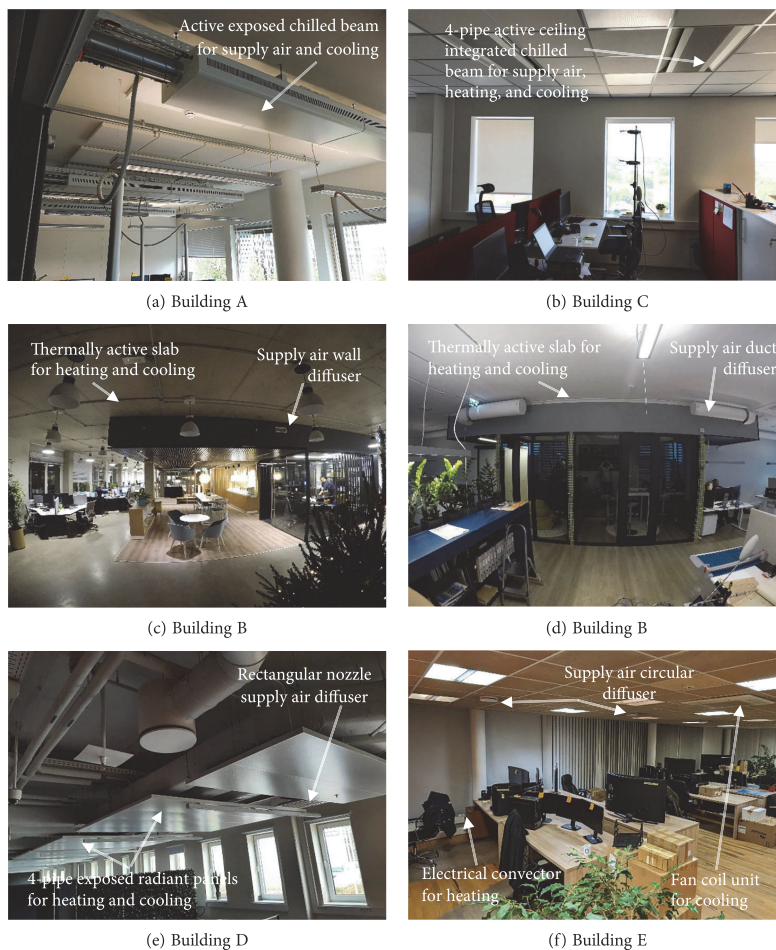
FIGURE 2: Room conditioning units: (a) building A—active exposed chilled beam for supply air and cooling, (b) building C—four-pipe active ceiling integrated chilled beam for supply air, heating, and cooling, (c, d) building B—thermally active slab for heating and cooling, supply air wall diffuser, and supply air duct diffuser, (e) building D—four-pipe exposed radiant panels for heating and cooling and rectangular nozzle supply air diffuser, and (f) building E—supply air circular air diffusers, electrical convector for heating, and fan coil unit for cooling.

Consistent with the summertime study, a metabolic rate of 1.2 met for sedentary activity was assumed, and no mechanical power from sedentary activity was considered. The calculations were based on a clothing unit of 1.0 clo, as specified in EN 16798-1 [16]. Turbulence intensity (Tu) and DR were calculated at a height of 1.1 m, while *PMV* with *PPD* was calculated at a height of 0.6 m. The data was processed in Microsoft Excel.
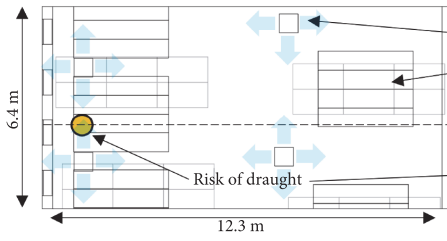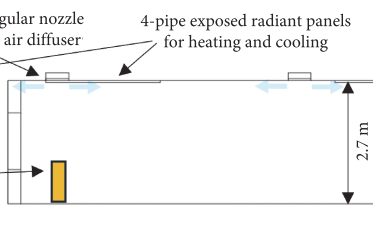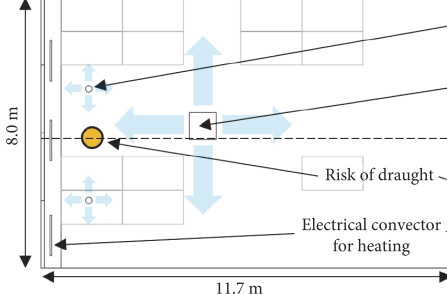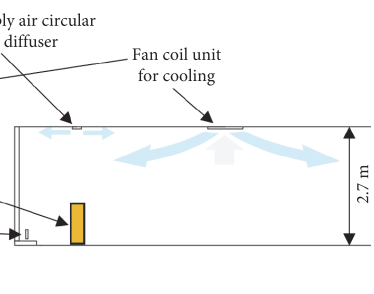
2.3. Measurements. On-site measurements were conducted in typical winter conditions during daytime operating hours of the buildings (Table 5). Measurement days were selected in collaboration with building owners to ensure a significant temperature difference between indoor and outdoor environments. The measurements followed ISO 7726 [19] guide-

lines, aiming to capture the conditions that align closely with occupant complaints. The occupants were replaced by a measurement tripod for 3 minutes (with a sampling rate of 20 Hz) as the duration of a single measurement, following EN 15726:2011 [52] methodology. Rooms were occupied, but occupants left the workplace when the measurement stand was installed. Precautions were taken to ensure that neither the fellow employees nor the measuring personnel had any influence on the results obtained. Windows and outdoor walls were deemed noncritical due to highly insulated thermal envelopes. Measurements were nearly simultaneous, conducted using a single measurement stand/equipment that was relocated from one workplace to another. Window opening was not observed and is not expected in these buildings due to cold outdoor temperatures. The measurement results

TABLE 3: Floor plan callouts and section views illustrating the critical locations of measurement points, marked with yellow dots/cylinders.

TABLE 3: Continued.

Building	Floor plan call-out	Section
D		
E		

Note: The blue arrows depict the potential air flow paths which may generate draught, and the grey arrows represent the circulation air.

were assessed according to the indoor climate categories (ICCs) that describe the quality of indoor climate, as provided in EN 16798-1 [16].

In order to enhance the evaluation of yearly t_i and t_{sup} data during heating, cooling, and midseason (ranging from +10°C to +15°C), we used Θ_{rm} equation from EN 16798-1 : 2019. The hourly t_i and t_{sup} analyses were conducted with 2020 weather data [51] in building C, and 15-min interval data was available in Building E. Data is filtered so that the results from occupied hours are shown.

2.4. ICQ. We conducted an online ICQ using Google Forms to assess the TC sensation of occupants. The questionnaire with 24 questions included standard EN 15251 [52] recommendations and additional questions for draught sensation in the past month and throughout all four seasons. No rapid fluctuations related to thermal conditions were observed during working hours in any of the buildings. The ICQ online form used in the study is provided in Appendix A in the Supporting Information section. However, in Building C, the ICQ was not possible due to the COVID-19 outbreak. Measurements were conducted simultaneously with the questionnaire, although the responses to the questionnaire came within a couple of days. Measurements and questionnaire results were analysed as separate samples.

3. Results and Discussion

In this study TC was analysed with short- and long-term measurements and with occupant questionnaires. Short-term air velocity/draught measurements were performed

during the heating season representative outdoor air temperature and specifically in areas where thermal discomfort complaints had either been reported or were anticipated as detailed in Table 3 of the methods section. Conducted according to the standard procedure in carefully selected locations, these measurements are expected to provide representative results of air velocity. To study draught perception more deeply, a focused ICQ was administered for the heating period, asking about the last month's occupant perceptions and concerns related to the indoor environment. While short-term measurements cannot represent temperature fluctuations, comprehensive year-round data on both indoor room air temperatures and ventilation supply air temperatures were analysed in two of the representative buildings. This longitudinal analysis was intended to support and contextualize the findings from the on-site measurements and questionnaire. The phased approach of this study, beginning with immediate on-site evaluations and extending to long-term environmental monitoring, was designed to create a robust framework for understanding the dynamics of indoor climate control and occupant comfort in office settings. This structure not only highlights the complexity of managing indoor environments but also underscores the necessity of integrating both immediate and extended temporal data to guide building management practices effectively.

This section reports a seasonal comparison of on-site measurements of v_a and t_i, providing detailed heating season measurement results from Building B as an example. The results for the remaining four buildings are provided in Appendixes B.1 to B.4 in the Supporting Information section. ICQ results are given with the ICQ template included
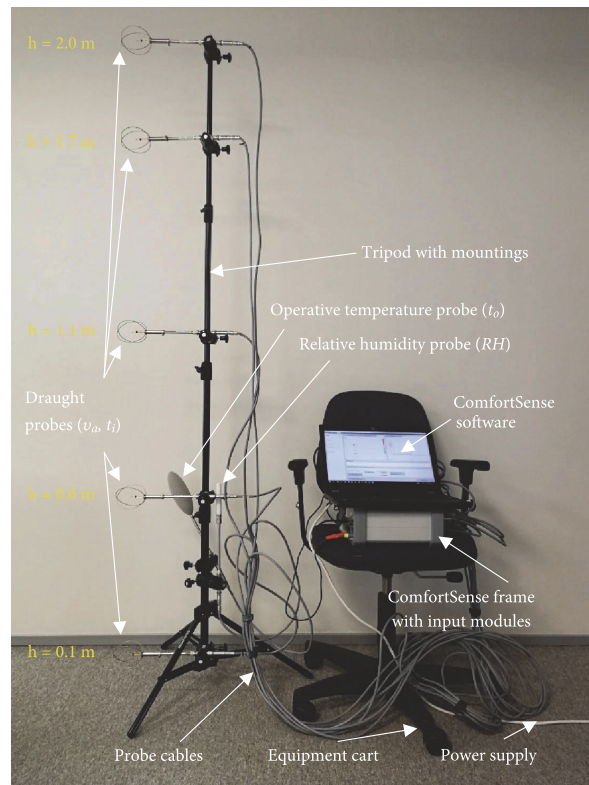
FIGURE 3: Measuring equipment setup including draught probes, an operative temperature probe, and a RH probe mounted on the tripod. Probes are connected through cables with the frame equipped with a power supply. ComfortSense software provides the measured data for the analysis.

TABLE 4: Measuring equipment specification [47–50].

	54 T33 draught probe	54 T37 relative humidity probe	54 T38 operative temperature probe	HOBO data logger U12-013	HLS 44 room controller	Duct temperature sensor NTC5k
Range	0.05–5 m/s $-20°C$ to $+80°C$	0–100%	0 to $+45°C$	$-20°C$ to $+70°C$	0 to $+50°C$	-30 to $+80°C$
Accuracy	±0.02 m/s ±0.2 K	$+1.5\%$	±0.2 K	±0.35 K	±0.5 K	±0.5 K

in Appendix A in the Supporting Information section. Long-term monitoring results of t_i and t_{sup} differences are presented, and the comfort temperature range is recalculated with changed clo value to explain the results. Based on the findings, temperature control recommendations are made.

3.1. On-Site Measurement and Seasonal Comparison of Air Velocity and Indoor Air Temperature.

In building A with wall-mounted water radiators, the t_i results do not meet the required criteria for new office buildings, as more than half of the results fall into the III ICC (Figure 4). The results of t_o show slightly better results, achieving II ICC in 13 positions out of 18. The v_a results fall within the I ICC, except for

measurement position #14, which falls into the III ICC due to unusually high internal heat gains from specific work equipment. The DR results also fall within the I ICC, with the exception of position #14, which falls into the III class.

Box and whisker plots are used to present the v_a values during a 180-s measurement period at three heights: 0.1, 0.6, and 1.1 m. The whiskers represent the minimum and maximum values, while round-shaped dots represent outliers that deviate significantly from the rest of the measured data. The box indicates the first and third quartiles, with the median displayed as a line within the box. The mean v_a value is denoted by a cross symbol in the box, representing the measurement position.

ina, 2024, 1, Downloaded from https://onlinelibrary.wiley.com/doi/10.1155/2024/9992937 by Tallin Technical University, Wiley Online Library on [10/10/2024]. See the Terms and Conditions (https://onlinelibrary.wiley.com/terms-and-conditions) on Wiley Online Library for rules of use; OA articles are governed by the applicable Creative Commons License

		1	2	3	4	5	6	7	8	9	10	11	12	13	14	15	16	17	18
$t_{i\,(1.1\,m)}$	°C	24.1	24.2	24.0	24.1	24.5	24.6	23.8	24.1	24.2	24.3	24.2	24.0	23.9	23.1	23.8	23.7	24.2	24.5
$v_{a\,(1.1\,m)}$	m/s	0.06	0.05	0.08	0.05	0.06	0.09	0.05	0.03	0.05	0.04	0.04	0.08	0.09	0.26	0.07	0.04	0.05	0.08
$Tu_{(1.1\,m)}$	%	66.7	88.8	102.2	43.3	52.6	34.9	51.8	49.3	58.8	57.9	64.4	64.0	69.3	41.5	68.5	65.5	54.2	57.1
$DR_{(1.1\,m)}$	%	2.9	0.0	6.9	1.3	2.1	5.3	0.0	0.0	1.0	0.0	0.0	5.6	7.2	29.9	4.9	0.0	1.5	5.5
$t_{i\,(0.6\,m)}$	°C	23.6	23.7	23.7	23.8	24.1	24.2	23.7	23.6	23.6	23.9	23.9	23.6	23.7	23.2	23.5	23.6	23.8	24.5
$t_{o(0.6\,m)}$	°C	24.1	24.1	23.6	23.7	24.2	24.2	23.4	23.7	23.9	24.0	23.8	23.3	23.8	23.4	23.3	23.4	23.8	24.4
$v_{a\,(0.6\,m)}$	m/s	0.03	0.11	0.09	0.07	0.06	0.07	0.02	0.06	0.04	0.06	0.05	0.04	0.04	0.17	0.05	0.04	0.04	0.10
$RH_{(0.6\,m)}$	%	24.9	26.5	24.9	24.9	25.0	26.5	24.7	25.2	25.6	24.6	24.1	24.8	23.3	23.0	23.6	23.8	25.8	24.2
$PMV_{(0.6\,m)}$	–	0.4	0.4	0.3	0.3	0.5	0.5	0.3	0.4	0.4	0.4	0.4	0.3	0.4	0.1	0.3	0.3	0.4	0.5
$PPD_{(0.6\,m)}$	%	8.8	7.8	6.9	7.5	9.3	9.6	6.8	7.7	8.1	8.4	7.8	6.5	7.6	5.3	6.3	6.6	7.8	9.5

■ I Cat.   ■ III Cat.

■ II Cat.   ■ IV Cat.

FIGURE 4: Air velocity and thermal comfort results in measurement Locations 1–18 in building A.

Average values of measured v_a and t_i from all buildings and locations are summarised in box and whisker plots (Figure 5). The on-site v_a measurements during the heating season exhibit better performance compared to the cooling season. During the heating season, buildings B and E reach v_a values in the II ICC, while the other three buildings are within the I ICC. For the cooling season, only building D remains in the I ICC. The III ICC is reached once in building C during the heating season and three times overall during the cooling season, including buildings B, C, and E. The v_a results during the cooling season show more variability, except for building D.

Compared to the cooling season study [35], building A with open ceiling chilled beams for cooling and wall-mounted water radiators showed slightly better results regarding v_a and DR during heating season measurements. While maintaining I ICC in most of the positions in summer, heating season measurements showed elevated t_i values, resulting in II and III ICC. On both occasions, no significant v_a value differences between 0.1, 0.6, and 1.1 m

TABLE 5: Time of thermal comfort measurements in workplaces and weather information from the Estonian Weather Service [51].

| Building	Time of measurements	Weather conditions	Minimum outdoor temp. ˚C	Daily mean outdoor temp. ˚C
A	21.02.2020 After midday	Cloudy skies light showers	+2.7	+0.5
B	17.12.2018 after midday	Cloudy skies light snowing	−4.0	−2.1
C	17.02.2020 before midday	Cloudy skies showers	+4.5	+6.2
D	18.02.2020 after midday	Cloudy skies light showers	+6.0	+5.0
E	14.02.2020 after midday	Partly cloudy skies No precipitation	−2.5	+0.1
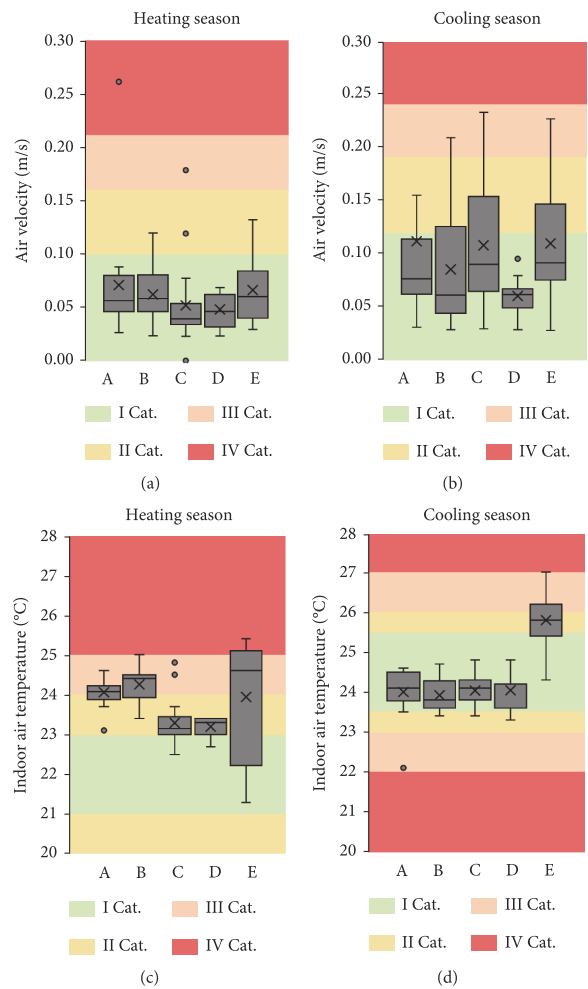
FIGURE 5: Air velocities recorded during the on-site measurements in the (a) heating and (b) cooling seasons and indoor air temperatures in the (c) heating and (d) cooling [35] seasons in buildings A to E.

measuring heights were observed. Heating season measurement results in building B with impinging jet ventilation confirmed higher v_a values and fluctuations on the lowest height of 0.1 m near the floor. During summertime, office spaces with higher ventilation rates (measurement points 4–8) stand out more clearly compared to heating season v_a values. This building was also strongly overheated during the heating season, showing the highest average value over 24°C. Building C that had active chilled beams similar to building A, achieved better results in the heating season with v_a and DR, while II and III ICCs were reached once. Building D with ceiling panels stands out on both summer and cooling season measurements, while all the results stay in the I ICC range. Building E with fan coil units was considered to be the least recommended configuration in the cooling season study [35]. While v_a was not an issue in the heating season, measured values of Tu exceed the standard [53] recommendation of Tu by 40%. Figure 6 compares all Tu and DR values, the latter calculated with the standard-recommended values and actual measured values. The slightly downward trend in the results indicates that the measured DR values are lower than the criteria based on the standard.

3.2. ICQ. The ICQ survey was conducted in four out of five buildings (building C was not included) in the heating season. Due to the low response rate, it is probable that complaints are overrepresented in the sample. The survey results are presented in Table 6 (ICQ), Figure 7 (draught), and Figure 8 (thermal environment).

In buildings A and D, about 1/3 of the ICQ respondents experienced draught. Such a high prevalence of draught could not be expected based on measured 1.1 m air velocities, which were below 0.1 m/s. If only the votes "often" would be counted as draught complaints, the prevalence of draught would remain below 20% in all buildings which is in line with measured results. Air velocities were slightly higher, especially in building D, at 0.1 m, which may indicate some cold draught from window surfaces. While t_i was 23°C–24°C, it is possible that a higher t_{sup} was applied to compensate draught complaints, resulting also in elevated t_i. In turn, this means higher heating energy costs and lower RH. In buildings B and E, which were similarly overheated, no significant draught complaints were reported.

Responses on the temperature show that occupants were either satisfied or would prefer higher temperature, which is in line with the reported neutral or slightly cool responses clearly dominating. Slightly warm was reported too, but the prevalence was lower, always below 20%. Also, the prevalence of cool and warm was always below 20%. In building A where t_i was as high as 24°C, slightly cool was reported more often than neutral, and reported preferences for higher and lower temperature were considerably higher, 26 and 22%, respectively. Building B had the highest t_i, and in this case, a high percentage of 89% was reported as neutral. In buildings D and E, the reported preference for a higher temperature was very high, 43 and 39% despite $t_i > 23$°C. Such results indicate that occupants have adapted to high t_i, and some draught may lead to even higher temperature preference. It has to be noted that t_i in all buildings was much higher than the expected neutral comfort temperature of 22°C, thus clothing must be less than 1.0 clo commonly assumed for the heating season. This phenomenon is further studied with t_i and t_{sup} long-term measurements in Section 3.3.

3.3. Analysis of Room Air and Supply Air Temperature Difference. To analyse the temperature difference between t_i and t_{sup}, adequate recommendations are available for dry cooling systems in general for condensation prevention as well as directly for active and passive chilled beams [54]. Guidelines for temperature differences between t_{sup} and air in the breathing zone to assure ventilation effectiveness are provided in CR 1752 : 1998 [55]. To separate midseason from heating and cooling seasons, we used Θ_{rm} running mean outdoor temperature formula B.2 from EN 16798-1 [16]. By defining the midseason as outdoor air temperatures of 10°C and 15°C, ICC temperature boundaries were set by merging the lower limits of the heating season and the upper limits of the cooling season, as shown in Figure 9. In this figure, t_i from a typical floor is reported as a cumulative frequency curve from occupied hours and t_{sup} as dots. Horizontal axis represents relative time 0%–100% for all three seasons, and the width of each season indicates the length of the season, that is, the heating season is much longer than the cooling and the midseason. *Rehva Guidebook* [54] instructions were used to define the recommended area suitable for maintaining convenient TC and draught risk control to assess the recommended temperature difference in Figure 10.

The t_{sup} in building C during the heating season mostly ranged between +20°C and +21°C. The scattered t_{sup} points above the t_i duration curve during heating mode can be attributed to the use of a four-pipe active chilled beam system for heating. These high t_{sup} values were often observed at the beginning of the workday, especially on Monday mornings, because heating setpoints were lowered during weekends. The gap between t_i and t_{sup} is more pronounced during the cooling season, although t_{sup} values exhibit greater variability. During the midseason, t_{sup} values are more scattered than in winter months, but they remain consistently below t_i. Thus, in building C, higher t_{sup} values are observed when additional heat is required from the ventilation system for room heating. However, this explanation does not work in the cooling season, albeit the number of points is very small and may be attributed to the situation where the cooling coil is not in operation for some reason. In contrast, during the midseason, t_{sup} remains consistently lower than t_i.

In building E, the t_i duration curves start from the lower limit of I ICC and exceed the upper limits of III ICC, indicating long time periods throughout the year when the building is overheated. Similar to building C, when defined by the midseason, t_{sup} remains well below t_i. During all seasons, there are scattered t_{sup} values that exceed the recommended limit of t_{sup} lower than 3°C compared to t_i, which is considered to increase the risk of draught. The disparity between

(a)

(b)
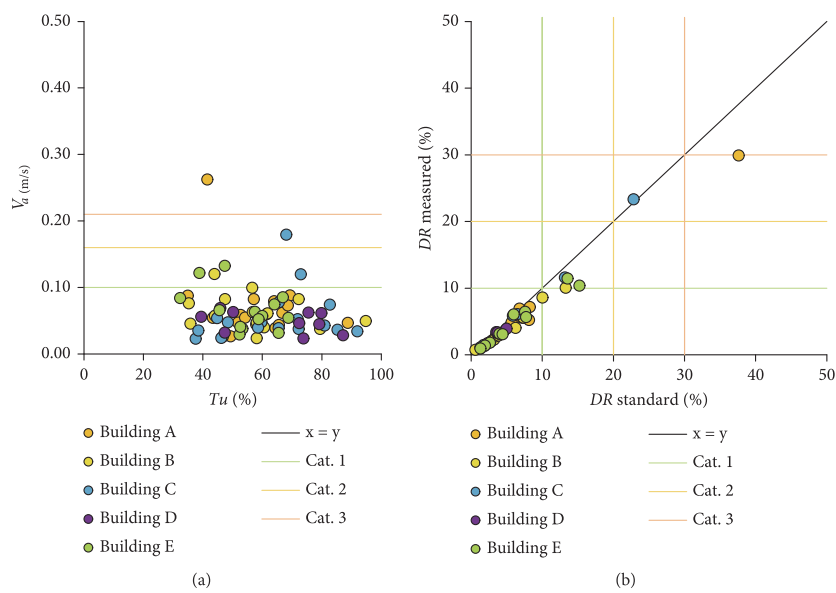
FIGURE 6: (a) Results of air velocity and turbulence intensity according to maximum air velocity Categories I–III in winter. (b) Draught rate correlation in measured and standard-based [53] conditions according to draught rate Categories I–III.

TABLE 6: Summary of the indoor climate questionnaire.

Building	A	B	D	E
Number of respondents	23	18	21	18
Male/female	5/18	8/10	5/16	8/10
Age	Majority 26-35 and 36-45	Majority 26-35 and 36-45	Majority 26-35	Majority 26-35
Location	Mostly open office	Open office	Mostly open office	Mostly open office
Working hours	Mostly whole workday	2/3 whole workday	Mostly whole workday	2/3 whole workday
Temperature	78% satisfied, but both cool and warm reported	95% satisfied	76% satisfied, but very high preferences for lower and higher temperature	88% satisfied
Draught	30% dissatisfied, draught reported both in summer and winter	No draught complaints, while few noted more draught in the summer season	33% dissatisfied, no draught complaints from summer	No draught complaints
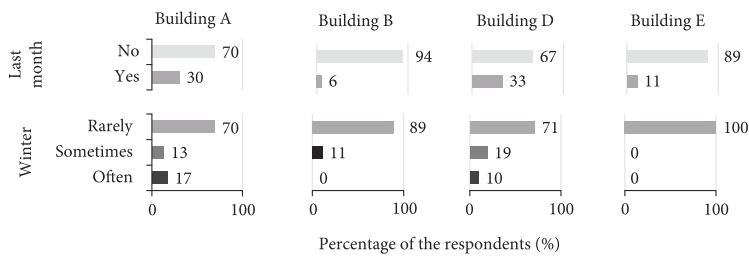
FIGURE 7: Results of the indoor climate questionnaire for draught complaints (heating season).
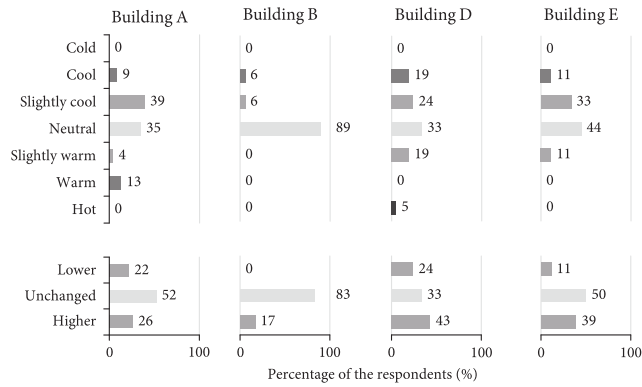
FIGURE 8: Results of the indoor climate questionnaire for indoor air temperature (heating season).

(a)

(b)
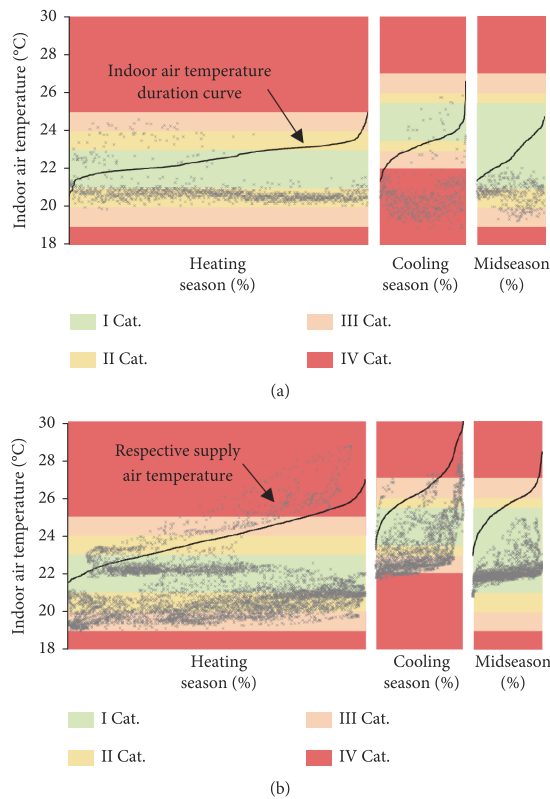
FIGURE 9: Yearly duration curves of indoor air temperature in (a) building C and (b) building E and respective supply air temperatures for heating, cooling, and midseason compared to recommended [16] indoor climate category values.

the two scattered point clouds in winter months is due to different setpoints during the heating season in different calendar years. During the cooling season, t_{sup} values are also excessively high. In the case of the midseason, when the tem-

perature difference is most stable, t_{sup} remains well below t_i. It was observed in building E that a systematic approach was employed in positioning the workstations to avoid areas and directions with a high risk of draught, as outlined in the
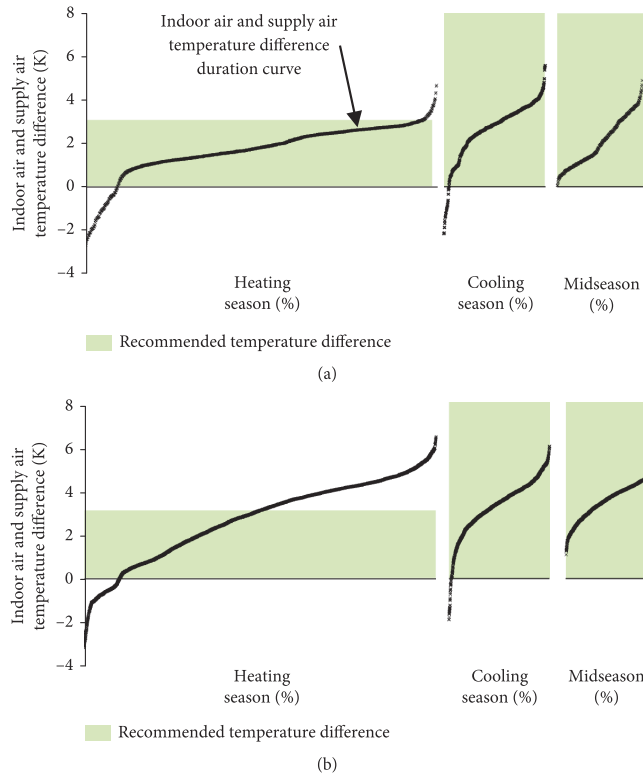
FIGURE 10: Yearly duration curve of the indoor air temperature and ventilation supply air difference for heating, cooling, and midseason compared to recommended [54] values in (a) building C and (b) building E.

cooling season study [35]. Nonetheless, the findings presented in the analysis of t_i and t_{sup} reveal significant deficiencies in the control of t_i, as well as manual adjustments to the t_{sup} settings.

3.4. Reduced Clothing Comfort Criterion for Measured Room Air Temperatures. To explain the acceptance of 23°C–25°C t_i values by occupants compared to a neutral temperature of 22°C at 1.0 clo, a new classification criterion for t_i based on the clothing value of 0.7 clo was calculated according to EN 16798-1:2019 (v_a of 0.1 m/s, RH of 40% for the heating season, and RH of 60% for the cooling season). It should be noted that the temperature scale difference between the heating and cooling graphs calculated with a 0.7 clo arises from the different RH values of 40% for the heating and 60% for the cooling season.

When applying the 0.7 clo criterion, the majority of measurement points in buildings A, B, C, and D stay within the II ICC, as shown in Figure 11. In building E, the temperature range is wider, but only one position falls into the III ICC. For the cooling season, the 0.7 clo criterion worsens the results in all five buildings, indicating that the 0.5 clo value is a sound assumption corresponding to occupants' perception.

Figures 5 and 12 show that there are no significant differences in the measured temperatures during the heating and the cooling season in buildings A and B. In building B, the average t_i values were slightly higher during the winter compared to the summer measurements. In buildings A to D, average t_i values were closer to average cooling season t_i values than to recommended heating period setpoints. This can be explained by two hypotheses. Firstly, raising the t_{sup} setpoint may be an effective strategy to avoid draught complaints. Secondly, the occupants have adapted their clothing to a lower value than the standard of 1.0 clo. Figure 12 shows that by adjusting the clo value from 1.0 to 0.7, the t_i values are within the I ICC for 79% of the measurement time, instead of the initial 18%. Therefore, it is likely that temperature control in the buildings studied is based on 0.7 clo in the heating season and 0.5 clo in the cooling season. This results only in 1°C temperature difference between the cooling and the heating season temperature scales.

3.5. Temperature Control Recommendations. One way to enhance indoor temperature control is to apply comfort temperature ranges according to Θ_{rm}; however, it was not implemented in the building automation and control system of any of the studied buildings. Θ_{rm} enables establishing
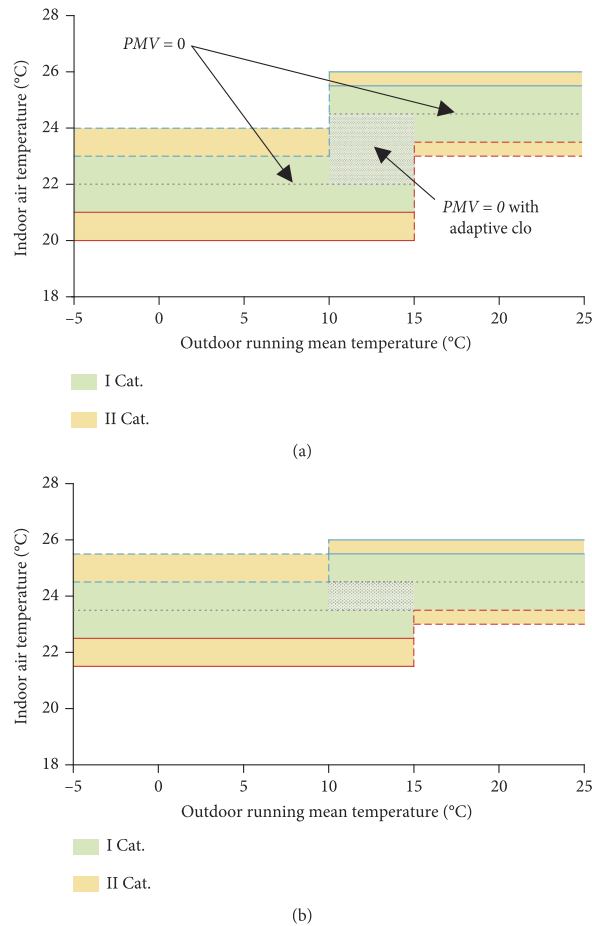
(a)

(b)

FIGURE 11: Room air temperature control recommendations for heating and cooling seasons, (a) based on the standard 1.0/0.5 clo and (b) based on the estimated 0.7./0.5 clo in the measured buildings.

temperature ranges for each season, which were not visible in the measured results, as shown in Figure 11. Optimal energy efficiency can be achieved by operating on the lower limit red line during the heating season and on the upper limit blue line during the cooling season. The dashed red line shows the heating limit during the cooling season (heating should be mostly avoidable through accurate t_{sup} control), while the dashed blue line represents the cooling limit during the heating season (which can be achieved with free cooling if needed). The grey dotted line represents a PMV value of 0 that can be employed as the t_i setpoint with a deadband, to program the control strategy based on the Θ_{rm}. In the midseason, the dashed area represents PMV = 0 with clothing adaption, that is, it is expected that occupants change clothing in between 0.5 and 1.0 clo as needed. The right figure describes the situation in the buildings with a probable 0.7 clo in the heating season.

Because temperature control shown in Figure 11 was not applied in any of the buildings, we converted these values to controller setpoints for practical application, as shown in Table 6. Outdoor running mean temperature formula and three setpoint and deadband values are to be programmed to controllers. For instance, in I ICC, <10 C Θ_{rm} controller setpoint is $22 \pm 1°C$. The $\pm 1°C$ indicates a deadband of 2°C, resulting in a heating limit of +21°C. The values in Table 7 are rounded to the nearest 0.5°C, and the cooling deadband is slightly smaller due to the impact of RH on PMV. In Table 7, ideal control accuracy is assumed; Therefore, in practice, small adjustments depending on the system may be needed to ensure that the temperature remains within the green or yellow areas.

Another observed challenge was in the controlling of t_{sup} that was a potential reason for elevated t_i. Constant air volume systems used in buildings A and C with chilled beams
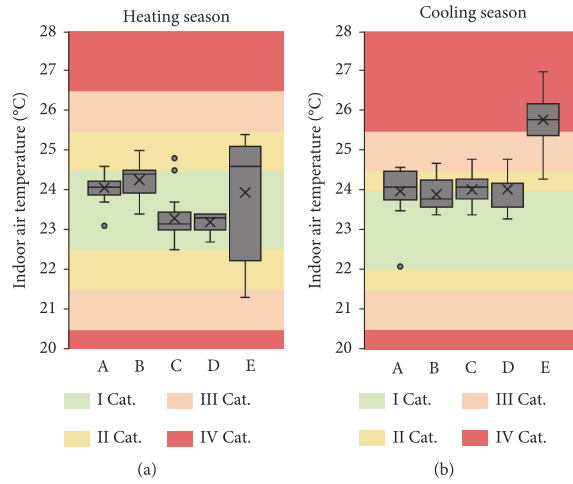
FIGURE 12: Indoor air temperatures recorded during on-site measurements in (a) the heating and (b) the cooling [35] seasons on the 0.7 clo temperature scale in buildings A to E.

TABLE 7: Controller setpoint and deadband values as a function of outdoor running mean temperature converted from Figure 11(a).

Outdoor running mean temperature (°C)	Controller setpoint, Category I	Controller setpoint, Category II
< 10 (heating)	22 ± 1	22 ± 2
10–15 (midseason)	23.25 ± 2.25	23 ± 3
> 15 (cooling)	24.5 ± 1	24.5 ± 1.5

rely on seasonal resetting of t_{sup}, ranging from +18°C to +20°C during the cooling season and from +19°C to +21°C during the heating season [54]. In impinging jet ventilation (B), approximately 1 to 2 K lower temperatures should be employed for t_{sup} compared to mixing ventilation to prevent short circuits caused by buoyancy-driven upward air movement [55, 56]. It is recommended to maintain a minimum t_{sup} of +18°C for impinging jet ventilation. Furthermore, when combining impinging jet ventilation with a high-temperature cooling system, the air distribution may transition to a mixing air system [57]. To achieve satisfactory t_{sup} control for the studied supply air and room conditioning units, a recommended t_{sup} curve based on design values proposed in *Rehva Guidebook* No. 5 [54] was used, which is supported by the measurement results in building C depicted in Figure 13. This curve is aimed at striking a compromise between preventing overheating and avoiding draught discomfort. The proposed t_{sup} control method is effective when room conditioning units are designed to maintain low air velocities. However, in practice, the manual resetting of t_{sup} in the studied buildings was performed randomly based on the season [58], indicating that t_{sup} was

gradually increased during both the heating and the cooling season to mitigate draught complaints.

3.6. Limitations and Future Work. In this study, on-site measurements are subject to limitations in terms of boundary conditions control and may not have captured the most critical scenarios. The interpretation of the findings of the study is most applicable in heating-dominated climatic conditions. Additionally, while the study examined five different HVAC system configurations and included up to 80 measurement points in office buildings, it does not encompass the full spectrum of systems found in real-world office buildings. Moreover, the retrospective analysis of t_i and t_{sup} was restricted to two buildings, limiting the generalizability of the results. Therefore, it would be reasonable to validate these findings in future studies with more comprehensive setups. Future measurements should consider additional factors to enhance accuracy and efficiency. These include finding suitable methods to assess HVAC system performance by incorporating subjective information from building managers and postproject technical documents, without the need for detailed building inspections. Addressing specific complaints over time intervals or extended periods is another crucial aspect to consider. Utilizing mobile phone-based web applications could improve the ability to pinpoint the location of the room and individual respondents, ensuring more precise data collection about indoor climate satisfaction. Additionally, surveying specific individuals within shorter time frames enables better assessment of HVAC parameters at their respective locations. Offering some bonuses to respond to the questionnaire could increase the response rate. Moreover, it would be beneficial to include clothing-related queries in ICQs and systematically collect clothing information within the buildings during surveys.
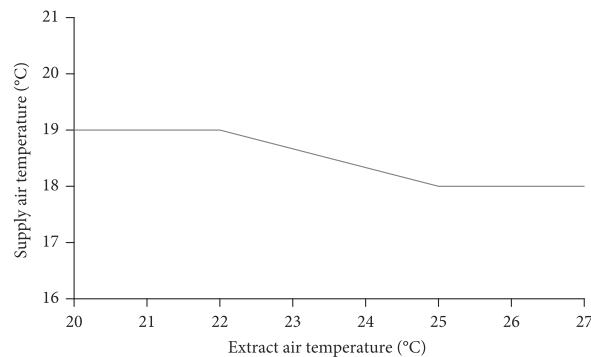
FIGURE 13: Recommendation for a control curve of ventilation supply air setpoint depending on the ventilation extract air temperature.

4. Conclusions

This study focuses on TC and draught in five office buildings in Tallinn, Estonia. Room conditioning units in these buildings included various configurations, such as open ceiling active chilled beams with radiator heating, thermally activated building systems, suspended ceiling four-pipe active chilled beams for heating and cooling, open ceiling four-pipe radiant panels, and multisplit fan coil units for cooling with electrical radiators for heating. General TC and local thermal discomfort measurements and a questionnaire study were conducted. Comparisons of supply air and room temperature were performed for heating, midseason, and cooling seasons using calculated outdoor running mean temperature.

Our findings revealed a limited or no draught discomfort during the heating season. However, the general TC criteria were not met in three out of five buildings because of too high indoor temperatures that ranged from 23°C to 25°C in the heating season. For a better understanding of the clothing adaption by occupants, the ranges of the temperature criterion for the heating season were recalculated by assuming a lower clothing value of 0.7 clo. With this adjustment, two buildings achieved Category I TC, while three buildings were within Category II. In the cooling season, the application of 0.7 clo temperature ranges worsened the results, revealing that 0.5 clo corresponds to occupants' preferences in clothing and is the correct value to be used in the assessment. Generally, our findings confirm the hypothesis that air velocities, room, and supply air temperatures are not well controlled in the current design and operation practices.

Regarding air velocities, the office with four-pipe radiant ceiling panels performed best, exhibiting low air velocities both in summer and winter. Buildings with active chilled beams demonstrated the potential to meet Category II requirements for air velocity and room air temperature simultaneously. The building with slab-based TABS had air velocities similar to those with active chilled beams but experienced significant overheating during the heating season.

While in some buildings, the measured indoor air temperature during the heating season was even higher than in the cooling season, the indoor and supply air temperature control was studied. It was observed that elevated setpoints are likely to be used to compensate for draught, resulting in overheating. Consequently, to adapt with 23°C–25°C indoor temperatures in the heating season, occupants had adjusted their clothing to 0.7 clo, estimated from reported satisfaction with the temperature in the occupant questionnaire. To improve the temperature control and to avoid overheating, we propose a control curve for room temperature being based on outdoor running mean temperature and for supply air temperature control based on the extract air temperature. As all the office buildings studied had some room for improvement in the temperature control, it is important to avoid draught both with design and correct setpoints, at the same time maintaining a lower supply air temperature compared to the room temperature. While the overheating reported in this study indicates an extensive energy penalty, in the future research, it is worth applying the proposed improvement measures to find out how effectively they can solve the problem.

Nomenclature

DR	draught rate (%)
Θ_{rm}	outdoor running mean air temperature (°C)
HVAC	heating, ventilation, and air conditioning
ICC	indoor climate category
ICQ	indoor climate questionnaire
PMV	predicted mean vote
PPD	predicted percentage dissatisfied (%)
RH	relative humidity (%)
TABS	thermally active building systems
TC	thermal comfort
t_i	indoor air temperature (°C)
t_o	operative temperature (°C)
t_{sup}	supply air temperature (°C)
Tu	turbulence intensity
v_a	air velocity (m/s)

Data Availability Statement

The measurement data used to support the findings of this study are included within the article and supporting information. Long-term temperature measurement data is available from the authors.

Conflicts of Interest

The authors declare no conflicts of interest.

Author Contributions

J.K. designed the experiments. M.K. prepared agreements with the building owners, performed the measurements, and analysed the data. M.T. and J.K. helped to perform the data analysis. M.K., R.S., M.T., and J.K. wrote this paper.

Supporting Information

Additional supporting information can be found online in the Supporting Information section. Supporting Information contains the form (Appendix A) used to survey participants regarding their perceptions of indoor climate conditions. The questionnaire includes sections on thermal comfort, air quality, lighting, and acoustic conditions, designed to gather comprehensive feedback from occupants. Appendixes B.1 to B.4 with Figures 1, 2, 3, and 4, respectively, represent the detailed measurement results for indoor climate parameters in building B to building E. The data includes temperature, humidity, and draught results, allowing for comparative analysis across different buildings. (Supporting Information)

References

[1] I. Mujan, A. S. Anđelković, V. Munćan, M. Kljajić, and D. Ružić, "Influence of indoor environmental quality on human health and productivity-a review," *Journal of Cleaner Production*, vol. 217, pp. 646–657, 2019.

[2] Y. Al Horr, M. Arif, A. Kaushik, A. Mazroei, M. Katafygiotou, and E. Elsarrag, "Occupant productivity and office indoor environment quality: a review of the literature," *Building and Environment*, vol. 105, pp. 369–389, 2016.

[3] J. Sundell, "On the history of indoor air quality and health," *Indoor Air*, vol. 14, no. s7, pp. 51–58, 2004.

[4] P. Wargocki and R. Djukanovic, "Simulations of the potential revenue from investment in improved indoor air quality in an office building," *ASHRAE Transactions*, vol. 111, 2005.

[5] W. J. Fisk and A. H. Rosenfeld, "Estimates of improved productivity and health from better indoor environments," *Indoor Air*, vol. 7, no. 3, pp. 158–172, 1997.

[6] R. Valancius, A. Jurelionis, and V. Dorosevas, "Method for cost-benefit analysis of improved indoor climate conditions and reduced energy consumption in office buildings," *Energies*, vol. 6, no. 9, pp. 4591–4606, 2013.

[7] R. Djukanovic, P. Wargocki, and P. O. Fanger, "Cost-benefit analysis of improved air quality in an office building. In proceedings of the proceedings of indoor air 2002," *Citeseer*, vol. 1, pp. 808–813, 2002.

[8] A. Leaman and B. Bordass, "Productivity in buildings: the 'killer'variables," in *In Creating the productive workplace*, pp. 181–208, Taylor & Francis, 2006.

[9] L. Lan, P. Wargocki, and Z. Lian, "Thermal effects on human performance in office environment measured by integrating task speed and accuracy," *Applied Ergonomics*, vol. 45, no. 3, pp. 490–495, 2014.

[10] S. Lamb and K. C. S. Kwok, "A longitudinal investigation of work environment stressors on the performance and wellbeing of office workers," *Applied Ergonomics*, vol. 52, pp. 104–111, 2016.

[11] O. A. Seppänen and W. Fisk, "Some quantitative relations between indoor environmental quality and work performance or health," *Hvac&R Research*, vol. 12, no. 4, pp. 957–973, 2006.

[12] L. Yang, H. Yan, and J. C. Lam, "Thermal comfort and building energy consumption implications–a review," *Applied Energy*, vol. 115, pp. 164–173, 2014.

[13] H. Liu, X. Ma, Z. Zhang, X. Cheng, Y. Chen, and S. Kojima, "Study on the relationship between thermal comfort and learning efficiency of different classroom-types in transitional seasons in the hot summer and cold winter zone of China," *Energies*, vol. 14, no. 19, p. 6338, 2021.

[14] J. Jiang, D. Wang, Y. Liu, Y. Xu, and J. Liu, "A study on pupils' learning performance and thermal comfort of primary schools in China," *Building and Environment*, vol. 134, pp. 102–113, 2018.

[15] O. Seppanen, W. J. Fisk, and Q. H. Lei, "Effect of temperature on task performance in office environment," Department of Energy, United States, 2006.

[16] European Committee for Standardization (CEN), *EN Standard. 16798-1. Energy performance of buildings - Ventilation for buildings - Part 1: Indoor environmental input parameters for design and assessment of energy performance of buildings addressing indoor air quality, thermal environment, lighting and acoustics - Module M1-6*, European Committee for Standardization (CEN), Brussels, Belgium, 2019.

[17] European Committee for Standardization (CEN), *EN 16798-2: 2019 Energy performance of buildings - Ventilation for buildings - Part 2: Interpretation of the requirements in EN 16798-1 - Indoor environmental input parameters for design and assessment of energy performance of buildings addressing indoor air quality, thermal environment, lighting and acoustics (Module M1-6)*, European Committee for Standardization (CEN), Brussels, Belgium, 2019.

[18] International Organization for Standardization (ISO), *EN ISO 7730: 2005 Ergonomics of the thermal environment — analytical determination and interpretation of thermal comfort using*

calculation of the PMV and PPD indices and local thermal comfort criteria, International Organization for Standardization (ISO), Geneva, Switzerland, 2005.

[19] International Organization for Standardization (ISO), *EN ISO 7726: 1998 Ergonomics of the thermal environment - instruments for measuring physical quantities*, International Organization for Standardization (ISO), Geneva, Switzerland, 1998.

[20] M. Geshwiler, *ASHRAE pocket guide for air conditioning, heating, ventilation, refrigeration*, ASHRAE, Atlanta, United States, IP Edition edition, 2005.

[21] American National Standards Institute/American Society of Heating and Refrigerating and Air-Conditioning Engineers (ANSI/ASHRAE), *ASHRAE Standard 55 American National Stadards Institute/American Society of Heating, Refrigerating and Air-Conditioning Engineers*, American National Standards Institute/American Society of Heating and Refrigerating and Air-Conditioning Engineers (ANSI/ASHRAE), Atlanta, GA, USA, 2020.

[22] S. Gao, R. Ooka, and W. Oh, "Experimental investigation of the effect of clothing insulation on thermal comfort indices," *Building and Environment*, vol. 187, article 107393, 2021.

[23] P. Jafarpur and U. Berardi, "Effects of climate changes on building energy demand and thermal comfort in Canadian office buildings adopting different temperature setpoints," *Journal of Building Engineering*, vol. 42, article 102725, 2021.

[24] M. Frontczak, S. Schiavon, J. Goins, E. Arens, H. Zhang, and P. Wargocki, "Quantitative relationships between occupant satisfaction and satisfaction aspects of indoor environmental quality and building design," *Indoor Air*, vol. 22, no. 2, pp. 119–131, 2012.

[25] J. A. Gärtner, F. M. Gray, and T. Auer, "Assessment of the impact of HVAC system configuration and control zoning on thermal comfort and energy efficiency in flexible office spaces," *Energy and Buildings*, vol. 212, article 109785, 2020.

[26] R. De Dear, "Thermal comfort in practice," *Indoor Air*, vol. 14, no. s7, pp. 32–39, 2004.

[27] S. K. Sansaniwal, J. Mathur, and S. Mathur, "Review of practices for human thermal comfort in buildings: present and future perspectives," *International Journal of Ambient Energy*, vol. 43, no. 1, pp. 2097–2123, 2022.

[28] W. Zhao, S. Lestinen, P. Mustakallio, S. Kilpeläinen, J. Jokisalo, and R. Kosonen, "Experimental study on thermal environment in a simulated classroom with different air distribution methods," *Journal of Building Engineering*, vol. 43, p. 103025, 2021.

[29] T. Cheung, S. Schiavon, L. T. Graham, and K. W. Tham, "Occupant satisfaction with the indoor environment in seven commercial buildings in Singapore," *Building and Environment*, vol. 188, p. 107443, 2021.

[30] D. Licina and S. Yildirim, "Occupant satisfaction with indoor environmental quality, sick building syndrome (SBS) symptoms and self-reported productivity before and after relocation into WELL-certified office buildings," *Building and Environment*, vol. 204, p. 108183, 2021.

[31] Z. Dong, K. Zhao, M. Ren, J. Ge, and I. Y. S. Chan, "The impact of space design on occupants' satisfaction with indoor environment in university dormitories," *Building and Environment*, vol. 218, p. 109143, 2022.

[32] S. Nkini, E. Nuyts, G. Kassenga, O. Swai, and G. Verbeeck, "Evaluation of occupants' satisfaction in green and non-green office buildings in Dar es Salaam-Tanzania," *Building and Environment*, vol. 219, p. 109169, 2022.

[33] K.-V. Võsa, A. Ferrantelli, and J. Kurnitski, "Cooling thermal comfort and efficiency parameters of ceiling panels, underfloor cooling, fan-assisted radiators, and fan coil," *Energies*, vol. 15, no. 11, p. 4156, 2022.

[34] W. Chen, Y. Deng, and B. Cao, "An experimental study on the difference in thermal comfort perception between preschool children and their parents," *Journal of Building Engineering*, vol. 56, p. 104723, 2022.

[35] M. Kiil, R. Simson, M. Thalfeldt, and J. Kurnitski, "A comparative study on cooling period thermal comfort assessment in modern open office landscape in Estonia," *Atmosphere*, vol. 11, no. 2, p. 127, 2020.

[36] P. O. Fanger and N. K. Christensen, "Perception of draught in ventilated spaces," *Ergonomics*, vol. 29, no. 2, pp. 215–235, 1986.

[37] B. Griefahn, C. Künemund, U. Gehring, and P. Mehnert, "Drafts in cold environments the significance of air temperature and direction," *Industrial Health*, vol. 38, no. 1, pp. 30–40, 2000.

[38] B. Griefahn, C. Künemund, and U. Gehring, "The impact of draught related to air velocity, air temperature and workload," *Applied Ergonomics*, vol. 32, no. 4, pp. 407–417, 2001.

[39] B. Griefahn, C. Künemund, and U. Gehring, "Evaluation of draught in the workplace," *Ergonomics*, vol. 45, no. 2, pp. 124–135, 2002.

[40] D. Pinto, A. Rocha, M. L. Simões et al., "An innovative approach to evaluate local thermal discomfort due to draught in semi-outdoor spaces," *Energy and Buildings*, vol. 203, article 109416, 2019.

[41] M. Borowski, R. Łuczak, J. Halibart, K. Zwolińska, and M. Karch, "Airflow fluctuation from linear diffusers in an office building: the thermal comfort analysis," *Energies*, vol. 14, no. 16, p. 4808, 2021.

[42] K. Tawackolian, E. Lichtner, and M. Kriegel, "Draught perception in intermittent ventilation at neutral room temperature," *Energy and Buildings*, vol. 224, p. 110268, 2020.

[43] K. Ahmed, T. Hasu, and J. Kurnitski, "Actual energy performance and indoor climate in Finnish NZEB daycare and school buildings," *Journal of Building Engineering*, vol. 56, p. 104759, 2022.

[44] T. Hoyt, E. Arens, and H. Zhang, "Extending air temperature setpoints: simulated energy savings and design considerations for new and retrofit buildings," *Building and Environment*, vol. 88, pp. 89–96, 2015.

[45] P. Raftery, S. Li, B. Jin, M. Ting, G. Paliaga, and H. Cheng, "Evaluation of a cost-responsive supply air temperature reset strategy in an office building," *Energy and Buildings*, vol. 158, pp. 356–370, 2018.

[46] A. A.-W. Hawila, A. Merabtine, M. Chemkhi, R. Bennacer, and N. Troussier, "An analysis of the impact of PMV-based thermal comfort control during heating period: a case study of highly glazed room," *Journal of Building Engineering*, vol. 20, pp. 353–366, 2018.

[47] "Dantec Dynamics ComfortSense specification," https://www.dantecdynamics.com/solutions/thermal-comfort/comfortsense/.

[48] "Onset Computer Corporation HOBO Temperature/Relative Humidity/2 External Channel Data Logger," https://www.onsetcomp.com/products/data-loggers/u12-013/.

[49] "Produal International Room controller HLS 44," https://www.produal.com/sku-1150250.html.

[50] "WOLF Anlagen-Technik GmbH & Co. KG Duct Temperature Sensor NTC5k," https://www.wolf.eu/fileadmin/Wolf_Daten/Dokumente/Technische_Dokus_EN/Airhandling/CONTROL_SYSTEM_AIR_HANDLING_-_WRS-K_201806.pdf.

[51] "EMHI Observation data," https://www.ilmateenistus.ee/ilm/ilmavaatlused/vaatlusandmed/tunniandmed/?lang=en.

[52] European Committee for Standardization (CEN), *EN 15251:2007 Indoor environmental input parameters for design and assessment of energy performance of buildings addressing indoor air quality, thermal environment, lighting and acoustics*, European Committee for Standardization (CEN), Brussels, Belgium, 2007.

[53] European Committee for Standardization (CEN), *EVS-EN 16798-3:2017 Energy performance of buildings - Ventilation for buildings - Part 3: For non-residential buildings - Performance requirements for ventilation and room-conditioning systems (Modules M5-1, M5-4)*, European Committee for Standardization (CEN), Brussels, Belgium, 2017.

[54] M. Virta, D. Butler, J. Gräslund et al., *Chilled beam application guidebook*, Rehva, Federation of European Heating and Air-conditioning Associations, 2007.

[55] H. Skistad, E. Mundt, P. V. Nielsen, K. Hagström, and J. Railio, *Displacement ventilation in non-industrial premises*, Rehva, Federation of European Heating and Air-conditioning Associations, 2004.

[56] M. Mundt, H. M. Mathisen, M. Moser, and P. Nielsen, *V Ventilation Effectiveness: Rehva Guidebooks*, Federation of European Heating and Ventilation Association, 2004.

[57] M. Virta, F. Hovorka, J. Kurnitski, and A. Litiu, *HVAC in Sustainable Office Buildings*, Rehva, Federation of European Heating and Air-conditioning Associations, 2012.

[58] M. Kiil, A. Mikola, M. Thalfeldt, and J. Kurnitski, "Thermal comfort and draught assessment in a modern open office building in Tallinn," *E3S Web of Conferences*, vol. 111, 2019.

Appendix A Indoor climate questionnaire

1. Gender – ( ) Female, ( ) Male

2. Age – ( ) 18–25, ( ) 26–35, ( ) 36–45, ( ) 46–55, ( ) 56–65, ( ) 66+

3. Workstation – ( ) Private office (max 3 people), ( ) Open office

4. Which amount of the workday you spend at your desk – ( ) Whole workday, ( ) Half of the workday (up to 4–5 h), ( ) Few hours (max 1–2 hours)

5. Which floor do you work on – ( ) 1-n

6. In which zone do you spend the most of your workday (1-n in picture) – ( ) 1-n

7. How do you rate your thermal sensation (choose neutral if you do not want a change in temperature) – ( ) Hot, ( ) Warm, ( ) Slightly warm, ( ) Comfortable, ( ) Slightly cool, ( ) Cool, ( ) Cold

8. How do you perceive odour intensity – ( ) No odour, ( ) Weak, ( ) Moderate, ( ) Strong, ( ) Very strong, ( ) Unbearable

9. Would you prefer the room temperature to be – ( ) Higher, ( ) Unchanged, ( ) Lower

10. Does the room lighting disturb working – ( ) Yes, ( ) No

11. Does the sunlight disturb working – ( ) Yes, ( ) No

12. Please rate (room temperature is) – ( ) Perfect, ( ) Good, ( ) Suitable, ( ) Unsuitable, ( ) Unbearable

13. Please rate (air quality is) – ( ) Perfect, ( ) Good, ( ) Suitable, ( ) Unsuitable, ( ) Unbearable

14. How do you perceive acoustic level (colleagues' speech and overall room acoustics) – ( ) Does not disturb at all, ( ) Rarely disturbs, ( ) Sometimes disturbs, ( ) Often disturbs, ( ) Disturbs all the time

15. How do you perceive other noise in your workplace – ( ) Does not disturb at all, ( ) Rarely disturbs, ( ) Sometimes disturbs, ( ) Often disturbs, ( ) Disturbs all the time

16. Whether and how often have you experienced the following symptoms (eye dryness or irritation) – ( ) Never, ( ) Rarely, ( ) Sometimes, ( ) Often, ( ) All the time

17. Whether and how often have you experienced the following symptoms (headache or fatigue) – ( ) Never, ( ) Rarely, ( ) Sometimes, ( ) Often, ( ) All the time

18. Whether and how often have you experienced the following symptoms (nasal or throat dryness or irritation) – ( ) Never, ( ) Rarely, ( ) Sometimes, ( ) Often, ( ) All the time

19. Whether and how often have you experienced the following symptoms (concentration problems) – ( ) Never, ( ) Rarely, ( ) Sometimes, ( ) Often, ( ) All the time

20. In the last month, has there been a feeling of draught at your workplace – ( ) Yes, ( ) No

21. Has there been and how often have you experienced draught at your workspace in summer – ( ) Never, ( ) Rarely, ( ) Sometimes, ( ) Often, ( ) All the time

22. Has there been and how often have you experienced draught at your workspace in autumn – ( ) Never, ( ) Rarely, ( ) Sometimes, ( ) Often, ( ) All the time

23. Has there been and how often have you experienced draught at your workspace in winter – ( ) Never, ( ) Rarely, ( ) Sometimes, ( ) Often, ( ) All the time

24. Has there been and how often have you experienced draught at your workspace in spring – ( ) Never, ( ) Rarely, ( ) Sometimes, ( ) Often, ( ) All the time

Appendix B.1 Building B air velocity and thermal comfort results

Building B with a slab-based TABS system, had better results for *DR* but worse for *PMV* and *PPD* (Figure 1). Compared to others, it had slightly higher v_a values near the floor compared to the abdomen or neck level of a seated person. The v_a and *DR* values at a height of 1.1 m fell within the I ICC, except for one position that fell into the II ICC. However, the v_a values at 0.6 m remained in the III ICC, with two instances exceeding the III ICC limit at a height of 0.1 m. Both t_i and t_o results at the abdomen level were divided between the II and the III ICC with one position achieving I ICC with t_o. Five measured positions did not meet the required II ICC for *PMV* and *PPD* indexes. The t_i results indicated that occupants preferred warmer temperatures, which was also confirmed by the ICQ survey.

		1	2	3	4	5	6	7	8	9	10	11	12	13	14	15	16
$t_{i(1.1\,m)}$	°C	25.0	24.5	24.6	24.1	23.8	23.4	24.4	24.1	24.01	23.8	24.8	24.4	24.5	23.9	24.4	24.4
$v_{o(1.1\,m)}$	m/s	0.06	0.05	0.08	0.06	0.12	0.10	0.08	0.05	0.05	0.08	0.02	0.04	0.05	0.06	0.04	0.06
$Tu_{(1.1\,m)}$	%	61.5	35.8	35.3	44.0	43.9	56.6	72.2	94.8	58.1	47.5	58.1	60.6	233.9	61.7	79.4	56.8
$DR_{(1.1\,m)}$	%	2.3	0.0	4.1	1.9	10.1	8.6	6.1	0.0	0.0	5.6	0.0	0.0	0.8	2.8	0.0	2.9
$t_{i(0.6\,m)}$	°C	25.0	24.5	24.4	24.0	23.7	23.2	24.2	23.8	23.8	23.6	24.6	24.2	24.3	23.6	24.3	24.2
$t_{o(0.6\,m)}$	°C	24.8	24.4	24.8	23.8	23.6	23.0	24.2	23.9	23.5	23.6	24.7	23.9	24.4	23.4	24.2	24.0
$v_{o(0.6\,m)}$	m/s	0.08	0.04	0.07	0.07	0.08	0.14	0.10	0.08	0.05	0.10	0.03	0.03	0.07	0.07	0.07	0.05
$RH_{(0.6\,m)}$	%	27.5	28.5	29.3	30.0	28.3	29.0	29.4	28.7	28.4	28.6	28.7	30.1	26.6	29.6	27.6	26.8
$PMV_{(0.6\,m)}$	-	0.6	0.5	0.6	0.4	0.3	0.1	0.4	0.4	0.3	0.3	0.6	0.4	0.5	0.3	0.5	0.4
$PPD_{(0.6\,m)}$	%	12.2	11.0	12.7	8.4	7.4	5.3	9.1	8.7	7.4	6.9	12.1	8.9	10.4	7.1	9.9	8.8

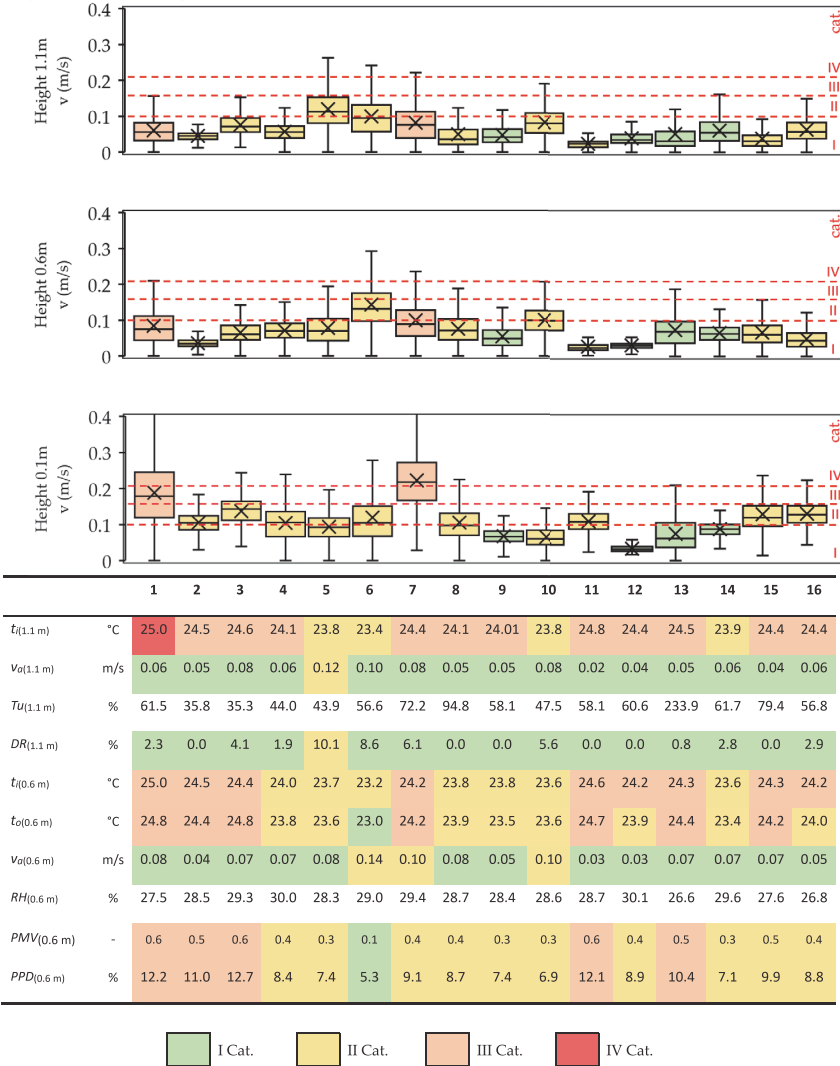I Cat.   II Cat.   III Cat.   IV Cat.

Figure 1. Building B air velocity and thermal comfort results in measurement points 1-16.

Appendix B.2 Building C air velocity and thermal comfort results

Building C, which is equipped with 4-pipe active beams, is presented in Figure 2. The measured values fall mostly into the I ICC, except for some t_i values. Half of the measured points for t_i meet the II ICC criteria, while two points fall into the III ICC. Two positions meet the II ICC, while other t_o values remain in I ICC. Air velocities are categorized as II ICC in one position and III ICC in another. The recorded v_a values show slightly more fluctuation at the neck height. Overall, Building C demonstrates a slightly better situation compared to Buildings A and B. Measurement point #14 is no longer available as it is no longer an occupied working area according to the room plan.
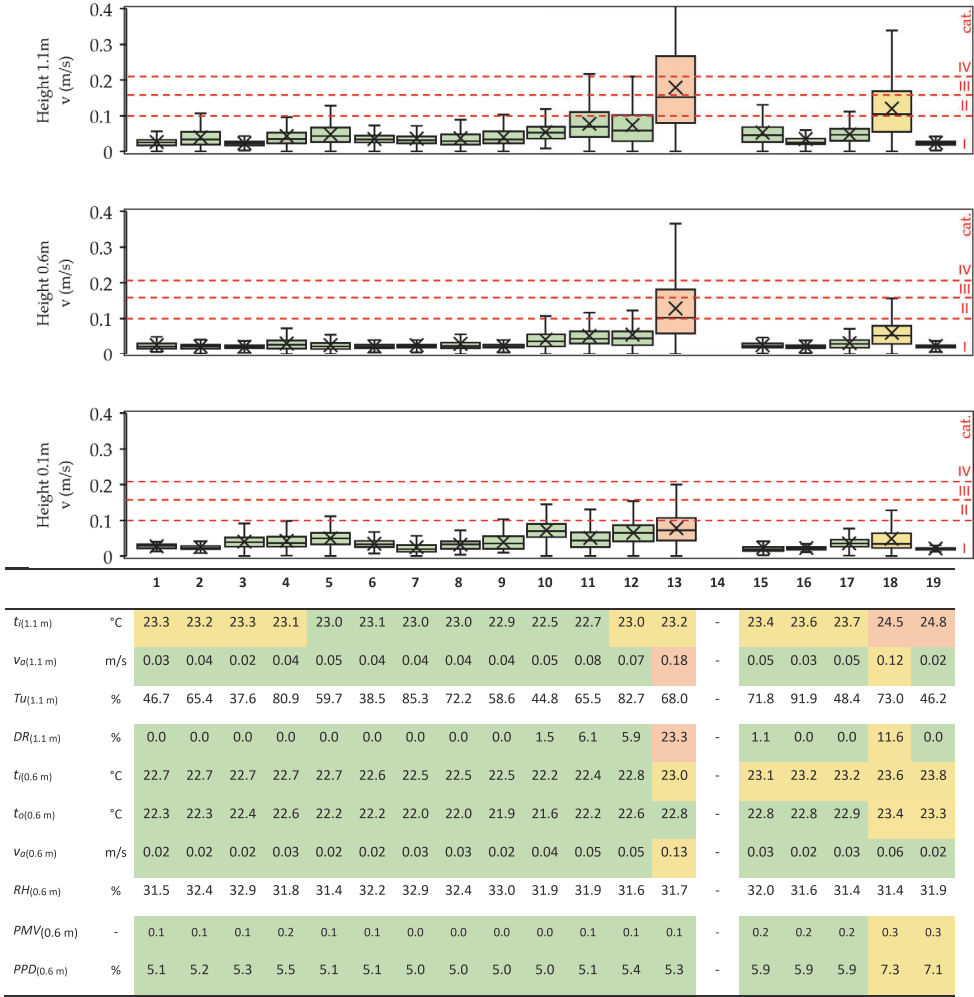
		1	2	3	4	5	6	7	8	9	10	11	12	13	14	15	16	17	18	19
$t_{i(1.1\,m)}$	°C	23.3	23.2	23.3	23.1	23.0	23.1	23.0	23.0	22.9	22.5	22.7	23.0	23.2	-	23.4	23.6	23.7	24.5	24.8
$v_{a(1.1\,m)}$	m/s	0.03	0.04	0.02	0.04	0.05	0.04	0.04	0.04	0.04	0.05	0.08	0.07	0.18	-	0.05	0.03	0.05	0.12	0.02
$Tu_{(1.1\,m)}$	%	46.7	65.4	37.6	80.9	59.7	38.5	85.3	72.2	58.6	44.8	65.5	82.7	68.0	-	71.8	91.9	48.4	73.0	46.2
$DR_{(1.1\,m)}$	%	0.0	0.0	0.0	0.0	0.0	0.0	0.0	0.0	0.0	1.5	6.1	5.9	23.3	-	1.1	0.0	0.0	11.6	0.0
$t_{i(0.6\,m)}$	°C	22.7	22.7	22.7	22.7	22.7	22.6	22.5	22.5	22.5	22.2	22.4	22.8	23.0	-	23.1	23.2	23.2	23.6	23.8
$t_{o(0.6\,m)}$	°C	22.3	22.3	22.4	22.6	22.2	22.2	22.0	22.0	21.9	21.6	22.2	22.6	22.8	-	22.8	22.8	22.9	23.4	23.3
$v_{a(0.6\,m)}$	m/s	0.02	0.02	0.02	0.03	0.02	0.02	0.03	0.03	0.02	0.04	0.05	0.05	0.13	-	0.03	0.02	0.03	0.06	0.02
$RH_{(0.6\,m)}$	%	31.5	32.4	32.9	31.8	31.4	32.2	32.9	32.4	33.0	31.9	31.9	31.6	31.7	-	32.0	31.6	31.4	31.4	31.9
$PMV_{(0.6\,m)}$	-	0.1	0.1	0.1	0.2	0.1	0.1	0.0	0.0	0.0	0.0	0.1	0.1	0.1	-	0.2	0.2	0.2	0.3	0.3
$PPD_{(0.6\,m)}$	%	5.1	5.2	5.3	5.5	5.1	5.1	5.0	5.0	5.0	5.0	5.1	5.4	5.3	-	5.9	5.9	5.9	7.3	7.1

I Cat.   II Cat.   III Cat.   IV Cat.

Figure 2. Building C air velocity and thermal comfort results in measurement points 1-19.

61 **Appendix B.3 Building D air velocity and thermal comfort results**

62   Building D, which has 4-pipe radiant panels, complies with the II ICC limits (Figure 3). The first ICC is
63 met for v_a in all measured locations. Air velocities are slightly higher at the lowest measurement height. Eight
64 out of eleven measured positions meet the II ICC criteria for t_i and four positions for t_o, while *PMV* and *PPD* fall
65 into the II ICC thrice. Like Building C, Building D demonstrates a slight advantage over Buildings A and B based
66 on the results.

		1	2	3	4	5	6	7	8	9	10	11
$t_{i(1.1\,m)}$	°C	22.7	23.0	23.3	23.2	23.4	23.3	23.0	23.4	23.2	23.3	23.4
$v_{a(1.1\,m)}$	m/s	0.03	0.06	0.05	0.06	0.04	0.06	0.02	0.05	0.06	0.07	0.03
$Tu_{(1.1\,m)}$	%	47.3	79.9	72.4	50.2	79.1	75.5	73.9	100.9	39.4	45.8	87.2
$DR_{(1.1\,m)}$	%	0.0	3.4	0.0	3.2	0.0	3.4	0.0	0.0	1.7	3.9	0.0
$t_{i(0.6\,m)}$	°C	22.6	22.8	23.1	23.1	23.3	23.1	22.5	23.0	23.0	23.0	23.1
$t_{o(0.6\,m)}$	°C	22.4	23.0	23.3	23.0	23.5	23.1	22.2	23.0	22.9	23.1	22.9
$v_{a(0.6\,m)}$	m/s	0.02	0.06	0.06	0.05	0.03	0.09	0.04	0.03	0.04	0.08	0.02
$RH_{(0.6\,m)}$	%	29.7	28.7	28.4	27.7	27.2	27.7	28.3	28.1	28.4	27.7	28.5
$PMV_{(0.6\,m)}$	-	0.1	0.2	0.3	0.2	0.3	0.2	0.0	0.2	0.2	0.2	0.2
$PPD_{(0.6\,m)}$	%	5.2	5.9	6.7	6.0	7.0	5.9	5.0	5.9	5.8	6.1	5.9

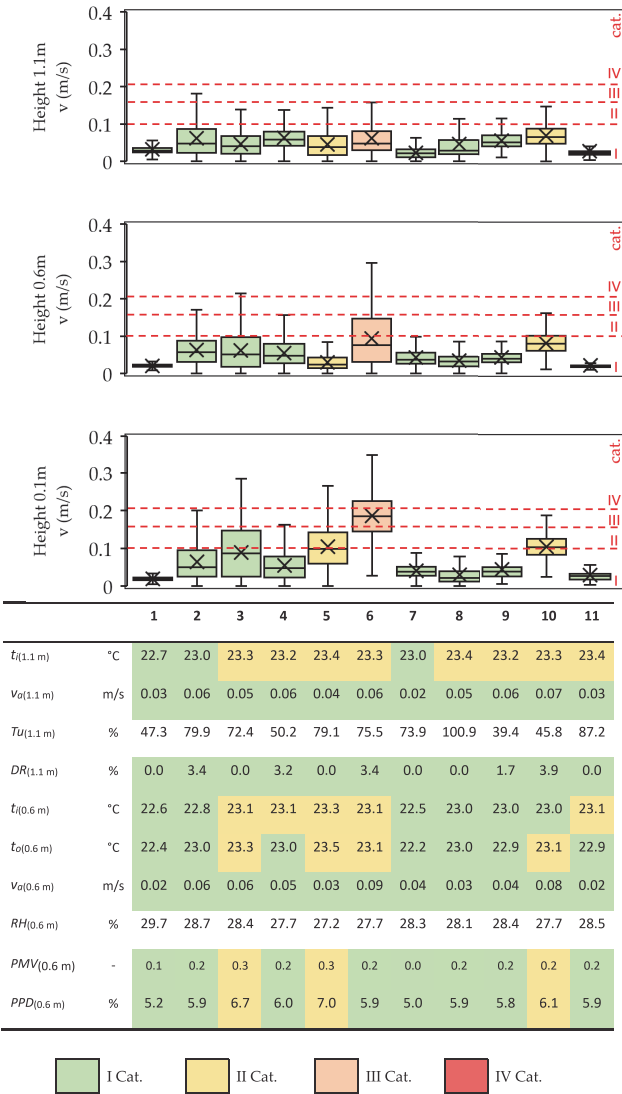I Cat.   II Cat.   III Cat.   IV Cat.

69 **Figure 3.** Building D air velocity and thermal comfort results in measurement points 1-11.

Appendix B.4 Building E air velocity and thermal comfort results

The office landscapes in Building E predominantly exhibited I ICC results for v_a (Figure 4). The fluctuations of v_a were random across different measurement heights. Regarding t_i, the lower temperatures observed in the first four positions can be attributed to low occupancy schedules in those areas. One position fell into the II ICC, five positions were classified as III ICC, and four positions were categorized as the worst IV ICC. The values of t_o are distributed among all ICC. *PMV* and *PPD* values were within the I and III ICC twice, while the remaining measurements were within the II ICC.

		1	2	3	4	5	6	7	8	9	10	11	12	13	14
$t_{i(1.1\,m)}$	°C	22.0	22.3	21.7	21.3	23.8	24.5	25.1	25.1	25.2	25.4	24.8	24.6	24.8	24.6
$v_{a(1.1\,m)}$	m/s	0.12	0.04	0.07	0.08	0.06	0.07	0.13	0.06	0.05	0.09	0.03	0.05	0.03	0.04
$Tu_{(1.1\,m)}$	%	38.9	53.3	64.0	32.4	57.5	45.6	47.4	60.0	68.7	66.9	52.3	58.7	65.5	52.6
$DR_{(1.1\,m)}$	%	11.5	0.0	6.1	6.5	3.2	3.1	10.4	1.8	1.4	5.7	0.0	0.9	0.0	0.0
$t_{i(0.6\,m)}$	°C	22.0	22.1	21.4	21.3	23.5	24.1	24.5	24.8	24.8	24.6	24.1	23.9	24.0	23.8
$t_{o(0.6\,m)}$	°C	22.0	21.8	20.8	20.8	24.3	24.5	24.7	24.5	25.1	24.6	23.5	23.7	23.7	23.4
$v_{a(0.6\,m)}$	m/s	0.13	0.02	0.08	0.06	0.02	0.03	0.07	0.03	0.06	0.07	0.02	0.04	0.03	0.05
$RH_{(0.6\,m)}$	%	21.9	22.1	22.9	23.4	22.2	21.9	21.7	21.8	21.8	21.8	23.4	23.5	23.6	23.7
$PMV_{(0.6\,m)}$	-	-0.1	-0.1	-0.3	-0.3	0.4	0.5	0.5	0.5	0.6	0.5	0.3	0.3	0.4	0.3
$PPD_{(0.6\,m)}$	%	5.4	5.1	6.6	6.6	9.1	10.0	11.2	10.4	13.2	10.5	6.8	7.5	7.6	6.7

I Cat.   II Cat.   III Cat.   IV Cat.

Figure 4. Building E air velocity and thermal comfort results in measurement points 1-14.

Appendix 3

Ventilation effectiveness in classroom infection risk control

Martin Kiil[1*], *Indrek* Valgma[1], *Karl-Villem* Võsa[1], *Raimo* Simson[1,2], *Alo* Mikola[1], *Teet* Tark[1], *Jarek* Kurnitski[1,2]

[1] Department of Civil Engineering and Architecture, Tallinn University of Technology, Tallinn, Estonia
[2] Department of Civil Engineering, Aalto University, Espoo, Finland

Abstract. The benefits of a good ventilation in classrooms are a well-studied topic regarding health and learning outcomes. However, many studies still show poor results regarding air quality, air change rate and air velocities. In this paper, typical Estonian classroom air distribution solutions were studied in an air distribution laboratory at Tallinn University of Technology. The air change efficiency was measured with CO_2 tracer gas concentration decay method. For determining the contaminant removal effectiveness, continuous dose method was used to create a constant contaminant source. In addition, by using air velocity probes, we conducted draught measurements in the mock-up classroom. Tests were conducted using dedicated room-based air handling unit and thermal mannequins for imitating heat sources from students. We found that all solutions studied ensured the air change efficiency roughly corresponding to fully mixing air distribution, but local ventilation effectiveness values of contaminant removal showed large variation from 0.6 to 1.7 stressing the impact of source location. Grouped ceiling supply circular diffusers and single vertical supply grille air distribution commonly used in renovated educational buildings resulted in higher draught risk on the border of the occupied zone. High air velocities recorded in some areas of the classroom perimeter, well explain why draught is considered as one of the main reasons why the airflow rates are reduced, or supply air temperatures are lifted compared to designed values. Perforated duct diffusers resulted in acceptable air velocities. In conclusion, local ventilation effectiveness of contaminant removal showed that fully mixing is not a case with a point source, although air change efficiency determined with equally distributed source showed fully mixing conditions. Therefore, in those cases, the air change rate should be increased to achieve the same ventilation effectiveness. Based on the experiments conducted, a point source ventilation effectiveness measurement method for the breathing zone is proposed. This value determined at least with two source locations can be used in infection risk-based ventilation design.

Keywords. Classroom, ventilation effectiveness, air velocity

1 Introduction

Studies have shown that poor indoor air quality in classrooms reduces students' performance and has a negative impact on the health. Inadequate ventilation increases the risk of asthma symptoms, absenteeism and respiratory disease among students [1–6]. Proper air change rates are found to ensure better results [7–10]. Air distribution plays a significant role in ensuring air quality, which determines how efficiently the contaminated air in the room is replaced with fresh, clean air.

Using carbon dioxide (CO_2) as a tracer gas for evaluating ventilation effectiveness is well validated [11–15]. The main alternative to the measuring techniques is to CFD simulate air distribution and quality. Ventilation strategies were studied by Novoselac and Srebic [16], indicating that overlapping results in the occupied zone and breathing plane lower the total number of necessary measurement points. Kosonen and Mustakallio [17,18] analysed mixing and displacement ventilation concepts in a mock-up classroom with follow-up CFD-simulations concluding

that heat gains in rooms with mixed air exchange may have a significant effect on the air distribution and draught. Lichtner and Kriegel [19] studied classroom ventilation in the view of the Covid-19 pandemics. The CFD-simulations indicated air quality in the breathing plane up to five times worse than expected. Strong correlation between ventilation strategy and airborne transmittable diseases is emphasised also by other studies [20,21]. However, mixing air distribution is the oldest and most common solution, the purpose of which is to ensure the most uniform removal of pollutants and temperature distribution in the occupied zone [22,23]. Furthermore, a new infection risk-based ventilation design method [24] was recently introduced. Infection-risk based ventilation equations apply for fully mixing and need to be divided by point source ventilation effectiveness for actual air distribution solutions [25].

The focus of this paper is to evaluate ventilation effectiveness simultaneously with draught risk in a mock-up classroom. Ventilation effectiveness indices and air velocities are presented. Main findings of the experiments indicate that the ventilation solutions do not always guarantee the expected efficiency, or the air velocities do not maintain the required limits in the occupied zone.

---

* Corresponding author: martin.kiil@taltech.ee

Nomenclature

ε^a	air change efficiency, %	ε_b	point source ventilation effectiveness for the breathing zone, -
ε_P^a	local air change index, %	t_i	indoor air temperature, °C
$\varepsilon^c = CRE$	contaminant removal effectiveness, -	t_{sup}	supply air temperature, °C
ε_P^c	local air quality index, -	v_a	air velocity, m/s
ε_b^j	point source ventilation effectiveness of measurement j, -		

2 Methods

This chapter provides information regarding ε^a, CRE and v_a measurements with the description of the ventilation laboratory used in the experiments. The research methodology flow chart is seen on Figure 1. Using air distribution laboratory at the campus of

Tallinn University of Technology, a mock-up classroom was set up for the experiments. Measuring equipment data is provided below in the second subsection of this chapter. The principles of the analysis based on the results of the carried-out experiments are described at the end of this chapter. SciPy and matplotlib software libraries in the Python programming language were used for visualisation of the results.
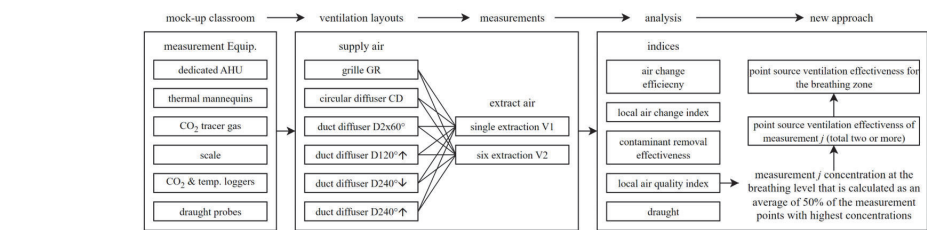
Figure 1. Flow chart of research methodology.

2.1 Mock-up classroom

The tests were conducted in an open ceiling mock-up classroom with a room height of 3.8 m and floor area of 5.2 × 8.7 m (45 m²). For 29 students and one teacher the required air change 240 l/s (5.3 l/s×m², 5 1/h) was used [26]. The ventilation layouts used in the experiments are

shown in Figure 2. The tests included ceiling diffusers, grille, and duct diffusers. The experiments included extract with individual location and with 6 points distributed evenly over the room. The indoor air and supply air temperatures during measurements were respectively t_i = +22 °C and t_{sup} = +18 °C using a dedicated air handling unit.
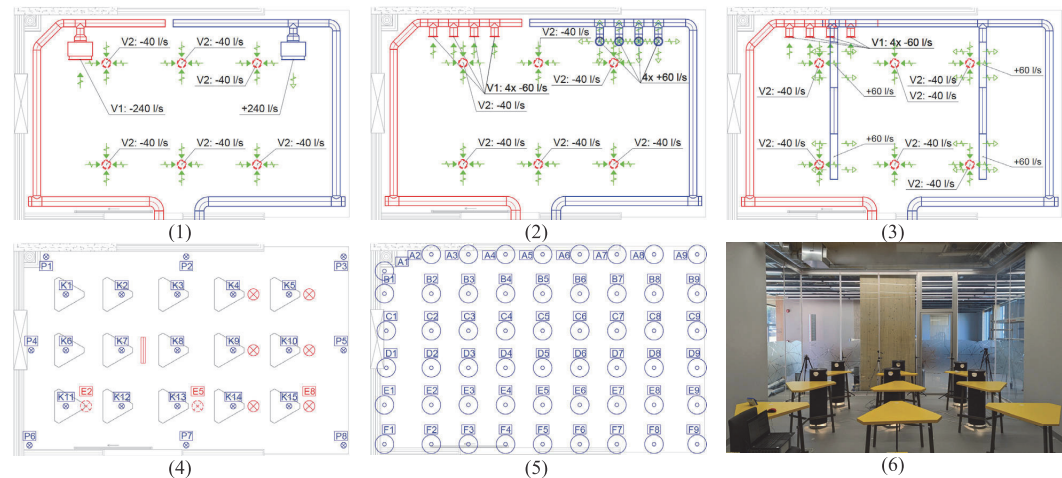

Figure 2. Ventilation layouts and measurement equipment used in the experiments: (1) grille, (2) circular diffuser, (3) duct diffuser, (4) "K" and "P"-labelled data loggers for occupied zone and room perimeter with the location of thermal mannequins (E2, E5 and E8 as contaminant source), (5) draught probes' measurement points (A1 to F9) and (6) photo of the mock-up classroom. V1 and V2 in the (1) to (3) layouts represent single and six extraction options.

2.2 Measurement equipment

To assess ε^a and *CRE*, we used CO_2 as a tracer gas respectively for concentration decay method and continuous dose method. To measure CO_2 concentrations, calibrated dataloggers were used: 15 on the tables (breathing plane, h=1.1 m), 8 in the perimeter (h=1.1 m), 1 in supply air duct for fresh air reference concentration and 1 in extraction duct for single location extract and 6 for multiple extract point layout (see Figure 2). For measuring gas dosage, scale was used. Air diffusers were balanced and measured for each layout using differential pressure manometer. In addition, to assess draught risk, each ventilation layout was measured as a level (h=1.1 m) by a set of 6 air velocity (v_a) probes with 1 m step. The experiments were conducted with t_i of +22.7±0.8 °C and t_{sup} of +19.9±0.7 °C, maintaining an Δt of t_i and t_{sup} with ~4 K. The specifications of measuring equipment are provided in Table 1.

Table 1. Specifications of measuring equipment : CO_2 concentration and temperature logger [27], differential pressure sensor [28], gas mass weighing scale [29], draught probe [30].

	Onset HOBO MX1102A Data Logger	Testo 440 dP	Kern FKB	Draught probe ComfortSense 54T35
Parameters	CO_2 concentration air temperature	differential pressure	weight	air velocity air temperature
Range	0…5000 ppm 0…50 °C	-150 to +150 hPa	0.002…65 kg	0.05-5 m/s -20 °C to +80 °C
Accuracy	±50 ppm + ±5 % ± 0.21 °C	<100 Pa ±0.05 Pa	±0.001 kg	±0.02 m/s ±0.2 K
Image				

The placement of thermal mannequins and one extra 1 kW electrical convector are seen in Figure 2. Before the ε^a assessment experiments, the room was filled with gas to fully mixed state. However, during *CRE* experiments, gas was injected as a contaminant continuously during the test. We used CO_2 tank connected to a dummy as a contaminant source (Figure 3) in three different positions.
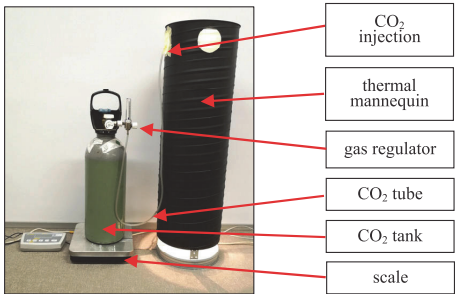

Figure 3. CO_2 tank connected with a thermal mannequin used as a contaminant source.

2.3 Data analysis of ventilation effectiveness

The ventilation effectiveness indicates the potential of a system to exchange the air in the room or to remove air-borne contaminants. Therefore, the first is subdivided to air change efficiency (ε^a) and local air change index (ε_P^a). Thus, the second is subdivided to contaminant removal effectiveness (ε^c) and local air quality index (ε_P^c). Another useful tool for evaluating ventilation effectiveness in the age of air. The local mean age of air ($\bar{\tau}_P$) is always equal to the nominal time constant (τ_n) in the exhaust, which can be found using Equation 1. [11]

$$\tau_n = V / q_v, \text{(h)} \quad (1)$$

where V stands for room volume and q_v as the air change rate. Using the ratio (Equation 2) between the lowest possible mean age of air and the actual room mean age of air, ε can be calculated. [11]

2.3.1 Calculating air change efficiency

The Equation 2' upper limit is 100 % in a piston flow situation. Between 50 % and 100 %, displacement flow is considered, while 50 % equals fully mixed flow and under 50 % efficiency indicates a short-circuit flow. [11]

$$\varepsilon^a = \frac{\tau_n}{2\langle\bar{\tau}\rangle} \times 100, \text{(%)} \quad (2)$$

Calculating conditions in a particular point, Equation 3 must be used, where $\bar{\tau}_P$ represent the local mean age of air: [11]

$$\varepsilon_P^a = \frac{\tau_n}{\bar{\tau}_P} \times 100, \text{(%)} \quad (3)$$

Determining airflow rates with traces gas dilution method is described in EN ISO 12569:2017 [14]. Methods for characterization of ventilation conditions with local mean ages of air is provided in ISO 16000-8:2007 [15]. Following procedure of multi-point concentration decay method, Equation 4 was used:

$$N = \frac{\left(\sum_{j=1}^{np} t_j\right) \times \sum_{j=1}^{np} \ln C(t_j) - n_p \times \sum_{j=1}^{np} t_j \times \ln C(t_j)}{n_p \times \sum_{j=1}^{np} t_j^2 - (\sum_{j=1}^{np} t_j)^2}, \quad (4)$$

where N stands for air change rate (1/h), t_j is a cumulative time step from the start of the experiment ($t_1 = 0$, h), $C(t_j)$ represents the traces gas concentration at a time step j (ppm) and np shows the sum of measuring points. Finally, using Equation 5, local mean age of air is calculated as an inverse value of local air change rate (λ, 1/h) [15].

$$\bar{\tau}_P = \frac{1}{\lambda}, \text{(h)} \quad (5)$$

2.3.2 Calculating contaminant removal effectiveness

Using ratio (Equation 6) between the steady state concentration (c_e) and the steady state mean concentration of the room ($\langle c \rangle$), ventilation effectiveness of contaminant removal (ε^c) can be calculated. While as Equation 7 was used to calculate ε_P^c, where represents the concentration of contaminant at the point P. On both cases, supply air concentration c_{sup} is subtracted from extract air concentration c_{ext} and from mean concentration $\langle \bar{c} \rangle$ (Equation 6) or local concentration c_P (Equation 7) [11]. According to EN 16798-3:2017 [31], Equation 6 is called ventilation effectiveness.

$$\varepsilon^c = \frac{c_e}{\langle c \rangle} = \frac{(c_{ext} - c_{sup})}{(\langle \bar{c} \rangle - c_{sup})}, (-) \qquad (6)$$

$$\varepsilon_P^c = \frac{c_e}{c_P} = \frac{(c_{ext} - c_{sup})}{(c_P - c_{sup})}, (-) \qquad (7)$$

2.3.3 Calculating ventilation for infection risk

Breathing zone ventilation rate ($q_{V,bz}$) divided with ventilation effectiveness (ε^c) from Equation 6 represents the ventilation outdoor air volume flow needed at the room supply diffusers, Equation 8:

$$q_{V;ODA} = \frac{q_{V,bz}}{\varepsilon^c}, (m³/s) \qquad (8)$$

Breathing zone ventilation rate ($q_{V,bz}$) can be calculated as the infection risk-based ventilation rate as shown in [24]. The main aim of this paper is to provide information about ε^c values in classrooms. Instead of the breathing zone mean concentration (Equation 6) we use local breathing zone values (Equation 7). In the case of the point source (an infectious person) the latter should be used as the denominator in the Equation 8, to apply the formula in the new infection risk-based design method [24] recently proposed. The latter in turn has been supplemented with quanta emission input data to simplify the ventilation rate (Q) calculation directly for common room types as design ventilation airflow rate at actual air distribution solution (Q_s)[25] as in Equations 9 to 11:

$$Q_s = \frac{Q}{\varepsilon_b}, (l/s) \qquad (9)$$

where ε_b stands for point source ventilation effectiveness for the breathing zone:

$$\varepsilon_b = \frac{\Sigma_j \varepsilon_b^j}{m}, (-) \qquad (10)$$

where ε_b^j represents point source ventilation effectiveness of measurement j. Henceforth, the ε_b^j differs from ε_P^c (Equation 7) in that:

$$\varepsilon_b^j = \frac{c_{je} - c_{jo}}{c_{jb} - c_{jo}}, (l/s) \qquad (11)$$

where c_{je} represents measurement j concentration in the extract air duct (c_{ext}), c_{jb} represents measurement j concentration at the breathing level that is calculated as an average concentration of 50% of the measurement points having the highest concentrations, c_{jo} represents concentration in the supply air (c_{sup}) and m means the total number of measurements (two or more) with different point source locations.

Results and discussion

In this section, the main results of the experiments conducted are provided and discussed. Not all the ventilation layout options provided in Figure 1 are reported in the results. Duct diffusers with horizontal 2x60°, upward (↑) 120°, and 240°↑ settings did not perform as well as downward (↓) 240° version regarding ε_b values. The duct diffuser setting with 120°↓ showed air velocities up to 0.45 m/s in the occupied zone. We noticed that increasing the supply air temperature to the room air temperature level did not reduce the performance of these ventilation solutions significantly. The results of calculated ε^a with minimum and maximum ε_P^a, calculated ε^c with ε_b (calculated from ε_P^c values), and measured v_a values, all without perimeter, are provided in Table 2. The results of calculated ε_P^a as colour-maps are provided in Figure 4 and the results of ε_P are reported in Figure 5. Measured values of v_a are seen below on Figure 6.
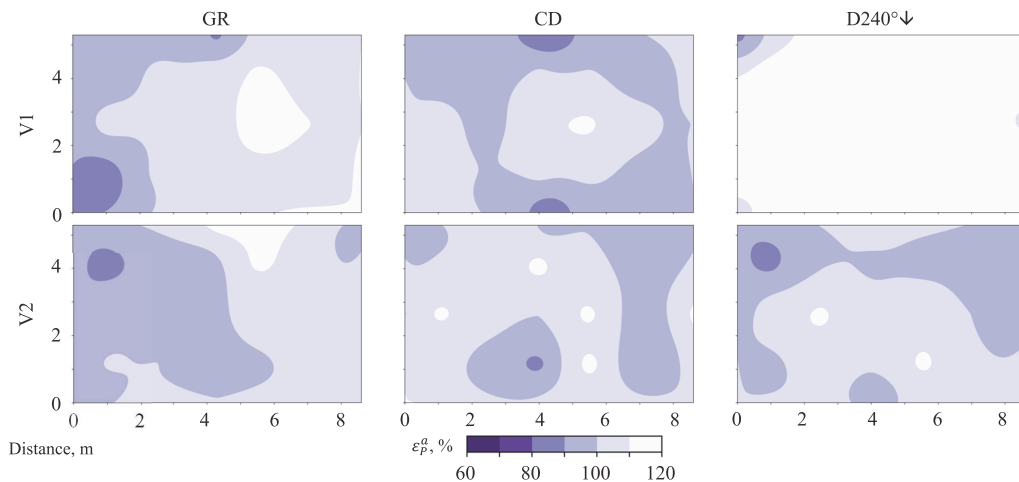
Table 2. Results of calculated air change efficiency (ε^a) and local air change index (ε_P^a), calculated ventilation effectiveness of contaminant removal (ε^c) and point source ventilation effectiveness of measurements with positions of 1-3 (ε_b^j) with point source ventilation effectiveness (ε_b), and measured air velocity (v_a) for grille (GR), circular diffuser (CD), and downward 240° duct diffuser (D240°↓) supply comparing single (V1) and six (V2) extraction layouts in the occupied zone on the breathing plane.

| Experiment | Air change efficiency, local air change index | | | Contaminant removal effectiveness, point source ventilation effectiveness for the breathing zone | | | | | | Average point source ventilation effectiveness | Air velocity | |
| | | | | Position 1 (E2) | | Position 2 (E5) | | Position 3 (E8) | | | | |
	ε^a %	$\varepsilon_{P,min}^a$ %	$\varepsilon_{P,max}^a$ %	ε^c -	ε_b^1 -	ε^c -	ε_b^2 -	ε^c -	ε_b^3 -	ε_b -	v_a m/s	$v_{a,max}$ m/s
GRV1	51	92	107	1.06	0.88	1.07	0.85	1.06	0.98	0.90	0.09	0.40
GRV2	50	94	106	0.90	0.65	0.98	0.82	1.09	1.03	0.83		
CDV1	50	97	106	1.73	1.51	1.62	1.39	1.20	1.12	1.34	0.10	0.31
CDV2	51	94	107	1.34	1.17	1.23	1.01	1.05	0.97	1.05		
D240°↓V1	56	107	124	1.09	1.02	0.97	0.87	0.87	0.82	0.91	0.11	0.21
D240°↓V2	50	94	106	1.09	1.03	1.00	1.00	0.99	0.98	1.00		

Figure 4. Results of calculated local air change index (ε_P^a) representing mock-up classroom breathing plane colour-maps from CO_2 concentration decay method measurements. Grille (GR), circular diffuser (CD), and duct diffuser (D240°↓) compared with single (V1) and six (V2) extraction (for measurement grid and equipment, see Figure 2).

In all cases, the ε^a results show equivalent values to the theoretical mixing ventilation value of 50%. The lowest values for $\varepsilon_{P,min}^a$ were calculated 92% according to the measurements. Duct diffuser option with single extraction can be highlighted with both better air change efficiency and local air change index. In general, except for the last-mentioned case, as seen on Figure 4, ε_P^a is comparably uniform with other layout settings. Thus, according to the Equation 8 and the average ε^a results indicating mixing ventilation situation (ε^a =50%), increasing of the air change rate would not be needed.

Comparing ε^c results, better contaminant removal effectiveness is achieved on all cases, when contaminant source is positioned in the middle P2 (E5) of the classroom. The results presented in the middle column in the Figure 5 show slight symmetry, if at all. In general, grille with six extraction layout in P3 (E8), all the circular diffuser and both P1 (E2) duct diffuser settings stand out with less spreading of the "contaminant". In the middle position P2 (E5), CO_2 concentration was measured slightly more distributed around the source in case of duct diffuser layouts. The outspread becomes more diffusing for grille option, except for P3 (E8) with six extraction option, as mentioned earlier. The most critical areas are measured for duct diffuser settings with contaminant source positioned in P3 (E8). Left P1 (E2) position shows 0.90 and right P3 (E8) position shows 0.87 for ε^c with grille (GR) with six extraction (V2) and duct diffuser (D240°↓) with single extraction (V1) respectively.

However, ε_b results for positions 1 to 3 are more varying together with middle P2 (E5) position not having an advantage. The lowest point source ventilation effectiveness for position P1 (E2) is 0.65 with grille and six extraction, for position P2 (E5) 0.82 with grille and six extraction (0.85 with one extraction)

and for position 3 (E8) the least value dropped to 0.82 with duct diffuser and single extraction layout. In terms of better performance, for position P1 (E2), circular diffuser with single extract achieved ε_b 1.51. Position 2 (E5) follows with 1.39 and position 3 (E8) with 1.12.

Similarly, to the comparison of the general ventilation efficiency according to the Equation 8 in the mock-up classroom with ε^a, mixing ventilation occurs with ε^c=1. Therefore, in position 1 (E2), the ventilation rate should be increased by 11% for the grille and six extract layout (ε^c=0.90). For position 2 (E5), lower ε^c values can be rounded up to 1. If duct diffuser single extract solution ε^c=0.87 could be rounded to 0.9, again ventilation rate should be increased by 11%. In the case of duct diffuser, the ventilation rate can be reduced.

Hence, according to ε_b, the ventilation rates should be adjusted up to 14% (ε_b=0.88 in P1) in case of grille with single extract and up by 54% (ε_b=0.65 in P1) in case of six extraction. Less conservative would be to use average value of three contaminant source positions, 0.90 and 0.83 respectively, with the need of higher ventilation rate by 11% and 20%. In case of duct diffusers, the same approach would indicate 22% (ε_b=0.82 in P3) demand for ventilation increase with single extract and 2% (ε_b=0.98 in P3) for six extract. The less conservative average values based on three contaminant source positions would be 0.91 and 1.00 with the need for ventilation rate increase of 10% and no need respectively. Therefore, using ε_b values instead of ε^c as a correction factor for dimensioning ventilation rate, presuming mixing ventilation, would be preferred. It is likely enough conservative to use an average of the two or more measurement positions ε_b values and not the random single nor the lowest measurement ε_b value available which may result in excessive over dimensioning of the ventilation rate.
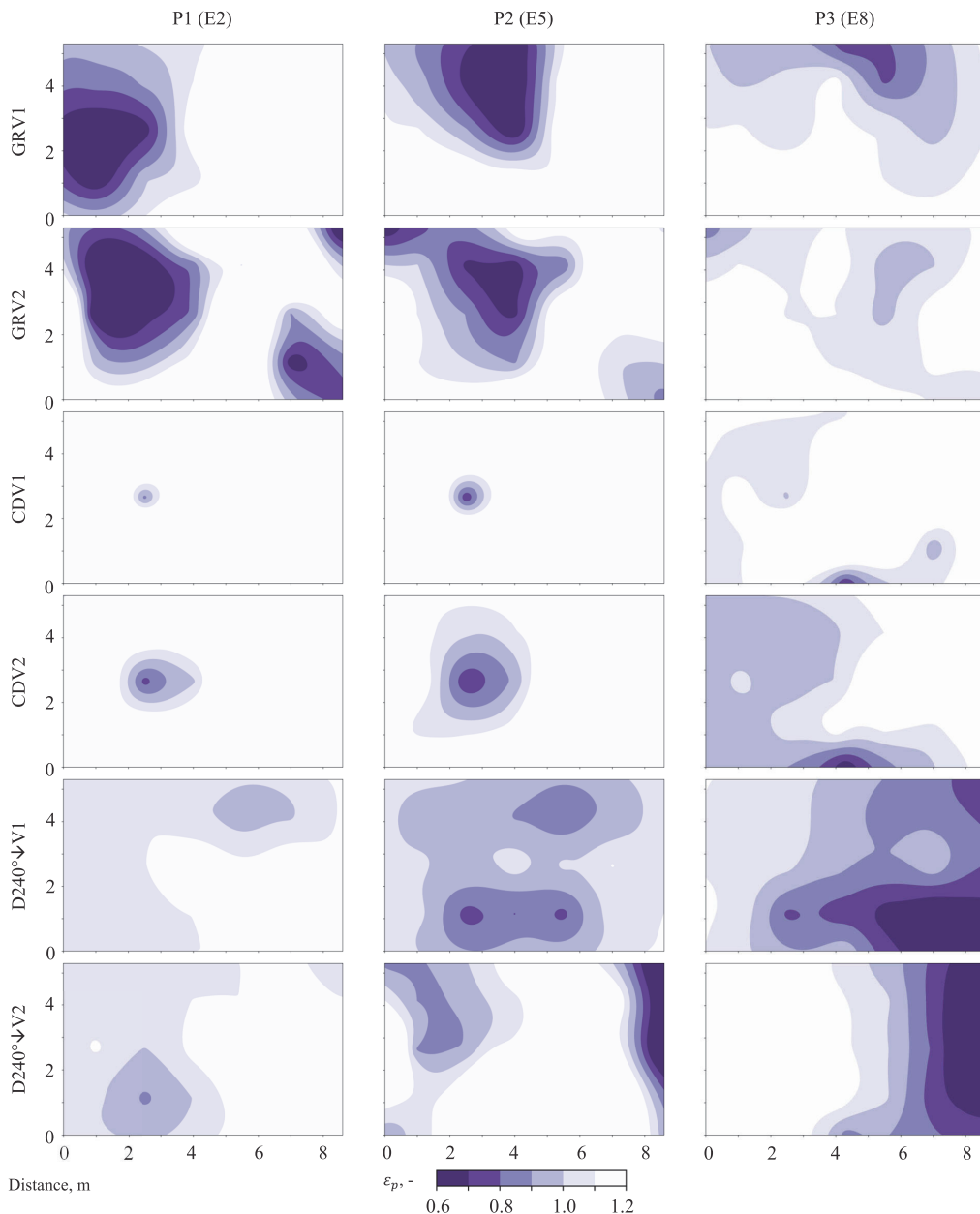
Figure 5. Measured local air quality index (ε_P) from which point source ventilation effectiveness can be calculated, representing mock-up classroom breathing plane colour-maps from continuous injection method. Grille (GR), circular diffuser (CD), and duct diffuser (D240°↓) compared with single (V1) and six (V2) extraction for each contaminant source position P1-P3 (for measurement grid and equipment, see Figure 2).

The Category I, II, and III air velocities are 0.10, 0.16, and 0.21 m/s during winter and 0.12, 0.19, and 0.24 m/s during summer respectively [32]. Measured air velocities on the breathing plane in the occupied zone reached maximum values 0.40 m/s for grille, 0.31 m/s for circular diffuser, and 0.21 m/s for duct diffuser. Average v_a values were measured 0.09 m/s, 0.10 m/s, and 0.11 m/s respectively. According to Figure 6, the grille and circular diffuser colour-plots indicate the

highest draught risk in the occupied zone border and room perimeter area. In the occupied zone, there is one area where duct diffuser reaches 0.21 m/s and drops to Category III. The rest of occupied zone well fulfils second Category.

Considering all the variation provided in Figure 1, the layout of internal heat gain sources or air terminals did not have a substantial impact on the results generally. We measured only three air distribution

solution in this study indicating the need to measure other possible solution. Measurements are highly needed because the result of ventilation effectiveness >1 for circular diffusers was impossible to predict. Similarly, increasing the number of extraction points from 1 to 6 in some cases decreased the performance (grille and circular diffuser) but in the case of duct diffusers enhanced the performance. Results are promising, showing that ventilation effectiveness values equal or higher than 1 are possible. This allows not to increase the ventilation rate that may result in elevated draught risk and not to mention higher space demand or cost- and energy efficiency parameters. To sum up, the need for further research regarding ventilation effectiveness values is crucial, essentially in case of infection risk-based ventilation design.
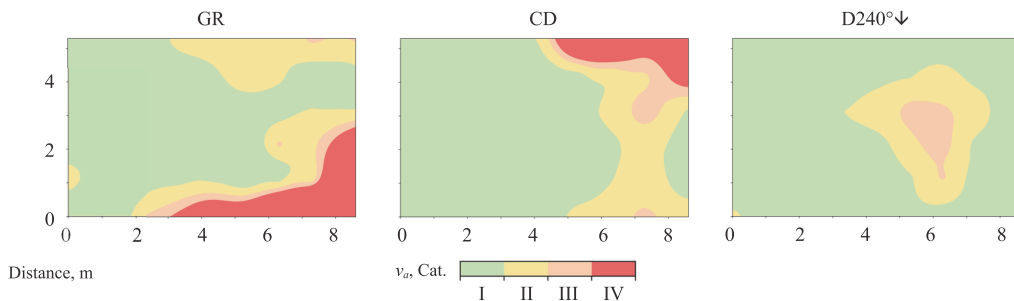
Figure 6. Results of measured air velocity (v_a) representing a mock-up classroom breathing plane colour-maps. Green stands for I Category (<0.10 m/s), yellow for II Category (0.10-0.16 m/s), light red for III Category (0.16-0.21 m/s), and dark red for IV Category (>0.21 m/s) during summer [32]. Grille (GR), circular diffuser (CD), and duct diffuser (D240°↓) are compared (for measurement grid and equipment, see Figure 2).

3 Conclusions

In this paper, ventilation effectiveness indices including air change efficiency (ε^a) and contaminant removal effectiveness (ε^c) simultaneously with air velocity were studied in a mock-up classroom. Supply grille, circular diffuser, and duct diffuser with single and six extract air terminal layouts were compared. We propose point source ventilation effectiveness (ε_b) approach to be calculated as an average of the two or more measurements with different contaminant source locations as a conservative efficiency value allowing to recalculate the fully mixing airflow rate to the actual ventilation air distribution solution. Further research regarding ventilation effectiveness values measured with point source would be crucial. Therefore, more combinations for air terminals, temperature amplitudes, room layouts etc must be investigated. In conclusion, we found that:

- There was no good correlation between ε^a and ε^c. Local ventilation effectiveness of contaminant removal showed that fully mixing is not a case with a point source, although air change efficiency determined with equally distributed source showed fully mixing conditions.
- Circular diffuser showed surprisingly ventilation effectiveness values >1 whereas six extraction points did not always perform better than single extract.
- In the infection risk-based ventilation design with contaminant point source (Covid-19), point source ventilation effectiveness ε_b values can be used as a correction factor for mixing ventilation airflow rate.

References

1. Duffield, T.J. School ventilation. Its effect on the health of the pupil. *Am. J. Public Health* **1927**, *17*, 1226–1229.
2. Toyinbo, O.; Shaughnessy, R.; Turunen, M.; Putus, T.; Metsämuuronen, J.; Kurnitski, J.; Haverinen-Shaughnessy, U. Building characteristics, indoor environmental quality, and mathematics achievement in Finnish elementary schools. *Build. Environ.* **2016**, *104*, 114–121.
3. d'Ambrosio Alfano, F.R.; Bellia, L.; Boestra, A.; van Dijken, F.; Ianniello, E.; Lopardo, G.; Minichiello, F.; Romagnoni, P.; da Silva, M.C.G. *Indoor Environment and Energy Efficiency in Schools*; Rehva, Federation of European Heating and Air-conditioning Associations, 2010;
4. Johnson, D.L.; Lynch, R.A.; Floyd, E.L.;

Wang, J.; Bartels, J.N. Indoor air quality in classrooms: Environmental measures and effective ventilation rate modeling in urban elementary schools. *Build. Environ.* **2018**, *136*, 185–197.

5. Stafford, T.M. Indoor air quality and academic performance. *J. Environ. Econ. Manage.* **2015**, *70*, 34–50.

6. Simons, E.; Hwang, S.-A.; Fitzgerald, E.F.; Kielb, C.; Lin, S. The impact of school building conditions on student absenteeism in upstate New York. *Am. J. Public Health* **2010**, *100*, 1679–1686.

7. Wargocki, P.; Wyon, D.P. The effects of moderately raised classroom temperatures and classroom ventilation rate on the performance of schoolwork by children (RP-1257). *Hvac&R Res.* **2007**, *13*, 193–220.

8. Salthammer, T.; Uhde, E.; Schripp, T.; Schieweck, A.; Morawska, L.; Mazaheri, M.; Clifford, S.; He, C.; Buonanno, G.; Querol, X. Children's well-being at schools: Impact of climatic conditions and air pollution. *Environ. Int.* **2016**, *94*, 196–210.

9. Bakó-Biró, Z.; Clements-Croome, D.J.; Kochhar, N.; Awbi, H.B.; Williams, M.J. Ventilation rates in schools and pupils' performance. *Build. Environ.* **2012**, *48*, 215–223.

10. Wargocki, P.; Wyon, D.P. Providing better thermal and air quality conditions in school classrooms would be cost-effective. *Build. Environ.* **2013**, *59*, 581–589.

11. Mundt, M.; Mathisen, H.M.; Moser, M.; Nielsen, P. V Ventilation effectiveness: Rehva guidebooks. **2004**.

12. Batterman, S. Review and extension of CO2-based methods to determine ventilation rates with application to school classrooms. *Int. J. Environ. Res. Public Health* **2017**, *14*, 145.

13. Chung, K.-C.; Hsu, S.-P. Effect of ventilation pattern on room air and contaminant distribution. *Build. Environ.* **2001**, *36*, 989–998.

14. ISO/TC 163; CEN/TC 89 EVS-EN ISO 12569:2017 Thermal performance of buidlings and materials. *Determ. Specif. airflow rate Build. - Tracer gas dilution method* **2017**.

15. ISO/TC 146 ISO 16000-8:2007 Indoor air - Part 8: *Determ. local mean ages air Build. Charact. Vent. Cond.* **2007**.

16. Novoselac, A.; Srebric, J. Comparison of air exchange efficiency and contaminant removal effectiveness as IAQ indices. *Trans. Soc. Heat. Refrig. Air Cond. Eng.* **2003**, *109*, 339–349.

17. Mustakallio, P.; Kosonen, R. Indoor air quality in classroom with different air distribution systems. *Indoor Air* **2011**, 5–10.

18. Kosonen, R.; Mustakallio, P. Ventilation in classroom: a Case-study of the performance of different air distribution methods. In Proceedings of the Proceedings of 10th REHVA World Congress-Clima; 2010.

19. Lichtner, E.; Kriegel, M. Pathogen spread and air quality indoors-ventilation effectiveness in a classroom. **2021**.

20. Li, Y.; Leung, G.M.; Tang, J.W.; Yang, X.; Chao, C.Y.; Lin, J.Z.; Lu, J.W.; Nielsen, P.V.; Niu, J.; Qian, H. Role of ventilation in airborne transmission of infectious agents in the built environment-a multidisciplinary systematic review. *Indoor Air* **2007**, *17*, 2–18.

21. Zhang, J. Integrating IAQ control strategies to reduce the risk of asymptomatic SARS CoV-2 infections in classrooms and open plan offices. *Sci. Technol. Built Environ.* **2020**, *26*, 1013–1018.

22. Cao, G.; Awbi, H.; Yao, R.; Fan, Y.; Sirén, K.; Kosonen, R.; Zhang, J.J. A review of the performance of different ventilation and airflow distribution systems in buildings. *Build. Environ.* **2014**, *73*, 171–186.

23. Müller, D.; Kandzia, C.; Kosonen, R.; Melikov, A.K.; Nielsen, P.V. *Mixing Ventilation Guide on mixing air distribution design*; Rehva, Federation of European Heating and Air-conditioning Associations, 2013;

24. Kurnitski, J.; Kiil, M.; Wargocki, P.; Boerstra, A.; Seppänen, O.; Olesen, B.; Morawska, L. Respiratory infection risk-based ventilation design method. *Build. Environ.* **2021**, *206*, 108387.

25. Nordic Ventilation Group; Rehva Technology and Research Committee COVID-19 Task Force Health-based target ventilation rates and design method for reducing exposure to airborne respiratory infectious diseases. *Rehva* **2022**, 6.

26. EVS/TC 27 EVS 906:2018 Ventilation for non-residential buildings. *Perform. Requir. Vent. room-conditioning Syst. Est. Natl. Annex EVS-EN 16798-32017* **2017**.

27. Onset Computer Corporation HOBO MX1102A data logger Available online: https://www.onsetcomp.com/products/data-loggers/mx1102a/.

28. Testo SE & Co. KGaA Testo 440 dP datasheet Available online: https://www.testo.com/en-US/testo-440-dp/p/0560-4402.

29. KERN & SOHN GmbH Kern FKB datasheet Available online: https://www.kern-sohn.com/en/FKB.

30. Dantec Dynamics A/S ComfortSense Probes Available online: https://www.dantecdynamics.com/product-category/thermal-comfort/comfortsense-probes/.

31. CEN/TC 156 EVS-EN 16798-3:2017 Energy performance of buildings. *Vent. Build. - Part 3 Non-resid. Build. - Perform. Requir. Vent. room-conditioning Syst. (Modules M5-1, M5-4)* **2017**.

32. 156, C. 16798-1. Energy performance of buildings—Ventilation for buildings—Part 1. *Therm. Environ. Light. Acoust. M1-6.(16798-1)* **2019**.
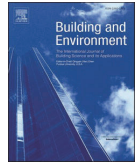
Appendix 4

Ventilation effectiveness and incomplete mixing in air distribution design for airborne transmission

Martin Kiil [a,*], Alo Mikola [a,b], Karl-Villem Võsa [a], Raimo Simson [a,b], Jarek Kurnitski [a,b]

[a] Department of Civil Engineering and Architecture, Tallinn University of Technology, Tallinn, Estonia
[b] Department of Civil Engineering, Aalto University, Espoo, Finland

ARTICLE INFO

ABSTRACT

How ventilation should be arranged to be effective at reasonable air change rates is one key question as ventilation criteria and standard airborne disease transmission models are based on the well-mixed assumption, but air distribution patterns lead to non-uniform spatial concentrations. In this study a new method for ventilation effectiveness application in ventilation design for airborne transmission was developed and tested with tracer gas measurements in 22 rooms. Contrary to existing ventilation effectiveness values measured with distributed source, the developed method uses a couple of point source locations corresponding to an infector to quantify infection risk for each occupant. Novelty of the method is new ventilation effectiveness indicator that makes it possible to describe the effect of spatial variation of concentration and risk with single parameter. Quanta were used as input data to calculate the ventilation rate supplied by air distribution system corresponding to a specified risk level, but the differences between studied cases do not significantly depend on the quanta values. Application of the method to measured rooms showed that simple ventilation effectiveness calculation from average concentration at the breathing height, not requiring quanta data, provided lower ventilation effectiveness and higher ventilation rate in all cases. In many cases the difference in required ventilation rates was only a few percent, but in some large spaces it exceeded 10% with maximum of 39% in large open plan office with high concentration differences. Measured ventilation effectiveness values ranging from 0.5 to 1.4 indicate a substantial improvement potential in many cases.

None Para

Nomenclature

A	floor area of the room (m^2)
ACH	air change per hour (1/h)
C	average quanta concentration in the breathing zone (quanta/m^3)
C_0	quanta concentration in the supply air (quanta/m^3)
C_e	quanta concentration in the extract air (quanta/m^3)
C_{ex}	quanta concentration in the exhaled breath of infector (quanta/m^3)
C_i	quanta concentration at the location i (quanta/m^3)
D	duration of the occupancy (h)
D_l	dilution ratio (-)
D_{inf}	the total interaction time when an infectious individual is in the vicinity of any susceptible persons during the whole pre-symptomatic infectious period (h)
$\varepsilon_{P,i}$	local air quality index at the measurement point i (-)
ε_b	ventilation effectiveness (contaminant removal effectiveness) $\varepsilon_b = 1$ for fully mixed conditions (-)

(continued on next column)

(continued)

Nomenclature

ε_b^j	point source ventilation effectiveness of measurement with source location j (-)
$\varepsilon_{b,loc}$	ventilation effectiveness taking into account the spatial variation of concentration (-)
$\varepsilon_{b,loc}^j$	point source ventilation effectiveness of measurement with source location j taking into account the spatial variation of concentration (-)
h	room height (m)
I	number of infectious persons (-)
k	virus decay (1/h)
λ_{dep}	deposition onto surfaces (1/h)
λ_{rest}	other removal mechanisms than ventilation (1/h)
λ_v	outdoor air change rate, i.e., removal rate due to ventilation (1/h)
n	number of quanta inhaled (quanta)
K	number of measurement points (-)
m	number of tracer gas experiments with different point source locations (-)
N_c	number of disease cases (-)
N_s	number of susceptible persons in the room (-)

(continued on next page)

* Corresponding author.
  E-mail address: martin.kiil@taltech.ee (M. Kiil).

(*continued*)

Nomenclature	
p	probability of infection for a susceptible person (-)
p_i	probability of infection for a susceptible person at location i (-)
q	quanta emission rate per infectious person (quanta/h)
Q	outdoor and non-infectious supply air target ventilation rate for the breathing zone (m^3/h)
Q_b	volumetric breathing rate of an occupant (m^3/h)
Q_s	ventilation rate supplied by ventilation air distribution system (m^3/h)
$Q_{s,loc}$	ventilation rate supplied by ventilation air distribution system taking into account the spatial variation of concentration (m^3/h)
Q_{act}	actual measured design ventilation rate supplied by the ventilation system (L/(s·m^2))
R	event reproduction number (-)
R_0	basic reproduction number that describes the spread of an epidemic in the population (-)
R_i	fraction of the reproduction number (-)
V	volume of the room (m^3)

1. Introduction

The emergence of the COVID-19 pandemic, triggered by the SARS-CoV-2 virus has precipitated an unparalleled global health emergency, profoundly impacting public health frameworks, economic infrastructures, and the very essence of daily human interactions worldwide. The crisis has underscored the critical importance of maintaining high standards of indoor air quality and robust ventilation systems as frontline measures against the spread of respiratory infections [1–3]. Research has identified the predominant modes of COVID-19 transmission to be expelled respiratory droplets almost instantly desiccating to aerosols, remaining airborne for extended periods and enabling transmission over distances much longer than initially recommended 2-meter distancing [4,5].

Ventilation supported with particle filtration and air disinfection are the main removal mechanisms in mitigating long range airborne transmission by reducing infectious aerosol concentrations in shared indoor spaces [3]. Ventilation replaces indoor air with outdoor or otherwise treated non-infectious supply air, diluting the accumulation of airborne pathogens, that lowers transmission risk among indoor occupants significantly [6]. One key question is how ventilation should be arranged to be effective at reasonable air change rates (*ACH*). The ability of a ventilation system to remove airborne contaminants does not only depend on the *ACH* but also on the ventilation effectiveness [7]. In this study, we focus on the problem that any ventilation criteria, either being based on perceived air quality, threshold concentration of a specific pollutant, or airborne transmission, will provide a target ventilation rate at fully mixed conditions. In reality ventilation is arranged in indoor spaces by mechanical or natural means with air distribution patterns which may lead to considerable contaminant concentration differences. This is a problem in the infection risk assessment because a standard airborne disease transmission Wells-Riley model is based on the well-mixed assumption that the distribution of pathogen-laden aerosols is spatially uniform [8]. With this assumption, the airborne infection risk is reported to be potentially underestimated [9–11].

Non-uniform concentration can be taken into account with ventilation effectiveness which values are summarised in reviews [12,13] for many air distribution systems. However, as being measured with distributed contaminant source representing for instance bioeffluent and CO_2 emissions from all occupants in the room, existing ventilation effectiveness values do not apply for airborne transmission from an infector acting as a point source. Distributed emission sources are relatively equally distributed and thus easy to remove by mixing ventilation air distribution systems, which is the reason why a common design consideration is to use ventilation effectiveness value equal to one. In the case of airborne transmission, instead of distributed source, one person in a room may be an infector corresponding to a point source with many possible locations. While it is clear that the COVID-19 pandemic has intensified the urgency to develop, refine, and implement tailored ventilation guidelines to address the risks posed by respiratory infections across shared indoor settings [14,15] a research gap exists how the ventilation effectiveness concept can be applied for airborne transmission with a point source.

Spatial non-uniform concentration resulting from air distribution patterns has been analysed in many studies. The concentration field has been solved with CFD simulations [16] or with detailed measurements [8] enabling to calculate the infection risk in any point or for each occupant. Tan [17] has concluded that spatial variation in aerosol concentration is significant in indoor settings, with standard deviations comparable to the mean, and it should be accounted for during risk assessment. Jan [18] coupled CFD and modified Wells-Riley model based on the Lagrangian particle tracking framework. This allowed to conduct risk quantification for each occupant in the meeting room case study with two mixing ventilation configurations resulting in high spatial variation and revealing a higher inhalation possibility of droplets with nuclei size smaller than 5 μm. That cut-off size was found to be sensitive to ventilation. Son [19] studied experimentally the effect of floor and ceiling extracts with ceiling supply diffusers showing that floor extracts help to form a vertical airflow and reduce PM2.5 concentrations at the breathing level. Singer [20] showed in tracer gas experiments conducted for a meeting room and classroom that ceiling diffusers can achieve good mixing when supplying cooled or thermally neutral air, but heating with supply air will reduce ventilation effectiveness. CO_2 distribution within naturally ventilated classroom in wintertime was simulated with CFD in [21] showing considerable differences depending on opening configurations.

Therefore, it has been possible to show which air distribution solutions are more effective or in which locations the infection risk is lower for an occupant, but as methodology these approaches tend to be far too complicated to be applied for a robust ventilation design method. On the other hand, these studies demonstrate that it is possible to analyse spatial distribution of an infection risk with detailed measurements or CFD simulations. However, that is lacking, is a robust method for practical ventilation design purposes.

To bridge the gap, this study proposes new method for ventilation effectiveness application in ventilation air distribution design for airborne transmission based on tracer gas measurements with a couple of point source locations. Infection risk is quantified for each measurement point at the breathing height to show the sensitivity on the concentration differences and to compare with robust calculation based on average measured concentration in the breathing level. Novelty of the method is new ventilation effectiveness parameter that makes it possible to describe the effect of spatial variation of concentration and risk with single parameter that is especially important in cases with large concentration variations.

To test the developed methodology, in this study, tracer gas measurements were conducted in actual buildings and an air distribution mock-up laboratory at Tallinn University of Technology. For sensitivity analyses datasets from previously conducted CO_2 tracer gas measurements [22–26] were also used. Measured rooms represent typical modern or renovated non-residential spaces in educational, office and sports buildings, all equipped with ceiling distributed mixing ventilation air distribution systems. The room types included are classrooms, open plan offices, meeting rooms, fitness rooms, gym halls, dressing rooms, bars and restaurants. This comprehensive dataset of measurements with 2–3-point source locations all together in 22 rooms enabled to show some tendencies and high variations in ventilation effectiveness depending on air distribution system, room size and *ACH*. For the applications of practical ventilation design purposes, the results allow to draw conclusions about the benefits of the new developed method, and the drawbacks of its iterative calculations, as well as about possibilities to use conservative ventilation effectiveness values calculated from average concentration. The results can be potentially applied in ventilation standards and air distribution calculation tools.

2. Methods

2.1. General methodology

To analyse the effect of incomplete mixing in ventilation design for airborne transmission, average concentration at 1.1 m height corresponding to the sitting person breathing height or alternatively local concentrations are used as shown in Fig. 1.

In Sections 3.1 and 3.2 a set of equations is derived to solve the probability of infection as a function of ventilation rate and ventilation effectiveness in the steady state. Two alternative approaches are employed:

- By using average concentration in the breathing zone C as described in Section 3.1 and the event reproduction number (R) calculated from the scenario of exposure and the risk assessment model described in Section 2.4.
- With a new method where local concentrations C_i are used to calculate the local air quality index and the fraction of the event reproduction number (R_i) leading to iterative solving of the R equation as described in Section 3.2, allowing to take into account the spatial difference of the infection risk with new ventilation effectiveness parameter $\varepsilon_{b,loc}$.

To calculate the target ventilation rate, the quanta and risk assessment model related input data reported in Section 2.3 were taken from

[20]. This risk assessment model aims to reduce the secondary attack rates below 1.0 during the "subclinical infectious period" to slow down the spread of epidemic. The required ventilation rate supplied by the ventilation air distribution system is calculated from the measured local air quality index values which evaluation and measurement with tracer gas is reported in Sections 3.3 and 3.4.

Ventilation effectiveness values ε_b were computed based on the average concentration C at 1.1 m height of sitting person. These values were then compared to iteratively calculated $\varepsilon_{b,loc}$ values taking into account the spatial variation of the infection risk. In that way, two ventilation effectiveness values were calculated, allowing us to recalculate the fully mixing target ventilation rate to the required ventilation rate to be supplied by the actual air distribution system, accounting for non-uniform concentration and infection risk. The developed methodology was tested with tracer gas measurements with the constant injection method, conducted in total in 22 rooms by using 2–3-point source locations in each room.

2.2. Field and laboratory measurements in case study rooms

Case study rooms (Table 1) were selected from modern or renovated non-residential buildings with well-functioning mechanical supply and exhaust ventilation systems with heat recovery (no recirculation) located in Tallinn and Helsinki. The selected rooms represent typical shared indoor spaces in educational, office and sport buildings. Air distribution was organised in all rooms from ceiling with mixing
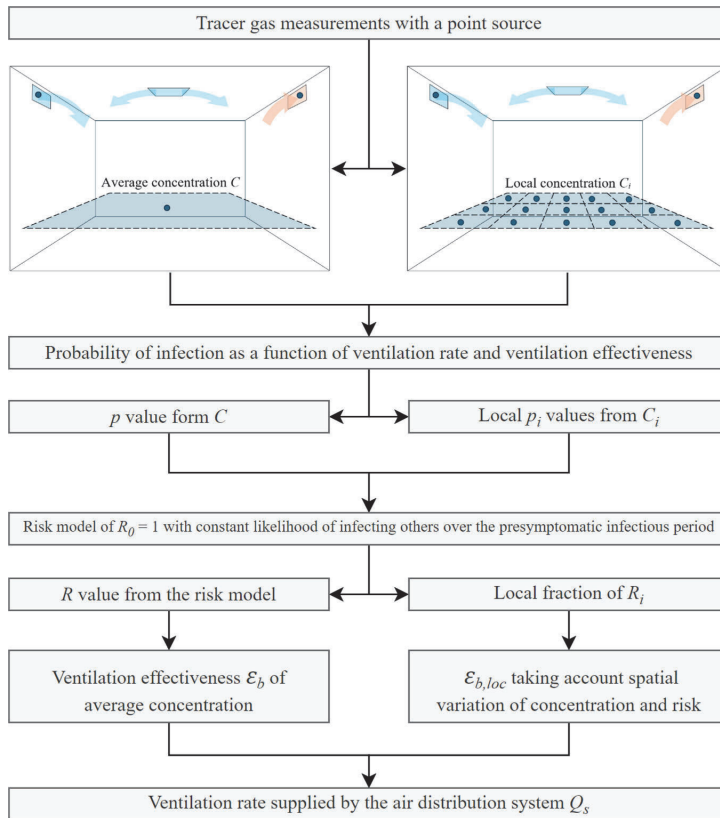

Fig. 1. Flow chart of the research methodology in the development the new method as the right path in the figure, to take the spatial variation of the infection risk into account in the air distribution design.

Table 1
Description of the case study rooms.

Classroom 1 Wall diffuser[1] 45.0 m², h = 3.8 m Q_{act} = 5.3 L/s·m²	**Classroom 2** Ceiling swirl diffusers 42.5 m², h = 2.9 m Q_{act} = 3.8 L/s·m²
Classroom 3 Ceiling swirl diffusers 30.5 m², h = 2.9 m Q_{act} = 6.2 L/s·m²	**Classroom 4** Ceiling swirl diffusers A = 56.5 m² h = 2.9 m Q_{act} = 3.9 L/s·m²
Classroom 5 Ceiling swirl diffusers 129.5 m², h = 2.9 m Q_{act} = 3.9 L/s·m²	**Classroom 6** Ceiling diffusers 45.1 m², h = 2.9 m Q_{act} = 4.0 L/s·m²
Dressing room 1 Ceiling diffusers 145.0 m², h = 2.8 m Q_{act} = 8.1 L/s·m²	**Dressing room 2** Ceiling diffusers 318.0 m², h = 2.5 m Q_{act} = 6.9 L/s·m²
Fitness 1 Conical ceiling diffusers 173.5 m², h = 3.5 m Q_{act} = 5.2 L/s·m²	**Fitness 2** Wall diffusers 117.0 m², h = 4.6 m Q_{act} = 6.4 L/s·m²
Fitness 3 Duct diffusers 153.0 m², h = 3.4 m Q_{act} = 4.9 L/s·m²	**Gym 1** Ceiling swirl diffusers A = 217.5 m² h = 6.0 m Q_{act} = 9.2 L/s·m²
Gym 2 Conical wall diffusers 331.0 m², h = 6.0 m Q_{act} = 6.0 L/s·m²	**Gym 3** Conical ceiling diffusers 987.0 m², h = 8.0 m Q_{act} = 4.1 L/s·m²
Canteen Ceiling diffusers 242 m², h = 2.5 m Q_{act} = 1.8 L/s·m²	**Restaurant** Ceiling diffusers 135.0 m², h = 3.1 m Q_{act} = 4.2 L/s·m²
Bar Ceiling diffusers 203.0 m², h = 3.1 m Q_{act} = 3.7 L/s·m²	**Nightclub** Ceiling diffusers 492.0 m², h = 4.5 m Q_{act} = 3.8 L/s·m²
Meeting room 1 Active chilled beams 52.5 m², h = 3.2 m Q_{act} = 3.8 L/s·m²	**Meeting room 2** Ceiling swirl diffusers 23.5 m², h = 2.7 m Q_{act} = 6.4 L/s·m²
Open office 1 Active chilled beams 45.0 m², h = 3.8 m Q_{act} = 2.0 L/s·m²	**Open office 2** Ceiling diffusers, ceiling panels 242.0 m², h = 2.7 m Q_{act} = 2.3 L/s·m²

[1] ceiling diffusers, duct diffusers, single and multiple extracts in other cases.

ventilation air distribution solutions. To have a good overview of mixing ventilation solutions performance, we used some previously reported measurements, and some original measurements conducted in this study. Multiple classroom configurations (Classroom 1 [22,24,25,27]) and Open office 2 [22] were laboratory mock ups measured at Tallinn University of Technology. Classroom 2 to 5 [28] consist of a large space that can be divided into three smaller classrooms. Measurements for the Canteen, Restaurant, Bar, and Nightclub were conducted on a cruise ship

[29] docked at the port of Helsinki. Dressing rooms, fitness rooms, gyms and meeting rooms were measured in this study.

Air distribution, room floor area (A), height, and design ventilation rates are provided in Table 1.

Primary equipment used in the experiments is detailed in Table 1 and Fig. 2. Field measurements with tracer gas were performed using the point source continuous injection method, which has been tested and compared with distributed source concentration decay method in [24].

In the experiments CO_2 concentration levels were measured at 1.1 m height corresponding to the sitting person breathing height, and in the supply and extract air, Fig. 2. Experiments were conducted under controlled conditions corresponding to normal operation, but without occupants to minimize external influences. Thermal dummies were employed to simulate internal heat gains of occupants. Thermal dummies were expected to generate a convective plume like persons, but they cannot reproduce a close proximity exhalation airflow and concentration field and thus are suitable for long range transmission experiments only. CO_2 injection inside the dummy representing an infector was adjusted by the regulator and measured using a scale. The HVAC operation/maintenance staff ensured that design airflow rates were maintained by manual 100% airflow rate setting in BMS system and occupied hours temperature setpoints were kept. According to BMS systems sensors, room temperatures were close to 22 °C and supply air temperature ranged 18–20 °C.

In the laboratory measurements the effect of the point source location was tested by repeating measurements with changed point source location. While this is time consuming, field measurements were conducted either with 2- or 3- point source locations. Locations representing typical occupant positions were used so that one location was selected as far as possible from extracts and another location from the middle of the room. An example of the measurement setup for a large teaching space, Classroom 5, is shown in Fig. 3 and the impact of point source locations is reported in Figs. 6 to 12. The number of measurement points used in each case is reported in Table 3.

The primary source of uncertainty in our measurements stems from the CO_2 sensor's accuracy, which includes errors of ±30 ppm ± 3% of the measured value, an additional 1% due to sensor non-linearity, and ±30 ppm from variations in CO_2 levels under quasi-steady state conditions. The total relative uncertainty of the calculated ventilation effectiveness indices ranges from 3% to 12% (Eq. (1)), with higher relative errors observed in tests with lower absolute CO_2 concentrations inside the measured rooms. This issue is particularly significant in large rooms, where dosing CO_2 in practical amounts during in-field measurements is challenging.

Table 2

Specifications of measuring equipment: CO_2 concentration logger [30] and gas mass weighting scale [31].

Parameters	Aranet4 Data Logger	Kern FKB
	CO_2 concentration	weight
Range	0…9999 ppm	0.002…65 kg
Accuracy	±30 ppm + ±3 %	±0.001 kg
Image		

$$u_T = \frac{H^2}{i} \sqrt{\sum \left(\frac{u_j}{\left(\varepsilon_b^j\right)^2} \right)^2} \tag{1}$$

where

u_T	total uncertainty of ventilation effectiveness (-)
H	harmonic mean value of the point source ventilation effectiveness at all source locations (-)
i	number of point source locations (-)
u_j	uncertainty of point source ventilation effectiveness of measurement with source location j (-)
ε_b^j	point source ventilation effectiveness of measurement with source location j (-)

2.3. Infection risk assessment parameters

Infection risk can be calculated for different activities and rooms using a standard airborne disease transmission Wells-Riley model calibrated to COVID-19 with the correct source strength (quanta emission rates). In this model, the viral load emitted is expressed in terms of the quanta emission rate (quanta/h). One quantum is defined as the dose of airborne droplet nuclei required to cause infection in 63% of susceptible persons. With the Wells-Riley model which history and modifications are explained in [32], the probability of infection (p) is related to the number of quanta inhaled (n) according to Eq. (2):

$$p = \frac{N_c}{N_s} = 1 - e^{-n} = 1 - e^{-\frac{IqQ_bD}{Q}} = 1 - e^{-CQ_bD} \tag{2}$$

where

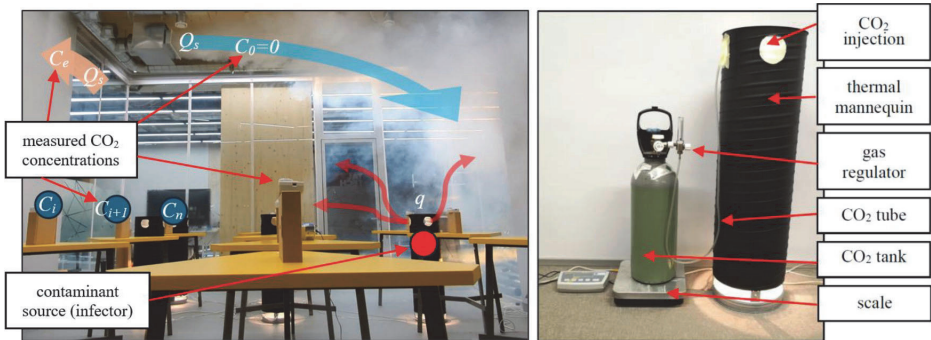|	
p	probability of infection for a susceptible person (-)
N_c	number of disease cases (-)
N_s	number of susceptible persons in the room (-)

Fig. 2. Left - measuring CO_2 concentrations at 1.1 m height of sitting person and in the supply and extract air. Right – contaminant source simulated with a CO_2 bottle connected to a thermal dummy.
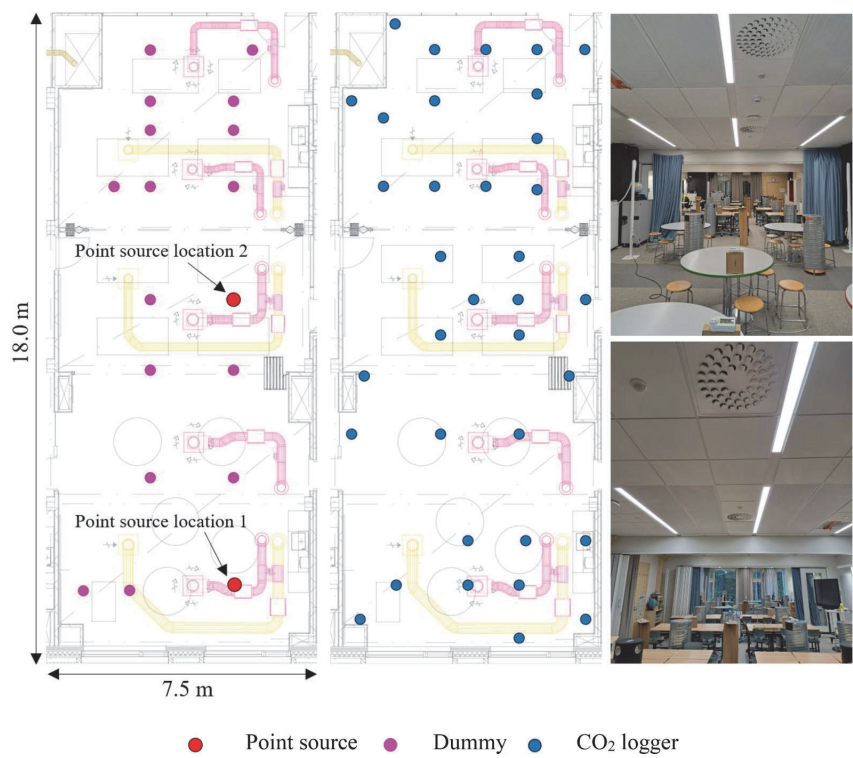
Fig. 3. An example of the measurement setup in Classroom 5: locations of the point source, dummies and measurement points. Upper right photo from the façade and lower right photo to the façade direction.

Table 3
Description of the infection risk-based target ventilation rate parameters in fully mixed conditions in the case study rooms.

Room	V (m³)	N_s (-)	K (-)	Q (quanta/h)	Q_b (m³/h)	D (h)	D_{inf} (h)	λ_{dep} (1/h)	K (1/h)	R (-)
Classroom 1	171	29	15	4	0.57	6	16	0.24	0.63	0.375
Classroom 2	123	24	18	4	0.57	6	16	0.24	0.63	0.375
Classroom 3	88	12	15	4	0.57	6	16	0.24	0.63	0.375
Classroom 4	164	24	14	4	0.57	6	16	0.24	0.63	0.375
Classroom 5	376	49	29	4	0.57	6	16	0.24	0.63	0.375
Classroom 6	131	24	12	4	0.57	6	16	0.24	0.63	0.375
Dressing room 1	406	28	22	10	0.65	2	16	0.24	0.63	0.089
Dressing room 2	795	37	20	10	0.65	2	16	0.24	0.63	0.089
Fitness 1	607	32	20	6	1.92	2	16	0.24	0.63	0.089
Fitness 2	538	17	13	6	1.92	2	16	0.24	0.63	0.089
Fitness 3	520	19	13	6	1.92	2	16	0.24	0.63	0.089
Gym 1	1305	24	30	6	1.92	2	16	0.24	0.63	0.089
Gym 2	1986	24	35	6	1.92	2	16	0.24	0.63	0.089
Gym 3	7896	48	34	6	1.92	2	16	0.24	0.63	0.089
Canteen	605	20	16	10	0.65	2	16	0.24	0.63	0.089
Restaurant	419	27	14	10	0.65	2	16	0.24	0.63	0.089
Bar	629	37	16	10	0.65	2	16	0.24	0.63	0.089
Nightclub	2214	93	16	10	0.65	2	16	0.24	0.63	0.089
Meeting room 1	168	12	13	10	0.65	9	22.5	0.24	0.63	0.089
Meeting room 2	69	7	20	10	0.65	9	22.5	0.24	0.63	0.089
Open office 1	171	6	7	6	0.6	9	22.5	0.24	0.63	0.4
Open office 2	450	21	25	6	0.6	9	22.5	0.24	0.63	0.4

I	number of infectious persons (-)	D	duration of the occupancy (h)
n	number of quanta inhaled (quanta)	C	average quanta concentration in the room (quanta/m³)
q	quanta emission rate per infectious person (quanta/h)		Virus and room specific parameters to calculate the target ventilation
Q_b	volumetric breathing rate of an occupant (m³/h)		rate Q in fully mixed conditions at specified risk level are provided in
Q	ventilation rate for the breathing zone (m³/h)		Table 3. The room volume V, N_s and the number of concentration

measurement points K are presented in the same room order as in Table 1. Virus risk specific parameters are from [25]. These parameters are necessary to calculate the required ventilation rates, but changing the values of parameters will not significantly change relative differences between the analysed cases that has been shown by relative risk of exposure analyses in [33]. Deposition and decay, λ_{dep} and k remain the same throughout the rooms. The quanta emission rate used were: 4 quanta/h in classrooms, 6 quanta/h in fitness, gym, and office rooms, and 10 quanta/h in dressing rooms, restaurants and bars, and meeting rooms. Breathing rate is 0.57 m³/h for classrooms, 0.6 m³/h for open office, 0.65 m³/h for dressing rooms, bars, and restaurants, and 1.92 m³/h for fitness and gym. Occupancy duration of 2 h is used, except for 6 h in classroom and 9 h in meeting rooms and open offices. Interaction time of an infectious individual in the vicinity of susceptible persons is assumed 16 h and 22.5 h in meeting rooms and open offices. R number used is 0.089, except for 0.375 for classrooms or 0.4 for open offices. Assuming a virus situation, occupancy reduction to 33 % in dressing rooms, 50 % in meeting rooms, and 80 % in open offices was applied.

2.4. Scenario of exposure and risk assessment model

It is shown that one infector in any room leads to the highest total removal rate needed to keep the specified value of new disease cases per infector [25,34] and thus can be used as relevant scenario of exposure in the design. The risk assessment model introduced in [25] aiming to secondary attack rates $R_0 \leq 1$ is applied. This model calculates acceptable room category specific R during one room-occupancy from the assumption that the likelihood of infecting others (i.e. the number of infections per unit time) is constant over the pre-symptomatic infectious period. It integrates the exposure over out-of-home-events by introducing an average interaction time [35] between the infector and susceptible occupants during the infectious period:

$$\frac{R}{R_0} \cong \frac{D}{D_{inf}} \ \Rightarrow R \leq \frac{D}{D_{inf}} \ \ when \ \ R_0 \leq 1 \tag{3}$$

where:
R event reproduction number, i.e. number of people who become infected per infectious occupant
D room occupancy period, i.e. length of time when both infectious and susceptible persons are present in the room at the same time (h)
D_{inf} total interaction time when an infectious individual is in the vicinity of any susceptible persons during the whole presymptomatic infectious period (h)
R_0 basic reproduction number describing the spread of an epidemic in the population (-)

The pre-symptomatic infectious period ends typically at the onset of symptoms when the infectious person self-isolates at home and is not any more in contact with susceptible individuals. For example, if an infectious person is in the vicinity of susceptible persons (e.g. on public transport, at work/school) for 20 h altogether during the pre-symptomatic infectious period, then he or she must not infect more than $R = 1/20 = 0.05$ persons per hour, on average, in order to remain within the limit of $R_0 \leq 1$. Room category specific R values based on the pre-symptomatic infectious period of 2.5 days [25] are reported in Table 3.

3. Results

3.1. Calculation of infection risk-based target ventilation rate

The Wells-Riley model applies for long range aerosol transmission in fully mixing conditions. In the case of incomplete mixing and one infector (point source) as a scenario of exposure, concentration C may vary in the room and can be measured with a tracer gas at points under

interest in the breathing height C_i to C_n (Fig. 4).

In [26] an explicit equation for ventilation rate in the steady state at given infection risk probability and fully mixing air distribution has been derived. The same approach can be used for incomplete mixing as follows. Quanta concentration C under steady state conditions may be solved from the pollutant mass balance:

$$Iq = C_e \lambda_v V + C \lambda_{rest} V \tag{4}$$

where
C_e quanta concentration in the extract air (quanta/m³)
C average quanta concentration in the breathing zone (quanta/m³)
V volume of the room (m³)
λ_v outdoor air change rate, i.e., removal rate due to ventilation (1/h)
λ_{rest} removal mechanisms other than ventilation (1/h)

The ratio of concentrations C_e and C is described with ventilation effectiveness as defined in EN 16,798–3:2017 (contaminant removal effectiveness in Rehva Guidebook No 2):

$$\varepsilon_b = \frac{C_e - C_0}{C - C_o} \tag{5}$$

where
C_0 quanta concentration in the supply air (quanta/m³)

Substituting ε_b to Eq. (4) and taking into account that the ventilation rate supplied by the ventilation air distribution system $Q_s = \lambda_v V$ one obtains:

$$C = \frac{Iq}{\varepsilon_b Q_s + \lambda_{rest} V} \tag{6}$$

where
Q_s ventilation rate supplied by the ventilation air distribution system (m³/h)

Probability of infection can be calculated by substituting C from Eq. (6) to Eq. (2):

$$p = 1 - e^{-\frac{IqQ_bD}{\varepsilon_b Q_s + \lambda_{rest} V}} \tag{7}$$

Considering that N_s susceptible persons are exposed to C, R (new disease cases per infectious person) can be calculated:

$$R = \frac{pN_s}{I} \tag{8}$$

For a given R value, the ventilation rate for the breathing zone Q can be solved from Eq. (7) because:

$$Q = \varepsilon_b Q_s \tag{9}$$

where
Q target ventilation airflow rate for the breathing zone (m³/h)

Target ventilation airflow rate for the breathing zone Q equals with the ventilation rate at fully mixing conditions ($C = C_e$ and $\varepsilon_b = 1$). To find the relevant R value, scenario of the exposure (one or more infector) and the risk assessment concept needs to be defined that is described in Section 2.4.

Equations 7 – 9 correspond to the target ventilation equation in [26]. Ventilation rate supplied by the ventilation air distribution system Q_s can be calculated if the ventilation effectiveness is known or measured. The results of ε_b and Q_s apply at a specific point source location, therefore multiple experiments with various point source locations are needed to determine representative values as reported in Section 3.4.

3.2. Calculation of infection risk from local concentration values

To analyse the effect of using an average concentration instead of local values, i.e. to take into account spatial variation of concentration C,
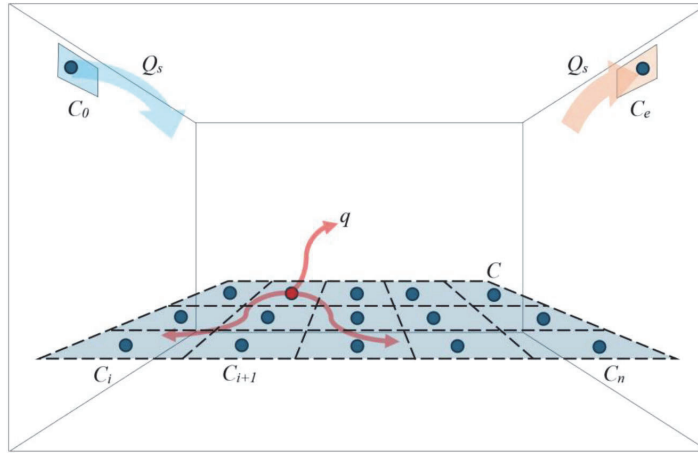
Fig. 4. Concentrations in the room and extract air in the case of incomplete mixing. Red arrows show one possible location of an infector that can be located at any point; therefore the measurements are to be repeated with multiple infector locations.

probability of infection can be calculated at each measured location i. In this case, quanta concentration C_i in the location i under steady state conditions is solved from pollutant mass balance:

$$Iq = C_e \lambda_v V + C_i \lambda_{rest} V \tag{10}$$

where

C_e quanta concentration in the extract air (quanta/m^3)
C_i quanta concentration at the location i (quanta/m^3)
V volume of the room (m^3)
λ_v outdoor air change rate, i.e., removal rate due to ventilation (1/h)
λ_{rest} other removal mechanisms than ventilation (1/h)

Local air quality index is defined:

$$\varepsilon_{P,i} = \frac{C_e - C_0}{C_i - C_0} \tag{11}$$

Substituting $\varepsilon_{P,i}$ to Eq. (10) and taking into account that the ventilation rate supplied by the ventilation system $Q_{s,loc} = \lambda_v V$ one obtains:

$$C_i = \frac{Iq}{\varepsilon_{P,i} Q_{s,loc} + \lambda_{rest} V} \tag{12}$$

where

$Q_{s,loc}$ ventilation rate supplied by the ventilation air distribution system taking into account the spatial variation of concentration (m^3/h)

Probability of infection at location i can be calculated by substituting C_i from Eq. (12) to Eq. (2):

$$p_i = 1 - e^{-\frac{Iq Q_b D}{\varepsilon_{P,i} Q_{s,loc} + \lambda_{rest} V}} \tag{13}$$

Considering that $N_{s,i}$ susceptible persons are exposed to C_i at location i, R_i (new disease cases per infectious person) can be calculated:

$$R_i = \frac{p_i N_{s,i}}{I} \tag{14}$$

R forms from the exposure of all susceptible persons:

$$R = \sum_i R_i \tag{15}$$

For a given R value, the ventilation rate supplied by the ventilation air distribution system $Q_{s,loc}$ can be iteratively solved from Eqs. (13) – 15. Ventilation effectiveness then can be calculated from the target

ventilation rate for the breathing zone that applies at fully mixing conditions:

$$\varepsilon_{b,loc} = \frac{Q}{Q_{s,loc}} \tag{16}$$

where

Q target ventilation airflow rate for the breathing zone (m^3/h)
$\varepsilon_{b,loc}$ ventilation effectiveness taking into account the spatial variation of concentration (-)

Target ventilation airflow rate for the breathing zone Q equals the ventilation rate at fully mixing conditions and it is calculated with Equations 7 – 9 so that $\varepsilon_b = 1$.

3.3. Ventilation effectiveness evaluation in case study rooms

The evaluation of ventilation effectiveness using carbon dioxide (CO$_2$) as a tracer gas is well-validated [7,36–38]. To calculate local air quality index values at measurement points, CO$_2$ is injected at a constant rate to the room and stabilised, steady state concentration values are used in Eq. (11).

Ventilation effectiveness ε_b quantifies a system's ability to remove airborne contaminants [7]. To compute ε_b that represents a conventional method based on the average concentration, an average is taken of the values derived from experiments at various point source locations j (ε_b^j), using Eqs. (17) and 18. For point source location j ventilation effectiveness based on the average concentration in the breathing zone is calculated from the local air quality index (Eq. (11)) measurement points ($\varepsilon_{P,i}$):

$$\varepsilon_b^j = \frac{1}{\dfrac{\sum_{i=1}^{K} \left(\dfrac{1}{\varepsilon_{P,i}} \right)}{K}} \tag{17}$$

Ventilation effectiveness for a room is calculated from m experiments with different point source locations as an average of weighted reciprocals:

$$\varepsilon_b = \frac{1}{\dfrac{\sum_{i=1}^{m} \left(\dfrac{1}{\varepsilon_b^j} \right)}{m}} \tag{18}$$

In the new method developed in this study, ventilation effectiveness

taking into account the spatial variation of concentration is calculated as a ratio of the target ventilation airflow rate for the breathing zone that equals the outdoor air ventilation rate at fully mixing conditions and the outdoor air ventilation rate supplied by the ventilation air distribution system taking into account the spatial variation of concentration:

$$\varepsilon_{b,loc}^{j} = \frac{Q}{Q_{s,loc}} \tag{19}$$

$$\varepsilon_{b,loc} = \frac{1}{\frac{\sum_{i=1}^{m}\left(\frac{1}{\varepsilon_{b,loc}^{j}}\right)}{m}} \tag{20}$$

To calculate $Q_{s,loc}$, R is solved from R_i Eqs. (13) – 15 by changing $Q_{s,loc}$ value until the R value specified in Table 3 is achieved. Target ventilation rate Q at fully mixing conditions is calculated with Equations 7 – 9. These calculations are reported in Table 4.

3.4. Ventilation effectiveness and target ventilation rate calculated from average and local concentration

To illustrate the spatial distribution of the concentration and to show tendencies of air distribution performance, local air quality index $\varepsilon_{P,i}$ distributions are visualised in selected rooms. In each room local air quality index $\varepsilon_{P,i}$ values were calculated with Eq. (11) in K measurement points at 1.1 m height (Table 3), from which values linearly interpolated colour plots are shown in Figs. 5–11. The visualization of results was performed using the SciPy and Matplotlib libraries within the Python programming language. The impact of the point source that is not fully mixed by mixing ventilation air distribution designed for the removal of distributed sources is well visible in Office 1 setup measured in the laboratory (Fig. 5). Despite active chilled beams providing high induction airflow and good mixing, higher concentration zones formed close to the point source with all three measured locations. Depending on the single or multiple extracts, ventilation effectiveness ε_b was 0.89 to 0.96

which is slightly below the fully mixing value of 1.0.

In relatively small 25-person classroom, Fig. 6 illustrates the impact of the location of extract air devices. In this classroom with two ceiling diffusers with plenum boxes, 12 concentration measurement points at a height of 1.1 m and one measurement from the extract air duct were used. With source locations far and close to extracts, high and low concentration zones formed resulting in ε_b^{j} values of 0.90 and 1.67 and $\varepsilon_b = 1.17$. This shows that the local exhaust effect improves ventilation effectiveness, and the source should not be located in the measurements just beneath the extract. A similar situation has been measured in Classroom 3 [28] and Meeting room 1 [25].

An extreme example of placing the source directly beneath the exhaust can be seen in Fig. 7. In this case the only extract in the room started to work as local exhaust providing as high ε_b^{j} as 1.86, but another source location showed accumulation of a contaminant that indicates poorly performing air distribution, i.e. air jets from ceiling diffusers were not reaching the floor level resulting in short circuiting with $\varepsilon_b^{j} = 0.53$. Such large differences in ε_b^{j} make it uncertain to calculate the average value, however as reciprocals are summed, the result $\varepsilon_b = 0.79$ indicates poorly performing air distribution. Another example from similar Fitness 2 in Fig. 8, shows good air distribution performance as both ε_b^{j} values 1.34 and 1.04 are higher than in fully mixed conditions and ε_b resulted in 1.17. In this case air distribution was organised with wall diffusers and extract grilles.

In gyms which are larger but have similar *ACH*, ventilation effectiveness smaller or higher than 1.0 was found similar to fitness examples. Gym 1 suffered from short circuiting because of too short jet throw length providing one of the lowest measured $\varepsilon_b = 0.49$, Fig. 9. In slightly larger Gym 2, all three measurements showed ε_b^{j} higher than one with resulting $\varepsilon_b = 1.17$, Fig. 10. However, in the upper left case, higher concentration formed around the source, indicating poor mixing in this part of the room. In the upper right case with a source in the middle of the room, the tracer gas was effectively removed so that breathing zone

Table 4

Comparison of the required ventilation airflow rates supplied by the air distribution system Q_s based on the measured ventilation effectiveness ε_b and iteratively calculated $Q_{s,loc}$ and $\varepsilon_{b,loc}$ which take into account the spatial difference of the infection risk.

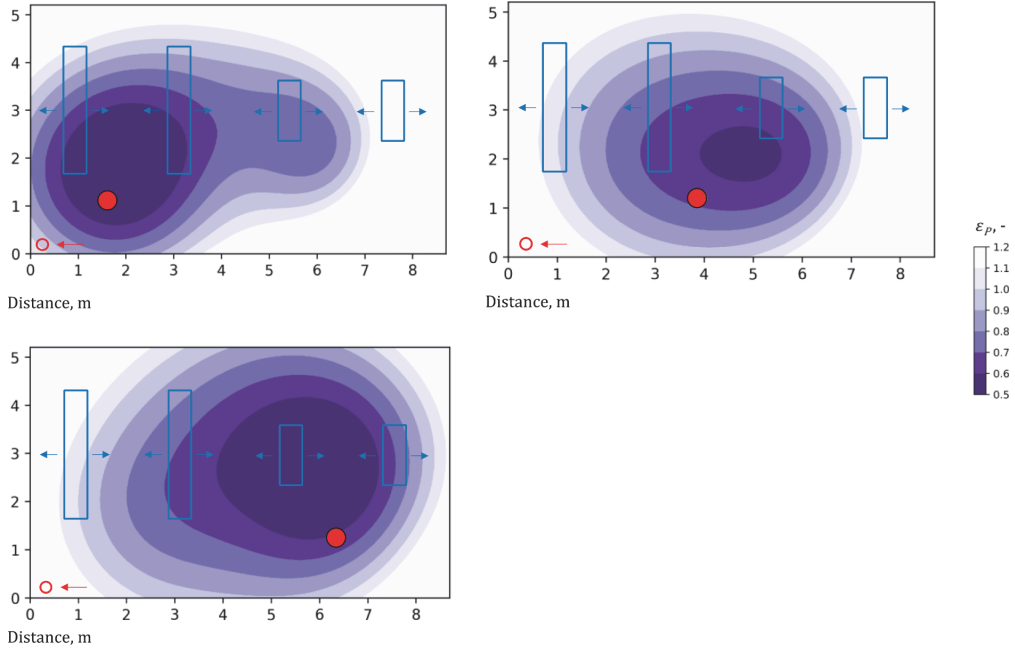| Room	ε_b^{j} -	ε_b -	Q_s m³/s	$\varepsilon_{b,loc}^{j}$ -	$\varepsilon_{b,loc}$ -	$Q_{s,loc}$ m³/s	Q m³/s	ΔQ_s %
Classr. 1	0.97, 0.97, 1.00	0.98	0.258	0.99, 0.98, 1.00	0.99	0.255	0.253	+1.4
Classr. 1	0.84, 0.95, 1.09	0.95	0.267	0.85, 0.95, 1.09	0.96	0.264	0.253	+1.0
Classr. 1	1.53, 1.43, 1.12	1.34	0.189	1.55, 1.46, 1.12	1.35	0.187	0.253	+1.0
Classr. 1	1.28, 1.17, 1.00	1.14	0.222	1.29, 1.18, 1.02	1.15	0.219	0.253	+1.1
Classr. 1	1.13, 0.98, 0.91	1.00	0.252	1.13, 0.98, 0.92	1.00	0.252	0.253	+0.2
Classr. 1	1.09, 0.89, 1.09	1.01	0.249	1.10, 0.89, 1.10	1.02	0.248	0.253	+0.4
Classr. 2	0.82	0.82	0.262	0.82	0.82	0.261	0.213	+0.2
Classr. 3	0.95, 1.77	1.24	0.081	0.95, 1.78	1.24	0.081	0.100	+0.4
Classr. 4	0.73	0.73	0.279	0.73	0.73	0.278	0.204	+0.7
Classr. 5	0.72, 0.76	0.74	0.547	0.74, 0.80	0.77	0.529	0.406	+3.5
Classr. 6	0.90, 1.67	1.17	0.181	0.90, 1.71	1.18	0.179	0.212	+1.1
Dress. 1	1.64, 1.03	1.26	0.823	1.69, 1.05	1.30	0.803	0.755	+2.6
Dress. 2	0.95, 1.27, 1.03	1.07	1.685	1.00, 1.47, 1.15	1.18	1.527	1.799	+10.4
Fitness 1	0.53, 1.86	0.79	2.624	0.54, 1.93	0.84	2.560	2.157	+2.5
Fitness 2	1.34, 1.04	1.17	0.934	1.35, 1.04	1.18	0.930	1.094	+0.4
Fitness 3	0.64, 1.05	0.79	1.570	0.67, 1.06	0.82	1.510	1.242	+4.0
Gym 1	0.56, 0.43	0.49	2.904	0.72, 0.44	0.55	2.575	1.413	+12.8
Gym 2	1.12, 1.12, 1.28	1.17	1.069	1.19, 1.18, 1.33	1.23	1.017	1.248	+5.1
Gym 3	1.52, 0.97, 0.74	0.99	1.563	1.68, 1.00, 1.07	1.18	1.307	1.548	+19.6
Canteen	0.97	0.97	0.684	1.10	1.10	0.605	0.666	+13.1
Restaur.	0.56, 0.87	0.68	1.465	0.59, 0.90	0.71	1.400	0.996	+4.6
Bar	0.64, 0.76	0.70	1.938	0.67, 0.79	0.72	1.865	1.351	+3.9
Nightclub	0.70, 0.50	0.59	5.521	0.79, 0.56	0.66	4.950	3.243	+11.5
Meeting 1	0.83, 1.37	1.04	0.431	0.84, 1.38	1.04	0.430	0.447	+0.1
Meeting 2	0.90, 0.96	0.93	0.288	0.91, 0.96	0.93	0.288	0.268	+0.2
Office 1	0.87, 1.02, 0.99	0.96	0.098	0.94, 1.17, 1.10	1.07	0.088	0.094	+10.8
Office 1	0.80, 1.08, 0.99	0.94	0.100	0.95, 1.16, 1.02	1.03	0.091	0.094	+9.9
Office 1	0.83, 0.98, 0.88	0.89	0.105	0.88, 1.06, 1.02	0.98	0.096	0.094	+9.6
Office 2	0.37, 0.69	0.48	0.657	0.56, 0.81	0.66	0.474	0.315	+38.8

Fig. 5. Local air quality index values in Office 1 (45.1 m^2) depending on the emission source location marked with red circle.
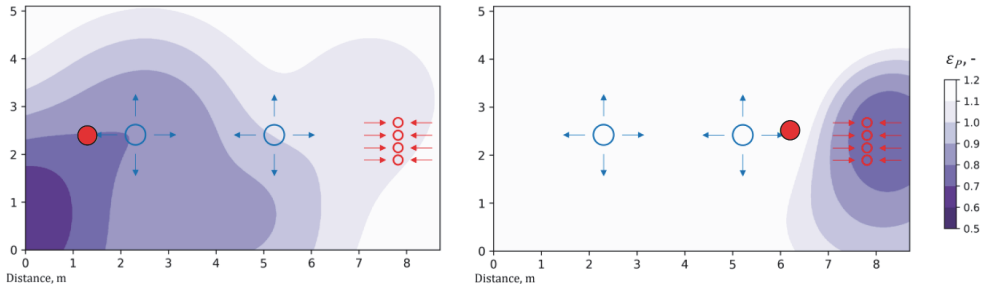

Fig. 6. Local air quality index values with left and right locations of point source in Classroom 6 of 45.1 m^2. Emission source is marked with red circle.
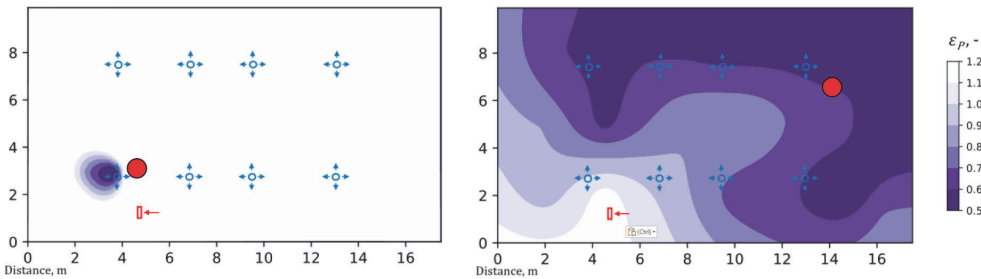

Fig. 7. Local air quality index values with left and right locations of point source in Fitness 1 of 173.5 m^2. Emission source is marked with red circle.

concentrations were clearly lower than the concentration in the extract duct.

While Fitness 1 and Gym 1 with ceiling diffusers suffered from short circuiting, Fitness 2 and Gym 2 with wall diffusers showed better effectiveness than that in fully mixing ventilation. This should not be taken as a rule, but rather as an issue of ceiling diffusers throw length control. In the largest Gym 3 with ceiling diffusers, close to fully mixing conditions were achieved with $\varepsilon_b = 0.99$ (Fig. 11).
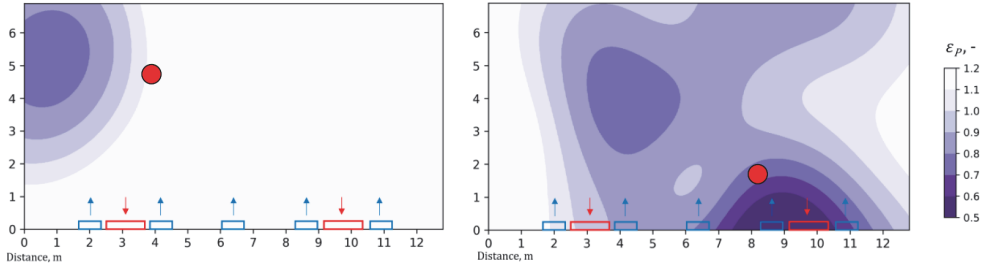
Fig. 8. Local air quality index values with left and right locations of point source in Fitness 2 of 117.0 m². Emission source is marked with red circle.
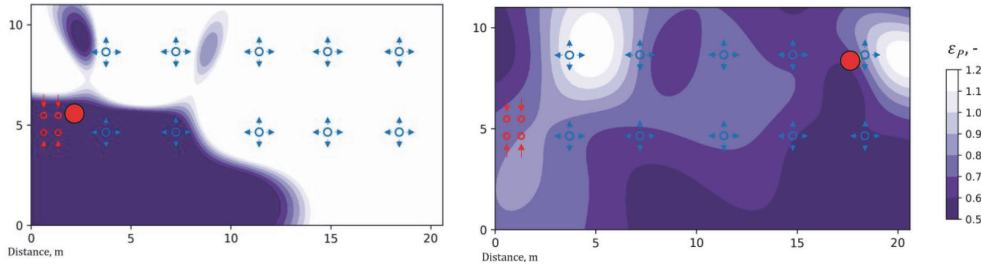

Fig. 9. Local air quality index values with left and right locations of point source in the gym (Gym 1) of 217.5 m². Emission source marked with red circle.
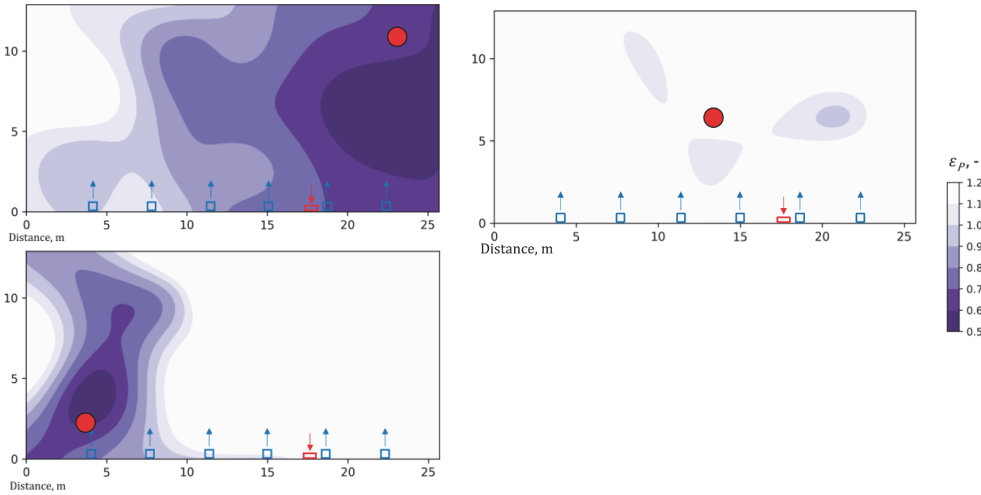

Fig. 10. Local air quality index values with three locations of point source in the gym (Gym 2) of 331 m². Emission source marked with red circle.

The rest of the measurement results are summarised in Table 4. It can be seen that ε_b values both lower and higher than 1 were measured in classrooms, dressing rooms, fitness, gyms and meeting rooms. In some cases, such as Classroom 1 and Classroom 3, higher ventilation rate lead to higher ventilation effectiveness, but also the opposite can be seen is some cases, such as Gym 1 and Gym 3. This may indicate that ventilation rates were enough high to control airflow patterns in these space categories. In offices where ventilation rates were smaller (2–2.3 L/s·m² compared to 4–9 L/s·m² in other rooms), ε_b values remained below 1 and the same applied for restaurants and bars in which air distribution was compromised by interior design.

On the other hand, measurements showed that the spatial difference of concentration is an issue in all measured cases conducted with the point contaminant source. Therefore, it is important to know how much the infection risk is increased in high concentration areas and correspondingly decreased in low concentration areas. This is not taken into account in ε_b and Q_s calculation that are based on the average concentration at 1.1 m height. Therefore Table 4 reports $\varepsilon_{b,loc}^j$ and $Q_{s,loc}$ that are iteratively calculated with Eqs. (12)-15 based on the local concentrations in each measurement point. $\Delta Q_s = (Q_s - Q_{s,loc})/Q_{s,loc} \cdot 100\%$ shows the difference in percentages between these two airflow rates. As ΔQ_s is positive in all cases, it shows that the calculation considering the spatial difference of the infection risk leads to lower required airflow rates. In
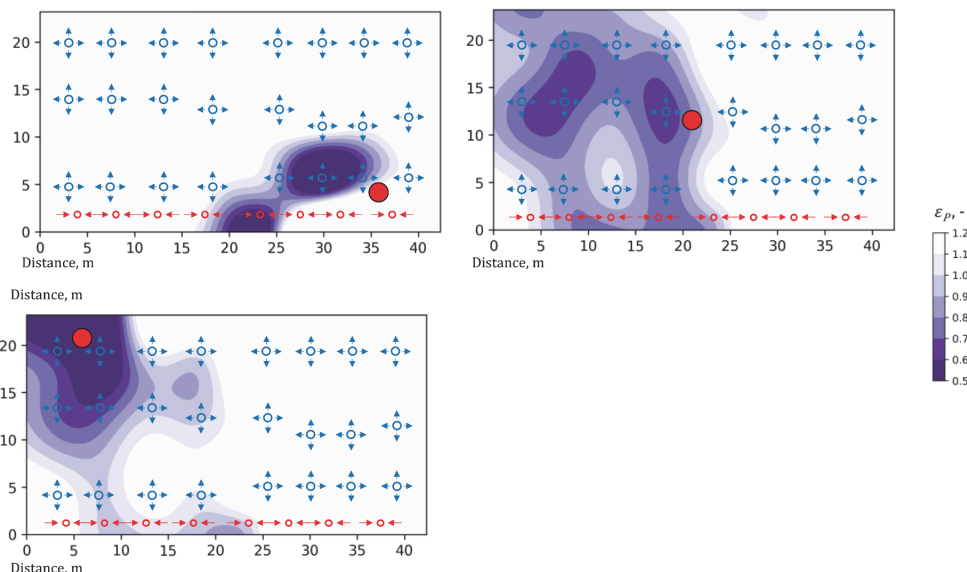
Fig. 11. Local air quality index values with three locations of point source in the gym (Gym 3) of 987 m². Emission source marked with red circle.

many cases the difference is only a few percent, but in some large spaces it exceeds 10% with a maximum of 39% in large open plan Office 2 where the highest concentration differences formed.

The airflow data in Table 4 is converted to L/s per floor m² units in Fig. 12 allowing comparison of the required ventilation rates to be supplied by air distribution systems in the measured rooms. There are considerable variations in between required ventilation rates in the same room type, which are caused by differences in ventilation effectiveness, occupancy and room volume.

In Fig. 13, the required ventilation rates are compared with indoor climate category I and II of EN 16,798–1:2019 [39]. Category I and II perceived air quality airflow rates include occupant component (I category – 10 L/(s·person); II category – 7 L/(s·person)) and floor area component to a low-polluting building (I category – 1.0 L/(s·m²); II category – 0.7 L/(s·m²)).

According to Fig. 11, in classrooms and open offices, ventilation rates based on the infection risk are mostly in between category I and II levels. However, in meeting rooms, infection-risk-based ventilation rates are substantially higher, suggesting that reducing occupancy and employing advanced air distribution might be practical solutions.

While the infection risk-based ventilation rates depend on the quanta values, measured ventilation effectiveness is a specific parameter of an air distribution system, which can be always used in relative risk reduction assessment. Variation of ventilation effectiveness values in the measured room categories is shown in Fig. 14. Values higher than 1.0 demonstrate that in carefully designed air distribution systems, the ventilation effectiveness achieved was higher than in fully mixed conditions. Among measured rooms, bars and the large open plan Office 2 were the only rooms where values higher than 1.0 were not achieved. While in bars this was clearly an air distribution design issue, large open plan offices may be the only room category where values close to 1.0 are difficult to achieve because of relatively small ventilation rates.
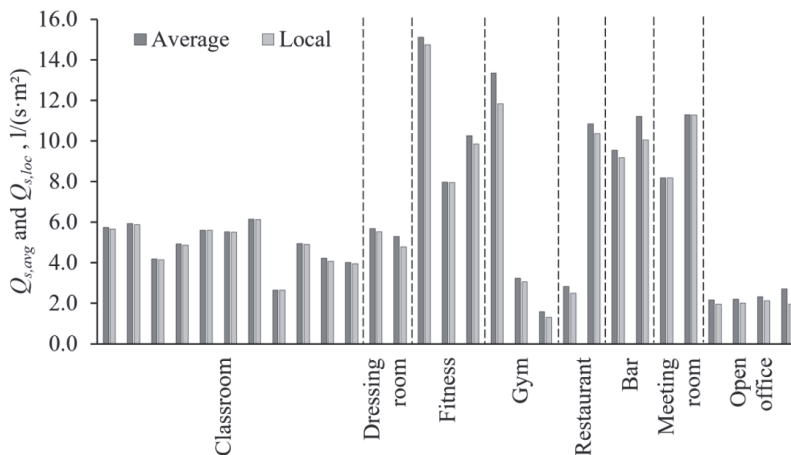

Fig. 12. Required ventilation rates to be supplied by air distribution systems in the measured rooms calculated from average and local concentrations.
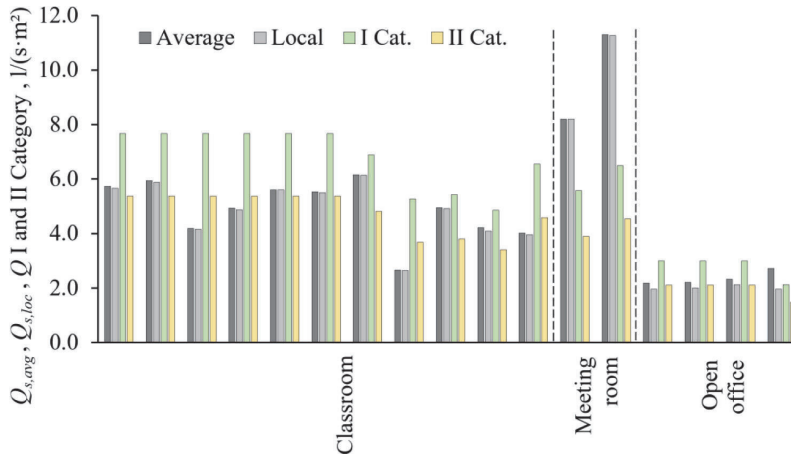
Fig. 13. Required ventilation rates to be supplied by air distribution systems calculated from average and local concentrations compared to EN 16798–1 [39] category I and II ventilation rates.
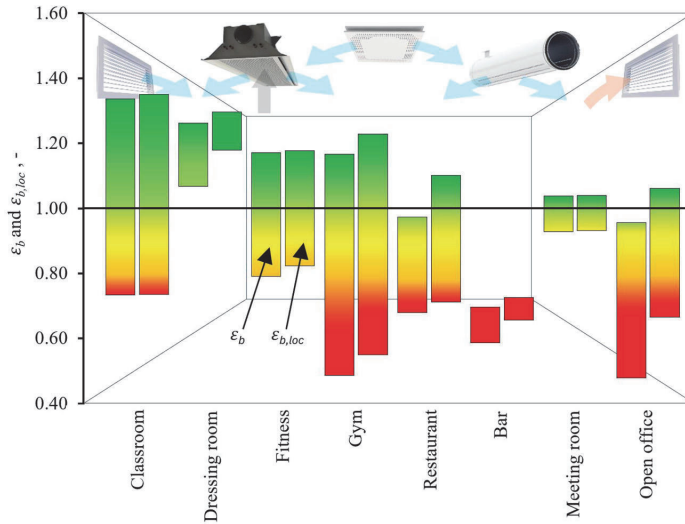

Fig. 14. Variation of ventilation effectiveness in measured room categories calculated from average (left columns, conventional method) and local concentrations (right columns, new method).

4. Discussion

In this study a new method to consider ventilation effectiveness in ventilation design for airborne transmission was developed. While local concentrations of the tracer gas or particles and infection risk maps have been analysed in previous studies, the advancement by this study is to describe the spatial variation of the concentration and infection risk with new parameter $\varepsilon_{b,loc}$ that has been calculated from the fraction of R_i. Therefore, the main novelty of the method is new ventilation effectiveness indicator that makes it possible to describe the effect of spatial variation of concentration and risk with single parameter. Compared to conventional ventilation effectiveness calculation from an average concentration, the new method improves the accuracy especially in cases with large concentration variations.

If the method is used in practice, there are some issues to consider.

Quanta emission rates, which can have high variation, are needed as input data to calculate the ventilation rate corresponding to a specified risk level. However, from methodological point of the view, the ventilation effectiveness is a parameter of an air distribution system that applies for any intensity of the emission source in similar fashion. Therefore, the differences between studied cases do not significantly depend on the quanta values. In that respect, the method has similar features with all other quanta methods: there is uncertainty in the absolute risk, but relative changes can be calculated accurately for different rooms and ventilation solutions.

Another consideration is needed for ventilation effectiveness measurement conditions and validity. Because of complexity of air flow patterns development in a room, affected by air jets, internal and solar heat gains, geometry etc., contaminant removal effectiveness measurement strictly applies only for those conditions in a room at measurement

time. This makes it highly important to conduct measurements in typical, representative situations. Internal heat gains are to be organised to the room, supply air temperature controlled, and the ventilation rate to be adjusted close to values under interest, because Archimedes number that is used to describe non-isothermal jets should not change significantly to keep the same air distribution patterns. Additional complexity is working with a point source which can have many possible locations in a room. In this study a tracer gas was introduced inside the dummy that is a simplification compared for instance to breathing manikin. This is justified, because it was not a purpose to simulate the close proximity exhalation and resulting concentration field, but the long-range transmission was studied. While some guidance on how to select relevant source locations was possible to provide, this topic evidently deserves future research efforts to ensure correct and practical application for ventilation design purposes.

The relevance of the contaminant removal effectiveness as a ventilation effectiveness indicator to describe spatial concentration differences can also be discussed. Another indicator used in many studies is the dilution ratio D_i of the exhaled breath of infector. D_i has not been used in this study, but equations can be rewritten so that the local air quality index would be replaced with dilution ratio. For this purpose, one can expand the source term introduced in Eq. (2):

$$Iq = IQ_b C_{ex} \qquad (21)$$

where

C_{ex} concentration in the exhaled breath of infector (quanta/m³)

From the D_i definition it is easy to show by substituting C_i from Eq. (12) that D_i is an alternative indicator for the local air quality index $\varepsilon_{P,i}$:

$$D_i = \frac{C_{ex}}{C_i} = \frac{q}{Q_b C_i} = \frac{\varepsilon_{P,i} Q_{s,loc} + \lambda_{rest} V}{IQ_b} \qquad (22)$$

Thus, D_i does not give more generic value, because it is in a similar fashion sensitive to heat gains and also on airflow rates if Archimedes number changes.

Measurements conducted in 22 rooms show some important tendencies in the air distribution systems performance. However, these measurement results should not be used to draw generic conclusions for studied room categories, because the selection criteria were to have enough large number of spaces which can show reasonably high variation in important parameters such as the room size, air change rates and concentration differences. More specifically, the interest was to see, how much spatial variation of concentration can be found in modern spaces equipped with mixing ventilation air distribution systems. The rooms included made it possible to show differences in ventilation effectiveness calculation with a conventional method based on the average concentration compared to the developed method taking into account the spatial variations. This means that any room category was not comprehensively studied for instance to find the best possible ventilation effectiveness values. Such analyses can be recommended for future studies because the results show high variations in most of measured room categories indicating that air distribution and ventilation effectiveness are important and there could be a substantial improvement potential in many cases.

5. Conclusions

In this study a new method for ventilation effectiveness application in ventilation design for airborne transmission was developed. While existing ventilation effectiveness values are based on tracer gas measurements with distributed source, the developed method uses a couple of point source locations corresponding to an infector and takes into account spatial non-uniform concentration resulting from air distribution patterns. Novelty of the method is new ventilation effectiveness parameter $\varepsilon_{b,loc}$ that makes it possible to describe the effect of spatial variation of concentration and risk with single parameter. The following

conclusions can be drawn:

- It was demonstrated that infection risk can be quantified for each measurement point at the breathing height, and it is possible to calculate the required ventilation rate supplied by the air distribution system corresponding to a specified risk level from the ventilation effectiveness tracer gas measurements with a couple of point source locations.
- The new method needs the quanta emission rate as input data, but the differences between the studied cases do not significantly depend on the quanta values used.
- Two or three point-source locations in tracer gas measurements were found to be sufficient for reasonably representative results. Locations representing typical occupant positions should be used so that one location is selected as far as possible from extracts and another location from the middle of the room. Locations just beneath extracts should be avoided.
- Simple ventilation effectiveness calculation from average concentration at the breathing height, not requiring quanta data, provided conservative results (lower ventilation effectiveness value and higher required ventilation rate) in all cases compared to iterative calculation with the new method taking into account the spatial difference of concentrations and infection risk.
- In many cases, the difference in required ventilation rates calculated with the new method and based on average concentration was only a few percent, but in some large spaces it exceeded 10% with a maximum of 39% in the large open plan office where the highest concentration differences formed.
- Ventilation effectiveness values both considerably lower and higher than one were measured in most of the room categories studied. The values ranged from 0.5 to 1.4. Values higher than 1.0 demonstrate that better ventilation effectiveness than in fully mixed conditions can been achieved with carefully designed air distribution systems.
- Higher ventilation rates did not consistently improve ventilation effectiveness indicating that ventilation rates were sufficiently high to control airflow patterns. Large open plan offices were the only room category where values close to 1.0 were difficult to achieve because of relatively small ventilation rates.
- The results can be potentially applied in ventilation standards and air distribution calculation tools. Ideally, it should not be too difficult to implement the new method in the calculation tools of air jet throw length and airflow patterns, which could in future report ventilation effectiveness values computed with the spatial difference of concentrations and infection risk taken into account.
- As the simple ventilation effectiveness calculation from average concentration revealed to provide conservative results, it can be seen suitable for practical design purposes, however in some cases leading to oversizing.

CRediT authorship contribution statement

Martin Kiil: Writing – original draft, Investigation, Formal analysis, Data curation. **Alo Mikola:** Writing – review & editing, Methodology, Data curation, Conceptualization. **Karl-Villem Võsa:** Visualization, Investigation, Formal analysis, Data curation. **Raimo Simson:** Writing – original draft. **Jarek Kurnitski:** Writing – original draft, Supervision, Methodology, Conceptualization.

Declaration of competing interest

The authors declare that they have no known competing financial interests or personal relationships that could have appeared to influence the work reported in this paper.

Acknowledgements

This work was supported by the Estonian Research Council grant (PRG2154), the Finnish Ministry of Education and Culture project HALLI-ILMA (OKM/3322/625/2021), the Finnish Work Environment Fund project LAIVA (TSR 220253) and by the Estonian Centre of Excellence in Energy Efficiency, ENER (grant TK230) funded by the Estonian Ministry of Education and Research. Nordic Ventilation Group and REHVA Technology and Research Committee COVID-19 Task Force are greatly acknowledged for support to develop this ventilation design method.

Data availability

Data will be made available on request.

References

[1] A. Flahault, A. Calmy, D. Costagliola, O. Drapkina, I. Eckerle, H.J. Larson, H. Legido-Quigley, C. Noakes, M. Kazatchkine, H. Kluge, No time for complacency on COVID-19 in Europe, Lancet 401 (2023) 1909–1912.

[2] Y. Li, P. Cheng, L. Liu, A. Li, W. Jia, N. Zhang, Predicting building ventilation performance in the era of an indoor air crisis, in: Proceedings of the Building Simulation; National Library of Medicine 16, 2023, pp. 663–666.

[3] L. Morawska, J. Cao, Airborne transmission of SARS-CoV-2: The world should face the reality, Environ. Int. 139 (2020) 105730.

[4] Y. Li, G.M. Leung, J.W. Tang, X. Yang, C.Y. Chao, J.Z. Lin, J.W. Lu, P.V. Nielsen, J. Niu, H. Qian, Role of ventilation in airborne transmission of infectious agents in the built environment-a multidisciplinary systematic review, Indoor Air 17 (2007) 2–18.

[5] M. Gormley, L. Marawska, D. Milton, It is time to address airborne transmission of coronavirus disease 2019 (COVID-19), Clin. Infect. Dis. 71 (2020) 2311–2313.

[6] R. Makris, C. Kopic, L. Schumann, M. Kriegel, A Comprehensive Index for Evaluating the Effectiveness of Ventilation-Related Infection Prevention Measures with Energy Considerations: Development and Application Perspectives, Indoor Air (2024) 2024.

[7] Mundt, M.; Mathisen, H.M.; Moser, M.; Nielsen, P. V Ventilation effectiveness: Rehva guidebooks. 2004.

[8] S. Zhang, Z. Lin, Dilution-based evaluation of airborne infection risk-Thorough expansion of Wells-Riley model, Build. Environ. 194 (2021) 107674.

[9] A.A. Aliabadi, S.N. Rogak, K.H. Bartlett, S.I. Green, Preventing airborne disease transmission: review of methods for ventilation design in health care facilities, Adv. Prev. Med. 2011 (2011) 124064.

[10] Z.T. Ai, A.K. Melikov, Airborne spread of expiratory droplet nuclei between the occupants of indoor environments: A review, Indoor Air 28 (2018) 500–524.

[11] S. Asadi, N. Bouvier, A.S. Wexler, W.D. Ristenpart, The coronavirus pandemic and aerosols: Does COVID-19 transmit via expiratory particles? Aerosol Sci. Technol. 54 (2020) 635–638.

[12] G. Cao, H. Awbi, R. Yao, Y. Fan, K. Sirén, R. Kosonen, J.J. Zhang, A review of the performance of different ventilation and airflow distribution systems in buildings, Build. Environ. 73 (2014) 171–186.

[13] B. Yang, A.K. Melikov, A. Kabanshi, C. Zhang, F.S. Bauman, G. Cao, H. Awbi, H. Wigö, J. Niu, K.W.D. Cheong, A review of advanced air distribution methods-theory, practice, limitations and solutions, Energy Build 202 (2019) 109359.

[14] H. Qian, T. Miao, L. Liu, X. Zheng, D. Luo, Y. Li, Indoor transmission of SARS-CoV-2, Indoor Air 31 (2021) 639–645.

[15] L. Morawska, J. Allen, W. Bahnfleth, B. Bennett, P.M. Bluyssen, A. Boerstra, G. Buonanno, J. Cao, S.J. Dancer, A. Floto, Mandating indoor air quality for public buildings, Science (80-.) 383 (2024) 1418–1420.

[16] W. Su, B. Yang, A. Melikov, C. Liang, Y. Lu, F Wang, A. Li, Z. Lin, X. Li, G. Cao, Infection probability under different air distribution patterns, Build. Environ. 207 (2022) 108555.

[17] S. Tan, Z. Zhang, K. Maki, K.J. Fidkowski, J. Capecelatro, Beyond well-mixed: A simple probabilistic model of airborne disease transmission in indoor spaces, Indoor Air 32 (2022) e13015.

[18] Y. Yan, X. Li, X. Fang, Y. Tao, J. Tu, A spatiotemporal assessment of occupants' infection risks in a multi-occupants space using modified Wells–Riley model, Build. Environ. 230 (2023) 110007.

[19] S. Son, C.-M. Jang, Effects of internal airflow on IAQ and cross-infection of infectious diseases between students in classrooms, Atmos. Environ. 279 (2022) 119112.

[20] B.C. Singer, H. Zhao, C.V. Preble, W.W. Delp, J. Pantelic, M.D. Sohn, T. W Kirchstetter, Measured influence of overhead HVAC on exposure to airborne contaminants from simulated speaking in a meeting and a classroom, Indoor Air 32 (2022) e12917.

[21] C.V.M. Vouriot, M. van Reeuwijk, H.C. Burridge, Robustness of point measurements of carbon dioxide concentration for the inference of ventilation rates in a wintertime classroom, Indoor Environ 1 (2024) 100004.

[22] M. Kiil, R. Simson, K.-V. Võsa, A. Kesküll, J. Kurnitski, Assessment of SARS-CoV-2 Transmission in Room with Mixing Ventilation Using CO2 Tracer Gas Technique, in: Proceedings of the Healthy Buildings America 2021, 2022; International Society of Indoor Air Quality and Climate (ISIAQ), Honolulu, Hawaii, USA, 2021. January 18-20.

[23] A. Aganovic, G. Cao, J. Kurnitski, A. Melikov, P. Wargocki, Zonal modeling of air distribution impact on the long-range airborne transmission risk of SARS-CoV-2, Appl. Math. Model. 112 (2022) 800–821.

[24] M. Kiil, I. Valgma, K.-V. Võsa, R. Simson, A. Mikola, T. Tark, J. Kurnitski, Ventilation effectiveness in classroom infection risk control, in: Proceedings of the E3S Web of Conferences 396, EDP Sciences, 2023, p. 1043.

[25] J. Kurnitski, M. Kiil, A. Mikola, K.-V. Vosa, A. Aganovic, P. Schild, O. Seppänen, Post-COVID ventilation design: Infection risk-based target ventilation rates and point source ventilation effectiveness, Energy Build 296 (2023) 113386.

[26] J. Kurnitski, M. Kiil, P. Wargocki, A. Boerstra, O. Seppänen, B. Olesen, L. Morawska, Respiratory infection risk-based ventilation design method, Build. Environ. 206 (2021) 108387.

[27] Rehva Health-based target ventilation rates and design method for reducing exposure to airborne respiratory infectious diseases. REHVA proposal for post-COVID target ventilation rates, Rehva (2023).

[28] A. Mikola, M. Kiil, K.-V. Võsa, M.F. Ejaz, S. Kilpeläinen, R. Kosonen, J. Kurnitski, Ventilation effectiveness measurements and CFD simulations in classrooms for infection risk control, in: Proceedings of the 17th Roomvent Conference, April 22-25, 2024, Stockholm, Sweden; E3S Web of Conferences, 2024.

[29] A. Mikola, M. Kiil, K.-V. Võsa, J. Kurnitski, Infection Risk-Based Ventilation Assessment in Cruise Ship Common Spaces Using Tracer Gas, in: Proceedings of the 17th Roomvent Conference, April 22-25, 2024, E3S Web of Conferences, Stockholm, Sweden, 2024.

[30] SAF Tehnika JSC Aranet4 TDSPC0H3 data logger Available online: https://aranet.com/about-us/.

[31] KERN & SOHN GmbH Kern FKB datasheet Available online: https://www.kern-sohn.com/en/FKB.

[32] A. Aganovic, G. Cao, J. Kurnitski, P. Wargocki, New dose-response model and SARS-CoV-2 quanta emission rates for calculating the long-range airborne infection risk, Build. Environ. 228 (2023) 109924.

[33] B. Jones, P. Sharpe, C. Iddon, E.A. Hathway, C.J. Noakes, S. Fitzgerald, Modelling uncertainty in the relative risk of exposure to the SARS-CoV-2 virus by airborne aerosol transmission in well mixed indoor air, Build. Environ. 191 (2021) 107617.

[34] Y. Guo, N. Zhang, T. Hu, Z. Wang, Y. Zhang, Optimization of energy efficiency and COVID-19 pandemic control in different indoor environments, Energy Build 261 (2022) 111954.

[35] The Lancet COVID-19 Commission *Proposed Non-infectious Air Delivery Rates (NADR) for Reducing Exposure to Airborne Respiratory Infectious Diseases.* November 2022.

[36] ISO/TC 146 ISO 16000-8:2007 Indoor air - Part 8: *Determ. local mean ages air Build*, Charact. Vent. Cond (2007).

[37] ISO/TC 163; CEN/TC 89 ISO 12569:2017 Thermal performance of buidlings and materials, Determ. Specif. airflow rate Build. - Tracer gas dilution method (2017).

[38] S. Batterman, Review and extension of CO2-based methods to determine ventilation rates with application to school classrooms, Int. J. Environ. Res. Public Health 14 (2017) 145.

[39] E.N. Standard, 16798-1. Energy performance of buildings—Ventilation for buildings—Part 1: Indoor environmental input parameters for design and assessment of energy performance of buildings addressing indoor air quality, Therm. Environ. Light. Acoust. M1-6.(16798-1) (2019).

Curriculum vitae

Personal data

Name:	Martin Kiil
Date of birth:	1989.03.09
Place of birth:	Kuressaare, Estonia
Citizenship:	Estonian

Contact data

E-mail:	martin.kiil@taltech.ee

Education

2018–2025	Tallinn University of Technology, Building and Civil Engineering and Architecture, PhD
2016–2017	Tallinn University of Technology, Building Energy Efficiency MSc (*cum laude*)
2016–2017	Tallinn University of Technology, Water Engineering, MSc
2011–2014	Tallinn University of Technology, Heating and Ventilation, MSc
2008–2011	Logistics, BSc
1996–2008	Co-ed Gymnasium of Saaremaa, secondary education

Language competence

Estonian	Native
English	Fluent
Finnish	Basic
Russian	Basic

Professional employment

2018–…	Tallinn University of Technology, Department of Civil Engineering and Architecture, Early-Stage Researcher/Expert
2016–2017	University of Applied Sciences, Institute of Civil Engineering, Lecturer
2013–2014	Tallinn University of Technology, Faculty of Civil Engineering, Department of Environmental Engineering, Engineer
2014–…	O3 Technology Ltd, Board Member

Chartered Engineer in Heating, Ventilation and Air Conditioning (HVAC), Level 8
Diploma Engineer in Water Supply and Sewerage, Level 7
Chartered Specialist in Energy Performance of Buildings, Level 8

Elulookirjeldus

Isikuandmed

Nimi:	Martin Kiil
Sünniaeg:	1989.03.09
Sünnikoht:	Kuressaare, Eesti
Kodakondsus:	Eesti

Kontaktandmed

E-post:	martin.kiil@taltech.ee

Hariduskäik

2018–2025	Tallinna Tehnikaülikool, Ehitus ja arhitektuur, PhD
2016–2017	Tallinna Tehnikaülikool, Hoonete energiatõhusus, MSc
2016–2017	Tallinna Tehnikaülikool, Veetehnika, MSc
2011–2014	Tallinna Tehnikaülikool, Küte ja ventilatsioon, MSc
2008–2011	Tallinna Tehnikaülikool, Logistika, BSc
1996–2008	Saaremaa Ühisgümnaasium, keskharidus

Keelteoskus

Eesti keel	Emakeel
Inglise keel	Kõrgtase
Soome keel	Algtase
Vene keel	Algtase

Teenistuskäik

2018–...	Tallinna Tehnikaülikool, Ehituse ja arhitektuuri instituut, nooremteadur/ekspert
2016–2017	Tallinna Tehnikakõrgkool, lektor
2013–2014	Tallinna Tehnikaülikool, Ehitusteaduskond, Keskkonnatehnika õppetool, insener
2014–...	O3 Technology OÜ, juhatuse liige

Volitatud kütte-, ventilatsiooni- ja jahutuseinsener, tase 8
Diplomeeritud veevarustuse- ja kanalisatsiooniinsener, tase 7
Volitatud energiatõhususe spetsialist, tase 8

Publications / Teaduspublikatsioonid

Articles in Journals:

Ventilation effectiveness and incomplete mixing in air distribution design for airborne transmission M Kiil, A Mikola, KV Võsa, R Simson, J Kurnitski *Building and Environment*, 112207.

Overheating and Air Velocities in Modern Office Buildings During Heating Season M Kiil, R Simson, M Thalfeldt, J Kurnitski *Indoor Air* 2024 (1), 9992937.

Post-COVID ventilation design: infection risk-based target ventilation rates and point source ventilation effectiveness J Kurnitski, M Kiil, A Mikola, KV Võsa, A Aganovic, P Schild, O Seppänen Energy and Buildings 296, 113386.

Kurnitski, J.; Kiil, M.; Wargocki, P.; Boerstra, A.; Seppänen, O.; Olesen, B.; Morawska, L. (2021). Respiratory infection risk-based ventilation design method. *Building and Environment*, 206. DOI: 10.1016/j.buildenv.2021.108387.

Kiil, M.; Simson, R.; Thalfeldt, M.; Kurnitski, J. (2020). A Comparative Study on Cooling Period Thermal Comfort Assessment in Modern Open Office Landscape in Estonia. *Atmosphere*, 11 (2), 127–149. DOI: 10.3390/atmos11020127.

Proceedings of scientific conferences:

How much active cooling is needed in Estonian multifamily apartment buildings to comply with Category II thermal comfort? M Kiil, K Onemar, K-V Võsa, R Simson, J Kurnitski Building Simulation Conference 2025, Brisbane 24-27.08.2025 (accepted for publication).

Battery storage potential in meeting NZEB energy performance requirements in Estonia M Kiil, T M Parts, M-L Sits, K-V Võsa, R Simson, J Kurnitski Building Simulation Conference 2025, Brisbane 24-27.08.2025 (accepted for publication).

Draught and ventilation effectiveness in large and high space with excessive heat gains M Kiil, K-V Võsa, R Simson, A Mikola, J Kurnitski REHVA HVAC World Congress CLIMA 2025, Milano 4-6.06.2025 (accepted for publication).

Relative risk reduction in ventilation design for airborne transmission J Kurnitski, M Kiil, A Aganovic, W Olesen REHVA HVAC World Congress CLIMA 2025, Milano 4-6.06.2025 (accepted for publication).

Point source Ventilation Effectiveness of mixing ventilation solutions used in non-residential Settings M Kiil, A Mikola, KV Võsa, R Simson, J Kurnitski Indoor Air 2024, Honolulu, Hawaii, USA, July 7-11, 2024.

Effect of Infector's location and occupants' activity level on airborne spread in a gym – an experimental and CFD study MF Ejaz, S Kilpeläinen, A Mikola, M Kiil, J Kurnitski, R Kosonen Roomvent Conference 2024, April 22-25, 2024, Stockholm, Sweden.

Using portable air cleaners to restrict airborne transmission in an open plan office – a field measurement and CFD study S Kilpeläinen, MF Ejaz, A Mikola, M Kiil, J Kurnitski, R Kosonen Roomvent Conference 2024, April 22-25, 2024, Stockholm, Sweden.

Infection Risk-Based Ventilation Effectiveness Assessment in Cruise Ship Common Spaces Using Tracer Gas Measurements A Mikola, M Kiil, KV Võsa, J Kurnitski Roomvent Conference 2024, April 22-25, 2024, Stockholm, Sweden.

Ventilation effectiveness measurements and CFD simulations in classrooms for infection risk control A Mikola, M Kiil, KV Võsa, MF Ejaz, S Kilpeläinen, R Kosonen, J Kurnitski Roomvent Conference 2024, April 22-25, 2024, Stockholm, Sweden.

Point source ventilation effectiveness in infection risk-based post-COVID ventilation design J Kurnitski, M Kiil, A Mikola, KV Võsa 43rd AIVC - 11th TightVent - 9th venticool Conference - Copenhagen, Denmark - 4-5 October 2023.

Ventilation effectiveness in classroom infection risk control M Kiil, I Valgma, KV Võsa, R Simson, A Mikola, T Tark, J Kurnitski E3S Web of Conferences 396, 01043.

Kiil, M.; Simson, R.; Võsa, K.-V.; Mikola, A.; Thalfeldt, M.; Kurnitski, J. (2022). Respiratory infection risk-based ventilation and room conditioning design method with year-round thermal comfort control in modern office buildings. Proceedings of The 16th ROOMVENT Conference. September 16-19, 2022, Xi'an, China.

Simson, R.; Võsa, K.-V.; Kiil, M.; Mikola, A.; Kurnitski, J. (2022). Air Leakages in Air Handling Units with Rotary Heat Exchanger: Estimating Extract Air Transfer to Supply Air Flow. Healthy Buildings America 2021, Honolulu, Hawaii, USA, January 18-20, 2022. International Society of Indoor Air Quality and Climate (ISIAQ).

Simson, R.; Kiil, M.; Võsa, K.-V.; Kesküll, A.; Kurnitski, J. (2022). Assessment of SARS-CoV-2 Transmission in Room with Mixing Ventilation Using CO2 Tracer Gas Technique. Healthy Buildings America 2021, Honolulu, Hawaii, USA, January 18-20, 2022. International Society of Indoor Air Quality and Climate (ISIAQ).

Sarevet, H.; Kiil, M.; Simson, R.; Thalfeldt, M.; Kurnitski, J. (2020). Undefined modelling parameters impact on building simulation results: using IDA ICE according to the Estonian methodology for calculating building performance. In: BuildSim-Nordic 2020. SINTEF Academic Press.

Kiil, M.; Käärid, M.-S.; Klõšeiko, P.; Võsa, K.-V.; Simson, R.; Sarevet, H.; Thalfeldt, M.; Kurnitski, J. (2020). PCSP's Diagonal Tie Connectors Thermal Bridges Impact on Energy Performance and Operational Cost: Case Study of a High-Rise Residential Building in Estonia. In: E3S Web of Conferences: 12th Nordic Symposium on Building Physics (NSB 2020) (#08006). EDP Sciences. DOI: 10.1051/e3sconf/202017208006.

Simson, R.; Rebane, T.; Kiil, M.; Thalfeldt, M.; Kurnitski, J. (2020). The Impact of Infiltration on Heating Systems Dimensioning in Estonian Climate. In: E3S Web of Conferences: 12th Nordic Symposium on Building Physics (NSB 2020) (#05004). EDP Sciences. DOI: 10.1051/e3sconf/202017205004.

Kiil, M.; Mikola, A.; Thalfeldt, M.; Kurnitski, J. (2019). Thermal comfort and draught assessment in a modern open office building in Tallinn. E3S Web of Conferences: CLIMA 2019 Congress, Bucharest 27-29.05.2019. EDP Sciences, 1–7. (E3S Web of Conferences; 111). DOI: 10.1051/e3sconf/201911102013.

De Luca, F.; Kiil, M.; Kurnitski, J.; Murula, R. (2019). Evaluating Daylight Factor Standard through Climate Based Daylight Simulations and Overheating Regulations in Estonia. Proceedings of 16th IBPSA International Conference and Exhibition (BS2019): 16th IBPSA International Conference and Exhibition (BS2019), Angelicum Congress Centre, Rome, Italy, 02-04 September 2019. Ed. V. Corrado, E. Fabrizio, A. Gasparella, and F. Patuzzi. International Building Performance Simulation Association, 3968–3975. DOI: 10.26868/25222708.2019.210915.

Kiil, M.; Simson, R.; De Luca, F.; Thalfeldt, M.; Kurnitski, J. (2019). Overheating and daylighting evaluation for free-running classroom designs. IOP Conference Series: Earth and Environmental Science, 352: 1st Nordic conference on Zero Emission and Plus Energy Buildings. IOP Publishing, 012059. DOI: 10.1088/1755-1315/352/1/012059.